

Stian Schencke Sivertsgård

Investigation of the Effect of Propeller Location with the use of CFD

Master's thesis in Marine Technology
Supervisor: Kourosh Koushan
June 2019

Stian Schencke Sivertsgård

Investigation of the Effect of Propeller Location with the use of CFD

Master's thesis in Marine Technology
Supervisor: Kourosh Koushan
June 2019

Norwegian University of Science and Technology
Faculty of Engineering
Department of Marine Technology

MASTER THESIS IN MARINE TECHNOLOGY

SPRING 2019

FOR

Stian Sivertsgård

INVESTIGATING THE EFFECT OF PROPELLER LOCATION WITH THE USE OF CFD

Propeller location can influence its performance and its effect on the ship hull. The propeller efficiency is clearly dependent on the inflow characteristics, which are dictated by its location. Also susceptibility of the propeller to cavitation is dependent on the inflow. The position of the propeller relative to the hull affects also amount of pressure pulses and vibration induced by the propeller.

Positioning of propellers is in general rather constrained but its exact positioning could be optimised based on the knowledge of the flow field in the wake of the hull. By taking advantage of the deep insight into the flow field obtained from CFD simulations, it is possible to evaluate the performance of a given propeller at a large array of potential position. This possibility gives the opportunity to optimise the exact propeller location. Application of pre-swirl energy saving devices (for example a pre-swirl stator) affects also the inflow to the propeller and therefore can be used to optimise the inflow to the propeller.

The candidate shall investigate the effect of inflow to the propeller, which is dependent on its location and possible pre-swirl device using the CFD software FineMarine. Calm water CFD analysis shall be performed with the hull but without the propeller to calculate the velocities at different possible positions for the propeller. Influence of these calculated inflows on propeller efficiency and cavitation performance of the propeller shall be investigated using the potential flow propeller code AKPA. In addition, effect of a pre-swirl stator on the inflow and consequently on the propeller efficiency and its cavitation performance shall be investigated using CFD software FineMarine and propeller analysis software AKPA. Further optimisation of the pre-swirl stator shall be performed. Coupling of AKPA with the CFD software FineMarine (online or offline) shall be envisaged. The candidate shall provide clear guidelines and recommendations for the positioning of the propeller. Possible constraints given by the classification rules should be described and taken into account.

In the thesis the candidate shall present his personal contribution to the resolution of problem within the scope of the thesis work.

Theories and conclusions shall be based on mathematical derivations and/or logic reasoning identifying the various steps in the deduction.

The thesis work shall be based on the current state of knowledge in the field of study. The current state of knowledge shall be established through a thorough literature study, the

results of this study shall be written into the thesis. The candidate should utilize the existing possibilities for obtaining relevant literature.

The thesis should be organized in a rational manner to give a clear exposition of results, assessments, and conclusions. The text should be brief and to the point, with a clear language. Telegraphic language should be avoided.

The thesis shall contain the following elements: A text defining the scope, preface, list of contents, summary, main body of thesis, conclusions with recommendations for further work, list of symbols and acronyms, reference and (optional) appendices. All figures, tables and equations shall be numerated.

The supervisor may require that the candidate, in an early stage of the work, present a written plan for the completion of the work. The plan should include a budget for the use of computer and laboratory resources that will be charged to the department. Overruns shall be reported to the supervisor.

The original contribution of the candidate and material taken from other sources shall be clearly defined. Work from other sources shall be properly referenced using an acknowledged referencing system.

The thesis shall be submitted electronically (pdf) in Inspira:

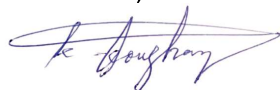
- Signed by the candidate
- The text defining the scope (signed by the supervisor) included
- Computer code, input files, videos and other electronic appendages can be uploaded in a zipfile in Inspira.
- Any electronic appendages shall be listed in the main thesis.

Supervisor : Professor Kourosh Koushan

Start : 15.01.2019

Deadline : 11.06.2018 at 14:00.

Trondheim, 15.01.2019



Kourosh Koushan

Supervisor

Preface

This master thesis have been written during my fourth and last semester at the Norwegian University of Science and Technology (NTNU) Department of Marine Technology.

Propeller hydrodynamic performance with respect to fuel consumption is a highly important research topic as we face the climate change problems we have today. Reducing the consumption of the shipping industry will in a significant way contribute to a greener fleet. This is widely accepted as a step towards a more sustainable way to operate older and newer vessels. I have been privileged to investigate the current state of knowledge within the field of propulsion.

During the writing of the thesis there has been many trial and errors. I have experienced that numerical computations is extremely sensitive and demands the user to have a deep understanding of the topic to obtain acceptable results. This has challenged me to dig into papers, analyse results from earlier studies and perform a literature study on this topic.

I would like to thank my supervisor Kouros Koushan for guidance and support through this task. A large gratitude is directed towards Eloïse Croonenborghs, Fengjian Jiang and Vladimir Krasilnikov for daily support in the use of numerical computations in general, CFD software FineMarine and propeller analysis software AKPA. I would also like to thank my fellow students for keeping the motivational spirit through the whole semester.



Stian Schencke Sivertsgård

Trondheim June 7, 2019

Abstract

The goal of this research is to investigate the propeller location with the use of numerical methods. The motivation of the study is mainly to lower the fuel consumption and thus lower the greenhouse gas emission. Other parameters such as disturbances to the marine environment and erosion on the propeller blades are also of importance. This thesis extends from the literature study made on the topic during the autumn of 2018.

A thorough study on the current state of knowledge within numerical methods in marine hydrodynamics and the influencing parameters on the propeller inflow are included. This part introduces how CFD may be applied to predict wake field and propeller performance. The classification society DNV GL's standards with respect to retrofitting of existing vessel is presented and discussed. Further is inflow to propeller, wake field, cavitation inception, ESD's and the location of the propeller presented and evaluated with respect to hydrodynamic performance.

All conducted simulations are performed on a chemical tanker with and without the presence of a PSS. The calm water numerical computations conducted in the study is performed in the CFD software FINE/Marine by NUMECA. Obtained wake field data is used to perform the propeller analysis at different longitudinal positions using the propeller program AKPA. An equal study was conducted by SINTEF both with CFD and EFD on the same vessel, where the presented results are used for comparison and verification. The hull testing with CFD is conducted on seven geometries at operational vessel speed, including naked hull, original PSS and five PSS adjustments. The pitch angle and angular position of the ESD fins is adjusted to quantify the effect on the propulsor efficiency. To determine the propeller performance at different advance numbers, a vessel speed of $1.21ms^{-1}$ and $1.61ms^{-1}$ in model scale, corresponding to 12 and 16 knots in full scale, respectively, are tested. All the conducted simulations are evaluated with respect to propeller location in the longitudinal direction. Parameters used to evaluate the most suitable position is thrust, torque, efficiency, required power and the effect of cavitation.

Sammendrag

Målet med denne masteroppgaven var å analysere propellens ytelse ved forskjellige plasseringer i lengderetning ved hjelp av numeriske metoder. Motivasjonen for studien er hovedsakelige å redusere drivstofforbruket og implisitt minske klimagassutslippet. Andre parametre av betydning er forstyrrelser av det marine havmiljøet, som støy, og erosjon på propellbladene. Oppgaven er en fortsettelse fra litteraturstudiet som ble utført høsten 2018.

Et nøye studie av nåværende kunnskap innen numeriske metode i marin hydrodynamikk samt parametre som påvirker innstrømmningen til propeller er presentert. Denne delen introduserer hvordan metoder innenfor CFD er brukt til å predikere medstrømsfordeling og propellens hydrodynamiske ytelse. Klaseselskapet DNV GLs regelverk med hensyn til ettermontering av geometri på eksisterende fartøy er presentert og diskutert. Videre er innstrømning til propell, medstrømsfeltet, kavitasjon, energibesparende geometri og plassering av propellen i lengderetning evaluert med hensyn til ytelse.

Alle numeriske simuleringer er utført på en kjemikalietanker med og uten energibesparende tilleggsgemetri. Stillevannskalkulasjonene utført i studien er gjort i CFD-programvaren FINE/Marine, levert av NUMECA. Medstrømsfeltene hentet ut fra de numeriske metodene brukes til å utføre propellanalyser ved forskjellige langsgående posisjoner ved hjelp av propellprogrammet AKPA. En studie utført på samme type fartøy med identisk tilleggsgemetri ved hjelp av numeriske og eksperimentelle metoder publisert av SINTEF med samarbeidspartnere er gjentatte ganger brukt til sammenligning og verifikasjon av resultater. Simulering ved hjelp av CFD er utført på syv forskjellige geometrier med tilhørende domener. Dette inkluderer skrog uten PSS, med PSS og fem forskjellige PSS-justeringer. Angrepsvinkel til PSS bladene og vinkelposisjon er justert for å kvantifisere effekten det påfører effektiviteten til propellen. Propellytelsen ved forskjellige fremgangstall er undersøkt, korresponderende til en hastighet på 12 og 16 knop i full skala. Alle utførte simuleringer vurderes med hensyn til propellens plassering i lengderetningen.

De numeriske beregningene viser god overenskomst med eksperimentell testing og konverger innen kort tid. Simulering uten overflateeffekter kan gi enorme besparelser med hensyn til konsumert tid. Propellanalysene viser at propellens kraftforbruk kan reduseres ved å bli plassert nedstrøms fra original posisjon, så langt det lar seg gjøre innenfor geometriske betingelser. En besparelse på 2.35% og 2.97% kan oppnås ved forflytte propellen til posisjon 8 for skrog henholdsvis med og uten PSS. Ved å endre geometri på PSS kan ytterligere 0.5% kuttes i forhold til original geometri. Forflytning av propell til posisjon 8 kan minske sannsynligheten for kavitasjon med 18.11% avhengig av geometri.

Contents

Preface	iii
Abstract	v
Sammendrag	vii
1 Introduction	1
1.1 Environmental Aspects	2
1.2 CFD in Wake Field Prediction and Propeller Optimisation	3
1.3 Retrofitting of Existing Vessel	5
1.3.1 Classification Standards and Rules	6
1.4 Objective	7
2 Propeller Inflow Characteristics	9
2.1 Optimal Propeller Inflow	9
2.1.1 Presence of the Propeller - Effective Wake	12
2.2 Propeller Cavitation	13
2.3 Energy Saving Devices	14
2.3.1 Pre-Swirl Stator	14
2.4 Location of the Propeller	15
3 Pre-Swirl Stator Optimisation	17
3.1 Stator Pitch Angle	17
3.2 Angular Position of Stator	18
3.3 Diameter of Stator Blade	20
3.4 Structural Optimisation	20
3.5 Difficulties with PSS Optimisation	21
4 Software	23
4.1 FINE/Marine	23
4.1.1 Domain and Grid	23
4.1.2 ISIS-CFD Numerical Flow Solver	26
4.2 AKPA - Propulsor Design and Analysis Software	27
4.2.1 Velocity Based Source BEM and Cavitation Analysis	28
4.3 Coupling of FM and AKPA	29
4.3.1 Step 1: Linux & Python - CFView	30
4.3.2 Step 2: MATLAB - AKPA	31

5	Numerical Simulation Set-up	33
5.1	Pre-Processing	33
5.1.1	Domain and Boundary Conditions	34
5.1.2	Discretisation of Domain and Grid	36
5.2	Numerical Test Set-Up	44
5.3	Post-Processing - FM Computation	46
5.4	Propeller Analysis - AKPA	47
6	Results - CFD and Propeller Analysis	51
6.1	Numerical Investigation and Validation	51
6.1.1	Resistance curve	51
6.1.2	Domain without FS	52
6.1.3	Nominal Wake Field	55
6.2	Resistance	61
6.2.1	Stator Drag Resistance	62
6.3	Wake Field Analysis	63
6.3.1	Effective Wake Field Analysis	65
6.4	Propeller Location Analysis	70
6.4.1	Hydrodynamic Performance - Hull w and w/o PSS	70
6.4.2	Hydrodynamic Performance - Forward velocity	72
6.4.3	Hydrodynamic Performance - Adjusted PSS Orientation	75
6.5	Pressure Distribution and Cavitation	77
6.5.1	Propeller Cavitation Analysis	77
6.5.2	Stator Fins - Pressure Distribution	83
7	Further Work	85
7.1	Presence of the Propeller and Rudder in CFD	85
7.2	Automatic Computation Processing	85
7.3	Other PSS adjustments	87
7.3.1	Diameter of PSS Blades	87
7.3.2	Number of PSS Blades	87
7.4	Long term goal - Establish Classification Rules for PSS	87
8	Conclusion	89
	Bibliography	91
	Appendices	I
A	Grid and Domain	III
A.1	Domain and boundary conditions	III
B	Correspondence with DNV GL personell	VI
B.1	Rognebakke, Olav (11.03.2019)	VI
B.2	Deinboll, Oddvar (12.03.2019)	VII
C	Propeller	VIII
C.1	Blade geometry	VIII
D	Resistance	IX
D.1	Convergence curve	IX
E	Propeller Performance	XII

	E.1	Original hull w and w/o PSS	XII
	E.2	Different advance number	XIII
	E.3	Adjusted PSS orientation	XIV
	E.4	Performance coefficients	XVI
F	Wake Field		XVII
	F.1	Naked hull	XVII
		F.1.1 Effective Wake	XX
	F.2	Hull with PSS	XXIV
		F.2.1 Nominal Wake	XXIV
		F.2.2 Effective Wake	XXVIII
	F.3	Wake Fraction	XLVI
G	Cavitation Analysis		XLVII
H	Pressure distribution PSS		XLVIII
I	Programming		LIV
	I.1	Python	LIV
	I.2	MATLAB	LV
		I.2.1 Code - Read FM data create AKPA file	LV
		I.2.2 Function - Read wake flow data	LVIII
		I.2.3 Function - Create AKPA Input files	LIX

List of Tables

1.1	Propeller Optimisation Trends	5
2.1	Pre-Swirl Stator savings	14
3.1	Adjustment of Pitch Angle	18
3.2	Original angular position PSS	18
3.3	Adjustment angular position of PSS	19
5.1	Simulated parameters FM	34
5.2	Main ship particulars	34
5.3	Domain 1 - Naked Hull	34
5.4	Domain 2 - Naked hull w/o Free-Surface	34
5.5	Domain 3 - Hull with PSS	34
5.6	Domain 4 - Hull with PSS w/o FS	34
5.7	Initial mesh - Naked hull	38
5.8	Box refinement parameters [m]	38
5.9	Refinements and total number of cells - Naked hull	40
5.10	Number of viscous layers - Naked hull	41
5.11	Free surface refinement target cell size	41
5.12	Free surface refinement parameters	41
5.13	Initial mesh - PSS	42
5.14	Box refinement parameters [m] - PSS	42
5.15	Refinements and total number of cells - Hull with PSS	43
5.16	Number of viscous layers - with PSS	43
5.17	Number of cells in direction (initial mesh) and total amount of cells - no FS	44
5.18	Fluid test parameters	44
5.19	Propeller parameters	47
5.20	Cavitation analysis parameters	48
5.21	Velocity vs Advance number	49
6.1	Comparison of numerical simulation	53
6.2	Nominal wake fraction for refinement 1-6	57
6.3	Resistance - Experimental and CFD of model scale vessel	61
6.4	Resistance - PSS Adjustments	62
6.5	Propeller plane evaluation	64
6.6	Propeller performance	70
6.7	Thrust coefficient - Naked	72
6.8	Torque coefficient - Naked	72
6.9	Efficiency in wake - Naked	73

6.10	Shaft delivered power - Naked	73
6.11	Thrust coefficient - PSS	74
6.12	Torque coefficient - PSS	74
6.13	Efficiency in wake - PSS	74
6.14	Shaft delivered power - PSS	74
6.15	Shaft delivered power - PSS Adjustments	76
6.16	Pressure coefficients - Cavitation data	77
6.17	Cavitation inception - ($-C_P/\sigma_0$)	79
6.18	Pressure distribution stator fins - PSS	84

List of Figures

1.1	Chemical tanker design	1
1.2	Environmental impact of marine vessels	2
1.3	Propulsion test setup with designed PSS	4
1.4	Energy savings on retrofitting of vessels	6
2.1	Nominal wake for a single screw vessel	10
2.2	Transverse nominal wake w/o and with ESD	11
2.3	EnergoFlow Pre-Swirl Stator	15
2.4	Streamlines aft of vessel	16
3.1	Adjustment of Pitch Angle	18
3.2	Adjustment angular position	19
3.3	Stator Blade Diameter	20
4.1	Tetrahedron, Hexahedron and Prism cell	24
4.2	Abrupt changes in pressure iso contour plot	25
4.3	Cavitation Pattern collected from AKPA	27
4.4	Offline Software Coupling	29
4.5	Automatic AKPA propeller analysis procedure	32
5.1	Domain 1 - with BC	35
5.2	Refinement of surface intersecting cells	37
5.3	Trimming of surface intersecting cells	37
5.4	Model of naked hull, no PSS	38
5.5	Refinement 5 of propeller location	39
5.6	Viscous layer insertion	40
5.7	Hull with PSS	42
5.8	Sinusoidal ramp profile	45
5.9	3D view of propeller	48
6.1	Resistance convergence - Naked hull [Half vessel]	51
6.2	Resistance convergence - PSS [Whole vessel]	52
6.3	Resistance convergence - No FS	53
6.4	Nominal wake field comparison - w FS vs. no FS (Naked)	54
6.5	Nominal wake field comparison - w FS vs. no FS (PSS)	54
6.6	Comparison of nominal wake - Naked	56
6.7	Tangential velocity comparison	57
6.8	Nominal wake field PSS - Refinement 1 Position 4	58
6.9	Nominal wake field PSS - Refinement 2 Position 4	58

6.10	Nominal wake field PSS - Refinement 3 Position 4	59
6.11	Nominal wake field PSS - Refinement 4 Position 4	59
6.12	Nominal wake field PSS - Refinement 5 Position 4	60
6.13	Nominal wake field PSS - Refinement 6 Position 4	60
6.14	Comparison of resistance reduction by PSS orientation	62
6.15	Propeller positions	64
6.16	Effective wake field Original PSS - Position 3	67
6.17	Effective wake field Original PSS - Position 4	67
6.18	Effective wake field Original PSS - Position 5	68
6.19	Effective wake field Original PSS - Position 6	68
6.20	Effective wake field Original PSS - Position 7	69
6.21	Effective wake field Original PSS - Position 8	69
6.22	Efficiency in Wake vs Propeller Position	71
6.23	Shaft delivered power vs Propeller Position	71
6.24	Shaft delivered power - Naked	73
6.25	Shaft delivered power - PSS	75
6.26	Efficiency in wake comparison for different PSS adjustments.	76
6.27	Thrust divided by power - Comparison for different PSS adjustments . .	76
6.28	Pressure distribution color bar	77
6.29	Propeller pressure distribution	78
6.30	Cavitation inception - Propeller blade at 9° rotation	80
6.31	Propeller cavitation inception	82
6.32	Pressure distribution stator fins - Original PSS	83
7.1	Automatic numerical computation outlay	86

Nomenclature

Abbreviations

<i>AP</i>	Aft Perpendicular
<i>AoA</i>	Angle of Attack
<i>BC</i>	Boundary Conditions
<i>BEM</i>	Boundary Element Method
<i>CFD</i>	Computational Fluid Dynamics
<i>CFL</i>	Courant-Friedrichs-Lewy
<i>ConRo</i>	Combination of RoRo and container ship
<i>DNS</i>	Direct Numerical Simulation
<i>EEDI</i>	Energy Efficiency Design Index
<i>ESD</i>	Energy Saving Devices
<i>FM</i>	FINE/Marine
<i>FP</i>	Fore Perpendicular
<i>FPP</i>	Fixed-Pitch Propeller
<i>LES</i>	Large Eddy Simulation
<i>LOA</i>	Length Overall
<i>MTE</i>	Modified Trailing Edge
<i>PDE</i>	Partial Differential Equation
<i>PID</i>	Propulsion Improving Devices
<i>PSD</i>	Pre-Swirl Devices
<i>PSS</i>	Pre-Swirl Stator
<i>RANS</i>	Reynolds-Averaged Navier-Stokes
<i>RPM</i>	Revolutions Per Minute

TEU Twenty-foot Equivalent Unit

VLCC Very Large Crude Carrier

Symbols

C_P Pressure coefficient

C_{TE} Total resistance coefficient model scale - experimental value

C_{TN} Total resistance coefficient model scale - numerical value

D Propeller diameter

F_i Force component i direction

K_Q Torque Coefficient

K_T Thrust Coefficient

P_D Shaft delivered power

R_P Pressure resistance

R_{TE} Total resistance model scale - experimental value

R_{TN} Total resistance model scale - numerical value

R_V Viscous resistance

R_{max} Maximum radius

R_{min} Minimum radius

U_∞ Local velocity

V_m Model scale velocity

V_{tan} Tangential velocity

V_{trans} Transferall velocity

ΔR_P Relative difference - Pressure resistance

ΔR_{TN} Relative difference - Total resistance

ΔR_V Relative difference - Viscous resistance

Δt Time Step

Δx Cell size

η_W Propeller Efficiency in Wake

η_C Conditional propulsive efficiency

ν	Kinematic Viscosity
\bar{p}	Mean pressure
\bar{u}_i	Mean local velocity in i direction
$\rho(\frac{\partial \overline{u'_i u'_j}}{\partial x_j})$	Reynolds stress component RANS
ρ	Water Density
σ_0	Cavitation number
h_0	Shaft Immersion
n	Propeller revolution
p_∞	Local pressure
p_a	Atmospheric Pressure
p_s	Pressure Surface
p_v	Vapour Pressure
r	Radial position on propeller blade
t	Thrust deduction
u_i	Local velocity in i direction
u_t	Velocity in x-direction - one single cell

Chapter 1

Introduction

During the last few decades, the demand for new technology within shipbuilding has increased and still is. A large number of vessels have been delivered both to the cruise, research and offshore industry with a purpose to solve complex tasks. This is a result of the industry always striving for better solutions, innovation and reduced costs, which is motivated by different factors. Combining climbing oil prices and strict environmental regulations followed up by the Energy Efficiency Design Index (EEDI), it all points towards improving the performance of the vessel and implicitly minimize the greenhouse gas emissions. Based on this, increasing the propulsive efficiency of a vessel is of major interest. There have been conducted several studies on how the geometry of and appendices in the vicinity of the propeller will influence the thrust performance, e.g. (Kim et al., 2013). Distributed propulsion, meaning many small propellers, have been investigated showing promising results and thus increased total efficiency (Nylund, 2017). Furthermore, the exact location and orientation may also be optimised with respect to the longitudinal position. This is often rather constrained by the shape of the hull and rudder arrangements, but there are possibilities to move the propeller a certain distance. By utilizing Computational Fluid Dynamics (CFD) tools, the flow field in the wake of a hull provides an indicator of what level of optimisation that is possible. This thesis aims to analyse and quantify the order of impact the location of the propulsive disc has on the hydrodynamic efficiency with and without the presence of an energy saving device (ESD). To quantify the level of change in hydrodynamic performance, a vessel with a sufficient amount of research data is chosen. The hull chosen has a central part in the NorSingProp research project, conducted by SINTEF and is a chemical tanker. Figure 1.1 illustrates a similar vessel, designed by ICE Marine Design (ICE Design, 2018).



Figure 1.1: Chemical tanker design by ICE Marine Design (ICE Design, 2018)

The project is still an ongoing process which is why the exact details are confidential. Thus, exact details regarding the vessel geometry will not be discussed. The model has a shape similar to the figure presented above and shall be analysed with NUMECAs FINE/Marine software.

1.1 Environmental Aspects

Ships will have a variety of tasks depending on the ship type, and will, in general, have a significant negative impact on the maritime environment (Andersson et al., 2016). The consequence of the operating vessel is dependent on different parameters, where newer vessels often are categorized as greener. This is a result of classification societies such as DNV GL and Lloyd's is pushing ship owners to comply with stricter rules when it comes to emissions of greenhouse gases. Figure 1.2 illustrates the general picture of how a vessel may have an impact on the marine environment and contribute with emissions to the air. Although the illustration shows several other possible impacts a ship may have on the environment, the two main parts related to propulsion is noise from propeller and emission of greenhouse gases due to fuel consumption.

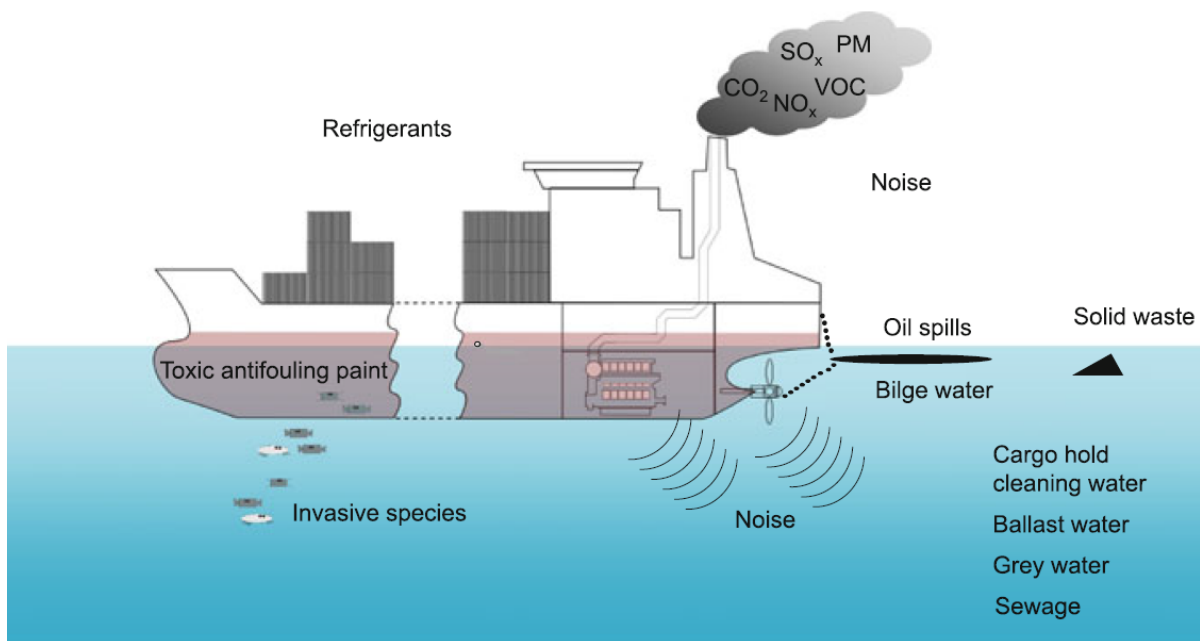


Figure 1.2: Environmental impact of marine vessels (Andersson et al., 2016)

The propulsion system of a vessel consists of an assembly of mechanical parts that produce a hydrodynamic thrust. To overcome the resistance of the ship, the propeller blades are often highly loaded which may generate the phenomena of cavitation. This event will produce intense noise, which is a source of disturbance to marine life. According to J.F. Lindgren (2016), there are four primary concerns due to the effect of elevated levels of anthropogenic noise (Andersson et al., 2016, p.231-232). These are permanent and temporary hearing losses, hindering communication and behaviour changes. Therefore, these issues need to be investigated properly to lower the damage maritime vessels may cause on the marine environment.

The fuel consumption is directly connected with the performance of the vessel and thus coupled with the delivered thrust by the propeller. This is also connected with the level of cavitation and therefore noise and vibratory problems. These challenges are two of many reasons why there is done research on how to increase the efficiency of ship propulsion systems.

1.2 CFD in Wake Field Prediction and Propeller Optimisation

CFD has become a widely used tool in the prediction of the ship wake field and thus highly important to determine the hydrodynamic performance of the propeller. It has over the last years played a significant role in optimising the propeller efficiency by improving the propulsor itself or by analysing how added geometry may increase the efficiency.

(Regener et al., 2018) studied the nominal and effective wake field and how they influence the propeller cavitation performance. The motivation for the research is that propeller designers often have to base their design on the nominal model scale wake. This introduces significant shortcomings to the final design as the total flow regime has not been analysed. A RANS code for the hull and a boundary element method (BEM) for the propeller flow (RANS-BEM coupling) was used to calculate both wake fields. The results show that using the model scale nominal wake field in propeller design leads to significant underprediction with respect to cavitation and pressure pulses compared to the prediction using the full scale effective wake field. Furthermore, the prediction based on a model scale effective wake field performs better on behalf of all parameters. Thus, highlighting the importance of knowing the effective wake in propeller design.

Another study on the same topic investigated the prediction of the effective wake field using a RANS code and an actuator disk model coupled in an iterative process (Sánchez-Caja and Pylkkänen, 2007). The actuator disk is based on an off-design lifting line method not taking into account the geometry of the propeller and about 2 million grid points was used for the numerical simulation. The results are as expected and the authors emphasize the importance of correct prediction of the effective wake field for propeller design. The researchers highlight that nominal wake, effective wake and ship hull geometry are strongly linked and should be taken care of in numerical calculations.

(Xing-Kaeding et al.,) investigated Pre-Swirl devices (PSD) and its life cycle with the use of CFD. The computations were conducted with a RANS code (FreSCo) solving the viscous flow along and aft of the hull combined with a BEM approach solving the propeller action. The number of grid points used in the numerical simulation ranged from 7-10 million and the obtained result was compared with full scale sea trials. Three different pre-swirl stator (PSS) designs were tested. These had the following geometry: four fins with hard tips in total, three on port and one on starboard side. The two others had only three port side fins where one of them had rounded blade tips. The results showed that the PSS consisting of three fins with rounded blade tips introduced the

highest power savings, around 2.8%. However, the PSS containing four fins introduced an increase in propeller performance of 14.5%, but also increased the thrust deduction by 11.0%. Thus resulting in an overall efficiency increase of 1.9%. Xing-Kaeding emphasises two main guidelines for a PSS design based on the result: to produce as much pre-swirl as possible and to moderate the increase in thrust deduction. Furthermore, the final result of the numerical simulations was compared with the sea trials. These indicated that the obtained CFD results are of conservative nature. Combined with the fact that CFD computations have a relatively low cost and obtains results in a relatively short time window, it is encouraged to use simulations in future power predictions.

Studies were made on the effect of about 70 variants of PSS' with a combination of the RANS code STAR-CCM+ and propeller analysis software AKPA (Krasilnikov et al., 2019). Both numerical computation and experimental testing were conducted and compared where the final PSS design in the propulsion test is presented in Figure 1.3. The final design resulted in almost 4% power savings on a chemical tanker and showed good agreement with experimental data. This study is conducted with equal hull and PSS variant as the one used in the current research and will frequently be used to compare and validate the obtained results.



Figure 1.3: Propulsion test setup with designed PSS (Krasilnikov et al., 2019).

Propeller Optimisation Trends

(Hollenbach and Reinholz, 2011) presented a paper investigating the trends in optimisation of propulsion. More complex methods such as optimising the hull form with respect to "off-design" condition and optimising twin screw appendages were summarised and discussed with respect to the design process and savings. However, no predicted reduction was specified due to the complexity each vessel introduce to the optimisation process. Furthermore, more specific cases were presented covering ESD's added in the vicinity of the propulsive disk. A sum up of some of the findings together with the respective developer obtained from the devices is presented in Table 1.1.

The presented results indicate that significant savings may be obtained by implementations in newbuildings and retrofitting existing vessels with such devices. It also emphasises the fact that further investigation of ESD's is an important topic.

Improvement	Comments	Developer	Gain in Power
PSS	Fins upstream of propeller. Generates pre-swirl to propeller.	DSME	1% - 6.3%
Thrust Fin	Fins aft of propeller on rudder.	HHI	4.9%
Post Stator	X-shaped fins aft of propeller. Reduces propeller hub vortices.	SHI	4.9%
Safer Fins	Vortex generator fins upstream improving inflow to propeller.	SHI	3.2%
Pre-Swirl Duct	Wake equalising duct with an integrated pre-swirl fin system.	MSH & BMS	3% - 9%

Table 1.1: Propeller Optimisation Trends (Hollenbach and Reinholz, 2011). Reduction presented is predicted by CFD and experimental testing. Multiple vessel types has been tested with a device if a percentage range is presented. Developers are: *Daewoo Shipbuilding & Marine Engineering (DSME)*, *Hyundai Heavy Industries (HHI)*, *Samsung Heavy Industries (SHI)*, *Mewis Ship Hydrodynamics (MSH)* and *Becker Marine Systems (BMS)*

1.3 Retrofitting of Existing Vessel

According to DNV GL there are four areas of retrofit that frequently yield the best return on investment. These include changing the bow shape, improving engines and auxiliary systems, propeller optimisation and ESD's and other appendages (DNV GL, 2018a). The two latter are of main interest due to the scope of the thesis. DNV GL presented in 2015 a study upon the energy management of the shipping industry (DNV GL, 2015). 31% of the ship owners replied that they had implemented propulsion retrofitting, thus increasing the efficiency of the ship propulsion system compared with the original set-up

at delivery of vessel. Furthermore, an additional 14% planned the same retrofit operation to be implemented during 2015. Figure 1.4 illustrates the applicability for (a) exchange of propeller and (b) implementation of ESD's on different types of vessels. It is seen that for tankers and bulk carriers the most suitable retrofit is implementation of ESD or appendages. It is also suitable for older vessels. Thus arguing that implementation of ESD is the most suitable solution for a wider range of ships while disregarding investment scope and payback time. Propeller exchange will not be discussed.

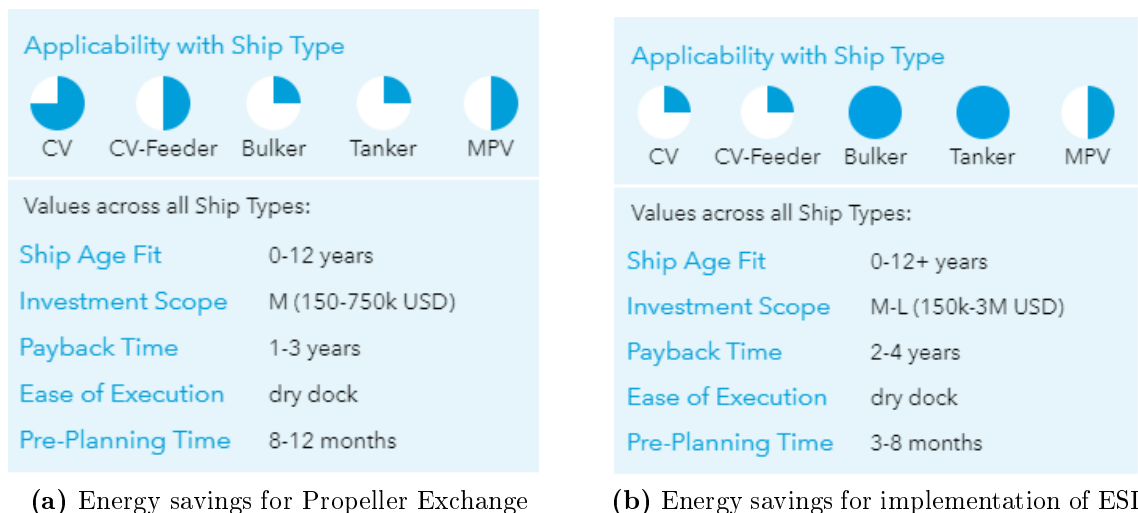


Figure 1.4: Energy savings on retrofitting of vessels (DNV GL, 2019)

1.3.1 Classification Standards and Rules

According to (Deinboll, 2019) there exists no prescriptive rules and standards made by DNV GL regarding PSD's, see Appendix B.2 for correspondence. It is stated that it has been discovered difficulties in defining design loads for such devices. This is supported by the fact that it has been reported that PSS' tends to fall of after a while in operation. This points towards unexpected dynamic loads resulting in fatigue failure. Therefore, such devices should be dimensioned accordingly to sustain significant hydrodynamic loads while serving its purpose.

Considering the propeller location, the classification society DNV GL does not have any clear guidelines nor constraints regarding the exact location of the rotative disc (Deinboll, 2019). However there are some important parameters to investigate before any changes are done, both with new and existing vessels. Deinboll highlights that moving the propeller in retrospect is not something that is desirable, due to it being costly and highly time consuming as the whole aft often has to be rebuilt. (Rognebakke, 2019) on the other hand highlights the importance of difference in bearing and shaft forces and moments when the propeller is moved in any direction. This has to be in accordance with the rules and standards by DNV GL. See Appendix B.1 for correspondence with DNV GL.

The rules and standards for rotating machinery given by DNV GL, “PT.4 CH.2 ROTATING MACHINERY, GENERAL”, on calculations directed towards shaft alignment presents guidelines that must be fulfilled before the vessel can enter operation (DNV GL, 2018c). In 2.1.2 through 2.1.4 the alignment conditions and influencing parameters for the shaft and bearings is highlighted with a demand of thorough calculations regarding reaction loads and pressure forces. Rognebakke (2019) emphasizes that noise and vibrations also has to be investigated if the vessel has a comfort class notation.

The noise and vibrations is often connected with structural damage in terms of fatigue. It is therefore important to conduct a thorough structural assessment in installation of such appendages. The assessment must consist of fatigue and ultimate strength analysis where the necessary safety factors must comply with specified recommendations from class societies, e.g. DNV GL “FATIGUE ASSESSMENT OF SHIP STRUCTURES” (DNV GL, 2018b).

There is not any prescriptive rules and standards towards the installation of PSD’s nor constraints with respect to moving the propeller in the longitudinal direction. As described, normal procedure with respect to loads on the shaft and bearings and investigation of noise and vibrations has to be followed according to class notation.

1.4 Objective

The objective of this thesis was to perform a thorough study on the effect of the longitudinal propeller location on its hydrodynamic performance and maximise power savings. The study consists of a literature research on the current state of knowledge around the topic and influencing parameters. A wide range of numerical CFD simulations was planned to be conducted in the CFD software FINE/Marine. Calm water analysis of a chemical tanker was planned to be performed with a naked hull, thus without the presence of the propeller. The goal of the research was to calculate the wake field at different possible positions for the propeller and analyse how these profiles affect the propeller efficiency and cavitation occurrence. To quantify how the propeller performs at the different positions, with regard to the respective parameters, the potential flow propeller code AKPA was utilised. Including this, the effect of a (PSS) was investigated by introducing the PSS geometry in the CFD simulations and analysed in AKPA. The effect of conducting the simulations without the free-surface was also investigated.

Post to the simulations described above, further optimisation of the PSS was performed. This includes adjustment of the geometry of the PSS and was conducted in accordance with the propeller location problem. Moreover, an online or offline coupling of the propeller analysis software AKPA and the CFD software FINE/Marine was encouraged to be envisaged. The online solution shall run the whole simulation in both programs and iteratively find an optimal position for the propeller. Clear guidelines and recommendations are presented with respect to the positioning of the propeller. These includes the recommendations made by classification societies with respect to adjusted geometries, relocation of the propeller and structural assessment.

Chapter 2

Propeller Inflow Characteristics

The propeller is working in a complex fluid flow, referred to as the wake field. In this environment the propulsion system is subject to varying velocities. These velocities is directly connected to fluctuating pressure forces, which may result in cavitation. Thus resulting in vibrations and noise, which are reasons for discomfort on board vessels and disturbance of the marine habitat. As the propeller is the part of the vessel that provokes these problems, it is important to understand and still look for solutions to improve its hydrodynamic performance. To do so, it is possible to look into the location of the rotative disc and determine if entities such as thrust and torque may be optimised by moving the propeller a certain distance. In addition, introducing an ESD at the aft of the hull may change the fluid regime seen by the propeller and indicate an entirely different propeller position. This chapter aims to discuss the inflow characteristics with respect to the hydrodynamic performance of the propeller. It includes the optimal inflow regime, the cavitation phenomenon, ESD's and finally how the location of propeller may influence this.

2.1 Optimal Propeller Inflow

The propeller geometry is designed for a specific inflow to deliver a desired thrust with as high efficiency as possible. To achieve these terms, the fluid inflow structure to the propeller is the most important parameter and will directly affect the hydrodynamic performance of the propulsion system, e.g. thrust, torque, efficiency and occurrence of cavitation. By considering these parameters it all comes down to how the fluid regime behaves at the rotative disc location, where a smooth and homogeneous inflow is desired in the design process of a propeller (Sivertsgård, 2018). Thus, the nominal wake field should have a smooth velocity transition in the radial distance going from the boss to the tip of the propeller blade combined with a small relative difference between maximum and minimum velocity.

The reason why velocity differences is undesirable is due to the fact that such variations may contribute to significant pressure differences and thus cavitation inception. Figure 2.1 illustrates both an axial contour plot and a velocity plot of one single radial position extracted from $r/R = 0.68$ in the axial contour. The plot is argued to be rather smooth and homogeneous due to no significant abrupt change in velocity seen in the contour plot in (a). However, in the radial plot (b), it is seen a relative difference of 0.5 in the

velocity ratio, which implies occurrence of pressure differences.

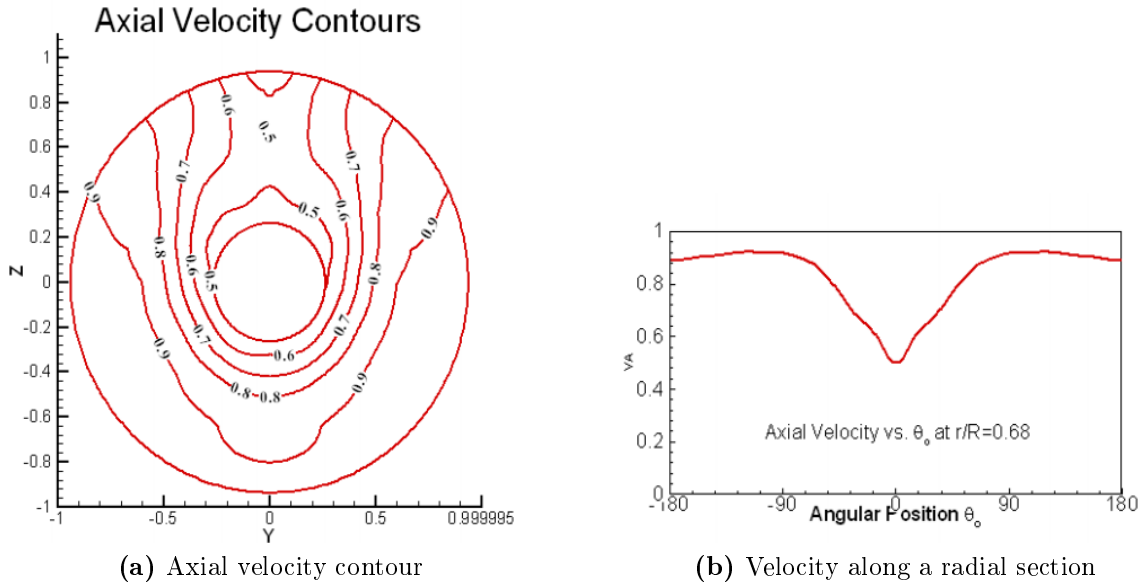
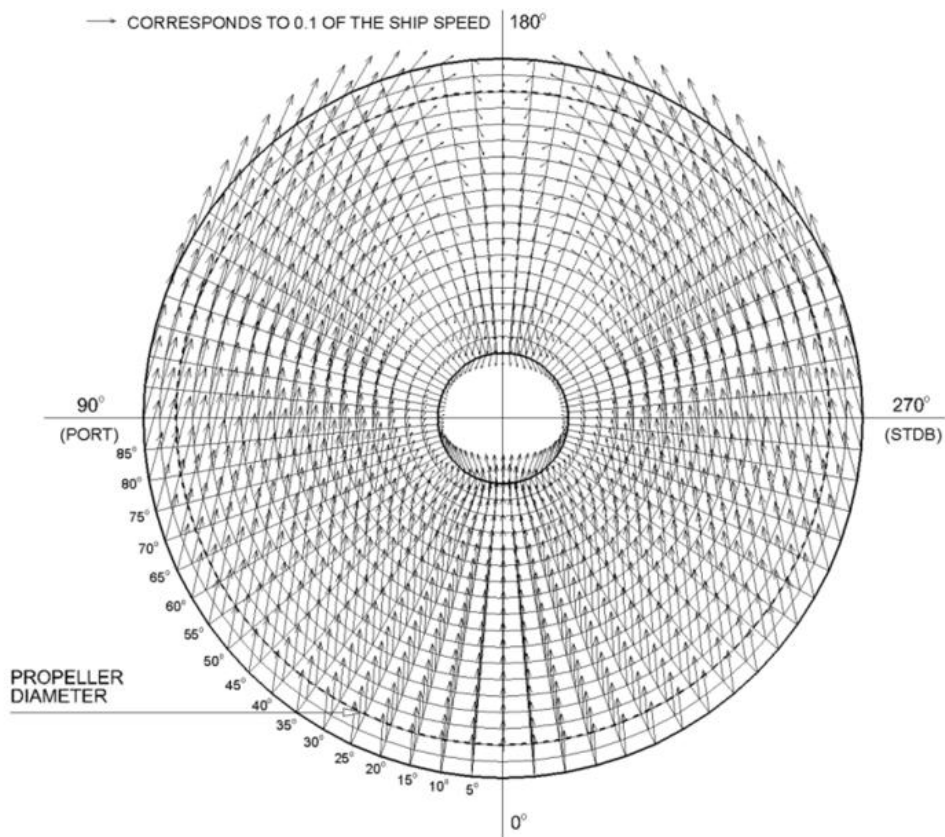


Figure 2.1: Nominal wake for a single screw vessel (Kerwin, 2001, p.149)

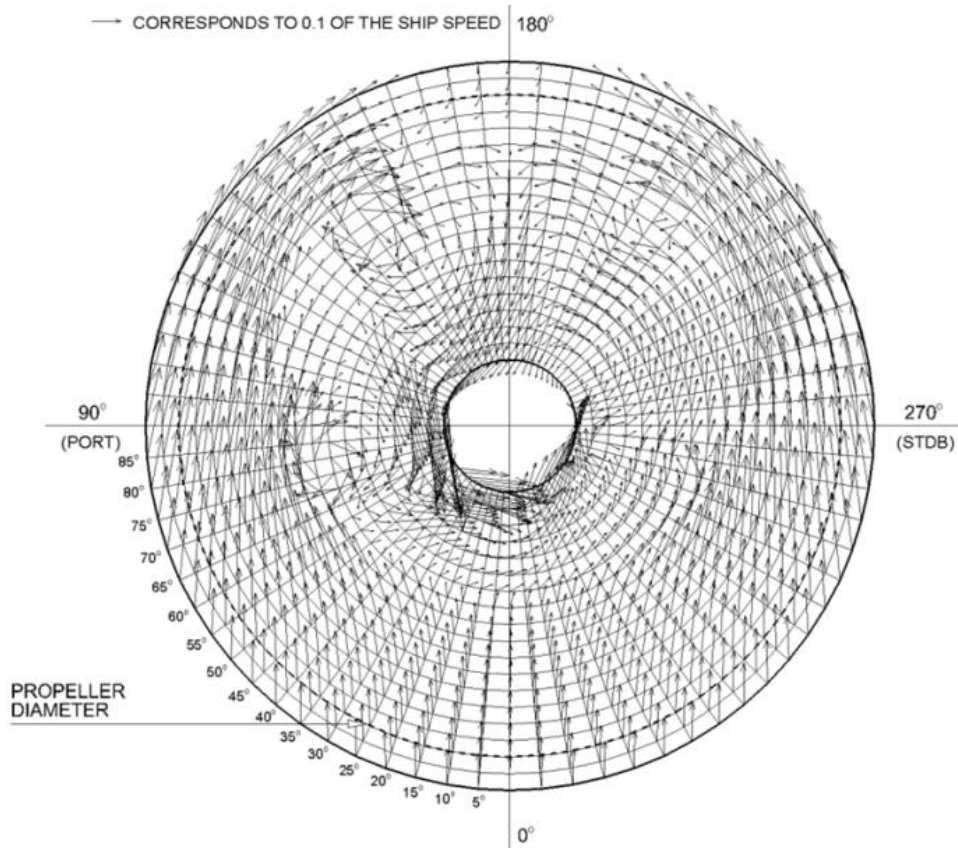
Another way of analysing the wake fields occurrence is the transverse velocity components. These will indicate the direction of the flow in the propeller plane, and contains valuable information regarding the performance of the propeller blades. In Figure 2.2 two transverse nominal wakes are presented for the same hull without (a) and with (b) ESD, and are collected from an ESD study (Dang et al., 2012). The hull without the presence of a ESD has a distinct pattern with the port side velocity field rotating slightly in the clockwise direction and the starboard side in the counter clockwise direction. This will introduce differences in the local velocity over the propeller blade where starboard side will have a higher local velocity than the port side. It should be mentioned this holds for a clockwise rotating propeller disc.

Furthermore, studying the influence of the ESD in (b) the resulting velocity profile is changed due to the presence of the added geometry. On the positive side, some portions of the flow field in the fourth quadrant has been manipulated to meet the clockwise direction of the rotating propeller. This may result in higher thrust and making it easier to predict the hydrodynamic performance. On the other hand the ESD introduces vortices at 90° , 145° and 215° . As vortices are chaotic and fluctuating this may result in unwanted pressure pulses leading to cavitation inception and thus vibrations and noise. Considering these examples it is safe to say that an optimal inflow to the propeller disc is hard to achieve and the design of an ESD is highly dependent on the desired hydrodynamic performance.

Looking from a propellers point of view, the most suitable wake flow regime is rather homogeneous, has no critical vortices and no abrupt changes in velocity. By tuning the ESD device and propeller blades, it is possible to control these parameters and achieve the desired result. However, in most cases a compromise has to be made.



(a) Transverse nominal wake, w/o ESD



(b) Transverse nominal wake, with ESD

Figure 2.2: Transverse nominal wake w/o and with ESD (Dang et al., 2012)

2.1.1 Presence of the Propeller - Effective Wake

The effective wake field is a result of the propeller interacting with the hull and thus introducing a different velocity field than given by the nominal wake. This is a highly complicated interaction where the flow at the propeller location consist of three components: flow resulting from the naked hull without the presence of the propeller (nominal wake), propeller induced velocities and the interaction between the two flow regimes (Sánchez-Caja and Pylkkänen, 2007). From the propeller design point of view, the effective wake field is the most important parameter as it is used as input for analysis and design procedures. The effective velocity field may be defined as given in Equation (2.1) or (2.2) (Carlton, 2012).

$$\text{effective velocity} = \text{nominal velocity} + \text{interaction velocity} \quad (2.1)$$

$$\text{effective velocity} = \text{total velocity} - \text{propeller induced velocity} \quad (2.2)$$

The latter is the most time consuming procedure as an iterative process is needed to calculate the effective velocity field. This however can only be done if the total velocity field is known just ahead of the propeller. The procedure starts by estimating an effective wake which is used to predict the propeller induced velocities. By subtracting this from the total velocity, the effective velocity is obtained. This is repeated until convergence is achieved (Carlton, 2012, p.74). Although it has been proven to converge the method is known to have shortcomings leading to incorrect assessment of the interacting velocities. The alternative procedure, presented in Equation (2.1), uses the nominal wake field as an input together with an actuator disk theory to predict the effective wake. Nominal wake may be obtained by experimental testing in a towing tank or by numerical calculations only considering the hull without the presence of the propeller. This procedure is considerably easier than the one presented in Equation (2.2), as the measurement of the total velocity field includes the presence of the working propeller.

Traditionally, the effective wake has been predicted by model scale tests and presented as an average volumetric quantity. However, RANS codes combined with potential methods, often represented by an actuator disk, is nowadays widely used for the same tasks and obtains satisfying results. The effective wake may therefore be presented with high accuracy along all angle and radial positions of the propeller blade by combining such methods. The numerical results is however highly dependent on the grid procedure and the available computational power.

By quantification of the effective wake in an accurate manner will strengthen the design procedure so that phenomena such as cavitation may be predicted more accurate. In addition, an impelling calculation of the effective wake may increase the accuracy in design procedures of ESD's. By doing so, the fluid inflow to the propeller may be tuned to fit the blade geometry so that the efficiency increases and less power is needed.

2.2 Propeller Cavitation

Cavitation is a complex phenomena which appears in high velocity flows wherein local absolute pressure drops to the vicinity of the vapour pressure of the fluid (Breslin and Andersen, 1996). For working propellers, the local velocity over the length of the blade often is of magnitudes that correlate to such pressure levels. The phenomenon is also highly important as it introduces damages to the metal blade, such as erosion and pitting. Therefore, the effective wake field that develops at the rotative disc location has a significant impact on propeller design and analysis.

To be able to determine the probability of cavitation some parameters of the fluid needs to be known. These are viscosity, density and vapour pressure and is highly dependent on the temperature of the fluid. Even though theory states that cavitation has a distinct limit being the vapour pressure, it has been observed at levels both above and below this pressure limit. This has been connected with other important parameters and Savio (2011) highlights that there are three main parts that increases the complexity in predicting of cavitation (Savio, 2011). These are presented below.

- Purity of water
- Suitable region extension
- Turbulence

The purity of the water is connected with the presence of a nuclei, also referred to as micro-bubbles. For a nuclei to be present, a work needs to be done for it to be created. Thus, these disturbances reduces the work that is needed to be done and therefore serves as a starting point for bigger vapour bubbles to grow. The second part states that a bubble needs sufficient time to develop. Therefore, given the velocity of the fluid, a certain length of the body must fall under vapour pressure. The third statement connects with the complexity and unsteadiness of the phenomena, due to most flow regimes are of turbulent nature. Although these parameters are important to consider in cavitation studies, the complexity is high. Thus, to easily quantify the plausibility of cavitation, the cavitation number is calculated using Equation (2.3). The cavitation inception criterion is given by Equation (2.4)

$$\sigma_0 = \frac{P_\infty - P_v}{\frac{1}{2}\rho U_\infty^2} \quad (2.3)$$

$$\sigma_0 \leq -(C_P) \quad (2.4)$$

Considering the nature of the phenomena it is impossible to predict exactly at which point a propeller will cavitate or not. However, by knowing the effective wake field and thus the pressure gradients it is possible to design a conservative propeller which is defiant to such disturbances.

2.3 Energy Saving Devices

Ship propulsion systems are complex structures with a significant cost to develop and manufacture, and the most optimal propeller geometry for a given inflow structure is desirable. However, it is nearly impossible to get a perfect result. Therefore, ESD has been introduced to the propeller geometry and in the vicinity of the rotative disc. (Hollenbach and Reinholz, 2011) defined ESD's to target improvements in the propulsion efficiency by recovering losses from the propeller slipstream or improvements in the water flow to the propeller allowing higher efficiency. Such devices are often implemented in retrofit and upgrade solutions and is connected with low-cost and improvement in the range of 2-9% (Babiczy, 2008). Thus, compared with complete renewal of a propulsion system, ESD's is the preferred solution in gaining power.

Propulsion improving devices (PID) are appendices fastened either to the ship structure or to the propeller geometry. It is defined as a stationary flow-directing device made to improve the hydrodynamic efficiency and thus lower the fuel consumption of the vessel. (Hollenbach and Reinholz, 2011) also studied the effect of different types of ESD's. The findings in the research pointed towards that the gain in power due to such devices may be as high as 6.3% for a PSS. Some of the findings for different vessel types is presented in Table 2.1 where all numbers is extracted for design draught.

<i>Ship type</i>	<i>Gain in Power</i>
ConRo Vessel	3.7%
Bulk Carrier	6.3%
16,000 TEU	3.8%
VLCC	5.6%

Table 2.1: Pre-Swirl Stator savings (Hollenbach and Reinholz, 2011)

2.3.1 Pre-Swirl Stator

Zondervan describes the PSS combined with a main propeller as the “poor man’s contra-rotating propeller”, due to this solution being cheap, effective and easy to apply in ship propulsion (Zondervan et al., 2011). Furthermore, from a hydrodynamic point of view there is little difference between this solution and a fully functional contra-rotating propeller.

The principle of a PSS is to recover rotational losses that are present at the propeller. This is done by decrease the rotational kinetic energy losses which increases the axial kinetic energy, momentum flux and thus thrust (van Terwisga, 2013). The flow is manipulated by introducing a swirling flow in the opposite direction of the rotation of the propeller. Thus, cancelling out the swirl that is produced by the presence of the propeller and at the same time increase the relative tangential velocity of the propeller blades (Breslin and Andersen, 1996, p.467-468). This will result in less fuel consumption to sustain the same thrust and forward speed of the vessel. Figure 2.3 illustrates how the PSS modifies the propagating flow to fit the propeller motion. The figure is Wärtsilä’s own PSS referred to as EnergoFlow (Wärtsilä, 2017). It is stated that by installing this design, the fuel consumptions may be cut by up to 10% for bulk carriers and provides a quick return on investment, typically one to two years.

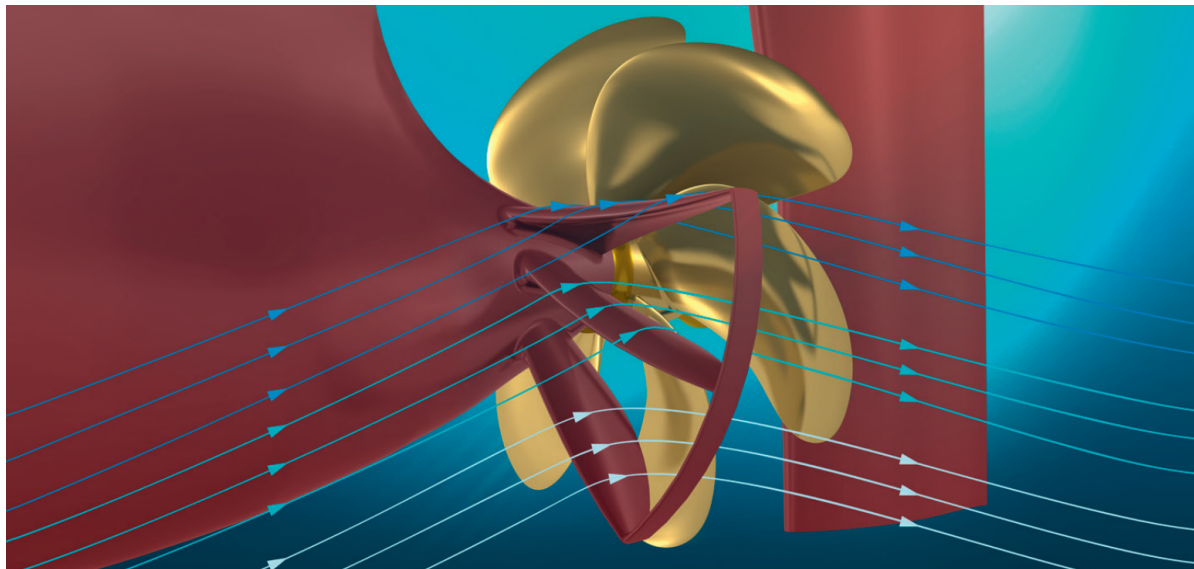


Figure 2.3: EnergoFlow Pre-Swirl Stator (Wärtsilä, 2017)

Daewoo Shipbuilding & Marine Engineering (DSME) has been manufacturing PSS systems for over a decade and claims that reduction in cavitation and fuel savings of 4-6% is expected by installing such systems (Gougoulidis and Vasileiadis, 2015). In their systems, for a right-hand rotating propeller there is usually installed three blades on the port side to reducing the slip-losses and one on the starboard side to increase the wake fraction. This also results in increased hull efficiency and less cavitation risk. On the other hand, increased thrust results in higher required torque.

Even though the main task for a PSS is to produce pre-swirl and thus recover the tangential flow energy it is crucial to investigate the whole flow picture with respect to savings. A design that produces less pre-swirl and therefore recovering less energy compared to other PSS designs may in fact have a higher power saving. This was seen in Krasilnikov's study comparing three different PSS designs (Krasilnikov et al., 2019), where the reason for the savings was a small reduction in axial wake at the PSS producing less pre-swirl. Such findings points out that small adjustments may improve the propeller performance and specifies the importance of thorough studies on the topic.

2.4 Location of the Propeller

The wake field will be highly dependent on the position of the propeller in the longitudinal direction. As the no-slip condition is valid at the surface of any geometry moving through a viscous fluid, there will be created a wake field near the body due to separation (Sivertsgård, 2018). Thus, arguing that moving the propeller further away from the geometrical obstacles the flow will become steadier and increasingly more homogeneous. Looking into the simple CFD computations conducted in the project thesis of Sivertsgård (2018) and comparing the positions of the rotative disc, the obtained results indicate that the propeller should be placed furthest downstream. On the other hand, the results presented were based on rather coarse numerical computations only taking into account the nominal wake from the naked hull.

Therefore, by conducting a thorough CFD analysis and looking into how the effective wake pattern develops at the evaluated positions may substantiate the presented research or indicate a different situation for the propeller. Taking into account cavitation pattern and the presence of a PSS upstream of the propeller the flow pattern may be entirely different. Thus, the location of the rotative disc may play a significant role in how the propeller works with respect to thrust, torque, efficiency and thus the power required to keep the vessel moving at constant speed. To substantiate how the fluid regime deviates moving further downstream an illustration of the streamlines around the PSS and aft of the vessel is presented in Figure 2.4. The magnitude of the relative velocity and direction of the flow is changing rapidly in the vicinity of the PSS, thus swirling around the hub.

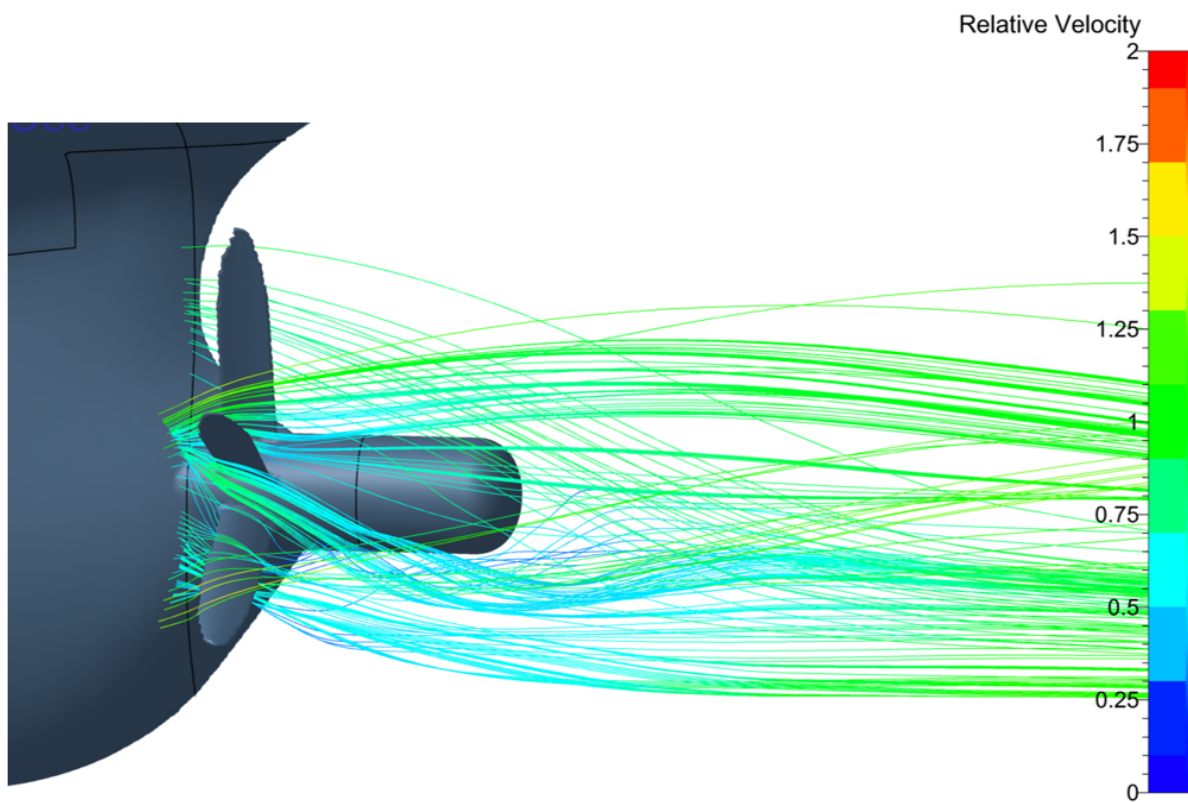


Figure 2.4: Streamlines aft of vessel

Chapter 3

Pre-Swirl Stator Optimisation

A PSS is added a short distance upstream of the rotative disc to manipulate the flow to fit the propeller action. The working principle of this device is discussed in Section 2.3. In the NorSingProp project and the testing conducted by SINTEF, a PSS consisting of three fins has been added to the geometry upstream on the port side of the vessel. This geometry is equal to the one in the current thesis. The angular position between the three blades is given in the research paper presented by (Krasilnikov et al., 2019), in Table 3.2 and is further discussed Section 3.2. During the testing, neither the geometry nor the direction of the fins have been adjusted and thus been held constant. By changing the pitch angle, thus angle of attack (AoA), and the angular position of the fins, the inflow to the propeller may change entirely and affect the most optimal position of the rotative disc in the longitudinal position. This chapter introduces how these changes are applied to further optimise the inflow to the rotative disc.

3.1 Stator Pitch Angle

By adjusting the pitch angle of the PSS blades the flow field seen by the propeller may look significantly different and could result in better hydrodynamic performance. With regard to the scope of this thesis, such adjustment may give an entirely different propagating wake flow and therefore indicate other plausible locations for the rotative disc. (Kim et al., 2013) made a study on hydrodynamic optimisation of PSS's with the help of CFD and model testing. The angle of attack on the inflow to the propeller generated by the PSS blades was one of the topics that were investigated. According to this research, gain in propulsion efficiency is often explained by the increase in the angle of attack of the inflow on the propeller generated by the presence of the PSS. By adjusting the pitch angle of the PSS blades, the flow seen by the propeller may have a more optimum angle directed towards the rotative disc resulting in higher efficiency. On the other hand, this may also result in higher resistance due to drag, cavitation due to higher velocities over the blade section and different dynamic loading due to the flow field.

The PSS blades are rotated about its own axis, going along the length of the fin. Figure 3.1 illustrates how the blade section of the fins is adjusted seen from the root of the blade. The dotted lines in purple colour illustrate the original position and green is the adjusted blade section. It should be mentioned that the adjusted pitch angle of the PSS blades, also referred to as stator blades, in this figure is exaggerated for illustrative

matter. Table 3.1 presents the change in pitch angle for the two different cases.

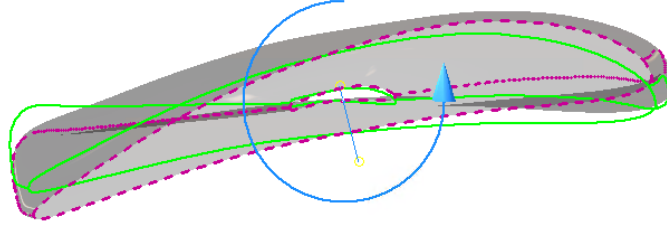


Figure 3.1: Adjustment of Pitch Angle - Positive direction counter clockwise

(Kim et al., 2013) adjusted the pitch angle of the blades with an increment of 4° in the range -8° to 8° . The obtained calculations showed varying results with a small and almost negligible relative difference. However, the plots presented in the paper clearly marked the optimum pitch angle range, indicating the importance of investigating the topic.

	Case 1	Case 2
AoA	-1°	$+1^\circ$

Table 3.1: Adjustment of Pitch Angle

3.2 Angular Position of Stator

The angular position of the stator has an effect on the inflow to the propeller in the same order as the pitch angle. To quantify the effect on the propagating wake flow and thus the choice of propeller location, the angular position is set to vary according to the three adjustments presented in Table 3.3. Upper, middle and lower fin corresponds to 1, 2 and 3 and α , β and ψ , respectively. Figure 3.2 illustrates how the blades are rotated to adjust the angular position. The adjustment is relative to the original angular orientation given in Table 3.2.

Stator fin number	1	2	3
Angle ($^\circ$)	68°	23°	-22.5°

Table 3.2: Original angular position PSS. Angle is defined from the y-axis (Krasilnikov et al., 2019).

The figure illustrates the y-axis which is the reference line of the rotation. The y-axis is the reference for 0° , and the blades are rotated about the x-axis. The outer line illustrates the rotative diameter.

	Adjustment angle	Adjustment 1	Adjustment 2	Adjustment 3
Upper fin (1)	α	-2.5°	-5°	0°
Middle fin (2)	β	0°	0°	$+2.5^\circ$
Lower fin (3)	ψ	$+2.5^\circ$	$+5^\circ$	$+2.5^\circ$

Table 3.3: Adjustment angular position of PSS. Numbering and angles correspond to Figure 3.2.

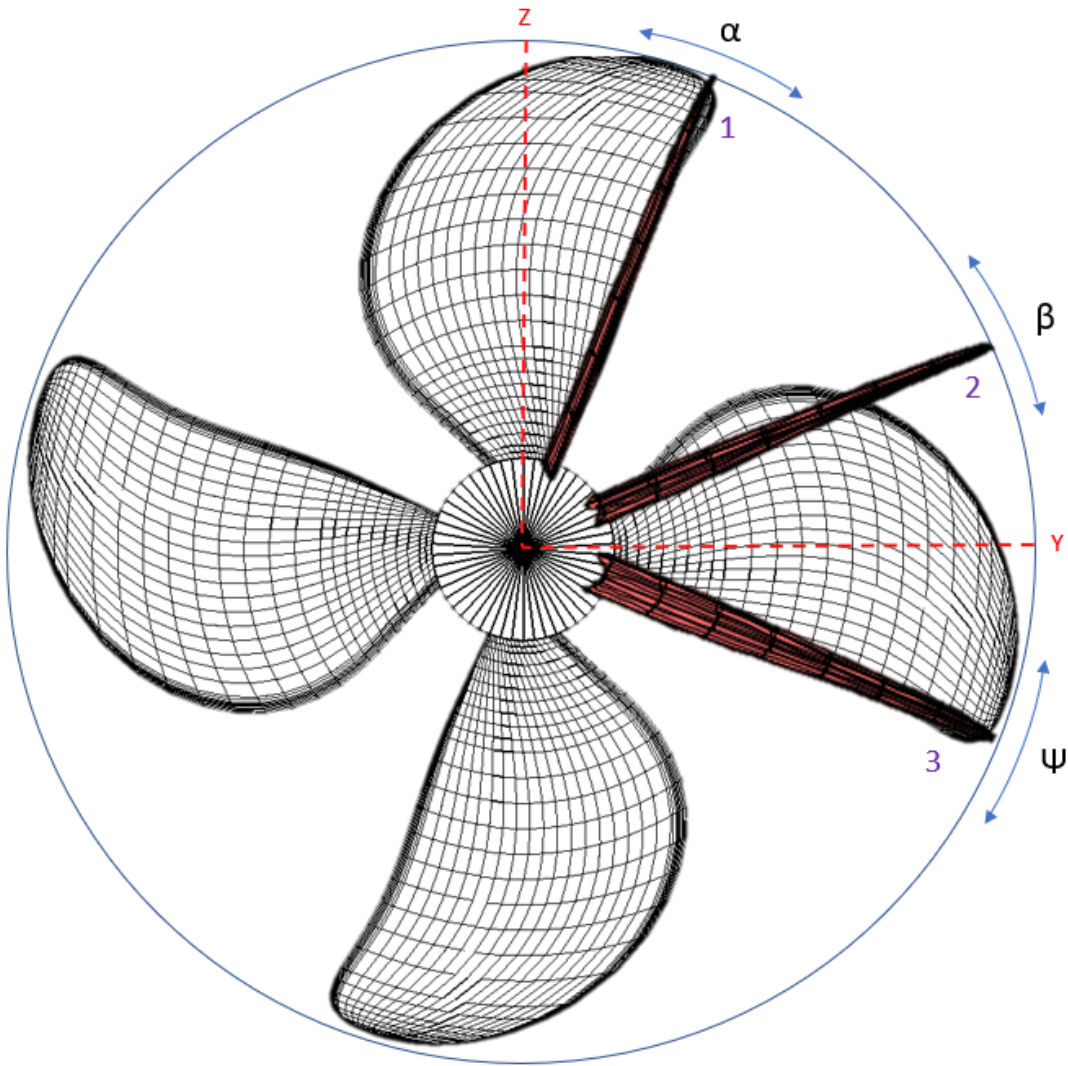


Figure 3.2: Adjustment angular position - Positive direction counter clockwise

3.3 Diameter of Stator Blade

The stator blade diameter may have an impact on the efficiency delivered by the PSS. (Kim et al., 2013) made a study on hydrodynamic optimisation of PSS looking into the diameter of the stator blades. The study indicated that the most optimal blade diameter is equal to the propeller size. The blade diameter was increased and decreased by 10% where larger diameter had a negative effect originating from the increased resistance. Decreasing the diameter may result in unfavourable tip vortices from the blades, which may result in cavitation inception. Figure 3.3 illustrates the case having an equal diameter of PSS and propeller.

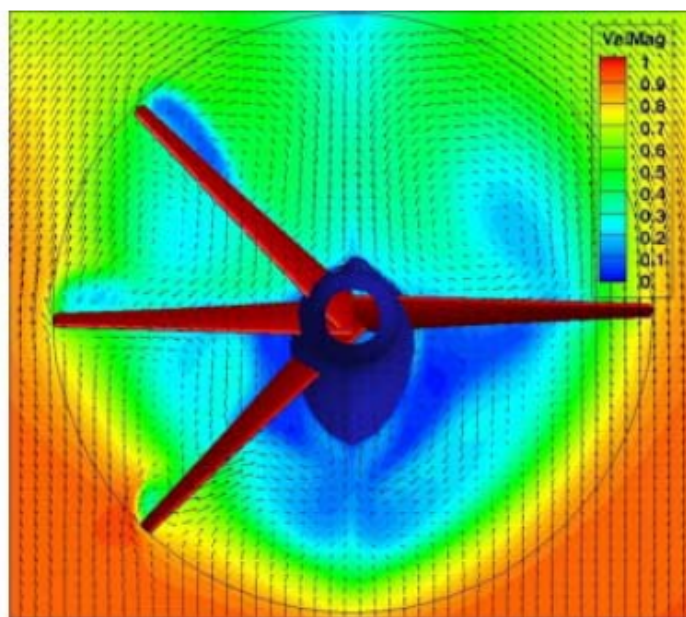


Figure 3.3: Stator blade diameter (Kim et al., 2013)

3.4 Structural Optimisation

The PSS experiences highly fluctuating hydrodynamic loads and according to (Voermans, 2019) the loads that are induced due to ship motion are highly relevant for fatigue lifetime. These loads are often connected with additional induced lift resulting from motions as pitch and roll. There are indicated loads with higher significance such as slamming, occurring when parts of the PSS has emerged above the free surface or loads that are induced during a hard ship manoeuvre. According to the research, slamming events, turning circle and crash stop resulted in significant off-design loads. This implies that a structural assessment of PSS devices is of importance and should be done thoroughly.

3.5 Difficulties with PSS Optimisation

Introduction of PSS blades near the propeller may result in increased drag and therefore not be favourable to install. According to (Kim et al., 2013) the increased resistance by adding a PSS with three blades was smaller than 0.6%. This may increase if the pitch angle of the blade is adjusted. A change in the angle of attack will result in a difference in the local velocity over the blade section, which may result in cavitation inception and pressure pulses on the structure. Also by changing the angular position of the blades, there may arise pressure differences in between the blades as the distance between them may be varied. Thus, as discussed by (Voermans, 2019), a fatigue assessment is most suitable for normal working conditions regarding the strength of the PSS.

Chapter 4

Software

To investigate the propagating ship wake field and to quantify the hydrodynamic differences that may be introduced by moving the propeller upstream or downstream of the original location two different software packages are utilized. The programs used are FINE/Marine and AKPA corresponding to full range CFD code and a narrow propeller analysis code, respectively. In this chapter the two different software and their working method are introduced. In the end, a discussion of how to couple them in an automatic process is included.

4.1 FINE/Marine

FINE/Marine is a CFD program utilizing the ISIS-CFD flow solver to evaluate turbulence flow regimes with RANS equations, further discussed in Section 4.1.2. NUMECA describes their software as: “An integrated CFD software environment for the simulation of mono-fluid and multi-fluid flows around any kind of ships, boats or yachts, including various types of appendages” (NUMECA, 2018a).

The software has a wide range of usage areas and has been utilized both commercially and in research by several universities. In 2011 (Guo et al., 2012) conducted a seakeeping simulation in head sea waves for the known KVLCC2 geometry. The software was used among others to analyse the wake field where the obtained numerical results had good accuracy. The program has been used in prediction of bank wall effects for a ship at different depths (Van Hoydonck et al., 2015) and to investigate how a damaged hull with flooded tanks would behave with respect to resistance (Bašić et al., 2017). For both research topics the results were satisfying.

4.1.1 Domain and Grid

To fully resolve the flow regime it has to be discretised into a numerical system of partial differential equations (PDE) (Thompson et al., 1998). The collection of all these PDE's is called the grid of the domain, also referred to as the mesh. The grid generation is essential for all types of CFD flow solvers on the market and there exist different ways to construct it. The two main categories of grids are structured and unstructured. The difference between the two is how they are addressed, where structured grids follow a uniform pattern that consists of hexahedral elements (quads in 2D). Unstructured mesh, which is used in the FM software, does not follow a uniform pattern and can consist of

tetrahedron, hexahedron and prism cell shapes as presented in Figure 4.1. FM however only uses hexahedral elements in their grid generator. The number of cells and the

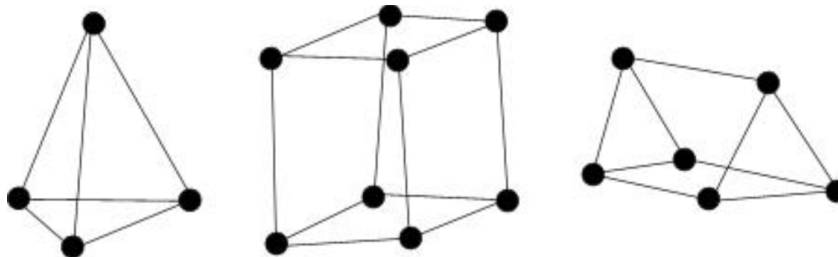


Figure 4.1: Tetrahedron, Hexahedron and Prism cell, respectively (Innovative-CFD, 2018)

domain size will directly influence the outcome of a numerical simulation. If the number of cells are too few it may result in inaccurate results. This also holds for the domain size. However, this often depends on the boundary conditions applied. Convergence studies are often made to identify and overcome such problems.

This demands a structured approach and is highly time consuming. In Gou's article from 2011, they analysed the seakeeping of a KVLCC2 in head sea waves with four different mesh sizes ranging from 0.35 million to 2.3 million cells (Guo et al., 2012). These were then compared with experimental results and the total resistance indicated a converging tendency. The course grid had a relative error of 9.26% and the finest an error of 2.6%. Measurements for pitch pointed towards the same conclusion. However, the heave motion gave unexpected results but was justified by the explanation of a relatively small absolute error. Also, the influence of small bias error could have largely affected the results. This indicates that increasing the number of cells will give a more accurate result. However, it has to be carefully evaluated by looking at the location and density of the cells.

Furthermore, there are several other parameters that must be carefully evaluated in a mesh study. Amongst one of them is the orthogonality of the various cells, where this can adversely affect solution accuracy and robustness (Devals et al., 2016). FM uses empirical methods and recommends that the minimal orthogonality to be higher than 5° to obtain satisfying results and low skewness (NUMECA, 2019). Devals also suggests that the distance of the first near wall point (Y^+ value) and mesh distance expansion factor should be taken into account.

The researchers emphasizes that the first near wall point must be controlled and kept in the range 30-300, using wall function (Devals et al., 2016). Mesh expansion factor defines at which rate the elements is increasing in size going from the wall and into the fluid, referred to as stretching ration in FM. It significantly increases the number of cells in the domain if the value is close to 1, and the recommended size for accurate results is 1.15 and not greater than 1.25.

Adaptive Grid Refinement

The adaptive grid refinement is an optional parameter that may be activated through the numerical simulation (NUMECA, 2019). It is an iterative process where the mesh is dynamically adapted to the requirements set by the user as the computation is on-going. This mesh adaptation may instantly insert fine cells where they are needed, making it a powerful tool for unsteady calculations such as wake flows and boundary layers. The refinement is cell-based, meaning that the existing cells are subdivided to create a finer local mesh. Thus, equal to normal refinement procedure. The adaptive control is highly dependent on the refinement criteria and the flow at the aft of the hull, pressure and velocity gradient criteria is suitable. These may be set so that the increase or decrease is lower than a given value, correcting abrupt changes that may be present in the solution. An example of such unwanted changes in a pressure contour plot is presented in Figure 4.2. The figure is collected from a simple unsteady flow simulation of a diamond square structure conducted in a prior course *Numerical Methods in Hydrodynamics* unaffiliated with the thesis. It should be mentioned that the figure is only for illustrative purposes.

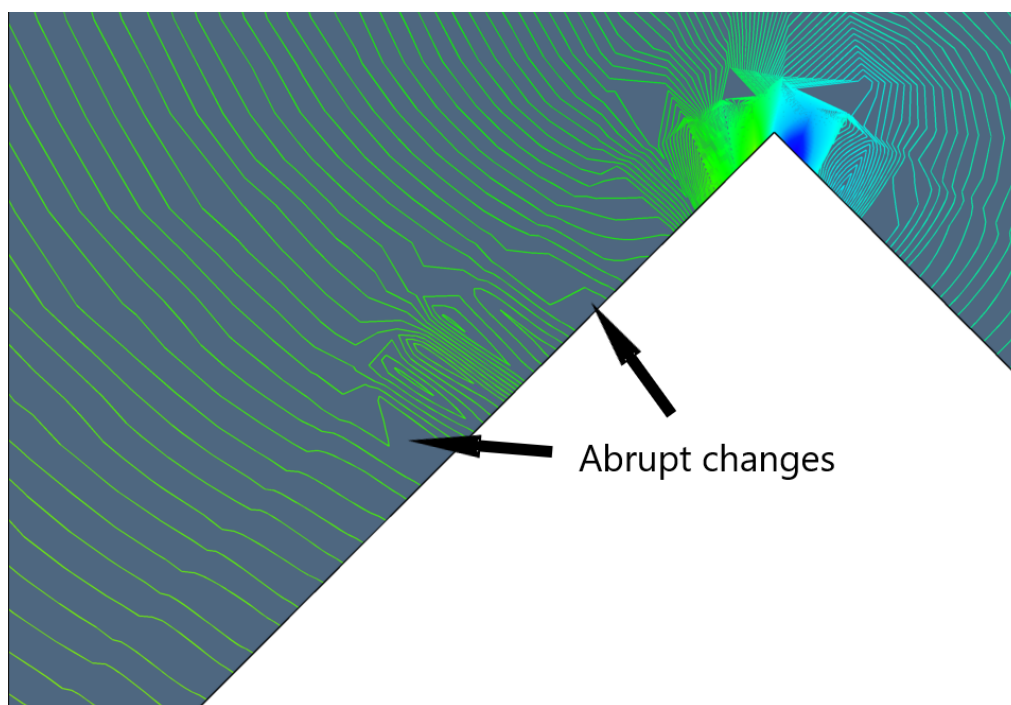


Figure 4.2: Abrupt changes in pressure iso contour plot

Although it is a powerful tool and will increase the accuracy of numerical computations it comes with a cost. A significant increase in computer power combined with higher computational time is two major challenges with the use of the tool. Additionally, it requires excessive knowledge about the software and nature of fluid behaviour. Therefore, the cost of using such functions must be evaluated up against the obtained winnings.

4.1.2 ISIS-CFD Numerical Flow Solver

The ISIS-CFD flow solver, developed by EMN (Equipe Modélisation Numérique), is the solver used in FM. It uses the incompressible unsteady RANS equations and is based on the finite volume method to build the transport equations. Together with SST $k - \omega$ turbulence model, this is a powerful tool implemented in the software.

RANS

The RANS equations is a widely used approximation method in numerical simulations. It describes the flow field in a statistical sense based on the Navier-Stokes equation given in Equation (4.1). The RANS equation results in time-averaging the pressure and velocity fields. This means that the turbulent velocity fluctuations is assumed to be distributed stochastically and thus, constant mean flow (Celik, 1999). For such methods, there occur additional terms in the equation because of the averaging. Consequently resulting in more variables than equations. This additional term can be seen in the RANS Equation (4.2), with the description *Reynolds - stress*, written in tensor form. Therefore, to be able to solve the equations in the flow solver, turbulence models are introduced.

$$\rho \frac{Du_i}{Dt} = F_i - \frac{\partial p}{\partial x_i} + \mu \Delta u_i \quad (4.1)$$

$$\rho \frac{D\bar{u}_i}{Dt} = F_i - \frac{\partial \bar{p}}{\partial x_i} + \mu \Delta \bar{u}_i - \underbrace{\rho \left(\frac{\partial \overline{u'_i u'_j}}{\partial x_j} \right)}_{\text{Reynolds-stress}} \quad (4.2)$$

Turbulence model

There are several turbulence models used in CFD calculations. Thus FM grants the user the possibility to choose between a wide range of models. However, the model that is preferred for simulation of a vessel in calm sea is the SST $k - \omega$ turbulence model. It is a combination of the $k - \omega$ model, used preferably near solid walls and the standard $k - \epsilon$ model used near boundary layer edges and in free-shear layers. Combined they modify the eddy viscosity with the shear stress transport modelling by introducing a constraint to the turbulent shear stress (NUMECA, 2019, Menter Two-Eq. mod.). Thus, in the simulation of a chemical tanker, the model will take care of the flow near the body and the wake field developed at the propeller location. Other models such as RST (Linear Pressure Strain formulation) have been investigated in wake field predicting and proven superior to the $k - \omega$ model as the former solves 7 equations for turbulence transport compared with only 2 in the latter (Krasilnikov et al., 2019). As a result, it demands a significant increase in computer power. In addition, the RST may experience instability and a converged $k - \omega$ solution is desirable as a starting value. Due to this the RST solver comes with an increased cost and is therefore not suitable for repetitive computations.

4.2 AKPA - Propulsor Design and Analysis Software

AKPA is a software developed by State Marine Technical University of St. Petersburg and MARINTEK intended for propeller design and analysis of open propellers and multi-component propulsors (SINTEF, 2004). The software includes three main features; PPD, AKPD and AKPA. These are aimed at preliminary design, blade design and propeller analysis, respectively. AKPA which is of main interest for this thesis is based on a velocity source Boundary Element Method, or panel method to solve the velocity field.

The analysis tool, AKPA, is mainly used to predict the total performance picture of the given propeller geometry in open water conditions (MARINTEK, 2012). The software also allows the user to define a specific inflow, thus introducing evaluation of the "effective" wake field. This is conducted by introducing the nominal wake, which will be found using numerical calculation methods in FM. Figure 4.3 illustrates how the pressure distribution and thus the cavitation pattern may be analysed using the tool. The software gives a full pressure picture in 3D illustrating where the pressure is low and cavitation may occur. This figure is based on the nominal wake of the hull with the presence of the ESD. It is seen that the blade tip has the lowest pressure, blue colour, but is still defiant to cavitation with a margin of around 83%. To understand how the software is built, a rough introduction to the theory of which AKPA is based on is presented in Section 4.2.1

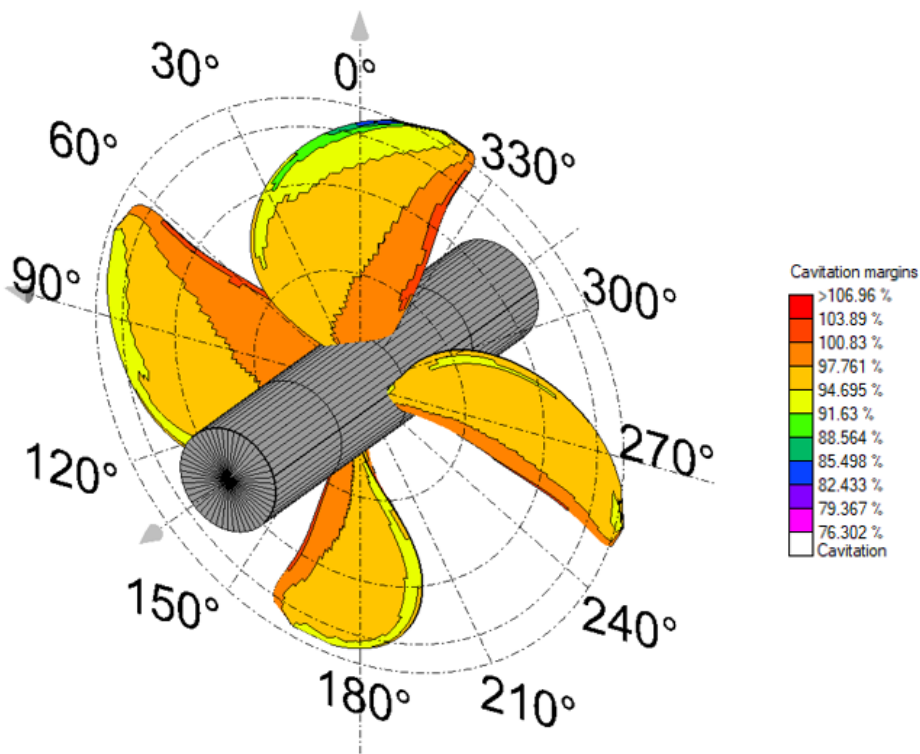


Figure 4.3: Cavitation Pattern collected from AKPA

4.2.1 Velocity Based Source BEM and Cavitation Analysis

The propeller analysis software AKPA is based on and classified as *Velocity Based Source BEM with Modified Trailing Edge*. The main features of the algorithm will be briefly presented and are solely based on the presentation in the user manual (MARINTEK, State Marine Technical University, Offshore Simulator Center, 2011, p.9-10). The method is given as follows:

- Propeller blade, rudder and hub surfaces are represented by the source layer of unknown strength to simulate the thickness effects. Furthermore, the circulation part of the flow is simulated by placing doublets along the blade mean surface with a semi-infinite vortex sheet behind the blade. Hub is considered a non-lifting surface. The form of the chordwise vorticity distribution can be arbitrary, and in AKPA it is assumed to be constant along the nose-tail section line. The unknown quantity, defining the vortex strength, is the circulation strength around the given blade section. To obtain this value a special kinematic boundary condition is applied to the modified trailing edge (MTE). The condition satisfies the Kutta-Joukowski condition and states that there shall be no flow across the MTE panels.
- To implement the kinematic condition as mentioned above, an additional panel is introduced behind the trailing edge of the blade section. This is thoroughly described in (MARINTEK, State Marine Technical University, Offshore Simulator Center, 2011). The method also allows to include the effect of viscosity on circulation.
- The geometry of the vortex wake that is created behind the trailing edge is according to the Generalized Linear Model as given in (MARINTEK, State Marine Technical University, Offshore Simulator Center, 2011).
- Inflow to the rotative disc is considered nominal, thus not influenced by the propulsor. For steady calculations, the mean axially and radially flows at the prescribed sections is the basis of the calculations. Simulating the unsteady case, the inflow field is defined in the propeller disc and the components are considered as given periodical functions of angular coordinate.

The effective wake field obtained through the software is based on a V-shape method algorithm solving axisymmetric Euler equation with respect to axial velocity. It assumes that all viscosity effects are included in the prescribed nominal wake field and resolves the interaction between the propeller and nominal wake while omitting the interaction between the hull and propeller.

The cavitation analysis in AKPA grants the user three alternatives, *Non-cavitating*, *2D cavitation analysis* and *3D cavitation analysis*. The former considers a fully wetted calculation but neglects all effects from cavitation and cavity volumes. The 2D analysis allows for a prediction of the effect of cavitation on the blade using the method of equivalent 2D flow. The latter includes a full analysis of cavity volumes and forces at cavitation with high accuracy.

4.3 Coupling of FM and AKPA

Every step in running FM and AKPA as a stand-alone software is time consuming and therefore a costly procedure. Due to this, the possibility of an online or offline coupling has been investigated. The online connection, meaning an automatic process running the simulation in FM, collecting the wake flow data in CFView and analysing the propeller in AKPA to obtain parameters such as the effective wake, pressure distribution and cavitation pattern was disregarded as an option. This conclusion was based on the fact that there was no possibility of having both software on one computer due to license problems and insufficient computational power.

The offline option on the other hand, grants the possibility of having two computers and thus one software on each machine. This is more time consuming than the options of an online function but is significantly better than doing all operations manually. Figure 4.4 illustrates the procedure of the computations from the starting point in FM's in built function HEXPRESS to the propeller analysis in AKPA. None of the mentioned coupling functions can automatically operate the first step as the grid and domain generation is different for each setup. Moreover, the increasing refinements are often based on the empirical data from the former computation. Considering the second step, the boundary conditions and simulation setup is held constant for every single case to minimize errors. However, this step does not acquire much effort to do manually. Therefore the offline function for the FM software starts at the third step and thus only considering the post-processing.

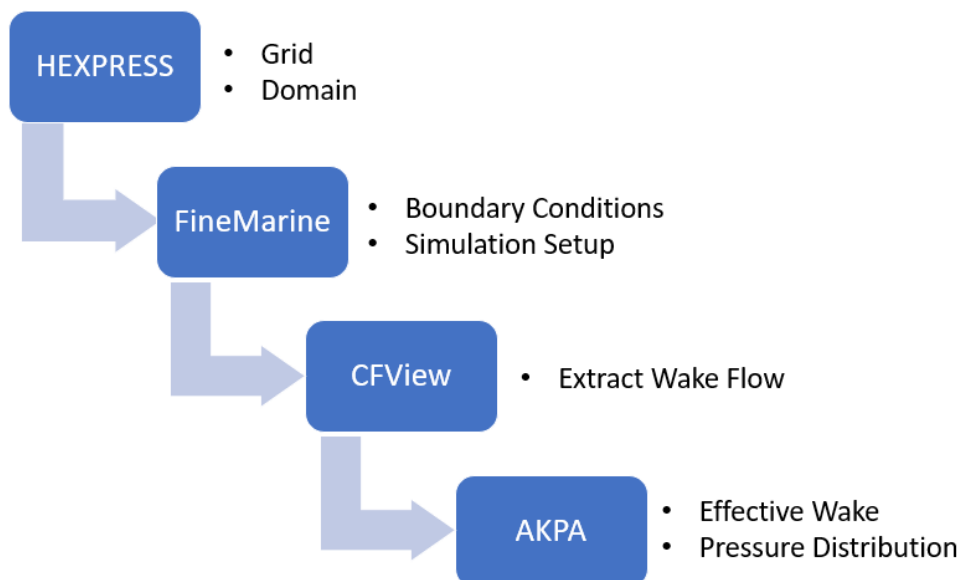


Figure 4.4: Offline Software Coupling - FM and AKPA

4.3.1 Step 1: Linux & Python - CFView

Controlling the post-processing in CFView with an automatic procedure reduces the manual workload and also introduces a lower probability of human error in the process of collecting desired data. CFView has a built in possibility to be controlled by python coding, where commands to control the macros are easily executed and thoroughly explained in the documentation of the software (NUMECA, 2019, CFView). Collecting the wake flow data in CFView is executed through the wake flow macro tool that is a part of the software and only extracts data for one specified position for one specific computation.

To extract the data at six different propeller locations for a significant number of computations a Linux and Python script has been utilized. The code is written with respect to Linux operation system and is presented below including comments. Desired positions and directories of the simulations are defined in line 4 and 7 as *positions* and *DIRS*, respectively. The values are imported and fed into the wake flow tool executed in line 25, using the *wake_flow_ppmarine72* command as given in the documentation (NUMECA, 2019, Wake_Flow_PP). New folders for the extracted wake flow for each position is created in line 27-29.

```

1  #!/bin/bash
2  # list of distances to propeller plane
3  positions=(0.0615 0.0410 0.0205 0 -0.0205 -0.0410)
4  # list of directories to explore SIMULATIONS WITH ESD
5  DIRS=( NorSingProp_w_ESD_Ref_1/NorSingProp_w_ESD_Run_1)
6
7  # save current directory as top directory
8  topDir='pwd'
9
10 # loop over list of directories run wakeflow tool
11 for DIR in "${DIRS[@]}"
12 do
13     # loop over list of distances to propeller plane
14     for pos in "${positions[@]}"
15     do
16         # print case
17         echo "${DIR} ${pos}:"
18         # replace keyword "position" in input file with numerical value and
19         # copy input file to sim directory
20         sed "s/position/${pos}/" wake_flow_pp.input > $DIR/wake_flow_pp.
21         input
22         # move to simulation directory
23         cd "${DIR}"
24         # run wake flow tool
25         wake_flow_ppmarine72 -print -relative < wake_flow_pp.input
26         # save wake flow output to separate subdirectory (overwrites
27         # previous files)
28         rm -r "Wake_pos_${pos}"
29         mkdir "Wake_pos_${pos}"
30         mv wake* "Wake_pos_${pos}"/
31         # move back to top directory
32         cd "$topDir"
33     done
34 done

```

4.3.2 Step 2: MATLAB - AKPA

FM creates text files containing the velocity field parameters such as axial, radial and tangential velocity. These are the same values that is needed to conduct the propeller analysis in AKPA and thus, the data does not need to be processed any further. However, the format of the text file is not identical from FM to AKPA. This means that MATLAB is utilized to create AKPA compatible files which are required to conduct the analysis. This is easily done by copying the text layout from AKPA's project library. The code that imports the wake flow data for all positions and computations are given in Appendix I.2.1. Furthermore, a function creates new unique folders in the AKPA directory and saves new velocity field files, *inputvel.frw*, in each folder. The code that creates these files is presented in Appendix I.2.3.

It was desirable to create a script that easily handled the AKPA simulations automatically. This would reduce the manual workload significantly as it is highly time consuming to manually set up and start each simulation. Combined with creating readable files this solution would make the analysis significantly easier to conduct with less chance of human errors. A proposed procedure to investigate is presented as a flow chart in Figure 4.5. The procedure starts with the extracted wake field data from FM at all eight propeller positions. Each position is automatically loaded into MATLAB which generates AKPA compatible files, runs the propeller analysis, collects the obtained data and repeats the procedure until all positions are simulated. After all computations have been conducted, the MATLAB code illustrates, compares and suggests the most suitable placing of the propeller.

Creating a code that handles this procedure automatically is highly time consuming. Evaluating the winnings of doing so up against doing it manually did not prove to be sufficient. Therefore, all simulations conducted in AKPA was done manually. However, for further work, it is highly encouraged to investigate the possibility of making a code that implements this procedure. Additionally, including the FM simulation procedure in an online coupling is of interest but not pursued.

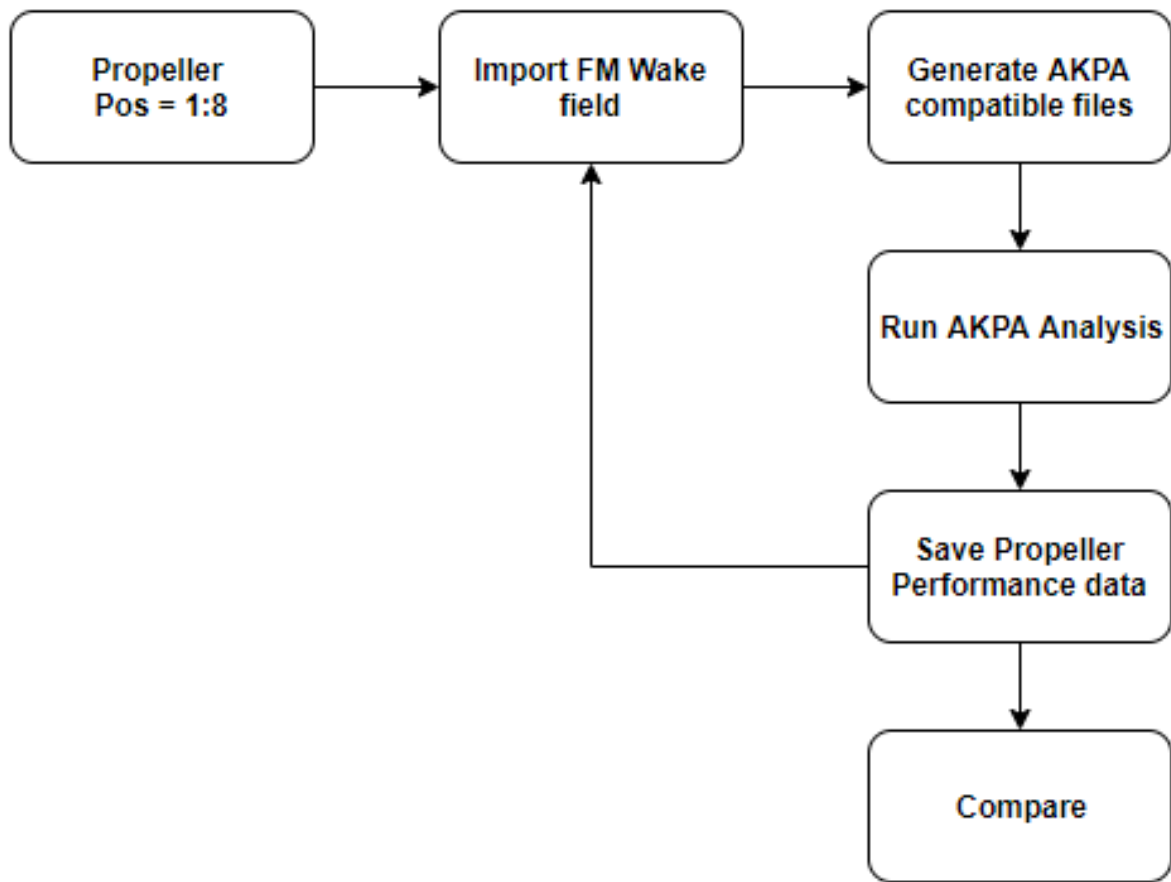


Figure 4.5: Automatic AKPA propeller analysis procedure

Chapter 5

Numerical Simulation Set-up

To quantify how the location of the propeller affects the efficiency and cavitation pattern it is necessary to conduct a thorough analysis of the subject. This would preferably be done with experimental testing, and therefore conducting well known procedures to determine how the different involving parameters interfere with the performance of the propulsor. Due to such testing is highly costly and demands a significant amount of man hours in a lab, a less costly and equally exact method is desired. CFD is rapidly growing and has become a good substitute for EFD, being able to present good results for early stage designs and indications for fluid flow regimes that show good correlation with EFD. In this chapter, the simulation set-up for a number of different computations is presented. Firstly how the hull is simulated in FM and thereafter how the propeller analysis software AKPA is set-up and utilised to analyse the given case.

5.1 Pre-Processing

The hull is numerically simulated propagating through calm water at the operational speed. Additionally, two other velocities corresponding to two knots higher and lower than the operational speed is simulated to quantify if the most optimal propeller location may be different depending on the forward velocity. This is however only executed with the original PSS and naked hull. The different parameters are presented in Table 5.1. To resolve the complex flow pattern and present an accurate prediction of the ship wake field in the studied case, the ISIS-CFD flow solver combined with the RANS equations and $k - \omega$ (SST-Menter) turbulence model is utilized.

To determine how the propeller operates both with and without the presence of a PSS, two different geometries is presented with two different domains. These will be further discussed. The domains are then discretised with an increasing amount of grid points obtaining enough data to quantify any deviation the grid may introduce. Both cases are simulated for about 30-60 seconds until the resistance and flow regime has stabilised. The main ship particulars are presented in Table 5.2.

	Model scale	Froude number	Full scale
Operational	1.210 [ms^{-1}]	0.1487 [-]	12 [kn]
	1.412 [ms^{-1}]	0.1735 [-]	14 [kn]
	1.614 [ms^{-1}]	0.1983 [-]	16 [kn]

Table 5.1: Simulated parameters FM

	Symbol	Model scale	Full scale
Length between PP	L_{PP}	6.7538 [m]	175.60 [m]
Breadth moulded	B	1.2395 [m]	32.229 [m]
Draught	T	0.4556 [m]	11.846 [m]
Block coefficient	C_B	0.8123	0.8123

Table 5.2: Main ship particulars

5.1.1 Domain and Boundary Conditions

The two models are discretised in two domains each, thus with and without PSS and with and without the presence of FS. The main distances of the domains is presented in Table 5.3, 5.4, 5.5 and 5.6 corresponding to naked hull, naked hull w/o FS, hull with PSS and hull with PSS w/o FS, respectively. The reference length is the vessel length overall (LOA) assumed to be equal to LPP. The size of the discretised area is according to the recommendations given by FM (NUMECA, 2018b) and guidelines presented by ITTC (Procedures, ITTC Recommended,), where the outlet is to be placed 3-5LOA downstream and inlet 1-2LOA upstream. The origin of the cartesian coordinate system is located at the aft perpendicular (AP) with $z = 0$ at the keel.

Domain 1		
-3LOA	$\leq x \leq$	2LOA
0	$\leq y \leq$	2LOA
-1.1LOA	$\leq z \leq$	1.1LOA

Table 5.3: Naked hull

Domain 2		
-3LOA	$\leq x \leq$	2LOA
0	$\leq y \leq$	2LOA
0	$\leq z \leq$	1.1LOA

Table 5.4: Naked hull w/o FS

Domain 3		
-3LOA	$\leq x \leq$	2LOA
-2LOA	$\leq y \leq$	2LOA
-1.1LOA	$\leq z \leq$	1.1LOA

Table 5.5: Hull with PSS

Domain 4		
-3LOA	$\leq x \leq$	2LOA
-2LOA	$\leq y \leq$	2LOA
0	$\leq z \leq$	1.1LOA

Table 5.6: Hull with PSS w/o FS

The four different domains will have deviating boundary conditions due to different size and simulation settings. The boundary conditions for domain 1 are set so that the upper and lower boundary has a prescribed pressure corresponding to atmospheric and hydrostatic pressure, respectively. For the surface laying parallel to the x-z plane in

the positive y -direction and those being parallel to the y - z plane, a far field definition to the condition is applied. On the inlet boundary, the far field condition applies calm water entering the box. At the outlet boundary, it allows the water to freely exit the computational domain. As the ship is symmetric about the longitudinal axis only half the ship is simulated. Thus, the boundary conditions are mirrored around the center plane (x - z plane). Figure 5.1 illustrates the boundary conditions set for domain 1.

Figure A.1 in Appendix A depicts domain 2 which is rather similar to the one presented in domain 1. The only difference here is that the simulation only considers the wetted part of the vessel. Therefore, the domain is cut at the free surface and the boundary condition in the x - y plane is set to represent a mirror plane.

Domain 3 and 4 include the complete geometry, thus including the three blades of the PSS on the port side of the vessel. The respective domain and their coordinates is presented in Table 5.5 and 5.6. As the blades of the PSS only is present on one side, a full simulation including the whole vessel is needed to catch the full nature of the flow. Thus, the domain needs to correspond to the full geometry of the vessel and is therefore significantly larger in size than domain 1 and 2. The boundary conditions applied for domain 3 are set so that the upper and lower boundary has a prescribed pressure similar to domain 1. For the surfaces laying parallel to the x - z and y - z plane, a far field definition to the condition is applied. This allows calm water to enter the box and freely exit the computational domain at the outlet boundary. Domain 4 has equal boundary conditions as domain 3, except for the cutting plane at the free-surface which is set as a mirror plane. The two different domains with their respective boundary conditions is presented in Figure A.2 and A.3, respectively.

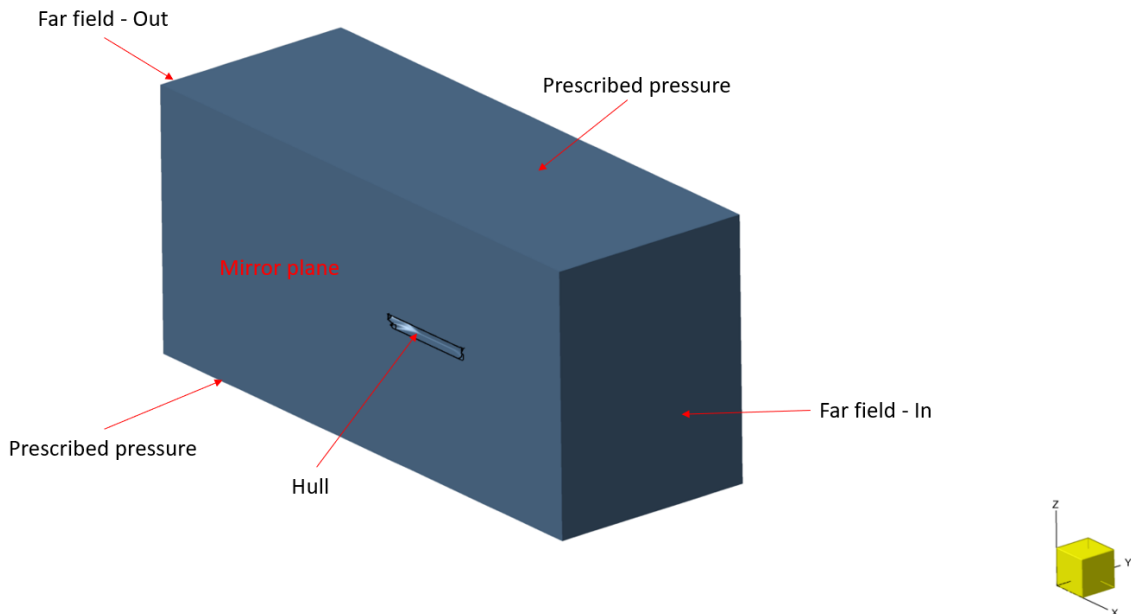


Figure 5.1: Domain 1 with applied boundary conditions

The boundary condition for the solid parts is divided into wet and dry surfaces. The dry surface, namely the deck is set to slip-condition. This ensures zero shear stress at this surface, thus not contributing to any resistance or disturbances in the fluid computation. The conditions along the wet surfaces such as the hull, bulb, bow, transom and hub is set to wall function. This is based on the no-slip condition and thus zero velocity at the wall. However, the difference between the two are that the no-slip boundary condition calculates all the velocity gradients in the boundary layer. The wall function, on the other hand, obtains the velocity gradients by assuming the shape of the velocity profile in the boundary layer. Furthermore, if the wall function is applied it is possible to apply a surface roughness to the simulation. This may increase the accuracy of the simulation. Due to the lack of knowledge around the true roughness of the model, this is neglected, substantiating the importance of careful evaluation of obtained results. The wall function tool is often used for complex geometries and bigger simulations. Thus, saving valuable computer power and computational time. This is why this is chosen for the numerical simulation of the chemical tanker. Nevertheless, using approximations such as this requires careful evaluation of the obtained results.

5.1.2 Discretisation of Domain and Grid

For discretisation of the respective domains, FM has a built in function named HEXPRESS which is designated for this type of task. It creates an unstructured hexahedral mesh around the input geometry, and the mesh generation follows the steps described below. The information is taken from the userguide (NUMECA, 2019).

1. Initial Mesh

- The initial mesh encompasses the whole computational domain and proposes automatically an isotropic subdivision of the defined box.

2. Adapt to Geometry

- This step is the most important parameter in terms of user interaction and is divided into two subgroups, namely refinement and trimming.
 - *Refinement* - in this part the user may define areas, volumes and surfaces of interest to have a higher order of refinement. Meaning that for a propeller plane and the flow in the vicinity of the rotative disc, a refinement box may be defined to catch the propagating wake flow in an effective manner. An example of refinement near a surface is given in Figure 5.2.
 - *Trimming* - this part removes all the cells overlapping or which is located outside the geometry. At the end of the process, a staircase mesh is obtained along the surface of the geometry. A trimming example with surface intersecting cells is presented in Figure 5.3 (NUMECA, 2019).

3. Snap to Geometry

- The snapping part is a fully automatic step that projects the obtained staircase mesh to the surface of the geometry. By doing so, a good quality body conforming mesh is obtained.

Refinement of Cells

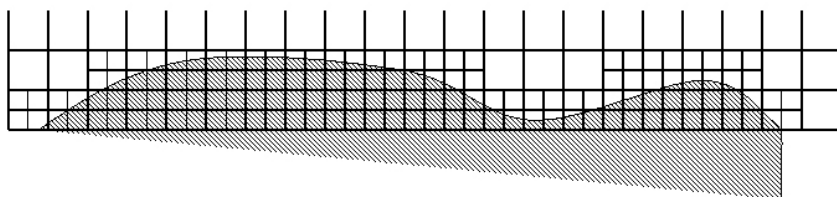


Figure 5.2: Refinement of surface intersecting cells (NUMECA, 2019).

Trimming

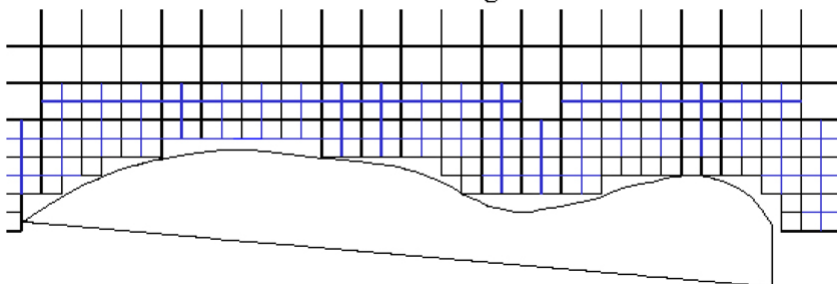


Figure 5.3: Trimming of surface intersecting cells (NUMECA, 2019).

4. Optimisation

- This step takes care of distorted cells that may be concave or even present a negative volume. Such errors may appear close to corners and curves. This step fixes such issues by slightly displacing their vertices.

5. Viscous Layer Insertion

- The insertion of viscous layers applies layers of large aspect ratio cells near the surface of the geometry to fully resolve the boundary layer flow.

Naked hull

The simulations disregarding the presence of the PSS is referred to as the naked hull and is illustrated in Figure 5.4, where there is no extra geometry at the hub. It should be mentioned that the added geometry in the vicinity of the propeller is the only difference between the two models. In the situation disregarding the PSS, the model is as stated, symmetric about the middle plane in the longitudinal direction. This implies that the discretisation may be simplified by creating a mesh of half the domain and then mirror the whole computation about the x - z plane. This results in a significantly lower number of cells and thus resulting in a lower demand of computer power for the computation of the simulation.

The initial mesh generation defines the starting cell size in the whole domain. As a rule of thumb, these starting values should correspond to a size so that the 8th refinement is approximately equal to $LPP/1000$ (NUMECA, 2019). The initial mesh and corresponding sizes are presented in Table 5.7. Furthermore follows the decision of grid density, also referred to as the number of refinements. This is where the user may

focus on the areas of interest and insert cell areas with a higher order of refinement. By doing so, the solver is able to catch the flow in a satisfactory manner. Figure 5.5 illustrates how the different refinement levels are set up for the 5th refinement of the numerical simulation of the naked hull. In the figure, it is seen that there is a significant difference in the refinement of the hull compared to skreg, hub and box refinement.



Figure 5.4: Model of naked hull, no PSS

	Cells along axis	Size 8th ref	LPP/1000
X	21	0.004371 [m]	0.006753 [m]
Y	8	0.006591 [m]	0.006753 [m]
Z	10	0.005804 [m]	0.006753 [m]

Table 5.7: Initial mesh - Naked hull

The box refinement differs from the other areas of interest as it is not a part of the surface on the vessel geometry. Normal surface refinement such as for the hull, skreg and the hub defines that the cells closest to the surface shall be of that specified size. For the box refinement, it is possible to refine all the cells that are inside the volume of which is covered by that box. In addition, the set up grants the user the possibility to focus on the refinement near the surfaces of the geometry that is inside the specified box refinement. For the case of this numerical set-up, the volume refinement with a cylindrical structure has been chosen where the parameters used to set up this refinement is presented in Table 5.8. By increasing the refinement level in this region the flow propagating along the hub may be captured more effectively and precisely. By doing this, the wake field is properly quantified at the plausible propeller positions.

X	Y	Z	R_{min}	R_{max}	Height
0.120	0.000	0.1625	0.0256	0.1250	0.1500

Table 5.8: Box refinement parameters [m]

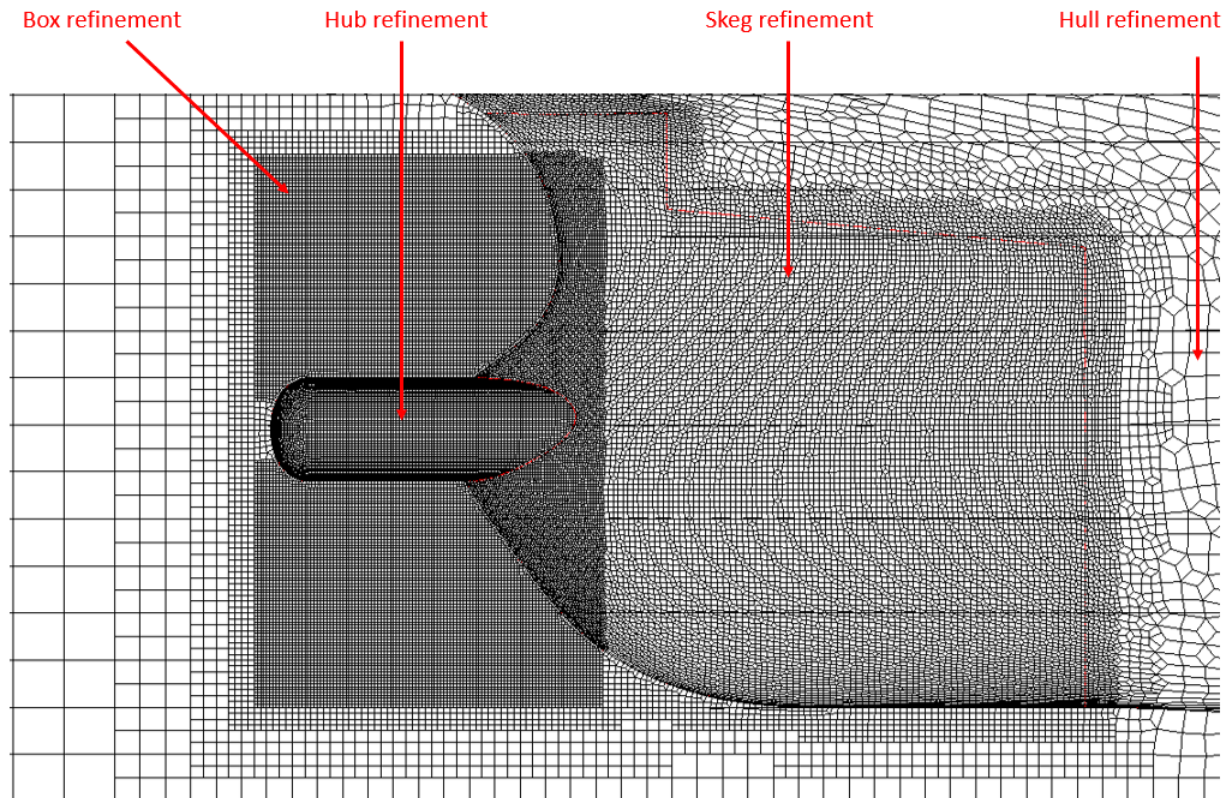


Figure 5.5: Refinement 5 of propeller location

The wet surface of the geometry propagating through the water will have a boundary layer resulting in viscous forces and therefore resistance. To fully capture these forces and the turbulent flow regime at these areas, cell structure (viscous layers) of high aspect ratio is placed from the solid wall of the structure and into the fluid with increasing thickness. The boundary layer and how it is solved will affect the wake field generated at the aft and is therefore important to take care of accordingly. With the viscous layer insertion in step 5 of the grid procedure, the software predicts how many layers which is necessary for solving the flow. It also suggests stretching ratio (increasing thickness) and the size of the first layer based on vessel speed, length and the Y^+ value.

The Y^+ quantity also referred to as the distance of the first near wall point, is according to Devals (2016) one of several parameters that govern mesh generation and influences the final solution of numerical computations (Devals et al., 2016). In the mesh generation conducted for the chemical tanker the Y^+ reference value was set to 40 according to ITTC's recommendations (Committee et al., 2011). SINTEF's study on the same vessel, in full scale, obtained an average Y^+ value of 150 on the hull surface and 90 on rudder and ESD (Krasilnikov et al., 2019). Furthermore, the value at the propeller blade was in the range from 30 to 80. Figure 5.6 illustrates the viscous layers that is placed at the transom of the vessel. In this area, there is placed five layers with a stretching ratio of 1.2.

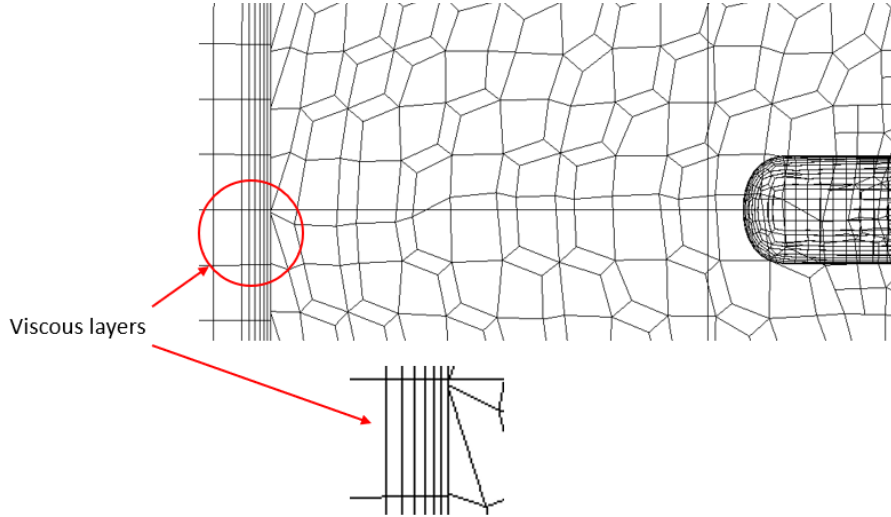


Figure 5.6: Viscous layer insertion - Transom (Hull with PSS)

To be able to quantify the effect of increasing mesh refinement at local areas and how it affects the obtained numerical solution, seven different refinements with a stepwise increase in cell number was prepared for the domain. Table 5.9 presents the respective refinements with the corresponding local refinement level for the geometry disregarding the PSS. The area of interest, propeller location represented by the box, has the main overall focus. However, areas affecting the wake flow such as skeg, hub and hull are also increased to account for differences that these areas impose. On the other hand, the overall grid generation and areas of interest must also be investigated properly to quantify how they affect the solution. This, however, is highly time consuming and therefore not prioritised in this thesis.

Maximum number of refinements

Area	Ref. 1	Ref. 2	Ref. 3	Ref. 4	Ref. 5	Ref. 6
Transom	8	8	8	8	8	8
Hub	8	8	8	8	8	8
Skeg	8	8	9	9	10	10
Hull	6	6	6	6	6	7
Deck	4	4	4	4	4	4
Bow	6	6	6	6	6	6
Bulb	8	8	8	8	8	8
Free Surface	8	8	8	8	8	8
Box	-	9	9	10	10	10
<i>Total cells</i>	1 067 399	1 329 404	1 435 849	2 644 865	3 039 530	3 498 487

Table 5.9: Refinements and total number of cells - Naked hull

Table 5.10 presents the number of viscous layers at the respective sections together with the corresponding stretching ratio. The layers are kept constant and according to the presented values for all computations. This will allow for equally comparable results and achieve Y^+ values in the same order. On the other hand, keeping them constant may impose an insufficient solved flow field if the number of layers is too low. Thus, suggesting to investigate how the layers may affect wake field behaviour. However, taking into consideration the goal of the thesis and the increase in computational time and power this introduces, the number of viscous layers is assumed to be sufficient.

Viscous layers		
Area	Layers	Stretch ratio
Transom	4	1.2
Hub	3	1.2
Skeg	3	1.2
Hull	10	1.2
Bulb	4	1.2
Bow	4	1.2

Table 5.10: Number of viscous layers - Naked hull

The presence of the free surface has an important impact on the numerical computation and must therefore be correctly discretised. The procedure executed is similar to the surface refinement of the geometry and is according to FM's tutorial and user guide (NUMECA, 2019). As it is not desirable to create a large number of cells and that the refinement in the z-direction is the most interesting area, the refinement in x- and y-direction is decreased. This is done by defining the target cell sizes in z direction close to zero and x and y-direction to be significantly larger. The maximum aspect ratio is set to 200 in order to allow the mesh anisotropy close to the free surface. All these values is presented in Table 5.11 and 5.12 and are equal for all simulations conducted with the presence of the free surface.

	Target cell size [m]
X	0.90000
Y	0.90000
Z	0.00617

Table 5.11: Free surface refinement target cell size (NUMECA, 2019)

Parameter	[-]
Aspect ratio	200
Refinement diffusion	4

Table 5.12: Free surface refinement parameters (NUMECA, 2019)

Hull with PSS

The geometry including the presence of the PSS has a similar mesh construction compared with the one disregarding the PSS. The only difference is that there is included refinements around the stator blades and that the number of total cells will be significantly higher due to the size of the domain. Initial mesh conditions are presented in Table 5.13 and is based on the same rule as for naked hull. The same holds for the procedure of refinements in areas of interest and the free surface discretisation. Box refinement, covering the rotative disc, is established in the same manner with some small adjustments. These are presented in Table 5.14. An illustration of the vessel with the added geometry (PSS) is presented in Figure 5.7 seen from the aft.

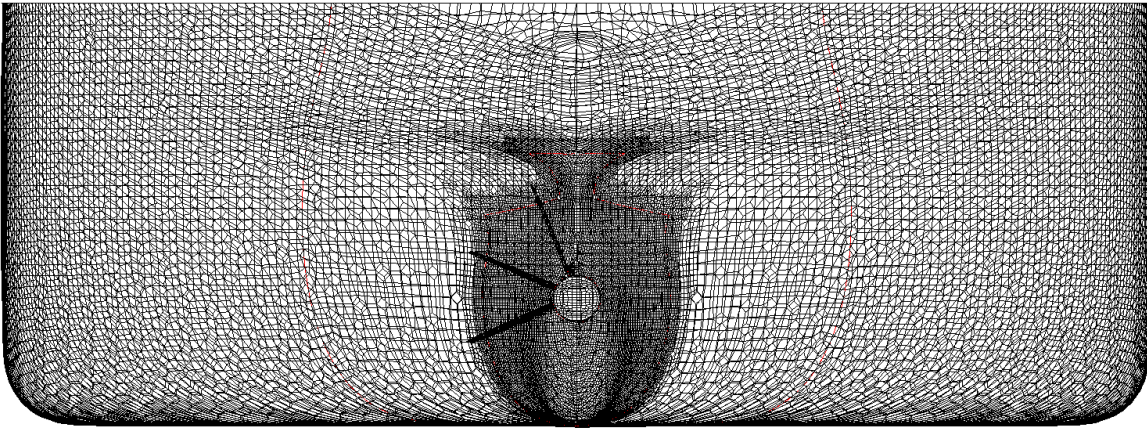


Figure 5.7: Hull with PSS seen from the aft

	Cells along axis	Size 8th ref	LPP/1000
X	20	0.006543 [m]	0.006753 [m]
Y	16	0.006591 [m]	0.006753 [m]
Z	10	0.005804 [m]	0.006753 [m]

Table 5.13: Initial mesh - PSS

X	Y	Z	R_{min}	R_{max}	Height
0.100	0.000	0.1369	0.0256	0.1380	0.2000

Table 5.14: Box refinement parameters [m] - PSS

Some minor adjustments were made in the discretisation of the hull with PSS. Due to the presence of the stator blades, the geometrical areas including skeg, hub and stator fins are merged. Meaning that this area is one single surface with equal local refinement, denoted "Skeg". This also holds for the grid generation for viscous layers. The rest of the refinements are equally set up and the respective local refinement numbers are presented in Table 5.15. The viscous layers are adjusted in the computation of the hull with PSS and is presented in Table 5.16. The adjustment are solely based on the recommendation of FM and thus due to the calculation made by the HEXPRESS function.

Maximum number of refinements

Area	Ref. 1	Ref. 2	Ref. 3	Ref. 4	Ref. 5	Ref. 6
Transom	8	8	8	8	8	8
Hull	6	6	6	6	6	8
Bow	6	6	6	6	6	6
Bulb	8	8	8	8	8	8
Deck	4	4	4	4	4	4
Skeg	8	10	10	10	10	10
Free Surface	8	8	8	8	8	8
Box	-	-	8	9	10	10
<i>Total cells</i>	1 760 000	3 071 744	3 150 074	3 555 026	6 381 223	11 147 317

Table 5.15: Refinements and total number of cells - Hull with PSS

Viscous layers

Area	Layers	Stretch ratio
Transom	5	1.2
Skeg + Hub + Blades	6	1.2
Hull	12	1.2
Bow	11	1.2
Bulb	6	1.2

Table 5.16: Number of viscous layers - with PSS

No Free Surface

To quantify the effect the domain size and thus the number of cells has on the simulations, one simulation was conducted without the presence of the free surface. This simulation was set up nearly equal to the other cases where local refinements correspond to refinement 4. To effectively remove the free surface from the numerical simulation, some minor changes were applied to the original domain. According to the domain settings discussed in Section 5.1.1 a plane cutting through the domain at the location of the free surface is

created. All boundary conditions are equal to the one presented for computation with FS except for the cutting plane which now is set to mirror. The initial refinement size is adjusted according to 8th refinement, presented in Table 5.17. Viscous layers are equal as formerly presented. This resulted in significantly lower number of cells in the domain with a decrease of -50.7% and -40.23% for naked and PSS, respectively.

	Naked	PSS
X	21	20
Y	8	16
Z	5	5
Total cell amount	1 301 998	2 124 791

Table 5.17: Number of cells in direction (initial mesh) and total amount of cells - no FS

5.2 Numerical Test Set-Up

The numerical computation set-up is conducted in the main FM software. An unsteady simulation approach is chosen in the general parameters so that the user has the possibility to control the maximum number of non-linear iterations and the number of time steps performed, which will aid the numerical results. Fluid parameters used in the computation is set to and correspond to the values presented in Table 5.18.

Parameter	Symbol	Value	Units
Water density	ρ	998.85	kgm^{-3}
Kinematic Viscosity	ν	1.11E-06	m^2s^{-1}

Table 5.18: Fluid test parameters

The chemical tanker has a minor difference in draught from FP to AP imposing a constant pitch angle. In the body motion section this is taken care of by imposing a constant pitch motion from the start of the simulation. The imposed pitch is set to -0.0018 radians based on simple hand calculations. As the vessel is moving forward with a constant speed a similar solution is exploited by imposing constant surge motion using the same menu. The inserted velocities correspond to the values presented in Table 5.1. To get a smooth translation from zero to operational velocity a sinusoidal ramp profile is used as presented in Figure 5.8. The acceleration of the tanker is controlled within a time window, t_0 to t_1 . This ensures that there is as little perturbations as possible from the acceleration of the vessel contributing to a faster convergence of the results. All other degrees of freedom (yaw, roll, heave and sway) are constrained from motion and therefore not solved during the computation.

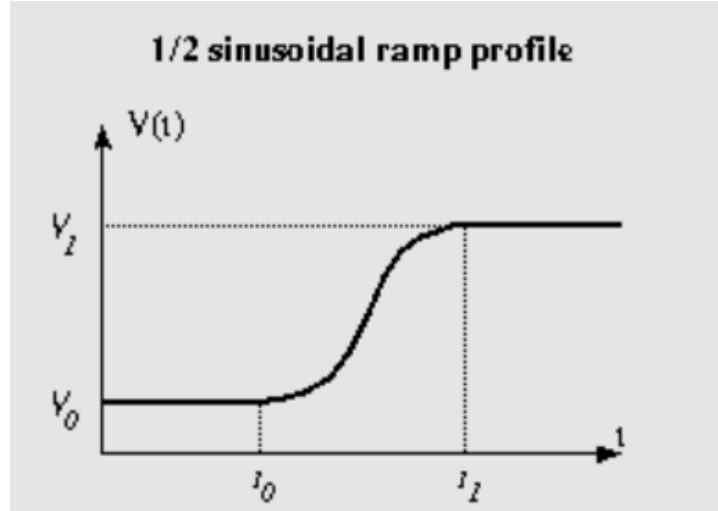


Figure 5.8: Sinusoidal ramp profile (NUMECA, 2019)

The software may resolve a significant number of equations and present parameters such as pressure distribution and forces, moments and motions in all degrees of freedom for all time steps. These may also be calculated in the post-processing in CFView but only for the final time step. As some parameters is desired to obtain for each time steps the *Outputs* in *Computation control* is utilised to select the desired variables. These are collected and stored for each time step interval and may be used to study and validate the numerical results.

In the *Control variables* other parameters connected with solving the equations and the total number of time steps is chosen. As the refinement in the vicinity of the propeller location is a local important refinement area the maximum number of non-linear iterations is increased to a number of 10 compared with the default value (8), which is in accordance with the recommendations of FM user manual (NUMECA, 2019). The convergence criteria is set to an order of 3, meaning the order of magnitude the infinite norm of the residuals must decrease during each time step.

In the *Time step Parameter* section the total number of time steps is set to be in the range of 3000-6000 with a time step of 0.01 seconds. This corresponds to a real time simulation of 30-60 seconds. The longest computations were conducted first so the stabilisation time was revealed. The chosen time step value is selected to save computational effort due to limited amount of computer power. The selected value is supported by the ITTC standard recommendations for resistance computations ($\Delta t = 0.001 \sim 0.0025 \frac{L}{U}$) (Committee et al., 2011). On the other hand, considering the Courant-Friedrichs-Lewy number (CFL) in may indicate that the time step is insufficient. The number describes how well the physical motion is captured in each cell and according to Trivelatto (2013) the value needs to be properly chosen to obtain accurate results (Trivellato and Castelli, 2014). Thus the selected time step must allow the information to have sufficient time to travel each cell element. The criterion for CFL number in one dimension is presented in Equation (5.1).

$$CFL = u_x \frac{\Delta t}{\Delta x} < 1 \quad (5.1)$$

The parameters chosen for the computations may thus be discussed in retrospect. Maximum number of non-linear iterations were increased by a number of 2. However, there is little knowledge regarding how the computation would respond to an even larger increase. Additionally the convergence criteria is also set without any proper study of how it influences the result. Considering all these arguments, there should be done a thorough study of the topic. However, as it is highly time consuming and not a part of the aim of the thesis, the set parameters is assumed to be sufficient.

Adaptive grid refinement is an iterative process in which the mesh is dynamically adapted to the requirements of the solutions. Due to the nature of wake field flows the tool may significantly improve the obtained results. However, the expected winnings connected with using this function in this research was found to be insufficient. The argument for this is the number of unique computations with deviating mesh constructions to be conducted. Thus, implementing the grid refinement with unique constraints and criterion's would significantly increase the computational time. Additionally, the limited available computer power comes with constraints and does not allow for trials and errors.

5.3 Post-Processing - FM Computation

CFView

FM has a built in post-processing tool named CFView which grants the user several possibilities to extract and view the obtained data. As the main objective of this thesis is collect the wake field flow data, FM's special designed wake flow tool is utilized to extract the velocity field in axial, radial and tangential direction. By specifying parameters such as location and size of the rotative disk, normal direction of the flow regime and mesh concentration these velocity values is extracted easily. To save time, a code in Python is made to execute this procedure automatically. This was explained in Section 4.3.1.

To validate the results obtained through the simulations it is necessary to look at other parameters such as pressure distribution, flow field along the hull and PSS and total resistance. These are easily collected through the convergence history presented by FM and in the post-processing interface in CFView.

MATLAB

The files that is created by FM has to be re-written to be compatible with AKPA format. This is done by importing the selected data from the FM format into MATLAB and creating new text files that is readable for the propeller analysis software. Due to the amount of simulations conducted combined with the six propeller locations, the number of files is significantly large. Thus, an automatic process is needed to post-process in an effective manner. A code that imports from FM folders and creates new folders in AKPA readable format depending on number of refinements, runs and positions is

therefore created. The main code with two additional functions is given in Appendix I.2.1, I.2.2 and I.2.3, respectively.

5.4 Propeller Analysis - AKPA

The AKPA compatible files is generated as described in MATLAB and thus the propeller analysis may be conducted. The correct propeller data such as diameter, shaft rotation speed and number of blades is loaded into the software. The propeller is a fixed-pitch propeller developed at SINTEF, is illustrated in Figure 5.9 and main parameters is given in Table 5.19. Exact blade geometry is given in Table 1 in Appendix C.

Parameter	Symbol	Value	Units
Propeller diameter	D	0.25	[m]
Shaft rotational speed	RPM	600	[1/min]
Number of blades	Z	4	[-]
Direction of rotation	Right-handed		

Table 5.19: Propeller parameters - Fixed-Pitch Propeller (FPP)

The effective wake computation is set to iterate 5 times and the wake is calculated at a distance of $X_{eff}/R = 0.2$ from the propeller plane, upstream. The distance defines the location of the control section at which the effective wake is computed. The reason for calculating at a distance away from the propeller blade is the singularities that are present on the blade in the panel method, also discussed and presented in (Regener et al., 2018). The number of iterations is according to the AKPA user manual stating that the suitable range of iterations to obtain convergence is 5-6 (MARINTEK, State Marine Technical University, Offshore Simulator Center, 2011, p.44).

In computation of the induced velocities, the Isolated Optimum Moderately Loaded Propeller (IOMPL) algorithm is chosen. This includes the effect of the wake and propeller loading in the wake on the geometry of the free vortices. Thus it predicts more accurate induced velocities compared with the other option, AKPA Analysis, which does not fully reflect these effects. Furthermore, the software is set to account for a finite number of blades to compute a more accurate total effective velocity field.

To account for and quantify the presence of cavitation inception and the effect it has on propeller performance, the software grants the user the possibility to choose between a 2D and 3D cavitation analysis. The former predicts the effect of cavitation on rudder forces using the method of equivalent 2D flow. The latter on the other hand includes a prediction of cavity volumes and forces that arise due to cavitation. The 3D analysis grants more thorough results but is highly time consuming. The 2D calculation method is argued to be sufficient as it demands less computer power combined with high accuracy on the result. Therefore, the 2D analysis is used for the cavitation calculation.

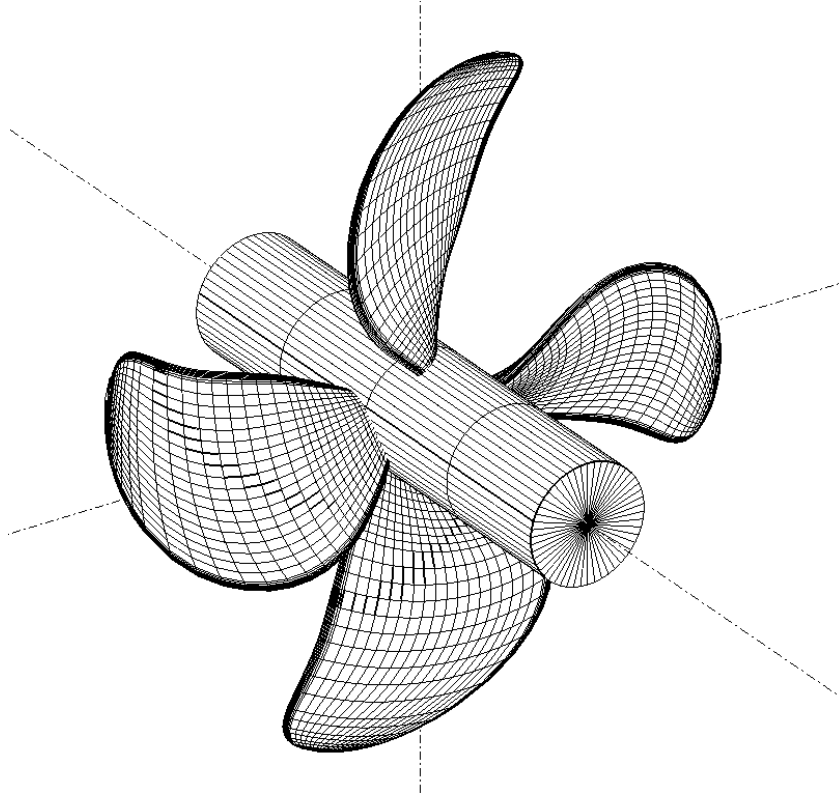


Figure 5.9: 3D view of propeller

In the cavitation analysis the software requests input parameters to quantify pressure differences with high accuracy. The parameters that must be given to the software are shaft immersion, atmospheric pressure and vapour pressure at the given water density. The data used in the computation is given in Table 5.20. Vapour pressure is obtained using ITTC's recommended procedures (in Marine Hydrodynamics, 2011) and linear interpolating between the water density values.

Parameter	Symbol	Value	Units
Shaft Immersion	h_0	0.2056	[m]
Atmospheric Pressure	p_a	101325	[Pa]
Vapour Pressure	p_v	1880.2	[Pa]

Table 5.20: Cavitation analysis parameters

The obtained results are written in a text file at the origin of the project folder. From this file, the corresponding hydrodynamic coefficients are collected and presented. The coefficient collected from AKPA are thrust (K_T), torque (K_Q), shaft delivered power (P_D) and efficiency in wake (η_w) given in Equation (5.2), (5.3), (5.5) and (5.4), respectively. Axial wake fraction WT is also extracted as a scalar. The values are presented with an advance number, J , obtained using Equation (5.6) and presented in Table 5.21.

$$K_T = \frac{T}{\rho n^2 D^4} \quad (5.2)$$

$$K_Q = \frac{Q}{\rho n^2 D^5} \quad (5.3)$$

$$P_D = K_Q 2\pi n^3 D^5 \quad (5.4)$$

$$\eta_w = \frac{K_T V}{K_Q 2\pi n D} \quad (5.5)$$

$$J = \frac{V}{nD} \quad (5.6)$$

The nominal and effective wake field may be visualised at the respective propeller location and is easily displayed entering *FRW Inflow (Nominal)* or *FRW Inflow (Effective)*, respectively. Both axial and transverse components are illustrated with color plot and vector representation, respectively. Additionally, density and transition of color bar and vector length may be adjusted to fit the desired presentation. To easily detect differences in the plots, the range of the color bar is set equal for all computations.

To analyse the pressure distribution and hence the cavitation pattern the propeller grid parameters must be selected in the *PREPARE* section. According to the manual (MARINTEK, State Marine Technical University, Offshore Simulator Center, 2011), the most suitable cell density is prescribed by default by the software. In the present case, it is set to 40 cells along both radius and chord length. The pressure distribution may be visualised in 3D or 2D represented by cavitation margins and areas and by pressure coefficient (C_P). An example of a cavitation margin visualisation has been presented in Figure 4.3.

Vessel velocity [V_m]	Advance number [J]	Propeller revolution [n]
$1.210ms^{-1}$	0.484	10
$1.410ms^{-1}$	0.564	10
$1.614ms^{-1}$	0.646	10

Table 5.21: Velocity vs Advance number - Propeller revolution (n) is kept constant for all three values.

Chapter 6

Results - CFD and Propeller Analysis

This chapter presents and discuss all obtained results from the numerical calculations conducted in FM and AKPA. It consists of six parts presenting a convergence study, resistance study, wake field analysis, propeller location analysis, cavitation analysis of the propeller blades and PSS pressure evaluation.

6.1 Numerical Investigation and Validation

6.1.1 Resistance curve

The propagating curve of the total resistance gives an indicator of the convergence of the numerical computation. Figure 6.1 and 6.2 illustrates the obtained results for the whole time domain given in (a), and a chosen time window where the resistance converges within an acceptable limit, in (b). As seen in (a) the plots indicate that the simulations has converged after about 20 seconds for all refinements. The narrow time window in (b) shows that the results are varying with time for each refinement. However the magnitude, oscillation frequency and period coincide, thus the varying results are negligible. The convergence may be rather rough if the goal is to quantify the resistance of the vessel, and it is within an acceptable limit for this thesis. Resistance curves for all computations are given in Appendix D.

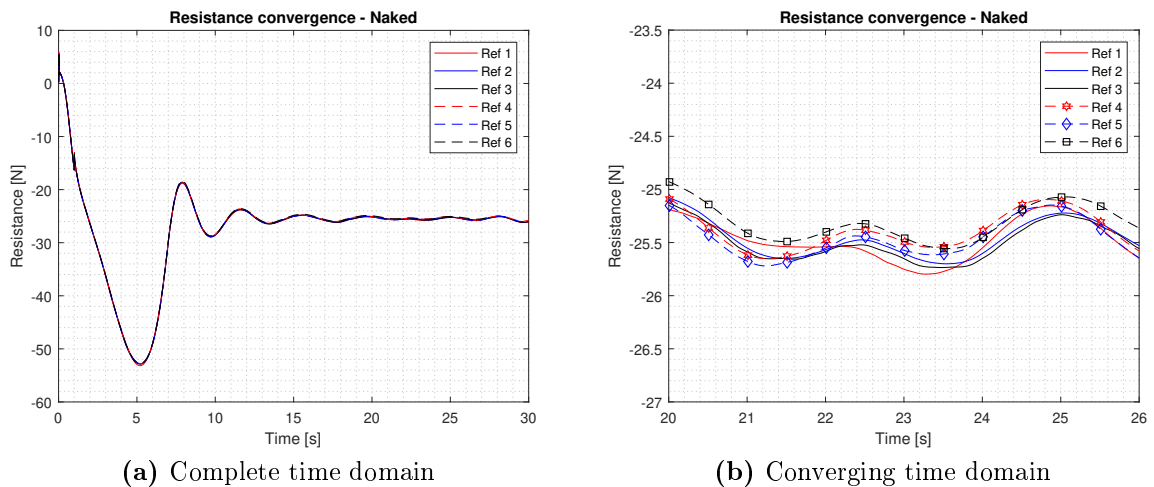


Figure 6.1: Resistance convergence - Naked hull [Half vessel]

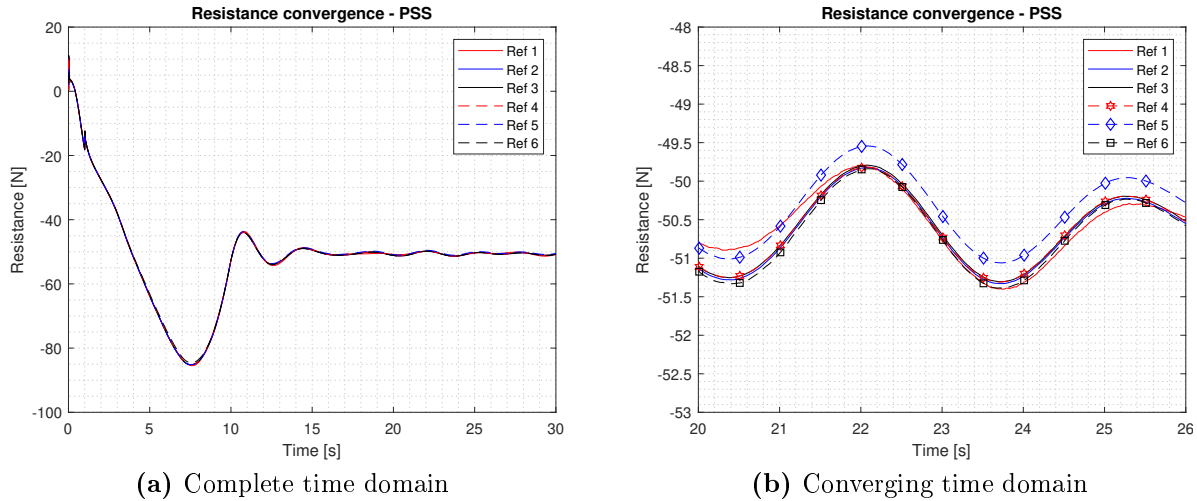


Figure 6.2: Resistance convergence - PSS [Whole vessel]

6.1.2 Domain without FS

Neglecting the effect of the FS may result in a faster convergence, when studying the resistance of the vessel. If this is the case, it may be more effective to conduct numerical computations without the presence of the free surface when the effect is not of importance. This would save time and money. Two extra cases have been simulated to quantify the effect of the FS may have on the resistance convergence. These correspond to the domains presented in Table 5.4 and 5.6. The tables correspond to Figure A.1 and A.3 in Appendix A, respectively. Furthermore, the refinement of the two computational settings are equal to refinement 4 for their respective cases.

Figure 6.3 presents the resistance convergence history of the computations conducted without the presence of the FS with both hull geometries. In (a) the whole computation is presented and a closer look at the time domain where the simulation stabilises is given in (b). It is clearly seen that the results converge at around 28 seconds for both cases. The computation disregarding the ESD fins stabilises at a value around $24N$ while the numerical computation with the PSS oscillates around a value of approximately $54N$. The oscillation at the latter may be due to the presence of the PSS which may generate fluctuating vortices and thus fluctuating forces. It also may be an effect of simulating the whole domain vs half a domain. However, it is hard to conclude without any further investigation on the topic.

Taking into account the magnitude of the resistance obtained, both are within acceptable limits. The naked hull obtains a value of $24N$ for half a vessel, which results in a total model scale resistance of $48N$. Although it is a bit low, it is in agreement with the resistance obtained with the presence of the FS indicating that simulation without the FS may be acceptable. For the computation with the presence of the PSS the resistance value obtained is $53.85N$. Thus showing good agreement with both formerly conducted CFD and EFD of around $54N$.

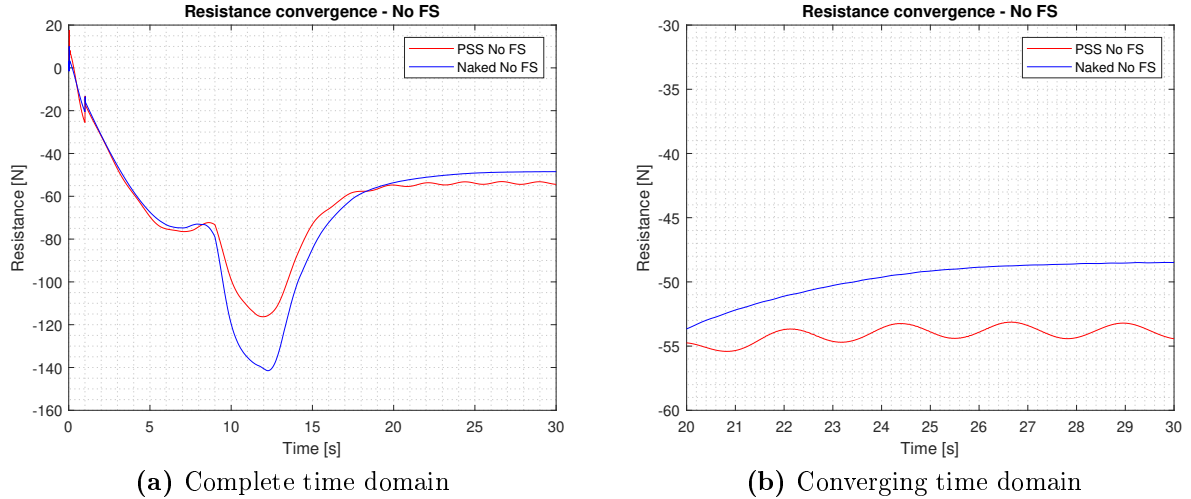


Figure 6.3: Resistance convergence - No FS

Comparing the convergence history for both with and without FS it is seen that the computation without the FS stabilises around 5 seconds (500 time steps) later for both geometries. Studying the amount of time spent in each computation, presented in Table 6.1, a significant difference is seen. The computational time decreased with 30.84% and 60.86% in for PSS and naked, respectively. This indicates that conducting numerical computations in cases where the FS is of no importance, may save valuable time and thus money. It should be mentioned that computational efficiency is highly dependent on computer architecture, therefore the current study had highly varying results with respect to computational time. Nevertheless, if the computer power is properly distributed and controlled it may introduce significant savings.

	PSS with FS	PSS no FS	Naked with FS	Naked no FS
Number of cores	30	30	16	16
Computational time	2181.225 min	1508.58 min	2112.99 min	826.97 min
Relative difference	30.84%		60.86%	

Table 6.1: Comparison of numerical simulation - with and without the presence of FS

The nominal wake field obtained with and without the presence of the FS is presented in Figure 6.4 and 6.5 for naked and PSS, respectively. Comparing the wake field obtained without and with the FS for naked hull it is seen that the wake without FS is captured in a satisfying manner. The wake fraction magnitude is, in general, nearly equal over the entire rotative disc. The bilge and keel vortices are present at the same location with axial velocity magnitude in the same order. This also holds for the high fraction area near the hub at 180° and the wake peak area. Some small, nearly negligible, deviations is seen in the outer region from 120° to 240°.

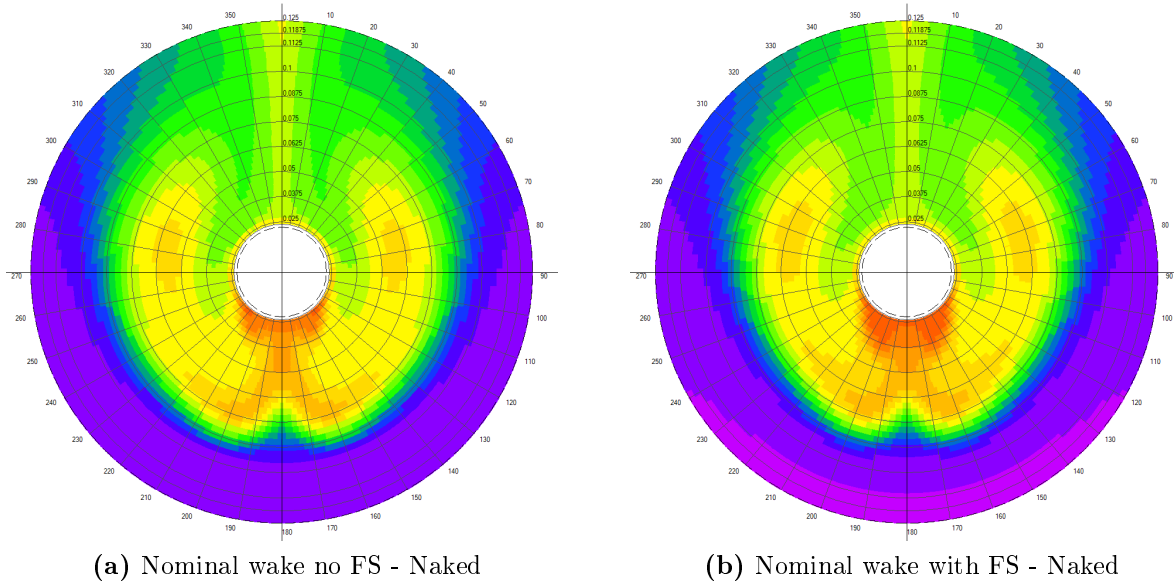


Figure 6.4: Nominal wake field comparison - w FS vs. no FS (Naked)

The computation of the hull with PSS while disregarding the FS also introduces promising results. The wake field distribution is nearly identical to the one obtained with the presence of the FS. The shadows of the ESD fins are distinctly presented and the high wake fraction near the hub is captured. Both bilge and keel vortices are captured at the correct location and the velocity component is in the same order. However, some small deviations in magnitude is seen at the wake peak area and at high wake fraction areas.

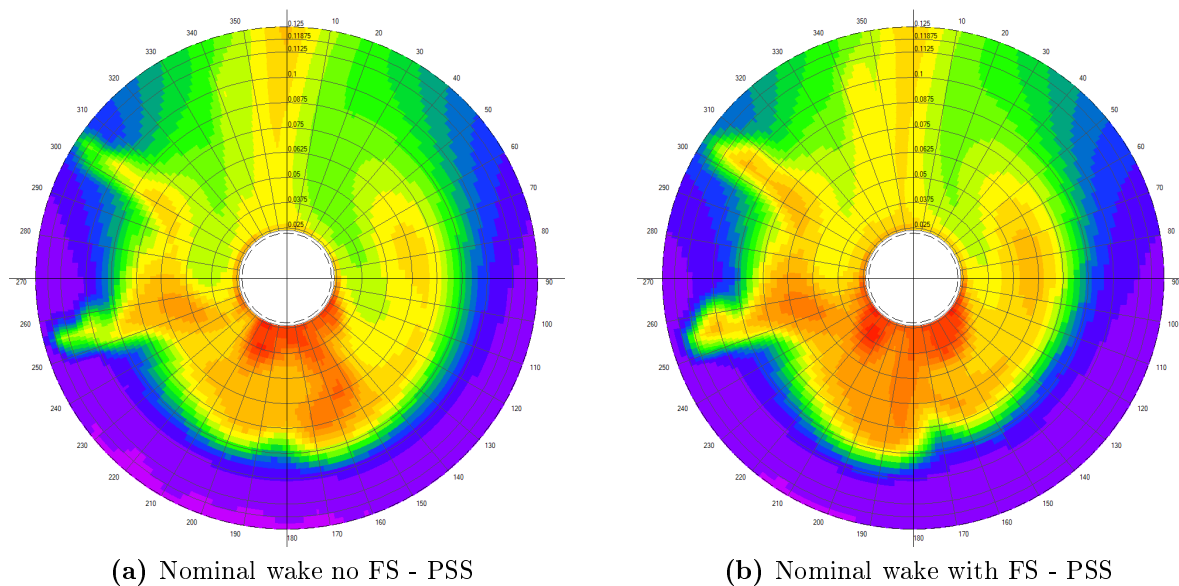


Figure 6.5: Nominal wake field comparison - w FS vs. no FS (PSS)

The presented results of computation without the presence of the FS a large reduction is seen. Up to 60% of computational time is reduced while the wake field is nearly identical with the one obtained with the FS. This points towards that significant savings may be achieved by introducing such methods to wake field and therefore propeller analysis. These results are however only indicators and does not conclude that all computations disregarding FS introduces savings. Each numerical computation must be properly interpreted with respect to the fluid dynamics and handled with care.

6.1.3 Nominal Wake Field

The nominal wake field changes as the refinement near the propeller location increase and may indicate a point of which the computations converge. Figure 6.8, 6.9, 6.10, 6.11, 6.12 and 6.13 illustrates how the nominal wake field of the computation including the presence of the PSS changes as the number of grid points in the refinement increases.

As the number of cells is increasing it is clearly seen that the velocity field changes. Studying the wake peak one can see the gradients of the velocity changing where the wake fraction is highest at the center section. Moving from the hub to the blade tip at 0° the velocity gradients are nearly equal for all refinements except refinement number 6. Furthermore, the low velocity regions close to the hub in the second and third quadrant is in the same order for all refinement. However, an oddly high wake fraction is observed close to the hub in refinement 6. Both these observations indicate that there may be something inaccurate with the numerics in refinement 6. Looking at how the computation catches the presence of the PSS indicates clearly that a higher number of cells has a higher accuracy in predicting the flow. This is seen by the change in axial velocity around the area of the PSS. Additionally a small change is seen in the vector representation of the combined tangential and radial velocity. Thus slightly changing direction as the number of grid points increase in the domain. The vector plot of tangential and radial velocities is given in Figure F.15 through F.20 in Appendix F.2.1 together with axial velocities for each refinement level.

Refinement 1 to 3 differs clearly from each other before the computation indicate convergence at refinement 4. Comparing the nominal wake obtained at refinement 4 with the nominal wake field obtained by SINTEF through former CFD studies substantiate that the computation is within acceptable limits. Here it is clearly seen that high wake fraction areas are present in the same section and in same order of magnitude. The comparison is illustrated in Figure F.21 in Appendix F.2.1.

The nominal wake field obtained from computations disregarding the PSS clearly illustrate that the obtained results show good agreement with formerly conducted CFD and thus EFD by SINTEF (Krasilnikov et al., 2019). The comparison is illustrated in Figure 6.6 with obtained results from FM in (a) and results obtained by SINTEF in (b). A velocity colour bar was not presented in the paper, making an exact comparison with respect to velocity magnitude difficult. On the other hand, the high wake fraction area close to the hub in between second and third quadrant has equal shape. Additionally the velocity gradient pattern on both starboard and port side correlate well, showing equal shape in most parts of the rotative disk. Tangential and radial velocity, presented as vectors, also

seem to show good agreement. The swirling flow introduced by the hull is as expected, clockwise and counter clockwise for starboard and port side, respectively. Furthermore, the pattern of vortices is clearly present on both starboard and port side at 70° and 290° , respectively. SINTEF's presented wake is computed at a location close to the ESD while the one computed in FM is a bit further downstream (Pos 1), resulting in a larger inner area for the former compared with the latter. This introduces deviation in the position of the vortices due to the no-slip condition at the wall. This may be seen by the difference in radial position of the two vortices being around 0.06m and 0.075m for (a) and (b), respectively. It may also be the reason for the deviation in tangential and radial velocity seen close to the surface at 190° .

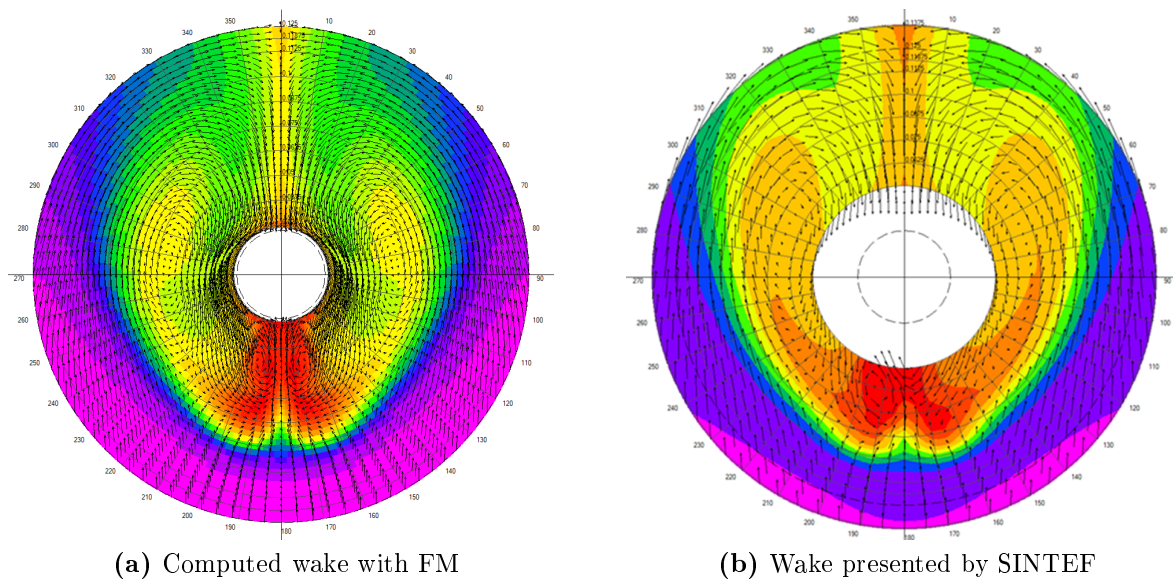


Figure 6.6: Computed naked nominal wake at the position closest to the ESD. Wake obtained by CFD in FM, (a), and wake obtained by SINTEF in the NorSingProp project (Krasilnikov et al., 2019), (b).

Table 6.2 presents the nominal wake fraction for both naked hull and hull with PSS collected from the numerical computations in FM. The values differs as the refinement increases and may indicate that the computations do not converge. This is due to the deviation that is present from refinement 4 to 5, being around 3.5% . On the other hand, the obtained nominal wake fraction supports the argument that refinement 6 is inaccurate as the value is significantly higher than the others.

The wake fraction obtained for the naked hull computation is lower than for PSS which is expected due to the higher loading coming from the adjusted flow. It should be noticed that the transition from refinement 4 to 5 may indicate shortcomings and uncertainties in the simulation as it increases significantly.

		Ref 1	Ref 2	Ref 3	Ref 4	Ref 5	Ref 6
W_T	[PSS]	0.38560	0.38072	0.37927	0.37735	0.36414	0.4005
W_T	[Naked]	0.38238	0.37427	0.37664	0.36539	0.37194	0.37610

Table 6.2: Nominal wake fraction at original propeller position - Ref 1-6 [$J = 0.56$]

The tangential velocity obtained may also strengthen the conclusion that refinement 4 has an acceptable convergence. Figure 6.7 compared the tangential velocity obtained in FM at the location of the original PSS (a) with the tangential velocity plot obtained by (Krasilnikov et al., 2019) in front of the propeller location. The high and low velocity areas close to the hub seem to match well both in placing and in magnitude. On the other hand, there is some deviation seen in magnitude close to the hub at 315° and in general over the whole disc. This is however expected as the conducted CFD only considers model scale, imposing a heavier wake due to Reynolds number effects. Additionally, it does not include the working propeller.

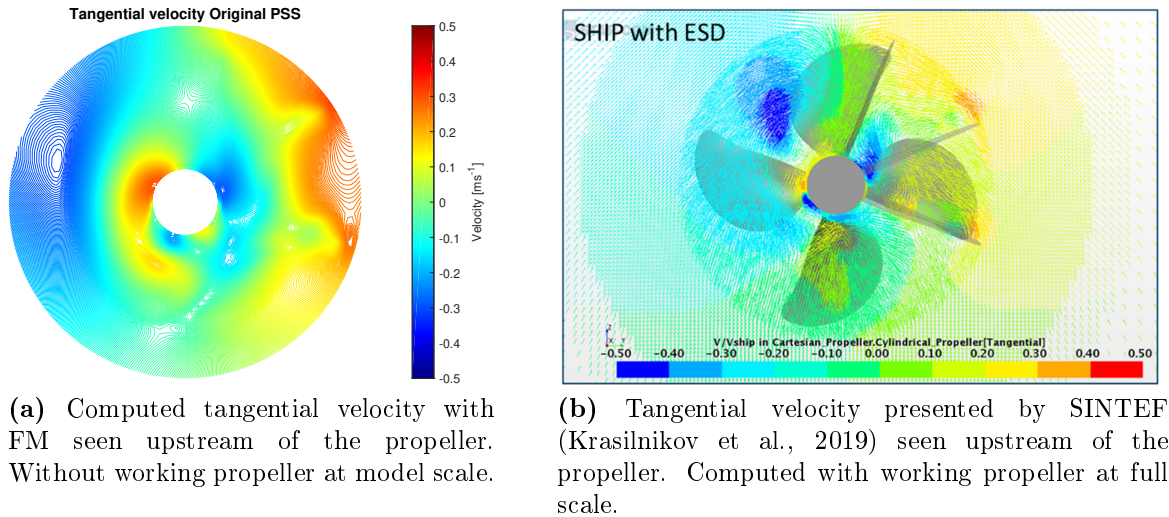


Figure 6.7: Tangential velocity comparison

The visual presentation of the nominal wake for all refinements compared with formerly conducted simulations indicates that the solution converges at an acceptable level at refinement 4. This is however not the case for the obtained nominal wake fraction as it has a significant change from refinement 5-6. On the other hand, it does substantiate that refinement 6 is inaccurate. As a concluding mark for further calculations, the obtained wake fraction, visual interpretation of nominal wake field, tangential velocity plot and the obtained resistance measurements all point towards that grid 4 or 5 should be used. Therefore, due to a significant lower number of grid points which demands higher computer power, refinement 4 is chosen for further consideration in FM and AKPA.

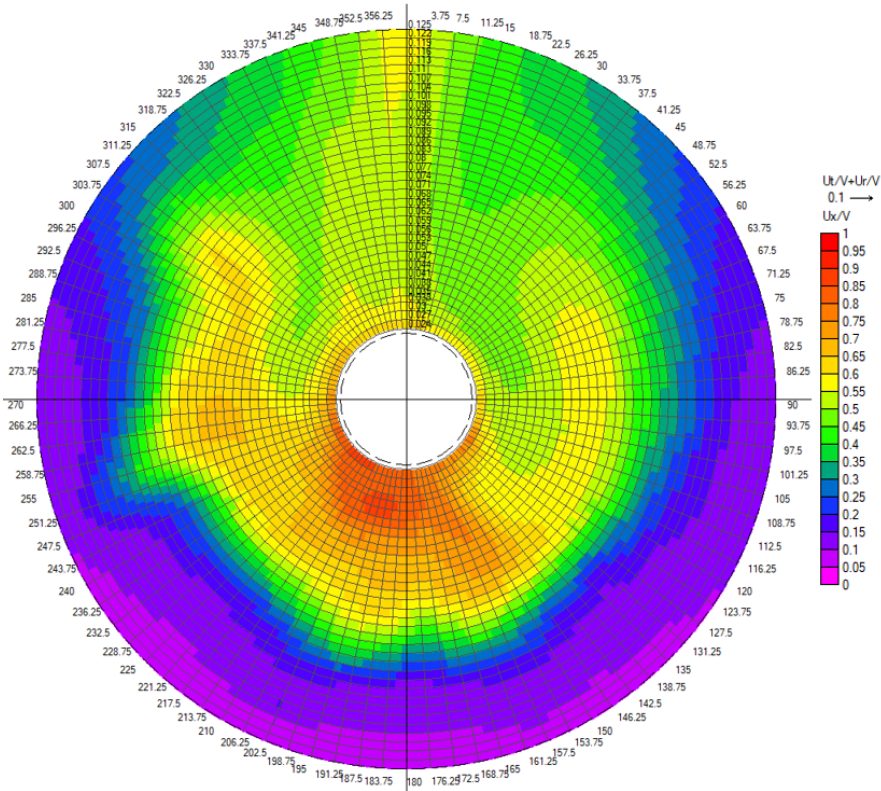


Figure 6.8: Nominal wake field PSS - Refinement 1 Position 4

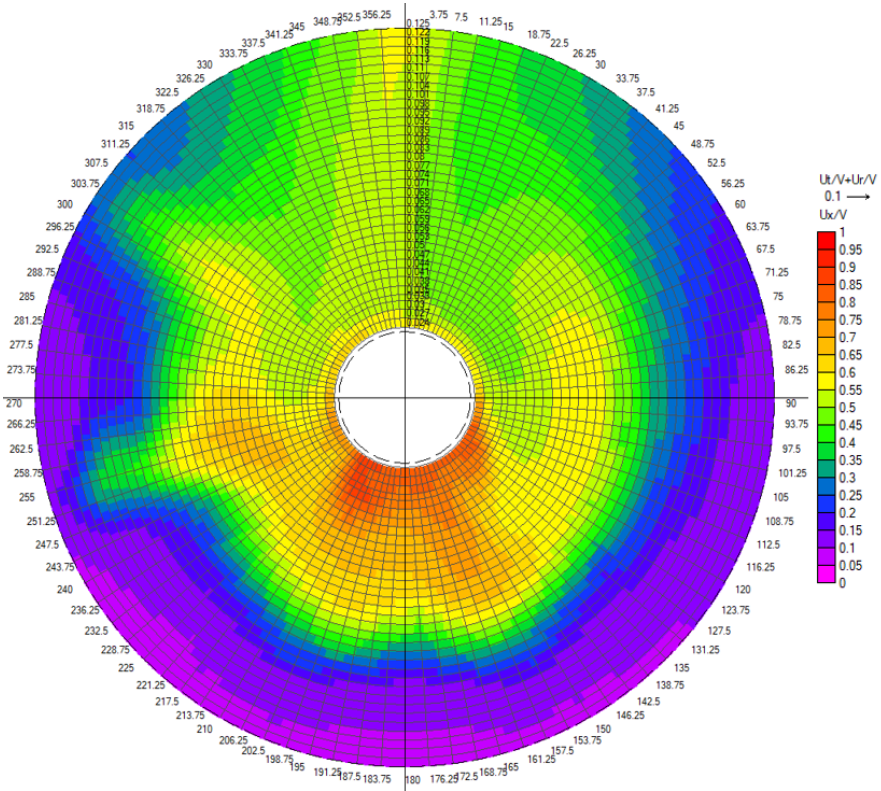


Figure 6.9: Nominal wake field PSS - Refinement 2 Position 4

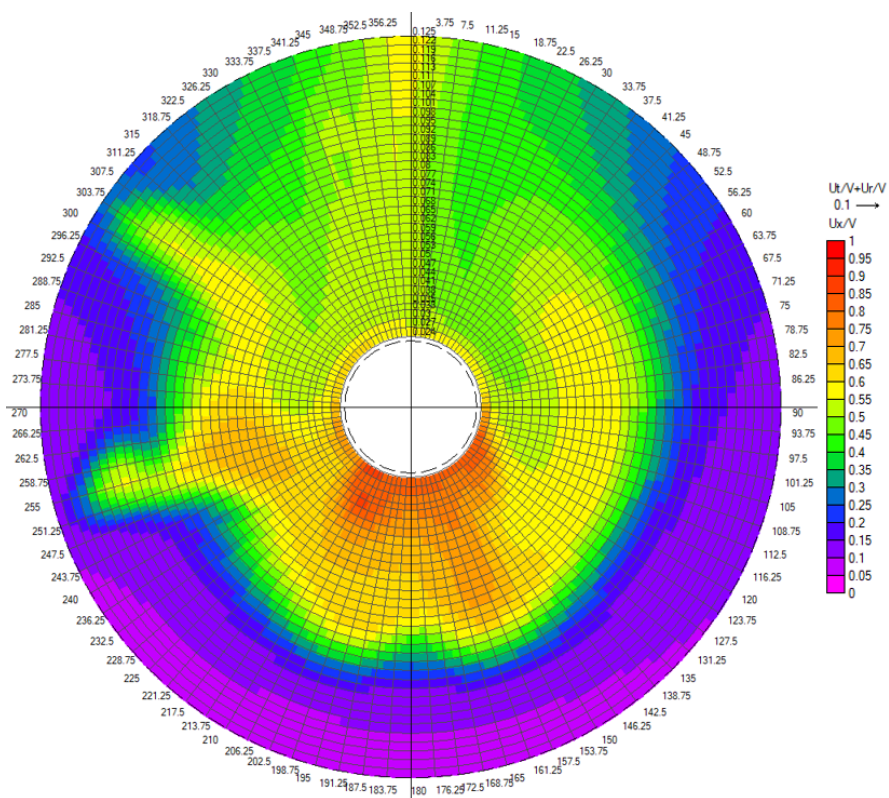


Figure 6.10: Nominal wake field PSS - Refinement 3 Position 4

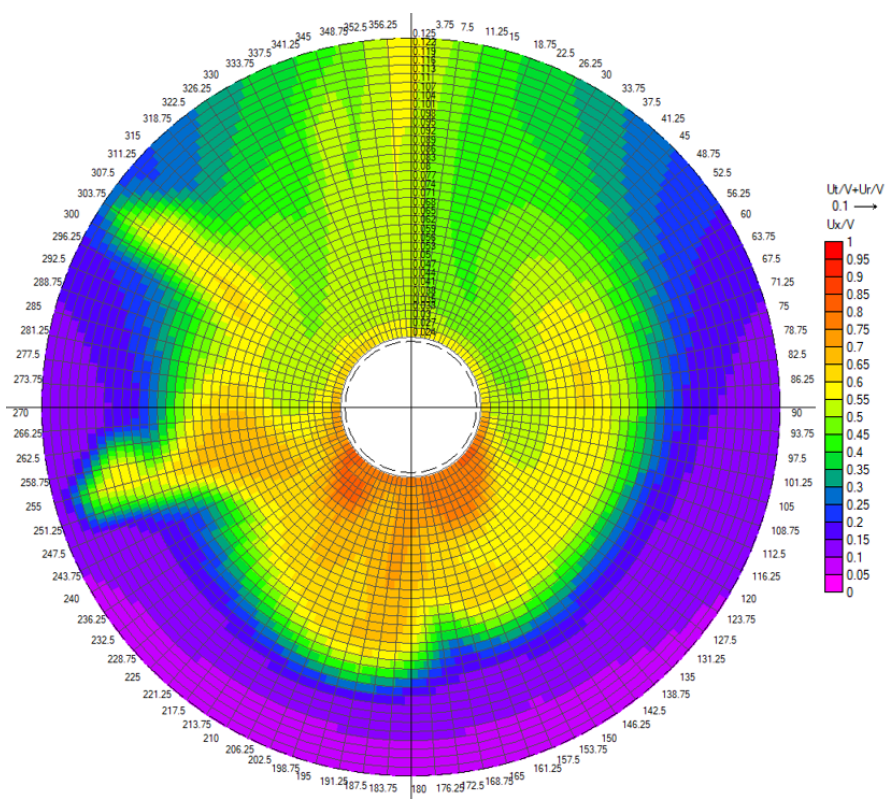


Figure 6.11: Nominal wake field PSS - Refinement 4 Position 4

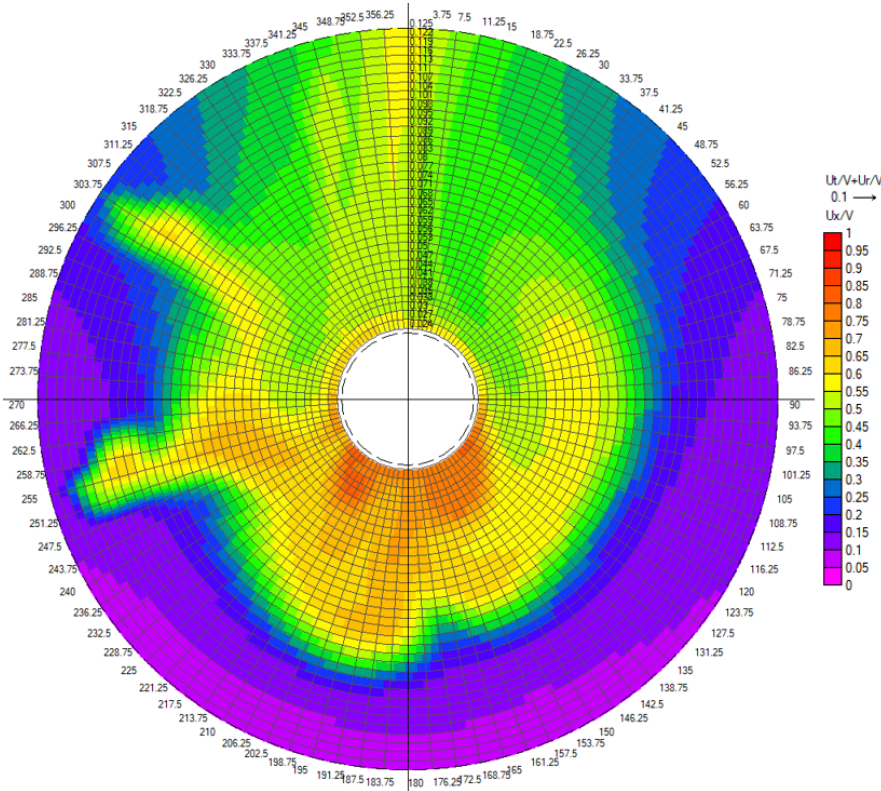


Figure 6.12: Nominal wake field PSS - Refinement 5 Position 4

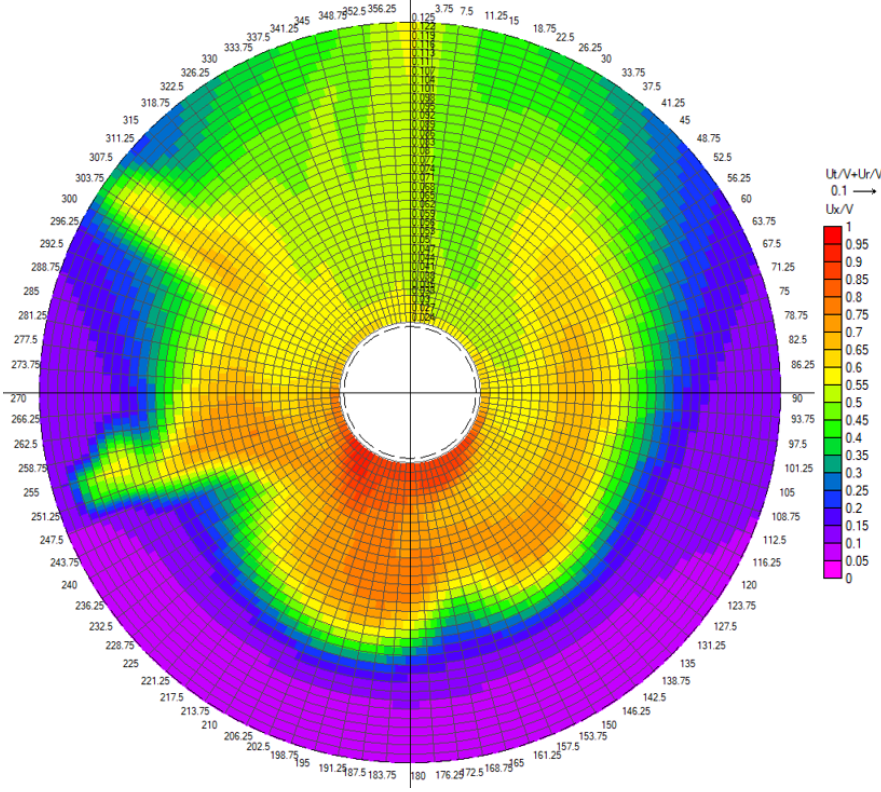


Figure 6.13: Nominal wake field PSS - Refinement 6 Position 4

6.2 Resistance

The total resistance is extracted from the raw numerical computation conducted in FM and is presented in Table 6.3. Experimental values are taken from model tests conducted by SINTEF Ocean in the NorSingProp project. The results obtained by the numerical computations shows good agreement with the experimental values, namely 5.77% and 7.38% lower resistance for naked hull and hull with PSS, respectively. This may be assumed to be within acceptable limits as the numerical model of the chemical tanker disregards air resistance of the superstructure and geometrical appendages such as bow tunnel thruster, bilge keels and rudder. From the obtained CFD results it is seen that resistance decrease by 0.49% when the PSS is introduced in the simulation. Although it is small and within an acceptable limit, it does not correlate with the experimental values and is not expected. The resistance should increase due to larger wet surface area and thus higher viscous resistance. Pressure forces, contributing as resistance, may also appear as a result of the PSS being present.

The deviation may come from the different methods of grid and domain in the numerical set up where the PSS geometry may have been insufficiently discretised. The geometry was discretised in a satisfying manner near the surface, but the box volume refinement did not cover the PSS. Thus, if the box refinement was increased in size so that it covered the PSS it may have increased the accuracy of the obtained resistance. This is however difficult to quantify without further analysis on the subject.

Symbol	Naked hull	With PSS	
R_{TE}	54.04 N	54.71 N	1.24%
C_{TE}	0.00418	0.00423	1.24%
R_{TN}	50.92 N	50.67 N	-0.49%
C_{TN}	0.00394	0.00392	-0.49%

Table 6.3: Total resistance of vessel for EFD compared with CFD of vessel with and without PSS in model scale. Numerical grid correspond to refinement 4.

6.2.1 Stator Drag Resistance

The total resistance may change in the case of adjusted geometry. Although adjusting the PSS geometry is mainly conducted to increase the propulsive efficiency it may also contribute to a lower total resistance. Five different adjustments of the PSS have been numerically simulated in FM and the total resistance is obtained from the same computation. The adjustments are as presented in Table 3.1 and 3.3 in Chapter 3. The total resistance (R_{TN}) is presented in Table 6.4 where it is divided into viscous (R_V) and pressure (R_P) resistance. Furthermore, the relative difference between the original PSS orientation and the adjustment is denoted with the symbol Δ . Figure 6.14 illustrates the relative difference of the respective contributions compared with original PSS.

PSS Adjustment	R_{TN}	ΔR_{TN}	R_V	ΔR_V	R_P	ΔR_P
Original	50.6787 N	—	37.9006 N	—	12.7781 N	—
Adjustment 1	49.9894 N	-1.360%	37.5573 N	-0.905%	12.4320 N	-2.708%
Adjustment 2	50.2692 N	-0.808%	37.5555 N	-0.910%	12.7136 N	-0.505%
Adjustment 3	50.2502 N	-0.845%	37.5553 N	-0.905%	12.6949 N	-0.651%
AoA 1	50.2032 N	-0.938%	37.5569 N	-0.906%	12.6462 N	-1.032%
AoA 2	50.2753 N	-0.796%	37.5566 N	-0.908%	12.7187 N	-0.465%

Table 6.4: Total resistance of vessel for each PSS adjustment. Including viscous and pressure resistance. Adjustments is according to Table 3.1 and 3.3. Numerical grid correspond to refinement 4.

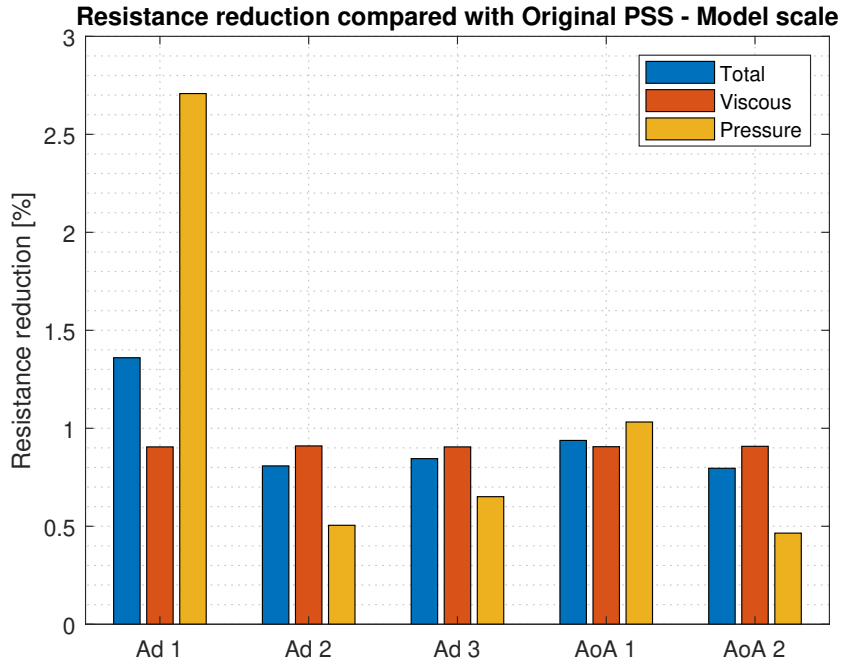


Figure 6.14: Comparison of resistance reduction by PSS orientation. The obtained respective reduction is calculated with respect to obtained value for original PSS orientation. Thus viscous resistance for original PSS is compared with Ad 1 PSS orientation etc.

From the obtained results it is seen that all adjustments impose a lower resistance for both components of the total resistance. The main difference is seen in the pressure resistance where the highest difference is seen in *Adjustment 1* with a deduction of 2.708%. This corresponds to a total reduction in resistance of 1.36%. For the viscous resistance the difference is nearly equal for all five adjustments with a reduction of 0.905% to 0.91%. Based on this it indicates that *Adjustment 1* is the preferred option with respect to resistance. On the other hand, as the numerical computation is run without the propeller working at the aft of the vessel there is uncertainties regarding the presented results. The propeller will induce velocities on the fluid regime which results in a suction force on the hull. This contributes to an increase in resistance of the vessel and is referred to the thrust deduction.

The rudder was not included in the numerical model, introducing other uncertain parameters. The rudder is placed in the slip-stream of the propeller which is affected by the inflow and therefore the PSS. Studies has revealed that the rudder may decrease the gain in power of around 1.5% (Zondervan et al., 2011). Thus, adjusting the stator blades may adjust the slip-stream and therefore contribute to a different resistance contribution from the rudder based on viscous and potential forces. An example of varying resistance forces arising from adjusted PSS orientation was found in (Krasilnikov et al., 2019), where the presence of the PSS increased the rudder resistance coefficient with 2.25%, 6.01% and 3.76% for three different PSS orientations. It should also be mentioned that the study revealed that the stator blade orientation with an increase of 3.76% had the highest total saving with respect to power.

Although the obtained results is achieved conducting numerical computation with respect to the propeller performance it does indicate that the PSS may contribute in other means. Thus reducing the total resistance and gain reduction in power. The results also substantiates the importance of including the rudder in the computation and performing thorough studies on the matter.

6.3 Wake Field Analysis

The propeller wake field and hydrodynamic performance in Section 6.4 is analysed and evaluated at eight different locations including the original position. These are presented in Figure 6.15 where the red rotative disc represents the original propeller plane. The length between each disc is equal and set to $0.082D$. As seen by the figure, the first evaluation section is directly after the PSS location. This position is chosen to be able to quantify how the flow will propagate the total length of the hub, and to determine if the rotative disc should be placed closer or further away from the appended geometry.

Originally only six positions were planned for assessment, but the number was increased to eight as position 1 and 2 may not present a physical wake. This is due to the propeller blades would interfere with the PSS at these two locations. The refinement of the numerical CFD is not designed for a propagating wake field extending aft of the hub. Thus, the results may therefore be less accurate at this area. Furthermore position 7 and 8 may also introduce geometrical constraints due to the rudder placing. However, this

will not be considered in the evaluation of the results, but is highly important in further work. For the evaluation of the naked hull, disregarding the PSS, all eight locations are analysed. The parameters for the propeller positions is presented in Table 6.5.

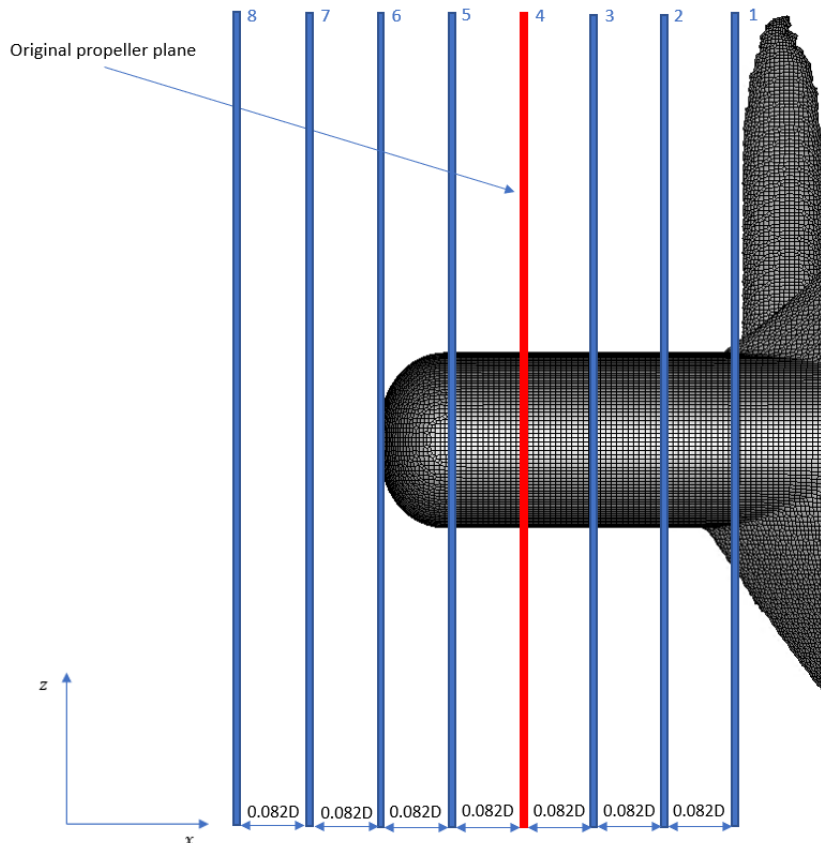


Figure 6.15: Propeller positions

	Position	X [m]	Y[m]	Z [m]	Inner radius [m]	Outer radius [m]
1	0.246D	0.0615	0	0.1369	0.0256	1.1R
2	0.164D	0.0410	0	0.1369	0.0256	1.1R
3	0.082D	0.0205	0	0.1369	0.0256	1.1R
4	Original	0.0000	0	0.1369	0.0256	1.1R
5	-0.082D	-0.0205	0	0.1369	0.0256	1.1R
6	-0.164D	-0.0410	0	0.1369	0.0256	1.1R
7	-0.246D	-0.0615	0	0.1369	0.0256	1.1R
8	-0.328D	-0.0820	0	0.1369	0.0256	1.1R

Table 6.5: Propeller plane evaluation - model scale [Origo (0,0,0) in numerical domain]

6.3.1 Effective Wake Field Analysis

The visual presentation of the effective wake field is an important tool in predicting the hydrodynamic performance of a propeller. Thus, this section will present and discuss axial and transverse components of the wake field for all the respective positions and cases.

Original PSS

Figure 6.16 to 6.21 illustrates the effective wake field for propeller location 3 to 8 for the original PSS orientation, respectively. The presented color scale for axial velocity fraction (U_x/V) is set from 0 to 0.7 to cover the highest and lowest value obtained. Above the color scale included in the figure, a reference vector for the transverse velocity is presented.

Studying the axial wake fraction as the propeller location is moved downstream it is clearly seen that high wake fraction areas decrease in magnitude from around 0.7 to 0.45 from position 3 to 8. This is seen at the wake peak area and in the vicinity of the PSS geometry at 250°, 300° and 345°. Additionally, studying the wake peak area the wake fraction is distinctly decreasing, being "sucked" into the wake peak. Meaning that the low wake fraction area is slowly growing from second and third quadrant into first and fourth quadrant, respectively. It should be noted that the most significant change is detected between position 3 and 4. This is explained by the short distance to the hull and thus higher impact by the boundary layer. In general the wake fractions are decreasing all over the disc section moving downstream, becoming more homogeneous. This is also substantiated by the obtained wake fraction (WT) values presented in Table 4 in Appendix F.3.

The transverse velocity component in the wake field decreases in the same manner as for axial velocity, clearly indicating the coupling between the two. Position 3 experiences two clear bottom stern vortices of significant magnitude close to the hub at 160° and 220°. Smaller vortices are detected as a result of the PSS, seen at the stator fin locations at a radial position of 0.075m. The effect of the PSS geometry is also distinctly marked, adjusting the flow to meet the clockwise rotating propeller motion. This is seen at the radial position going from the hub to about 0.065m in the angular position 235° to 330°. The wake peak area on the starboard side also benefits from the adjusted flow, but not at equal magnitude. Furthermore, a small vortices are present at 215° and 195° for radial position 0.075m and 0.0875m, respectively. However the strength of these are not of significance, additionally they do not seem to decrease downstream.

Studying the effect of moving the propeller location downstream, the bottom stern vortices diminish in strength and move closer to the hub. This is also seen for the vortices generated by the PSS. On the other hand, the adjusted flow on the starboard side does not decrease in strength. Therefore the effect of the PSS is sustained while achieving a better inflow condition to the propeller blades. Subsequently, this indicates that moving the rotative disc downstream will achieve better results. This often lowers the risk of cavitation, changes the obtained efficiency in a positive manner and lowers fuel consumption. Therefore, the position furthest downstream may be expected to deliver

better results. At position 6-7 there is seen a clear effect of the hub geometry ending, the swirling of flow towards the centre which in general is negligible due to it being non-physical if the propeller had been included at this location in the simulation.

Naked hull

The naked hull experiences similar trend as seen in previous section regarding the original PSS. The naked hull transition is illustrated in Figures F.7 to F.14 in Appendix F.1.1. The wake fraction reduces significant during position 1 to 4 and continues to decrease moving downstream. The bottom stern vortices are strong near the hull while the magnitude reduces at a steady rate over the length of the hub. The bilge vortices seem to be steady in position and strength over the whole length. This points towards a lighter wake and therefore more suitable design condition for the propeller.

Adjusting PSS Orientation

The effective wake fields for all five PSS orientations is presented in Appendix F.2.2. Studying the different orientations a nearly equal tendency is observed compared to the original PSS. The axial wake field reduces significantly over position 3-4 and continues decreasing further downstream. The high wake fraction areas seem to rotate and thus reducing from starboard and port side into the wake peak area. Additionally, the tangential velocity vector field experiences strong vortices at the same areas as for original PSS, at the bottom stern, stator blade position and bilge, results indicate that the vortices experience equal reduction in magnitude moving downstream while the effect of the PSS is still present. This indicates that for all the PSS orientations an increase in efficiency and thus lower fuel consumption may be expected.

To differentiate between the five PSS adjustments compared with original PSS, the original propeller location (4) is chosen as the comparison basis. These are illustrated in Figure F.52 to F.56 in Appendix F.2.2. A clear but minor difference between the orientations in both vector fields and wake fraction over the rotative disc is seen. The most distinct changes is seen at the location of the ESD fin at the wake peak. The magnitude of the axial flow is decreased for all except AoA 2. At the two lower fins the fraction is equal for AoA 1 and 2, but decreases for the other orientations. The transverse velocity field does not experience abrupt changes, but has some small deviation in magnitude. Area of highest interest for this component is also the wake peak. However, it is difficult to draw any conclusion with regard to propeller performance by only studying the effective wake field. Therefore, to differentiate between the cases the performance coefficients must be evaluated.

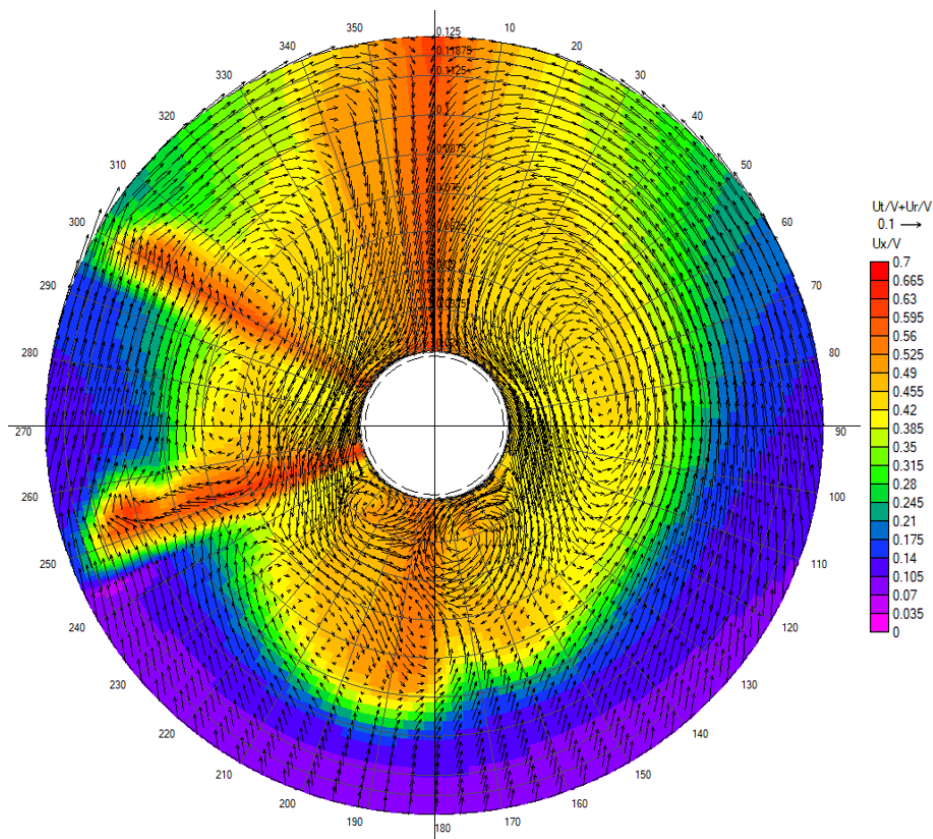


Figure 6.16: Effective wake field Original PSS - Position 3

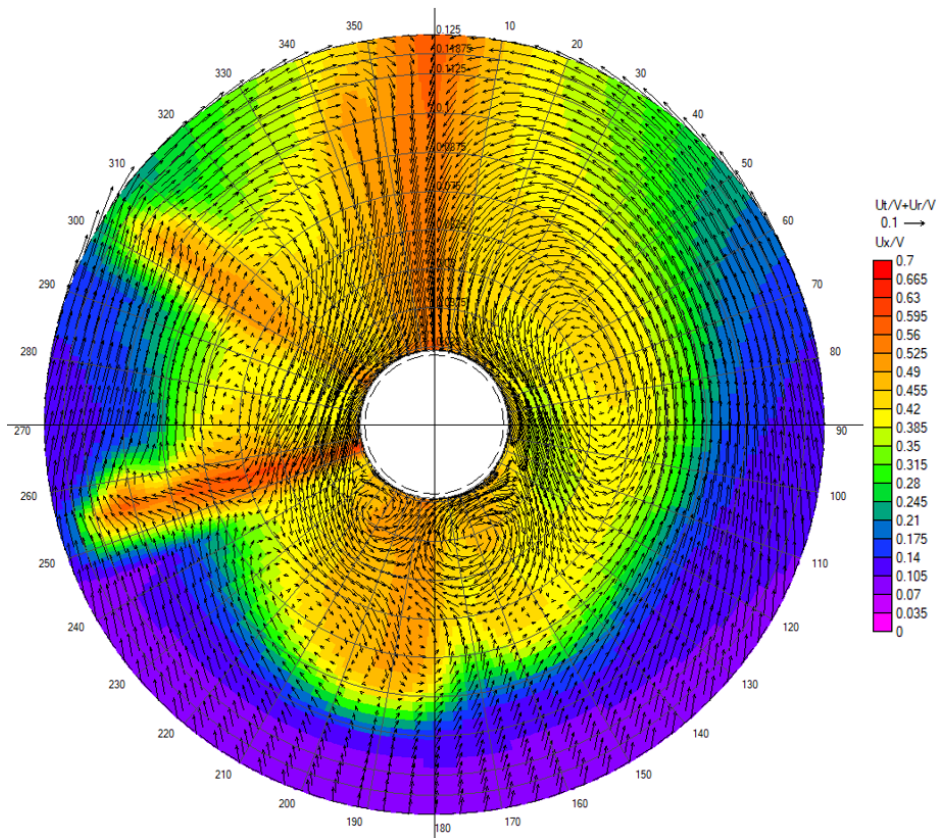


Figure 6.17: Effective wake field Original PSS - Position 4

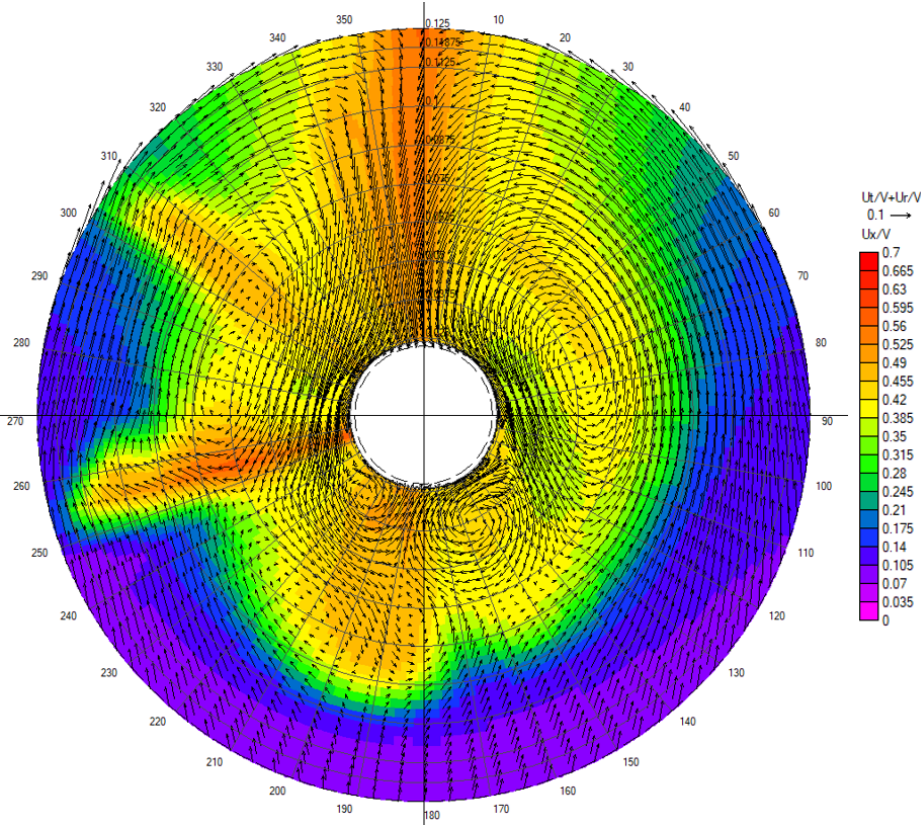


Figure 6.18: Effective wake field Original PSS - Position 5

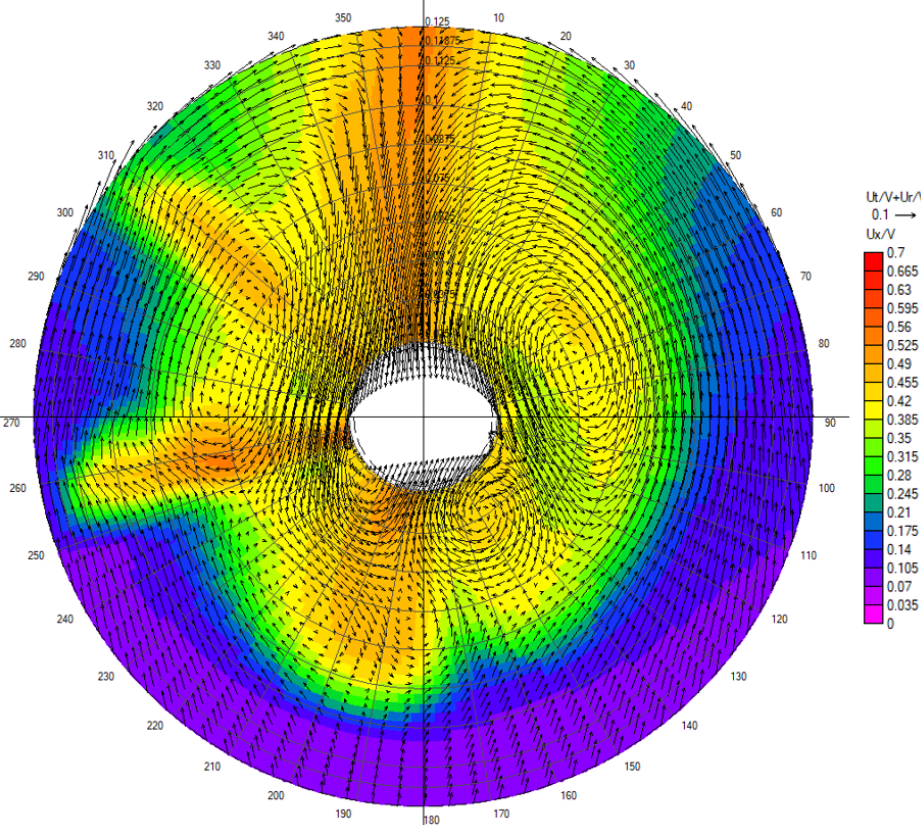


Figure 6.19: Effective wake field Original PSS - Position 6

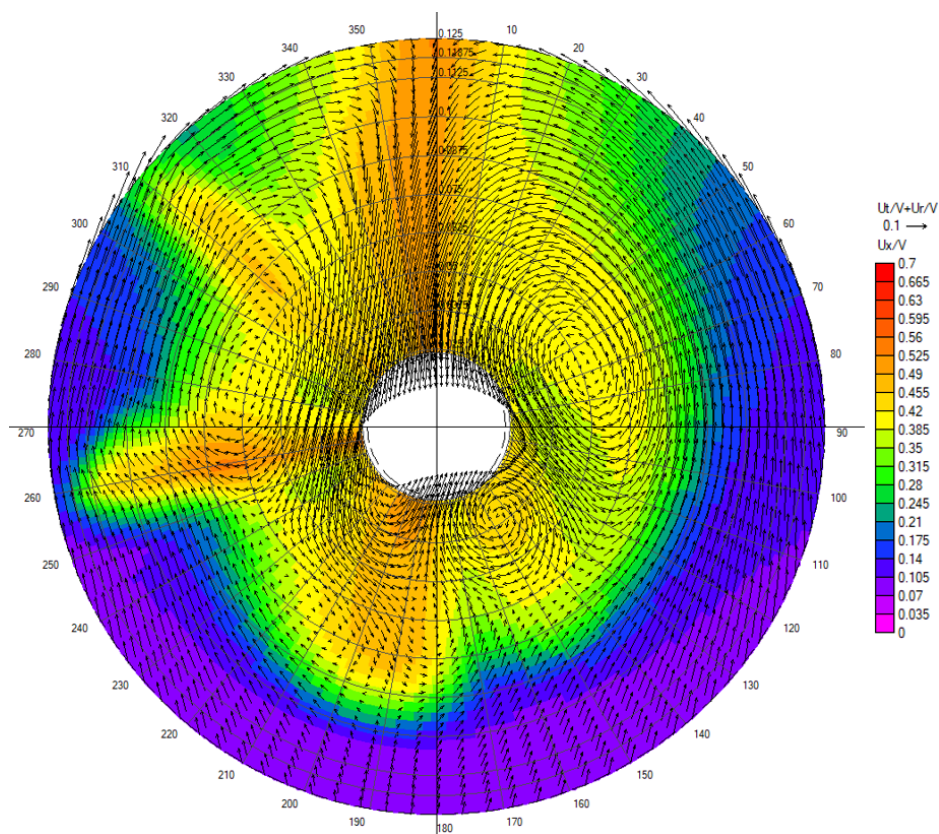


Figure 6.20: Effective wake field Original PSS - Position 7

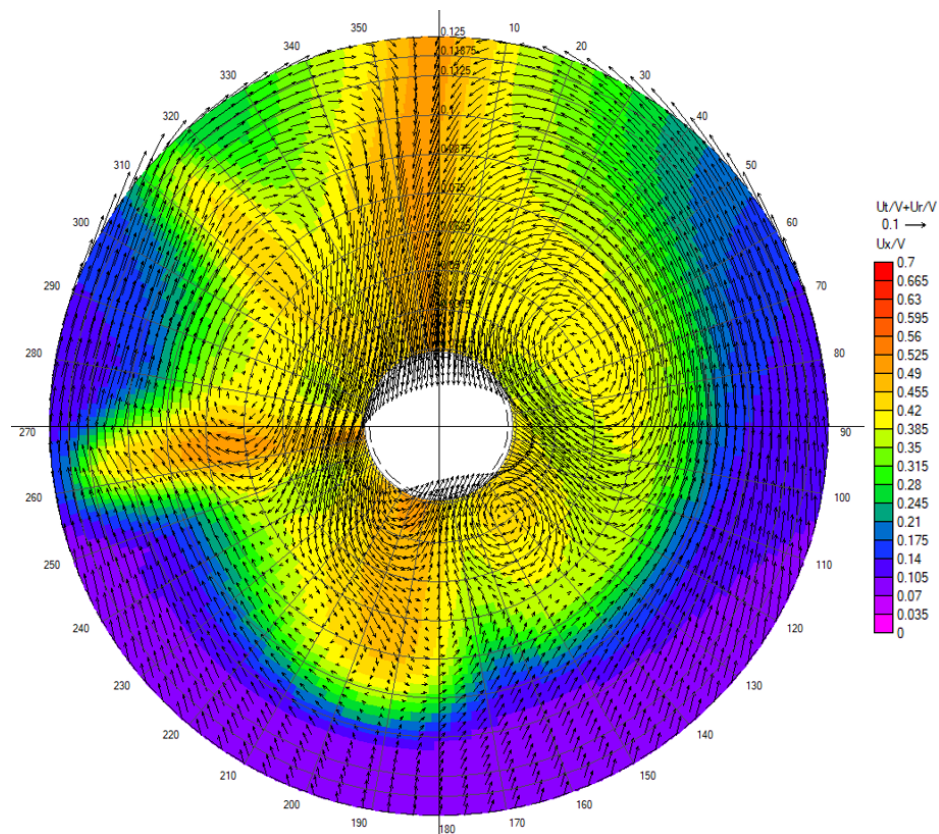


Figure 6.21: Effective wake field Original PSS - Position 8

6.4 Propeller Location Analysis

6.4.1 Hydrodynamic Performance - Hull w and w/o PSS

The propeller hydrodynamic performance is obtained through the AKPA analysis tool and the results are presented as dimensionless coefficients for the given locations. Due to the vortex sheets and high velocity gradients in the vicinity of the PSS, AKPA is not able to calculate the effective wake field and thus the hydrodynamic performance coefficients at location 1 and 2. Additionally, the placing of these two disks are not realistic due to the geometrical constraints as formerly discussed. Position 1 and 2 are therefore not considered in the evaluation of propeller location for hull with PSS.

The obtained hydrodynamic performance parameters for both geometries are presented for all eight positions in Table 6.6. Efficiency and shaft delivered power is presented in Figure 6.22 and 6.23, respectively. Thrust and torque coefficients is illustrated in Figure E.1 and E.2 in Appendix E for naked and with PSS, respectively.

Pos	Naked				PSS			
	K_T	K_Q	η_W	P_D [kW]	K_T	K_Q	η_W	P_D [kW]
1	0.26271	0.03329	0.7084	0.20402	—	—	—	—
2	0.25767	0.03279	0.7054	0.20097	—	—	—	—
3	0.25326	0.03236	0.7026	0.19831	0.26463	0.03359	0.7071	0.20590
4	0.24956	0.03199	0.7002	0.19609	0.26093	0.03323	0.7048	0.20366
5	0.24616	0.03165	0.6982	0.19395	0.25776	0.03291	0.7030	0.20172
6	0.24363	0.03136	0.6973	0.19222	0.25564	0.03269	0.7020	0.20034
7	0.24220	0.03124	0.6960	0.19144	0.25426	0.03256	0.7010	0.19955
8	0.24097	0.03113	0.6948	0.19079	0.25306	0.03245	0.7000	0.19888

Table 6.6: Propeller performance for both geometries.

The results show that both thrust and torque reduces as the propeller disc is moved further downstream and increases moving closer to the hull. This is expected as the wake fraction is high close to the hull and decreases moving downstream as seen by the wake field visualisation. Thus the loading on the propeller and torque reduces in the downstream direction and is seen for both naked hull and with PSS. The increase in wake fraction seen for PSS is a result of the stator fins producing pre-swirl and thus slowing down the fluid. The most interesting parameters are the efficiency of the propeller and the shaft delivered power. Efficiency is coupled with thrust and torque and is seen to increase closer to the hull and decrease moving downstream. As expected, the PSS is clearly more efficient for all positions. For both geometries, with respect to efficiency, it indicates that moving the propeller all the way upstream is the most optimal position.

On the other hand, this is not supported by the data obtained regarding the shaft delivered power. The delivered power required to keep the vessel speed constant reduces when the propeller location is moved downstream and increases closer to the hull. This is seen for both geometries and points towards the propeller consumes less power at a

location downstream. Comparing the results at the original propeller location (4) of the two geometries, see Figure 6.23, it is noticed that the required power is 3.86% higher for hull with PSS than naked. This does not match the presented savings of 3.97% by SINTEF (Krasilnikov et al., 2019). The deviation is however explained by the method of calculating the required power, where Krasilnikov has adjusted the propeller rotational speed (n) to meet some sort of equilibrium. In the presented results obtained in AKPA, n was kept constant for all computations. This results, as expected, in a higher required delivered power for the hull with PSS due to the higher wake fraction. Thus higher loading on the propeller and a higher demand of power to keep the rotational speed constant, explaining why naked hull obtains lower fuel consumption.

The unexpected deviation between efficiency and required power may be explained by the absence of the propeller in the numerical computations conducted in FM. The working propeller induces velocities and forces which interfere with the hull, referred to as the thrust deduction. Thus, the conditional propulsive efficiency (η_C), consisting of efficiency in wake and thrust deduction see Equation (6.1), would change. On the other hand, the shaft delivered power obtained in AKPA is not affected by the thrust deduction (MARINTEK, State Marine Technical University, Offshore Simulator Center, 2011). Using the thrust deduction presented by SINTEF in their study ($t = 0.0186$ for PSS) the obtained conditional propulsive efficiency is $\eta_C = 0.5737$ (Krasilnikov et al., 2019). This deviates around 18.6% compared with the efficiency in wake, indicating the importance of thrust deduction. Based on this the efficiency in wake is determined to be inconclusive and therefore not used for further consideration.

$$\eta_C = (1 - t)\eta_W \quad (6.1)$$

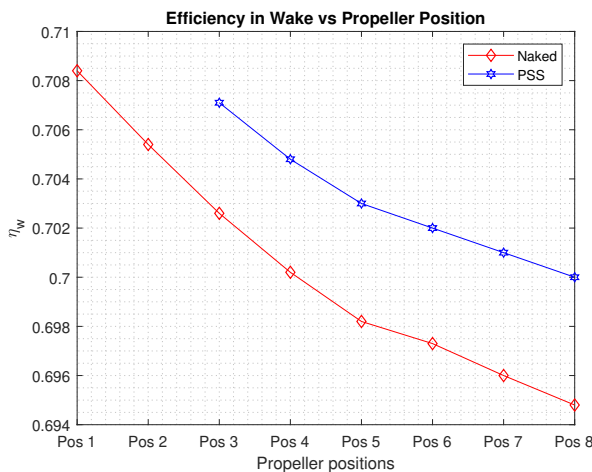


Figure 6.22: Efficiency in Wake vs Propeller Position

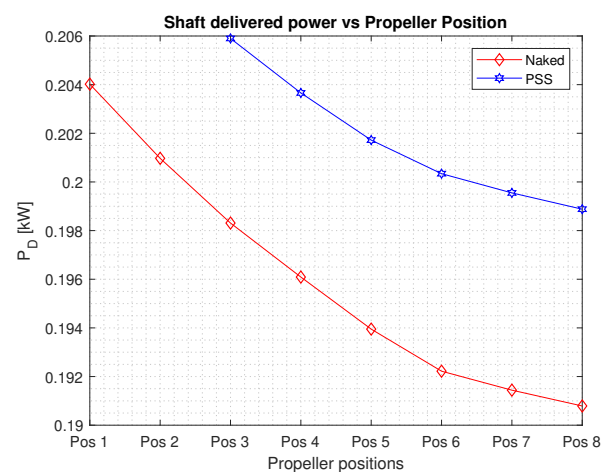


Figure 6.23: Shaft delivered power vs Propeller Position

Neglecting the fact that the thrust deduction may have a significant impact on the results, it points toward a clear conclusion. Moving the propeller further downstream may decrease the required power with 2.35% and 2.70% for PSS and naked hull, respectively. The difference is obtained by comparing original position (4) and position (8). It should be mentioned that the presence of the rudder may constrain the possibility of moving the propeller this far downstream. Nevertheless, the shortcoming of not including the propeller in the simulation introduces uncertainties to the results. This implies that further numerical computations including the propeller to obtain complete results with higher accuracy is encouraged.

6.4.2 Hydrodynamic Performance - Forward velocity

The forward velocity of the vessel may indicate a different propeller location for higher or lower velocities. Therefore, the hydrodynamic performance of the propeller is evaluated and compared for three different forward velocities.

Naked hull

The analysis is conducted for three different advance numbers, given in Table 5.21, and the obtained results presented as thrust coefficient, torque coefficient and efficiency in wake is presented in Table 6.7, 6.8 and 6.9, respectively. Thrust and torque for each advance number is plotted in Figure E.3, see Appendix E. Where the ship velocity is important, the advance number is presented. $J = 0.484$, $J = 0.564$ and $J = 0.646$ correspond to 12, 14 and 16 knots in full scale, respectively.

For all three advance numbers it is clearly seen that thrust and torque decreases as the propeller location is moving downstream and increase closer to the hull. Indicating that the loading on the propeller and thus wake fraction decreases further away from the hull. This is in accordance with the visual interpretation of the nominal wake fields in Section 6.3. The efficiency decays equal for all advance numbers at the positions downstream and is increased at the respective locations at higher advance number. The parameter is however inconclusive and not considered in the discussion of the results with respect to forward velocity. The reason for this is explained in Section 6.4.1.

K_T			
Pos	$J = 0.484$	$J = 0.564$	$J = 0.646$
1	0.28876	0.26271	0.23730
2	0.28452	0.25767	0.23168
3	0.28077	0.25326	0.22651
4	0.27747	0.24956	0.22218
5	0.27466	0.24616	0.21854
6	0.27239	0.24363	0.21590
7	0.27110	0.24220	0.21417
8	0.26985	0.24097	0.21281

Table 6.7: Thrust coefficient - Naked

K_Q			
Pos	$J = 0.484$	$J = 0.564$	$J = 0.646$
1	0.03591	0.03329	0.03069
2	0.03550	0.03279	0.03013
3	0.03514	0.03236	0.02961
4	0.03481	0.03199	0.02917
5	0.03454	0.03165	0.02880
6	0.03429	0.03136	0.02851
7	0.03417	0.03124	0.02834
8	0.03406	0.03113	0.02822

Table 6.8: Torque coefficient - Naked

Studying the shaft delivered power which does not seem to be affected by the thrust deduction, presented in Table 6.10 and illustrated in Figure 6.24, which indicates the opposite of efficiency. It points towards that the propeller needs less power to sustain forward velocity by placing the propeller further downstream. Additionally the steepness of the power curve seem to flatten out at position 8 indicating convergence. Although the rudder constraints the relocation of the propeller to this position it is interesting to see that it may be a converging limit.

η_w			
Pos	$J = 0.484$	$J = 0.564$	$J = 0.646$
1	0.6194	0.7084	0.7946
2	0.6174	0.7054	0.7900
3	0.6155	0.7026	0.7860
4	0.6139	0.7002	0.7826
5	0.6126	0.6982	0.7797
6	0.6120	0.6973	0.7781
7	0.6111	0.6960	0.7764
8	0.6104	0.6948	0.7747

Table 6.9: Efficiency in wake - Naked

P_D [kW]			
Pos	$J = 0.484$	$J = 0.564$	$J = 0.646$
1	0.22011	0.20402	0.18807
2	0.21758	0.20097	0.18469
3	0.21536	0.19831	0.18148
4	0.21337	0.19609	0.17879
5	0.21167	0.19395	0.17652
6	0.21014	0.19222	0.17474
7	0.20944	0.19144	0.17371
8	0.20873	0.19079	0.17299

Table 6.10: Shaft delivered power - Naked

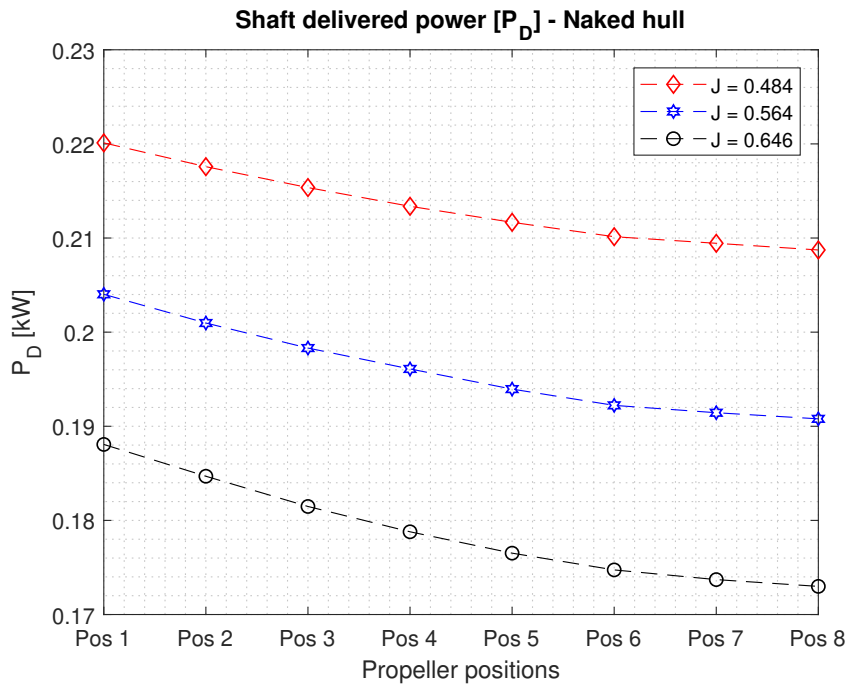


Figure 6.24: Shaft delivered power - Naked. Three different advance numbers.

Hull with PSS

Thrust and torque coefficients for each advance number with PSS is presented in Table 6.11 and 6.12 and is illustrated in Figure E.4, see Appendix E. Both thrust and torque decrease from position 3 to 8 at all three advance numbers. Compared with the naked hull, the thrust coefficient and consequently the torque is higher including the presence of the PSS. Similar to the naked hull, the same decreasing behaviour of efficiency is obtained and presented in Table 6.13. However it is neglected from discussion.

K_T			
Pos	$J = 0.484$	$J = 0.564$	$J = 0.646$
3	0.29183	0.26463	0.23879
4	0.28846	0.26093	0.23454
5	0.28565	0.25776	0.23098
6	0.28357	0.25564	0.22865
7	0.28253	0.25426	0.22701
8	0.28109	0.25306	0.22554

Table 6.11: Thrust coefficient - PSS

K_Q			
Pos	$J = 0.484$	$J = 0.564$	$J = 0.646$
3	0.03632	0.03359	0.03097
4	0.03599	0.03323	0.03054
5	0.03571	0.03291	0.03018
6	0.03548	0.03269	0.02993
7	0.03540	0.03256	0.02977
8	0.03526	0.03245	0.02963

Table 6.12: Torque coefficient - PSS

Considering the shaft delivered power, given in Table 6.14 and illustrated in Figure 6.25, it decreases moving downstream for all three advance numbers. Lower advance number is seen to require higher power and is expected, due to higher loading at lower velocity with equal propeller rotation. Comparing position 8 with respect to position 3, a relative reduction of 2.9%, 3.41% and 4.31% is obtained for low to high advance number, respectively. Thus implying higher savings at higher advance numbers and that propeller position 8 may introduce significant savings.

η_w			
Pos	$J = 0.484$	$J = 0.564$	$J = 0.646$
3	0.6190	0.7071	0.7922
4	0.6175	0.7048	0.7891
5	0.6162	0.7030	0.7863
6	0.6156	0.7020	0.7850
7	0.6148	0.7010	0.7835
8	0.6141	0.7000	0.7820

Table 6.13: Efficiency in wake - PSS

P_D [kW]			
Pos	$J = 0.484$	$J = 0.564$	$J = 0.646$
3	0.22257	0.20590	0.18981
4	0.22056	0.20366	0.18719
5	0.21886	0.20172	0.18498
6	0.21747	0.20034	0.18343
7	0.21696	0.19955	0.18246
8	0.21609	0.19888	0.18162

Table 6.14: Shaft delivered power - PSS

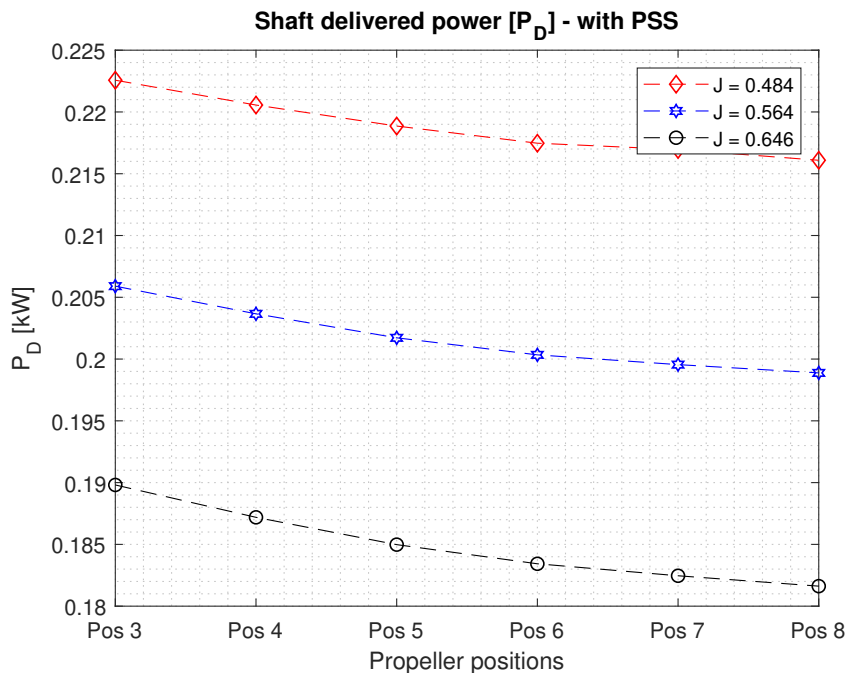


Figure 6.25: Shaft delivered power - PSS. Three different advance numbers.

6.4.3 Hydrodynamic Performance - Adjusted PSS Orientation

The optimal propeller location with respect to the propeller performance may be highly dependent on the PSS orientation due to the adjusted inflow it introduces. Therefore, in this section, the hydrodynamic performance parameters is quantified with respect to the different stator fin adjustments.

Similar to the presented performance coefficient with respect to normal working condition and adjusted forward velocity, thrust, torque and hence efficiency reduces as the propeller location is moved downstream and closer to the rudder. Obtained thrust and torque coefficients i presented in Table 2 and 3, respectively. Efficiency, presented in Figure E.7, follows the same trend and decreases in the same order. However, as discussed, the efficiency does not introduce the correct image of the propeller environment and is therefore not further considered.

The obtained shaft delivered power, presented in Table 6.15 and illustrated in Figure 6.26, decreases for all orientations moving downstream. Some interesting deviations is seen at the respective adjustments. At the first location (3) *Adjustment 1*, *Adjustment 3* and *AoA 1* show lower required power. The two remaining orientations obtains nearly identical values as the original. The highest difference seen at this position is obtained for the decrease in angle of attack (*AoA 1*), presenting a reduction of 0.52%. For the same adjustment, position 4, 5, 6, 7 and 8 obtains a reduction of 0.57%, 0.59%, 0.60%, 0.60% and 0.61%, respectively. These values are compared with original PSS at the respective positions. Thus, it indicates that *AoA 1* required less shaft delivered power at all positions. Studying the other orientations it is seen that all obtains nearly identical results at all positions except 3 and 5. At the latter, *Adjustment 1* has a small reduction, 0.277% , compared with original. The overall reduction of required power at all PSS

orientations moving the propeller further downstream correlates well with the visual evaluation of the wake fields in Section 6.3.

The presented results indicate that moving the propeller downstream will be beneficial for all orientations. However, to determine the effect the adjusted PSS orientation has on the total power consumption and thrust delivery a comparison of the two components is given in Figure 6.27. The thrust produced by the propeller is divided by the shaft delivered power. Although it is similar to efficiency calculation it, which is neglected, it is utilised to differentiate between the orientations. At the position closest to the hull (3) *Adjustment 3* delivers more thrust per unit power than all the other orientations. E.g. 0.12% more than the original PSS. The original orientation is the best option at all the other positions (4-8).

Considering the PSS orientations there is seen small differences in required power at the respective positions. Evaluating each adjustment unaccompanied, the computations indicate that moving the propeller further downstream, within the geometrical constraints, reduces the shaft delivered power and thus requiring less fuel. Comparing achieved thrust per power unit at every location and for all adjustments it indicates that the original PSS delivers the best outcome.

	Orig [kW]	Ad.1 [kW]	Ad.2 [kW]	Ad.3 [kW]	AoA 1 [kW]	AoA 2 [kW]
3	0.20590	0.20544	0.20585	0.20497	0.20482	0.20602
4	0.20366	0.20351	0.20346	0.20338	0.20250	0.20371
5	0.20172	0.20116	0.20173	0.20160	0.20053	0.20178
6	0.20034	0.20021	0.20035	0.20021	0.19913	0.20028
7	0.19955	0.19948	0.19960	0.19946	0.19835	0.19964
8	0.19888	0.19878	0.19876	0.19873	0.19766	0.19878

Table 6.15: Shaft delivered power - PSS Adjustments.

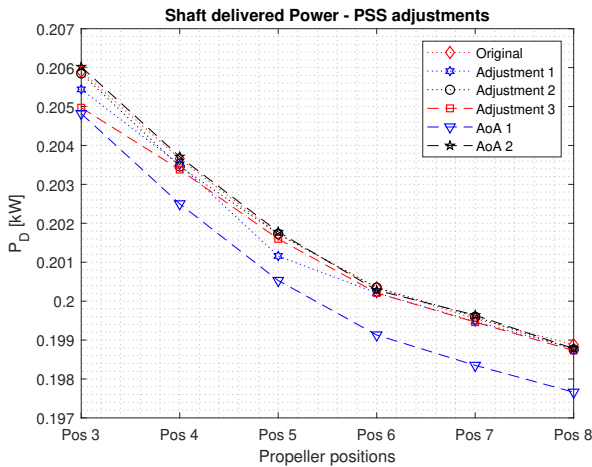


Figure 6.26: Efficiency in wake comparison for different PSS adjustments.

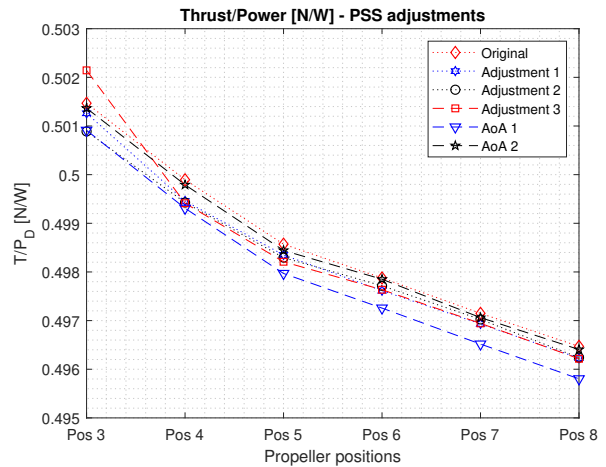


Figure 6.27: Thrust divided by power - Comparison for different PSS adjustments

6.5 Pressure Distribution and Cavitation

6.5.1 Propeller Cavitation Analysis

The pressure distribution over the propeller blade is collected from the visualisation tool in AKPA and is presented by the pressure coefficient for both upper (suction) and lower (pressure) surface at three different rotational angles. These are 0° , 27° and 63° relative to the starting position (0°), in Figure 6.29. Illustrating the propeller at the original position aft of the original PSS with obtained results from computation performed with refinement 4. Figure 6.28 indicates the pressure distribution color scale which is used in the illustration. The maximum obtained pressure coefficient for all cases and positions is presented in Table 6.16.

The total pressure coefficient distribution presented is obtained using the tangential velocity of the blade tip (nD), see Equation (6.2), and the maximum obtained value is located at the blade tip at 0° . The pressure starts to increase at around 330° , peaks at 0° and is reduced to a minimum at 150° . Compared with the findings of (Krasilnikov et al., 2019) the location and value of pressure distribution show good agreement. The cavitation areas at the blade tips presented in the study is not seen in the obtained results. This is explained by the fact that the study was conducted at full scale ballast draught, being more prone to cavitation, and the AKPA analysis is executed at model scale design condition. Considering all PSS orientations and velocity changes, equal results is obtained. Thus experiencing the highest pressure coefficient at the blade tip in the wake peak region.

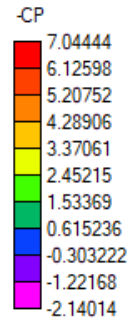


Figure 6.28: Pressure distribution color bar (C_P).

$$V_{tan} = nD \quad (6.2)$$

Propeller pos	1	2	3	4	5	6	7	8
Naked hull [12kn]	6.176	6.777	6.471	6.195	5.968	5.794	5.634	5.512
Naked hull [14kn]	6.041	5.611	5.287	4.996	4.751	4.562	4.359	4.226
Naked hull [16kn]	5.199	4.752	4.402	4.089	3.839	3.652	3.475	3.356
PSS Original [12kn]	–	–	8.421	7.964	7.681	7.278	7.255	7.054
PSS Original [14kn]	–	–	7.517	7.044	6.700	6.373	6.234	6.038
PSS Original [16kn]	–	–	6.621	6.131	5.785	5.460	5.325	5.125
PSS Adjustment 1	–	–	7.432	6.917	6.677	6.505	6.271	6.048
PSS Adjustment 2	–	–	7.242	6.980	6.780	6.542	6.298	6.071
PSS Adjustment 3	–	–	7.393	6.905	6.672	6.474	6.277	6.018
PSS AoA 1	–	–	7.471	7.006	6.666	6.343	6.203	6.029
PSS AoA 2	–	–	7.484	7.057	6.701	6.397	6.238	6.037

Table 6.16: Pressure coefficients $-(C_P)$ - Cavitation data. Highest value obtained is presented. All simulations are run at a velocity corresponding to 14 knots unless otherwise stated.

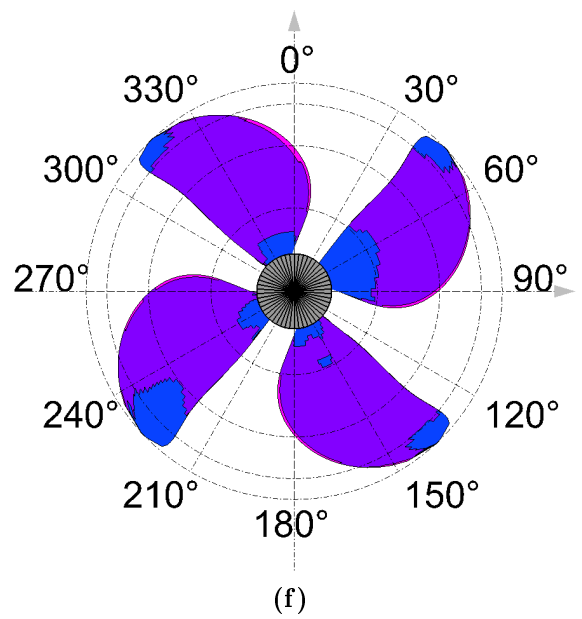
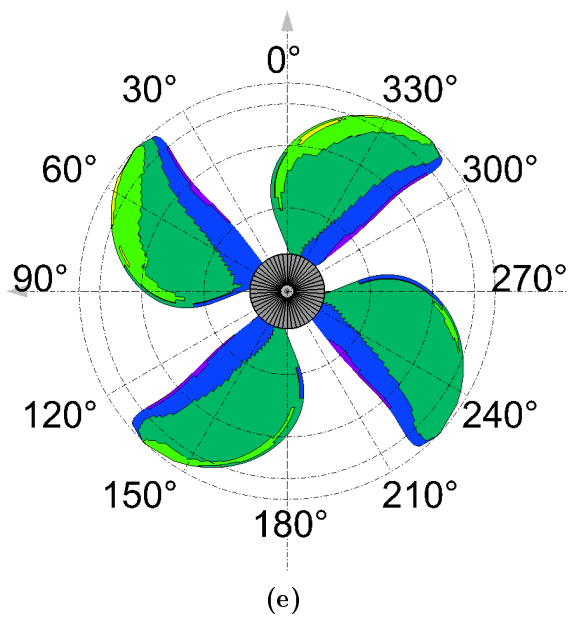
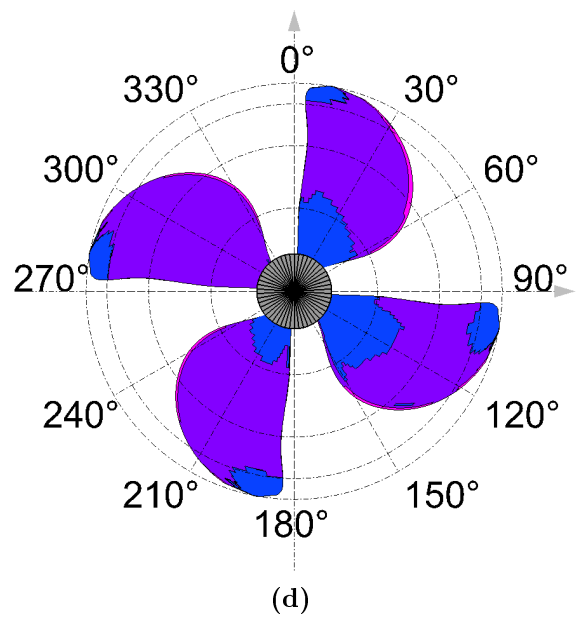
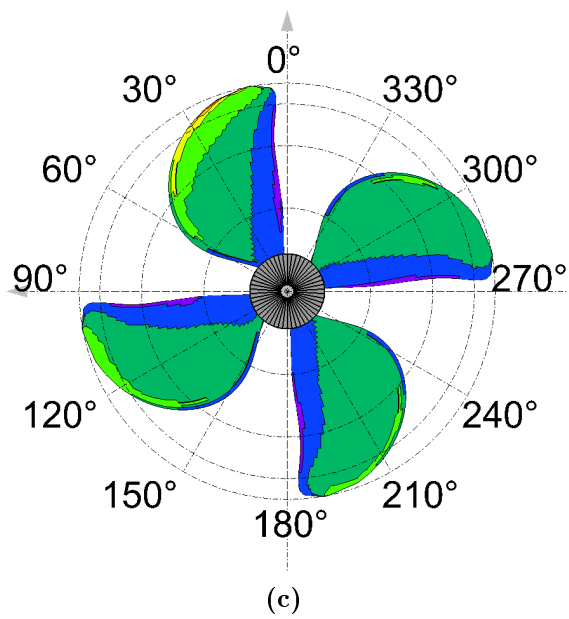
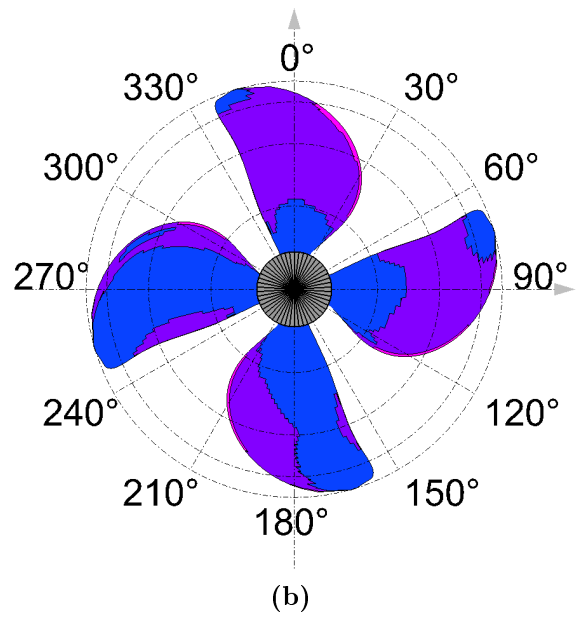
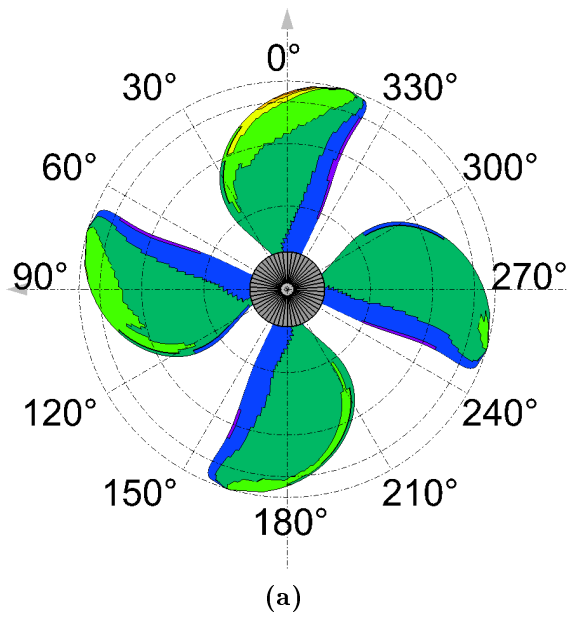


Figure 6.29: Pressure distribution ($-C_P$) PSS Original Pos 4: [(a)-(b) 0°], [(c)-(d) 27°], [(e)-(f) 63°]

The pressure coefficient alone does not reveal the probability of cavitation occurrence. The probability is evaluated by the cavitation number and the local pressure coefficient, with the inception criteria, along the propeller blade. The inception criteria, presented in Equation (2.4), defines a limit of which cavitation occurs, although it may be affected by other parameters. By calculating the cavitation number over the chord length at all radial positions and dividing the pressure coefficient on the obtained value it is possible to present the areas of the propeller that may experience cavitation. Thus, if the obtained number is equal or larger than one, presented in Equation (6.4), cavitation may occur. The local pressure coefficient is obtained using the local transferral velocity, see Equation (6.3), over each foil profile at every radial position.

$$V_{trans} = \sqrt{V_{\infty}^2 + (2\pi nr)^2} \quad (6.3)$$

$$1 \leq \frac{-C_P}{\sigma_0} \quad (6.4)$$

Table 6.17 presents the maximum values obtained in the propeller analysis with respect to the criterion. It also includes the relative difference between position 4 and 8, denoted Δ_{4-8} . An illustration of the cavitation exposed areas is presented in Figure 6.31 and is based on the transferral velocity component at every blade section. It is similar to the pressure coefficient, with three angular positions including both sides of the blade and an inflow from the original PSS at position 4. The color bar for the presentation is equal to the one in Figure 6.30 where the red color indicates the highest value obtained in the analysis.

Propeller pos.	1	2	3	4	5	6	7	8	Δ_{4-8}
Naked hull [12kn]	0.225	0.213	0.203	0.194	0.187	0.181	0.176	0.172	-11.34%
Naked hull [14kn]	0.189	0.176	0.165	0.156	0.148	0.142	0.137	0.133	-14.74%
Naked hull [16kn]	0.162	0.148	0.137	0.127	0.119	0.113	0.108	0.104	-18.11%
PSS Original [12kn]	–	–	0.266	0.251	0.242	0.229	0.228	0.222	-11.55%
PSS Original [14kn]	–	–	0.237	0.222	0.211	0.200	0.196	0.189	-14.86%
PSS Original [16kn]	–	–	0.208	0.193	0.181	0.171	0.167	0.160	-17.09%
PSS Adjustment 1	–	–	0.234	0.218	0.210	0.204	0.197	0.189	-13.30%
PSS Adjustment 2	–	–	0.228	0.219	0.213	0.206	0.198	0.190	-13.24%
PSS Adjustment 3	–	–	0.233	0.217	0.209	0.203	0.197	0.189	-12.90%
PSS AoA 1	–	–	0.235	0.221	0.209	0.199	0.195	0.189	-14.47%
PSS AoA 2	–	–	0.236	0.222	0.211	0.200	0.196	0.189	-14.86%

Table 6.17: Cavitation inception ($-C_P/\sigma_0$). All simulations is run at a velocity corresponding to 14 knots unless otherwise stated. Δ_{4-8} presents the relative difference between original position (4) and furthest downstream (8).

Both sides of the propeller blade is illustrated in Figure 6.31 indicating that the area experiencing the highest values is the front leading edge from radial position $r/R = 0.7$ to $r/R = 1.0$ in the wake peak area, more specific 0° to 9° . A closer look at this region is presented in Figure 6.30 depicting how the plausibility of cavitation increases closer to the blade tip. Although the values obtained indicates that the risk of cavitation is low it must be properly evaluated. Taking into account that the results is obtained in model scale and that Reynolds number effects arise when it is scaled up to ship size, thus it may indicate risk of tip cavitation. This is in agreement with the visual cavitation presentation in (Krasilnikov et al., 2019) conducted at full scale.

Studying the obtained results it is clearly seen that all the values is significantly lower than the criterion, indicating that cavitation inception most likely will not occur. Considering the propeller location, the risk of cavitation decreases moving further downstream from the body. This is in accordance with the reduction in wake fraction, resulting in a more homogeneous working environment for the propeller blades.

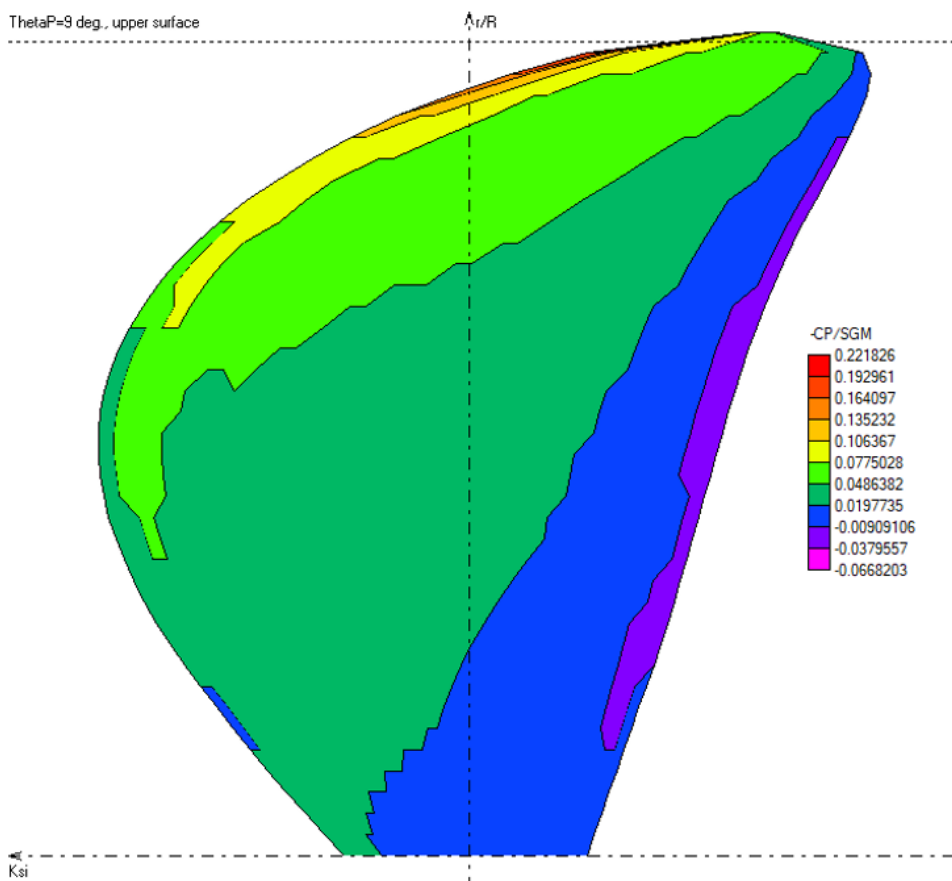


Figure 6.30: Cavitation inception - Propeller blade at 9° rotation. The pressure distribution at the radial position $r/R = 0.9895$ is presented in Figure G.1 in Appendix G.

Considering the original PSS at original propeller position, the blade is not expected to experience cavitation at any rotational angle. Furthermore, moving the propeller further downstream to position 8 decreases the criterion value by 14.86% compared with the original position. Moving the rotative disc upstream to location 3, the inception increase by 6.75%. Equal trend is registered for all velocities and PSS orientations, where the most significant reduction, 18.11%, occurs for the naked hull at a velocity corresponding to 16knots.

Comparing the values obtained for the different vessel velocities, it is noted that lower velocities results in a higher risk of cavitation. This is not expected as cavitation is often more pronounced at higher speeds. On the other hand, at lower velocity with constant propeller revolution the loading on the blades is higher. In these situations cavitation may be more prone for propeller blades (Harvald, 1983).

Summing up the cavitation analysis of the propeller blades for all the presented velocities and propeller locations there is not seen any indication that the phenomenon will occur. This is supported by the cavitation inception criterion making it is possible to conclude that the propeller most likely will not experience any cavitation at any of the evaluated situations. However, the criterion of cavitation inception is quite simple but does not consider important parameters such as purity of water nor turbulence (Savio, 2011). These may affect the inception limit to an extent that cavitation may occur at an earlier stage.

Studying the difference in cavitation inception value at the possible locations for the different cases there is seen a significant relative reduction. The obtained results indicate that moving the propeller further downstream will decrease the probability of cavitation for all cases. Nevertheless, the results obtained at model scale implies that the full scale propeller may experience cavitation. According to (Peters et al., 2018) it is difficult to predict full scale cavitation due to only a part of the scaling laws may be fulfilled at the same time. The researchers states that for full scale propellers cavitation inception occurs earlier with greater vapour production, which is connected with higher Reynolds number. This emphasises that full scale predictions must be properly executed and that full scale cavitation may occur. However, with respect to the aim of this thesis it may be assumed that full scale propeller analysis will obtain results in the same order, indicating lower cavitation risk moving the rotative disc further downstream.

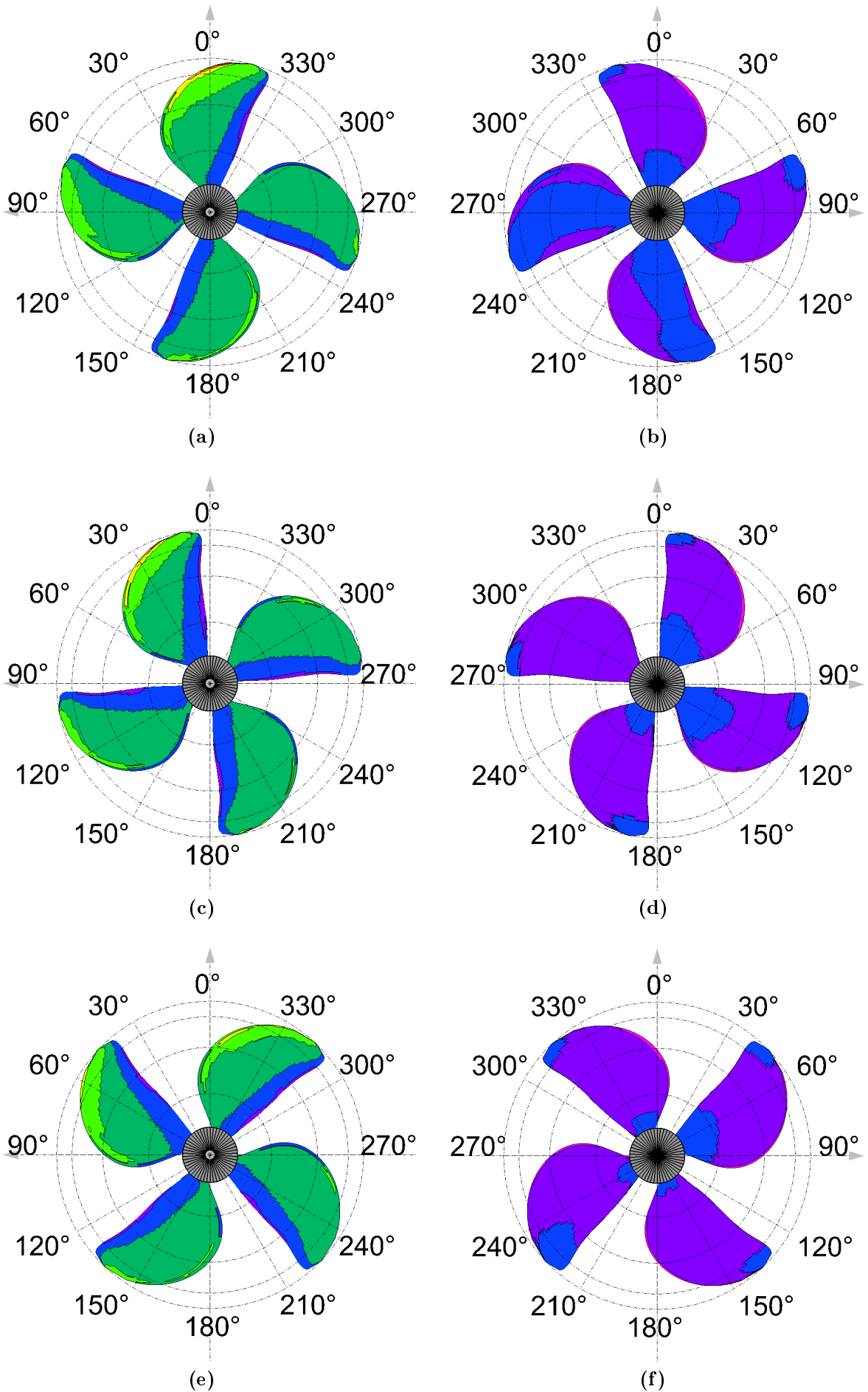


Figure 6.31: Propeller cavitation inception ($-C_P/\sigma_0$) PSS Original Pos 4: [(a)-(b) 0°], [(c)-(d) 27°], [(e)-(f) 63°]

6.5.2 Stator Fins - Pressure Distribution

Studying the pressure distribution over the stator fins it is seen that the lower and middle fin experiences the highest and lowest hydrodynamic pressure and is illustrated in Figure 6.32. Seen by the red color, the high pressure zone is located at the leading edge on the pressure side of the fins. Additionally the low pressure zone, seen in blue, is located at the leading edge on the suction side of the fins. This is expected due to the nature of the fins, having an angle of attack and camber which induces velocities over the chord length. This results in high and low pressure zones at the surface of the stator blades.

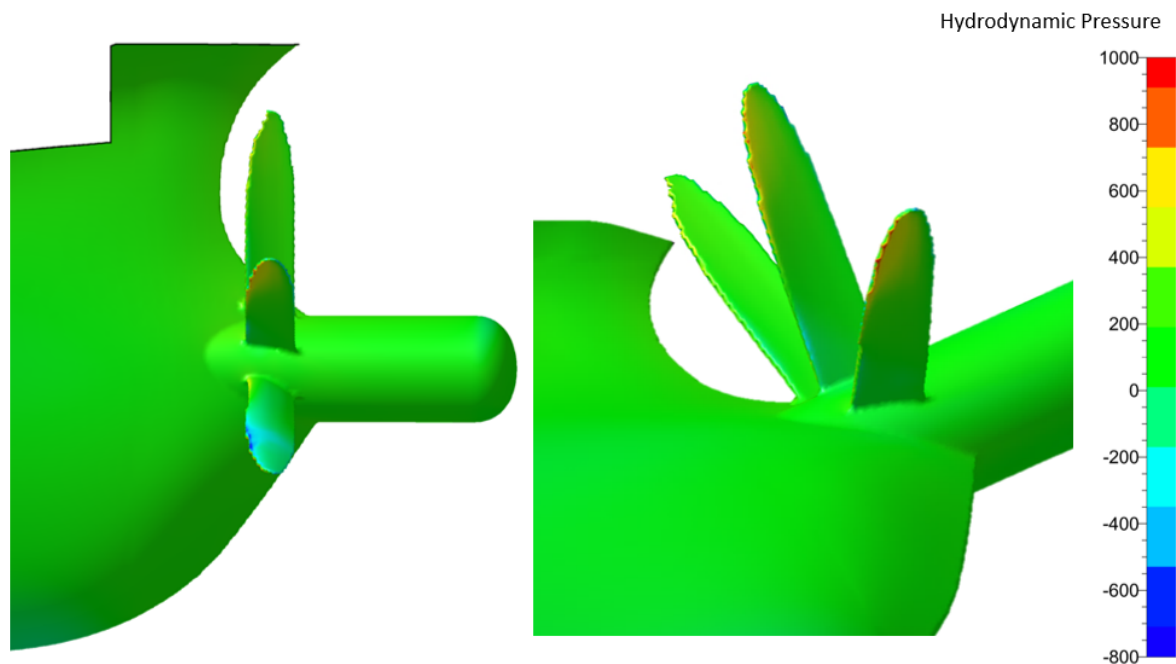


Figure 6.32: Pressure distribution stator fins - Original PSS

The pressure distribution is nearly identical for all PSS orientations and is illustrated in Appendix H. High pressure zones appear on the leading edge at the tip of the stator fins for all five orientations. Low pressure zones are identified at the same areas, thus at the upper side of the blades. Table 6.18 presents the maximum and minimum hydrodynamic pressure and pressure coefficients obtained at the respective PSS orientations.

The obtained pressure coefficients at the stator fins show good agreement with the results presented by (Krasilnikov et al., 2019), where low pressure zones showed values around -3.00. There is no risk of cavitation at the PSS due to the low velocity of the fluid. The main interest with the presented pressure distribution is the hydrodynamic load that is imposed on the structure. (Voermans, 2019) studied hydrodynamic loads on Wärtsilä's PSS EnergoFlow in sea states significantly more severe than tested in this study. It was emphasised that the PSS may need structural assessment with respect to fatigue and maximum off-design load for vessels operating in high waves and where a transient re-entry of PSS geometry occurs. Sea trial test conditions such as crash-stop and turning circle gave significantly high loads on the structure.

Thus, the hydrodynamic loads obtained while simulating the hull propagating through calm water is expected to be significantly lower than the critical values seen by Voermans. The pitch angle adjustment of the stator blades had an increase and decrease in high pressure at the leading edge corresponding to decreased (*AoA 1*) and increased (*AoA 2*) angle of attack, respectively. The same correlation is seen for the suction side of the blade where the pressure decreases and increases for *AoA 1* and *AoA 2*, respectively. Considering linear foil theory this is not expected. However, the deviation is explained by the fact that the inflow to the PSS in the wake of the hull is non-uniform and often chaotic. At the obtained hydrodynamic pressure areas on the angular position adjustment (1-3), there is a trend of decreasing maximum and minimum pressure. Due to the chaotic nature of the flow at this area it is not possible to justify the reason nor a trend. To do so further testing with respect to PSS geometry must be done.

Evaluating the force exerted on the fins by the hydrodynamic pressure and assuming a conservative area the obtained value is significantly lower than obtained by Voermans. Thus, a thorough fatigue analysis should be sufficient for normal operation conditions. Additionally, considering that the results are obtained for model scale there exists uncertainties about how these forces would scale up to full size structure. Furthermore, off-design peak loads must also be carefully evaluated.

PSS Orientation	Max p_s [Pa]	(C_P)	Min p_s [Pa]	(C_P)
Original	1057.14	-0.96	-768.32	-2.80
Adjustment 1	1003.63	-1.02	-714.49	-2.75
Adjustment 2	989.87	-1.03	-692.44	-2.73
Adjustment 3	979.66	-1.04	-713.06	-2.75
AoA 1	1070.50	-0.95	-837.09	-2.87
AoA 2	1036.89	-0.98	-711.69	-2.75

Table 6.18: Pressure distribution stator fins - PSS (Model scale speed $1.41m s^{-1}$)

Chapter 7

Further Work

During the computation in FM and propeller analyses conducted in AKPA there has been established interests of further investigation. In this chapter the topics that are most relevant for further work will be presented.

7.1 Presence of the Propeller and Rudder in CFD

The numerical computations performed in this study was conducted without the presence of the propeller and the rudder. This introduces uncertainties to the concluding marks of the study as there is some parameters that have not been fully resolved nor evaluated. By including the working propeller aft of the hull, the fluid regime may change entirely and affect the hydrodynamic performance of the propulsor at the respective longitudinal positions. The effect of the interaction between the hull and propeller, thrust deduction, directly changes the resistance components of the vessel and the final efficiency of the propeller. (Xing-Kaeding et al.,) showed that the presence of a PSS design increased the thrust deduction of a vessel with 11.0%, signifying the importance of the working propeller in studies with respect to propeller hydrodynamic performance. Thus, by properly including the rotative disc it will contribute to higher accuracy with respect to full scale propeller performance.

The presence of the rudder is also of interest in the performance of a vessel. As it is placed in the slip stream of the propulsor there may be significant differences in resistance forces. This is affected by the PSS where (Krasilnikov et al., 2019) showed that the rudder resistance increased by 3.62% by introducing ESD fins. Thus quantifying how the propeller location, in combination with the PSS and the rudder, influences the efficiency is of great interest.

7.2 Automatic Computation Processing

FM software is highly compatible with Python coding and the user guide has detailed information on how to implement it (NUMECA, 2019). This makes it applicable to develop a code that conducts pre-processing, simulation and post-processing in FM and couple it with the propeller analysis in AKPA in an iterative process. In this section a suggestion for further implementation of coding and coupling of the software described is presented.

Step 1: FM - Simulation & Post-Processing (Convergence)

By having a structured approach in the grid procedure, thus post-process and improve the grid at the aft of the vessel within constraints, and compare the obtained nominal wake fraction it may be possible to achieve a converging wake field. This procedure may be conducted without the working propeller to save computational time. The definition of constraints in the numerical grid procedure is however highly dependent on experience and physical understanding of the fluid behaviour and must be conducted properly.

Step 2: FM & AKPA Coupling

With a converged wake fraction the simulation with the working propeller may be conducted. A number of positions and propeller geometry is defined and simulated at each position. The suggested solution feeds AKPA with the nominal wake field, then feeds FM with the effective wake field and re-initiates the converged FM simulation. This loop is iterated until a propeller convergence is obtained. This may be controlled by Python which also collects, compares and suggest an optimal position for the propeller. A simple outlay of how the procedure may be accomplished is presented in Figure 7.1.

There are suitable functions in FM, where the software allows the user to introduce a propulsor aft of the hull to account for the propeller hull interaction. A more suitable solution for the current research is to introduce an actuator disk at the position of the propeller and feed AKPA with a result with higher accuracy. Doing so, the thrust deduction may be achieved. However, both these methods would have to be conducted at all the evaluated positions and introduces a significant increase in demanded computer architecture and power.

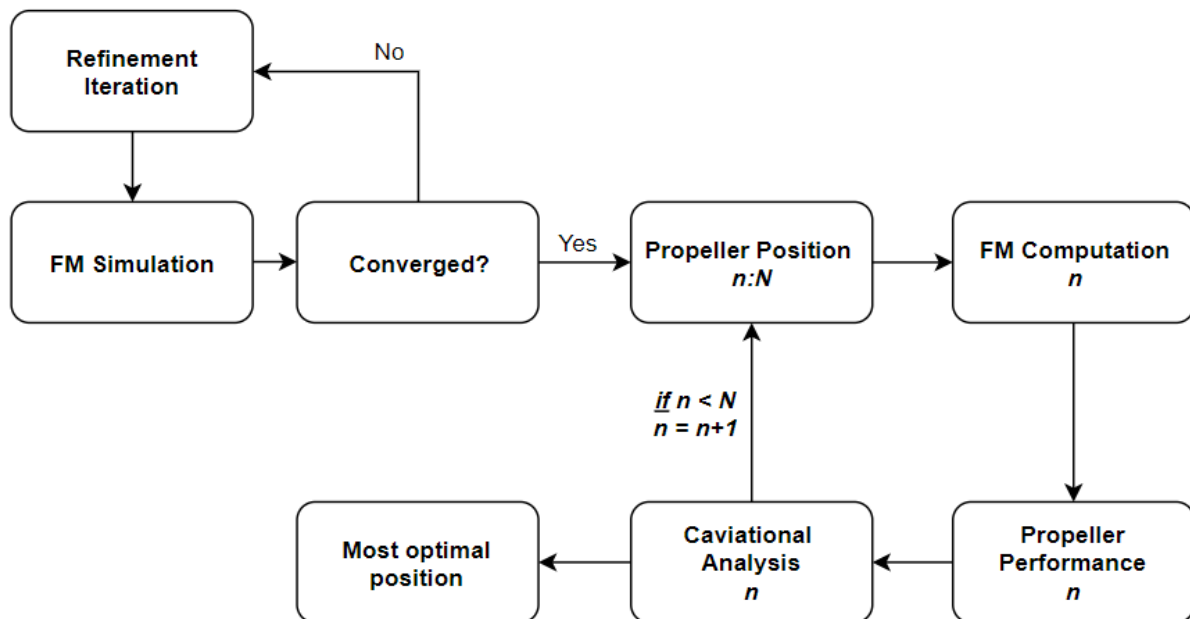


Figure 7.1: Automatic numerical computation outlay

As a long term goal, it may be interesting to look into the possibility of using optimisation methods such as particle swarm optimisation (PSO). Thus defining a set of different propeller geometries, a set of PSS geometries, propeller locations and type of rudder before conducting the analysis combined with PSO. The PSO method was used by (Nylund, 2017) to obtain initial values for a IP optimisation methods while analysing the possibility of distributed propulsion. Although it is of interest, this suggestion demands significant computational power and effort to accomplish.

7.3 Other PSS adjustments

7.3.1 Diameter of PSS Blades

The PSS fins introduces a change in the inflow regime to the propeller and is shown to increase and decrease the performance of the propeller based on angle of attack, foil geometry and angular position. In addition, deviating results is obtained while changing the propeller location upstream and downstream. By adjusting the diameter of the PSS blades it may also contribute to adjust the flow and indicate another feasible solution with better results. (Zondervan et al., 2011) states that the optimum diameter, with regard to efficiency, of the propeller should be less than the PSS diameter. (Kim et al., 2013) argues that the propulsor achieves the best performance at PSS diameter equal to the propeller diameter. Kim also emphasises that the PSS diameter must not be lower than the propeller diameter to avoid affect of stator tip vortices on cavitation risk. These arguments point towards that changing the diameter of the PSS may increase the propulsive efficiency.

7.3.2 Number of PSS Blades

The number of stator blades may affect the propeller performance and thus suggest a more feasible longitudinal position. Kim's study considered the number of stator blades and concludes that three port side blades and one starboard blade is the most optimum solution. This indicates that further investigation of the number of PSS fins may be favourable for the research.

7.4 Long term goal - Establish Classification Rules for PSS

The classification society DNV GL have not determined any specific rules with regard to PSS nor propeller location. The latter is normally covered by rules determining loads on shafts and bearing indicating that a stand alone document for propeller location is not of importance. This is also supported by the fact that relocation of propeller is very rare.

Considering the PSS arrangements normal procedures, with respect to welding and fatigue assessment published by DNV GL, in theory shall cover the topic. As there is reported accidents where the PSS structure has failed during design working conditions it indicates that the existing rules is insufficient. (Wärtsilä, 2017) introduced their own PSS including a load calculator for different operational environments. By combining CFD, EFD and load calculators as created by Wärtsilä, a stand alone classification definition with regard to PSS designs is of interest and encouraged to pursue.

Chapter 8

Conclusion

The results obtained through numerical calculations shows good agreement with the conducted EFD. The simulations converged and the nominal axial and tangential wake field prediction correlated well with formerly conducted CFD studies. Computations without the presence of the free surface indicated that significant savings, with respect to time, may be achieved with nearly identical results. However, it is highly dependent on the availability of computational power. The obtained resistance of the model had some minor deviations but was found to be within acceptable limits. A coupling of AKPA and FM was investigated but was not pursued as it is highly time consuming.

Seven computations were conducted with respect to resistance and propeller analysis, including naked hull, original PSS and five adjusted PSS orientations. All the adjustments indicates lower resistance compared with the original set-up where *Adjustment 1* shows the most promising result with a reduction in total resistance of 1.36%. Hydrodynamic loads on the PSS blades are of low magnitude and normal fatigue assessment is encouraged.

The effective wake field presentation obtained by the propeller analysis for all geometries experience equal transformation along the evaluated propeller locations. The strong vortices and high wake fraction areas in the rotative disc decreases significantly moving downstream from position 1 to 8. The effect of the PSS installation, swirl at port side, did not seem to reduce in the same magnitude. This indicates a more suitable working environment for the propeller further downstream and was substantiated by the performance coefficients obtained at all advance numbers and cases.

Efficiency of the propulsive system was found inconclusive due to CFD computation were executed disregarding the propeller hull interaction. The required power to sustain a constant vessel speed is decreased by moving the propulsive unit further downstream for all geometries, where the most optimal location is position 8. The obtained reduction in shaft power is 2.7% and 2.35% for naked hull and original PSS, respectively. The five PSS orientations gave an additional reduction around 0.6% compared with original PSS at equal propeller position. The achieved thrust per power unit exerted, the original PSS obtained the highest value at all locations except position 3, furthest upstream, where *Adjustment 3* performed best.

All cases studied obtains low risk of cavitation and the inception value may decay 18.11% by moving the propeller further downstream depending on geometry. The computations were done at model scale introducing uncertainties whether full scale propeller will experience higher risk of cavitation. However, the highest pressure coefficient seen at the blade tip in the wake peak area, indicates that tip cavitation may be a problem in full scale. The reduced risk of cavitation moving the propeller further downstream is assumed to be valid for full scale propeller.

As a concluding mark; moving the propeller in the downstream direction, within the geometrical constraints presented by the rudder, may reduce the required shaft power and the probability of cavitation, depending on hull geometry. The simulations are conducted at model scale without rudder and the interaction between hull and propeller. It is therefore emphasised that the results are only indications and may not be final. One of the large class societies, DNV GL, does not have any clear guidance on relocation of propeller nor installation of PSS. These issues fall under normal guidance for shaft and bearing and structural assessments.

Bibliography

- Andersson, K., Baldi, F., Brynolf, S., Lindgren, J. F., Granhag, L., and Svensson, E. (2016). Shipping and the Environment. In *Shipping and the Environment*, pages 3–27. Springer.
- Babicz, J. (2008). *Wärtsilä encyclopedia of ship technology*. Baobab Naval Consultancy.
- Bašić, J., Degiuli, N., and Dejhalla, R. (2017). Total resistance prediction of an intact and damaged tanker with flooded tanks in calm water. *Ocean engineering*, 130:83–91.
- Breslin, J. P. and Andersen, P. (1996). *Hydrodynamics of ship propellers*, volume 3. Cambridge University Press.
- Carlton, J. (2012). *Marine propellers and propulsion*. Butterworth-Heinemann.
- Celik, I. B. (1999). Introductory Turbulence Modeling. *West Virginia University, Lecture notes*.
- Committee, I. S. et al. (2011). ITTC–Recommended Procedures Guidelines Practical Guidelines for Ship CFD Applications. IITC.
- Dang, J., Dong, G., and Chen, H. (2012). An Exploratory Study on the Working Principles of Energy Saving Devices (ESDs): PIV, CFD Investigations and ESD Design Guidelines. In *ASME 2012 31st International Conference on Ocean, Offshore and Arctic Engineering*, pages 25–34. American Society of Mechanical Engineers.
- Deinboll, O. (2019). Email correspondence - "Masteroppgave - Retrofit existing vessel ESD. Correspondence: 2019-03-12.
- Devals, C., Vu, T., Zhang, Y., Dompierre, J., and Guibault, F. (2016). Mesh convergence study for hydraulic turbine draft-tube. In *IOP Conference Series: Earth and Environmental Science*, volume 49, page 082021. IOP Publishing.
- DNV GL (2015). Energy Management Study 2015.
- DNV GL (2018a). ECO Retrofit – vessel efficiency upgrades. <https://www.dnvgl.com/services/eco-retrofit-vessel-efficiency-upgrades-2673>. Accessed: 2019-03-11.
- DNV GL (2018b). Fatigue assessment of ship structures, DNVGL-CG-0129.
- DNV GL (2018c). Ships - Part 4 Systems and components, Chapter 2 Rotating Machinery, General.

- DNV GL (2019). Energy Efficiency. <https://www.dnvgl.com/maritime/energy-efficiency/efficiency-finder.html>. Accessed: 2019-03-11.
- Gougoulidis, G. and Vasileiadis, N. (2015). An Overview of Hydrodynamic Energy Efficiency Improvement Measures.
- Guo, B., Steen, S., and Deng, G. (2012). Seakeeping prediction of KVLCC2 in head waves with RANS. *Applied Ocean Research*, 35:56–67.
- Harvald, Sv, A. (1983). *Resistance and Propulsion of Ships*, volume 1. Ocean Engineering: A Wiley Series.
- Hollenbach, U. and Reinholz, O. (2011). Hydrodynamic trends in optimizing propulsion. In *Second International Symposium on Marine Propulsors-smp*, volume 11.
- ICE Design (2018). Proprietary Designs chemical tanker. <http://www.icedesign.info/services/proprietary-designs/tankers/>. Accessed: 2019-01-28.
- in Marine Hydrodynamics, I. S. C. C. (2011). ITTC–Recommended Procedures Fresh Water and Seawater Properties. IITC.
- Innovative-CFD (2018). CFD Grid types. <http://www.innovative-cfd.com/cfd-grid.html>. Accessed: 2019-04-17.
- Kerwin, J. E. (2001). Hydrofoils and propellers. *Lecture notes*.
- Kim, K., Leer-Andersen, M., Werner, S., Orych, M., and Choi, Y. (2013). Hydrodynamic optimization of pre-swirl stator by CFD and model testing. *International Shipbuilding Progress*, 60(1-4):233–276.
- Krasilnikov, V., Koushan, K., Nataletti, M., Sileo, L., and Spence, S. (2019). Design and Numerical and Experimental Investigation of Pre-Swirl Stator PSS. In *Sixth International Symposium on Marine Propulsion*.
- MARINTEK (2012). AKPA Fact Sheet. <https://www.sintef.no/globalassets/upload/marintek/pdf-filer/factsheets/akpa.pdf>. Accessed: 2019-02-12.
- MARINTEK, State Marine Technical University, Offshore Simulator Center (2011). *AKPA-CP-CT 5.6 Manual*.
- NUMECA (2018a). FINEMarine. <https://www.numeca.com/product/finemarine/>. Accessed: 2019-02-12.
- NUMECA (2018b). Numeca international. Tutorials FineMarine72. Accessed: 2019-04-12.
- NUMECA (2019). *FINEMarine72 Userguide 2018*.
- Nylund, V. (2017). Distributed propulsion for ships. *Master Thesis, NTNU*.
- Peters, A., Lantermann, U., and el Moctar, O. (2018). Numerical prediction of cavitation erosion on a ship propeller in model-and full-scale. *Wear*, 408:1–12.

- Procedures, ITTC Recommended. Guidelines: Practical Guidelines for Ship CFD Applications. *ITTC Report*, pages 7–5.
- Regener, P. B., Mirsadraee, Y., and Andersen, P. (2018). Nominal vs. Effective Wake Fields and their Influence on Propeller Cavitation Performance. *Journal of Marine Science and Engineering*, 6(2):34.
- Rognebakke, O. (2019). Email correspondence - "Masteroppgave - Retrofit existing vessel ESD. Correspondence: 2019-03-12.
- Sánchez-Caja, A. and Pylkkänen, J. (2007). Prediction of effective wake at model and Full Scale using a RANS code with an actuator disk model. In *2nd International conference on maritime research and transportation, Ischia, Italy*, pages 28–30.
- Savio, L. (2011). Propeller Cavitation. *Lecture notes*.
- SINTEF (2004). Propeller Design & Analysis. https://www.sintef.no/globalassets/upload/marintek/pdf-filer/software/akpd-akpa_programpackage.pdf. Accessed: 2019-02-11.
- Sivertsgård, S. S. (2018). Project Thesis - Investigation of Propeller Location with the use of CFD.
- Thompson, J. F., Soni, B. K., and Weatherill, N. P. (1998). *Handbook of grid generation*. CRC press.
- Trivellato, F. and Castelli, M. R. (2014). On the Courant–Friedrichs–Lewy criterion of rotating grids in 2D vertical-axis wind turbine analysis. *Renewable Energy*, 62:53–62.
- Van Hoydonck, W., Toxopeus, S., Eloot, K., Bhawsinka, K., Queutey, P., and Visonneau, M. (2015). Bank effects for KVLCC2. *Journal of Marine Science and Technology*, pages 1–26.
- van Terwisga, T. (2013). On the working principles of energy saving devices. In *Proceedings of the Third International Symposium on Marine Propulsors. Launceston, Tasmania, Australia*.
- Voermans, A. (2019). Experimental determination of hydrodynamic loads on the wtsilre-swirl stator energofflow and validation of a prediction methodology for design loads. Wärtsilä Netherlands, Marine Business.
- Wärtsilä (2017). Wärtsilä introduces an innovative pre-swirl stator to improve fuel efficiency. <https://www.wartsila.com/media/news/07-11-2017-wartsila-introduces-an-innovative-pre-swirl-stator-to-improve-fuel-efficiency>. Accessed: 2019-03-15.
- Xing-Kaeding, Y., Gatchell, S., and Streckwall, H. Towards practical design optimization of pre-swirl device and its life cycle assessment.
- Zondervan, G., Holtrop, J., Windt, J., and Terwisga, T. (2011). On the design and analysis of pre-swirl stators for single and twin screw ships. In *Second Intl Symposium on Marine Propellers*.

Appendices

A Grid and Domain

A.1 Domain and boundary conditions

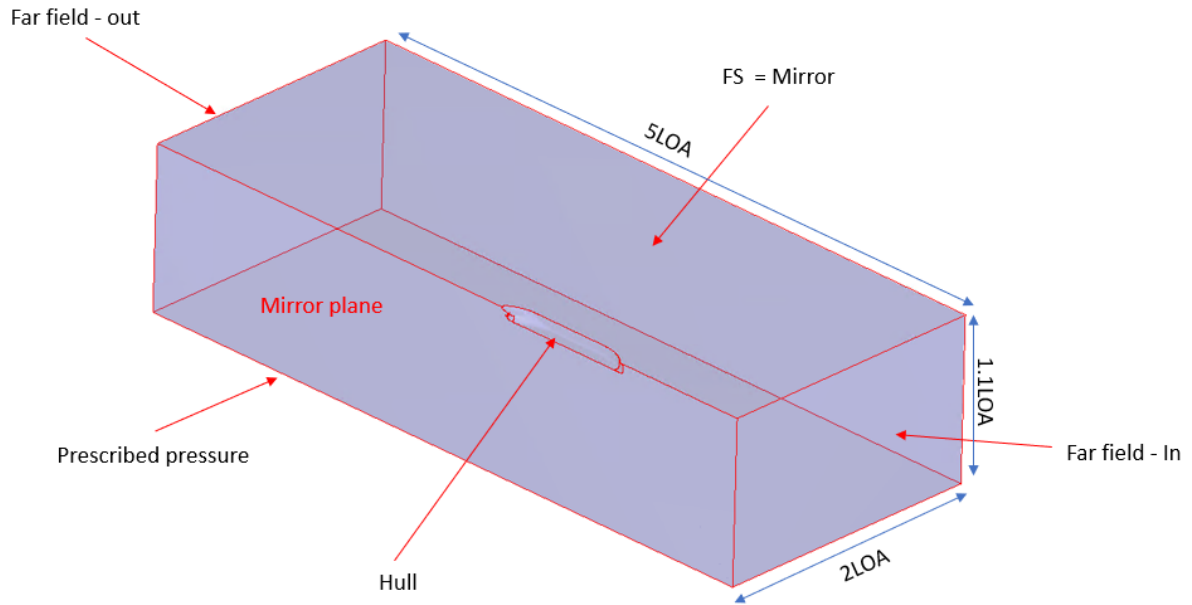


Figure A.1: Domain 2 with applied boundary conditions

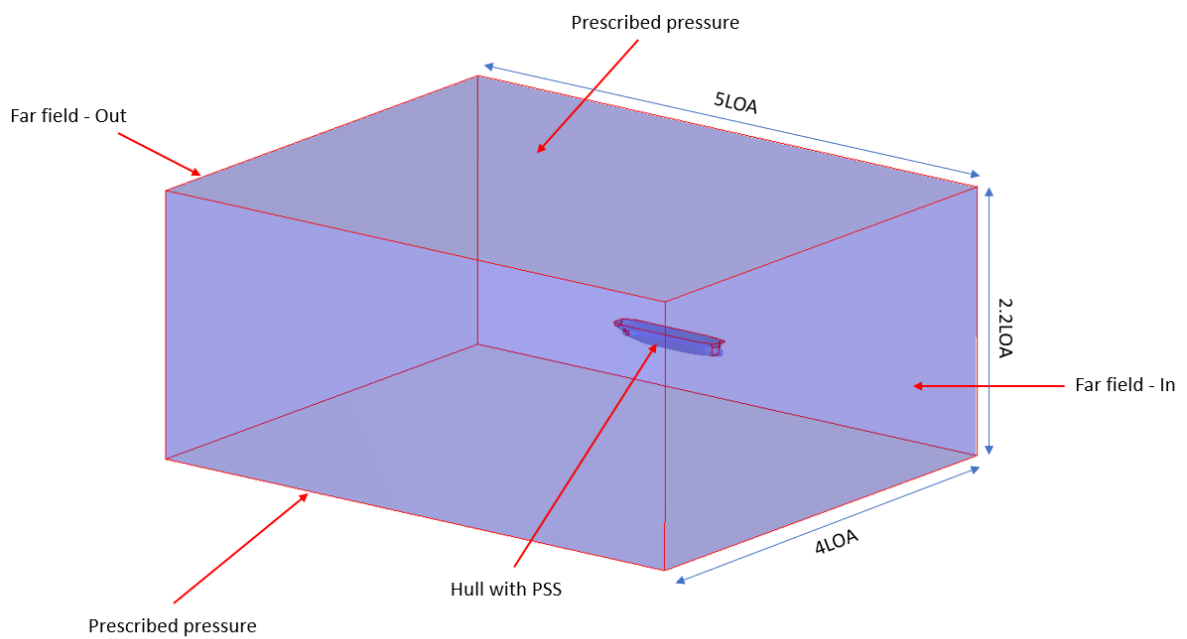


Figure A.2: Domain 3 with applied boundary conditions

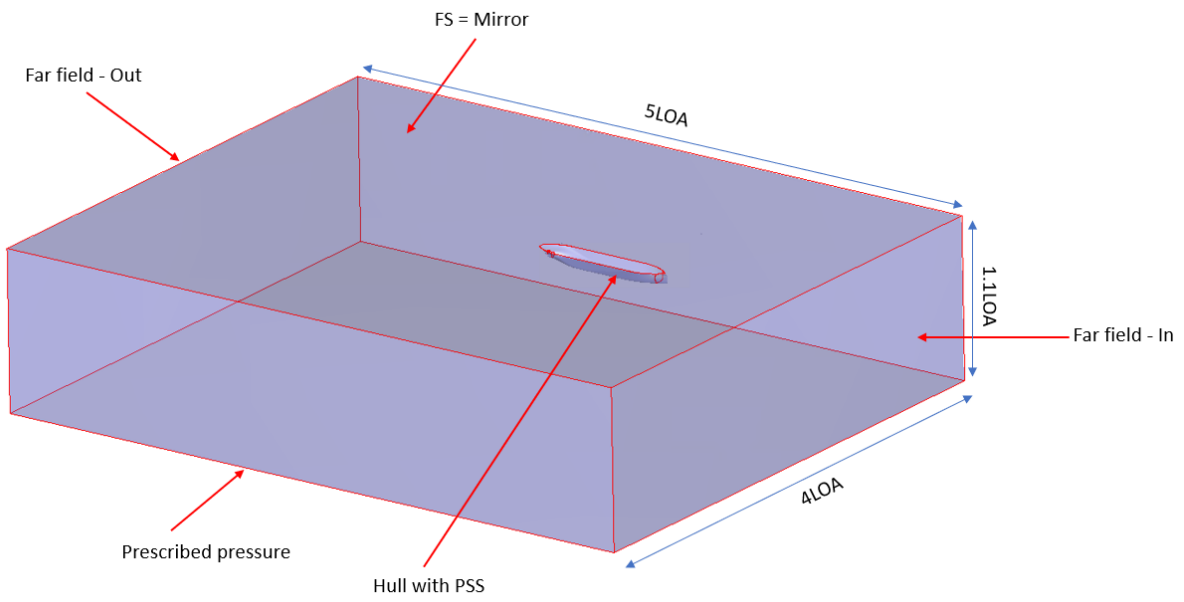


Figure A.3: Domain 4 with applied boundary conditions

B Correspondence with DNV GL personell

B.1 Rognebakke, Olav (11.03.2019)

13.3.2019

Gmail - Masteroppgave - Retrofit existing vessel ESD



Stian Schencke Sivertsgård <stianschencke@gmail.com>

Masteroppgave - Retrofit existing vessel ESD

Rognebakke, Olav <Olav.Rognebakke@dnvgl.com>
To: Stian Schencke Sivertsgård <stianschencke@gmail.com>
Cc: "Deinboll, Oddvar" <Oddvar.Deinboll@dnvgl.com>

Mon, Mar 11, 2019 at 3:47 PM

Hei Stian,

Du skulle egentlig snakket med en klassemann, men jeg synser litt uansett.

I hovedsak vil ikke energy saving devices være omfattet av klasseregler. Det har vært gjort vurderinger av f.eks. pre-swirl stator finner fordi disse kan skade propell hvis de faller av.

Jeg antar at vi ikke har spesielle regler for å flytte propell i lengderetning. Tenker at en må se på nytt på krav i forhold til lagerkrefter og aksling – som skulle dekkes gjennom vanlig regelverk (må tilfredstilles også etter retrofit).

Mulig at ror-regler har en kobling mot propell slik at roret også må sjekkes hvis avstand mellom propell og ror endres. Støy og vibrasjoner må nok vurderes, i hvert fall dersom fartøyet har en Comfort notasjon.

Mannen som vet best vet svar er nok Oddvar Deinboll. Tok meg den frihet å sette ham i CC.

Mvh Olav

[Quoted text hidden]

This e-mail and any attachments thereto may contain confidential information and/or information protected by intellectual property rights for the exclusive attention of the intended addressees named above. If you have received this transmission in error, please immediately notify the sender by return e-mail and delete this message and its attachments. Unauthorized use, copying or further full or partial distribution of this e-mail or its contents is prohibited.

B.2 Deinboll, Oddvar (12.03.2019)

13.3.2019

Gmail - Masteroppgave - Retrofit existing vessel ESD



Stian Schencke Sivertsgård <stianschencke@gmail.com>

Masteroppgave - Retrofit existing vessel ESD

Deinboll, Oddvar <Oddvar.Deinboll@dnvgl.com>
To: Stian Schencke Sivertsgård <stianschencke@gmail.com>
Cc: "Rognebakke, Olav" <Olav.Rognebakke@dnvgl.com>

Mon, Mar 11, 2019 at 10:53 PM

Hei igjen!

Her har nok Olav fra advisory svart godt på vegne av klasse – det finnes per i dag ikke konkrete beskrivende (preskriptive) regler på preswirl-devices. For hub cap fins har vi derimot sagt at dersom en av finnene bøyes / skades (mekanisk impact) så skal de ikke gi følgeskade på hub-cap'en såfremt denne er viktig for å forhindre at vann får tilgang til akslingen. I praksis har vi pleid å akseptere at vegtykkelsen i selve hub-cap'en er større eller lik rottykkelsen på finnen. For pre-swirl devices kan det være vanskelig å definere relevante designlaste. Enkelte påstår at slike har hatt en tendens til å falle av etter en stund, noe som kan indikere at de utsettes for dynamiske laste som kan gi utmatting – men her famler også vi litt i halvblinde. Skal du dimensjonere noe, er det sikkert lurt å ta litt godt i, dersom dette er forenelig med det du ønsker å oppnå hydrodynamisk. Så er det alltid en god ide å så langt det lar seg gjøre unngå skarpe kjerver der hvor belastningsnivået kan være betydelig.

Så vidt meg bekjent er det heller ikke konkrete regelkrav om avstand mellom rør og propell – dette er gjerne bestemt utfra at man skal kunne få til å montere/demontere propellen uten at roret også må tas av. Dersom man ønsker å flytte hele propellen lenger fram eller lenger akter ved en ombygging er dette etter min erfaring noe man søker å unngå – dette vil gjerne kreve en ombygging av hele akterskipet, noe som er kostbart og tidkrevende (hvis det da ikke allerede er en del av det man uansett skal gjøre). Dersom du beholder propellnavet i samme posisjon, og bare flytter bladene framover bakover i forhold til navet (f.eks. ved bruk av «rake») er dette mindre problematisk. En skal likevel være obs på at kaviterende tippvirvler kan medføre erosjonsskader på roret og således er noe man bør unngå, men konkrete regelkrav har vi altså ikke.

I forhold til støy og vibrasjoner, så har vi gjort oss noen erfaringer i retning av at propeller med en svært spesiell rakefordeling (spesielt ut mot tippen) KAN gi overraskende utslag, og noe man i såfall bør sjekke grundig.

Siden du som tidligere sommerstudent nærmest er for «in-house» å regne, må du gjerne ta opp konkrete forslag til diskusjon med oss – også på klasse. Om vi ikke har konkrete regelkrav kan vi sikkert i det minste ta en titt og kanskje bidra til at de største fallgrubene unngås.....

Ellers kan vi nevne at det for tiden ser ut til å være en bølge av retrofits der man de-rater motoren slik at man får ned turtallet ennå mer, og med den reduserte effekten så setter man på en ennå større propell enn man hadde – men retrofits på denne måten er kanskje litt kjedelige for en masteroppgave.

Lykke til med oppgaven.

Best Regards

for DNV GL AS

Oddvar Deinboll

<https://mail.google.com/mail/u/0?ik=80abaa102c&view=pt&search=all&permmsgid=msg-f%3A1627747751295601321&simpl=msg-f%3A1627747...> 1/2

C Propeller

C.1 Blade geometry

r/R	b/D	e0/D	cs/D	xr/D	P/D	f0/D
0.205	0.137	0.0335	0.00555	0	0.80712	0.00464
0.25	0.1652	0.0318	0.01175	0	0.80975	0.00619
0.3	0.1946	0.0301	0.0177	0	0.81211	0.00743
0.35	0.2232	0.0284	0.02305	0	0.8142	0.00835
0.4	0.2495	0.0265	0.0276	0	0.81601	0.00893
0.5	0.2889	0.0226	0.0326	0	0.81878	0.00917
0.6	0.311	0.0183	0.02945	0	0.82046	0.00852
0.7	0.3124	0.0141	0.01445	0	0.821	0.00734
0.8	0.2947	0.0107	-0.0167	0	0.8063	0.00562
0.9	0.2439	0.008	-0.0686	0	0.74344	0.00338
0.95	0.1913	0.007	-0.1039	0	0.68851	0.00205
0.975	0.1466	0.0065	-0.12415	0	0.65444	0.0013
0.99	0.1014	0.0062	-0.1372	0	0.63181	0.00076
0.995	0.0762	0.0061	-0.1417	0	0.62387	0.00052
1	0.0134	0.006	-0.1463	0	0.61575	0

Table 1: Blade geometry

D Resistance

D.1 Convergence curve

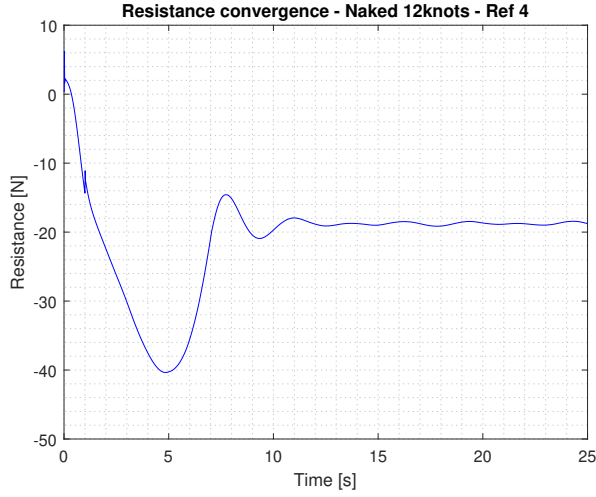


Figure D.1: Resistance convergence - Naked 12 knots conducted with gridding corresponding to refinement 4 given in Table 5.9.

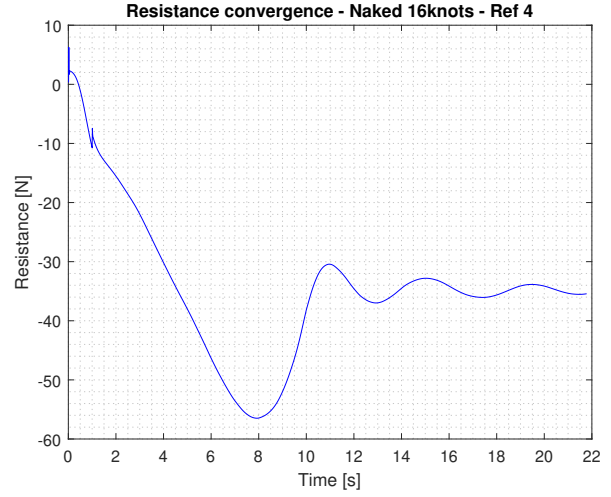


Figure D.2: Resistance convergence - Naked 16 knots conducted with gridding corresponding to refinement 4 given in Table 5.9.

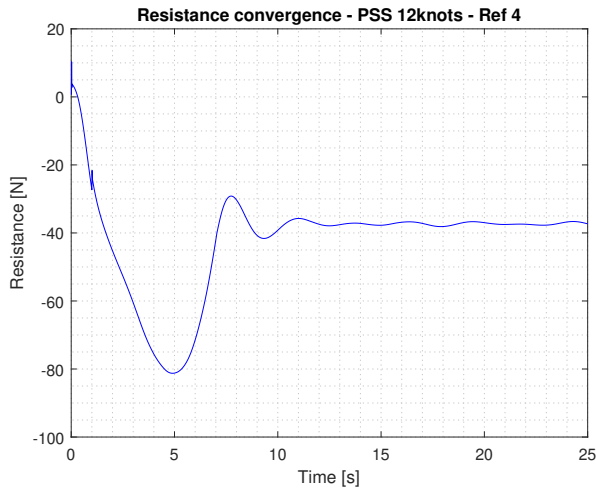


Figure D.3: Resistance convergence - PSS 12 knots conducted with gridding corresponding to refinement 4 given in Table 5.15.

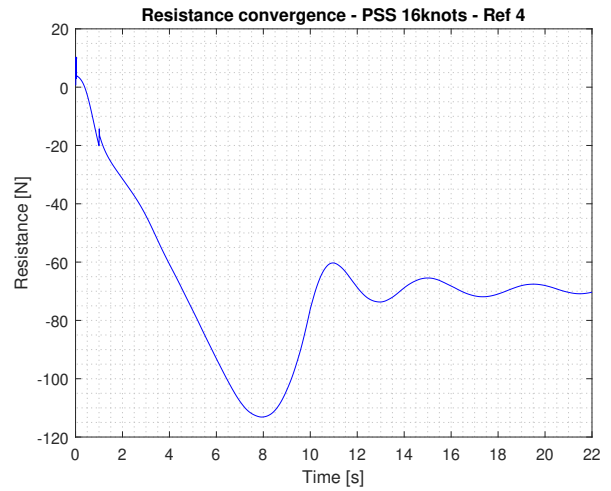


Figure D.4: Resistance convergence - PSS 16 knots conducted with gridding corresponding to refinement 4 given in Table 5.15.

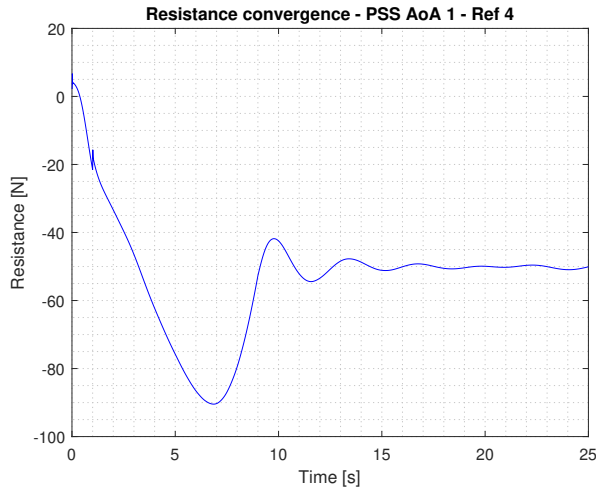


Figure D.5: Resistance convergence - Adjustment 1 of angle of attack. Conducted with gridding corresponding to refinement 4 given in Table 5.15 and adjustments of PSS as given in Table 3.1.

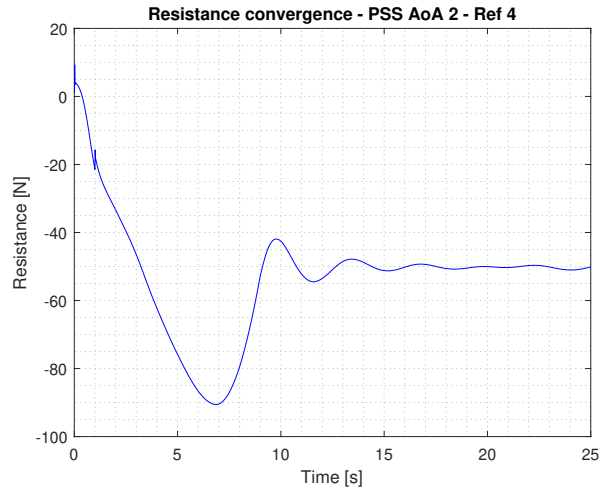


Figure D.6: Resistance convergence - Adjustment 2 of angle of attack. Conducted with gridding corresponding to refinement 4 given in Table 5.15 and adjustments of PSS as given in Table 3.1.

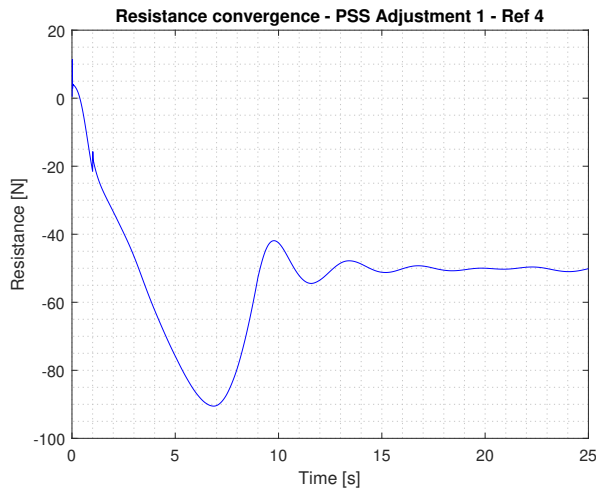


Figure D.7: Resistance convergence - Adjustment 1 of angular position of stator blade. Conducted with gridding corresponding to refinement 4 given in Table 5.15 and adjustments of PSS as given in Table 3.3.

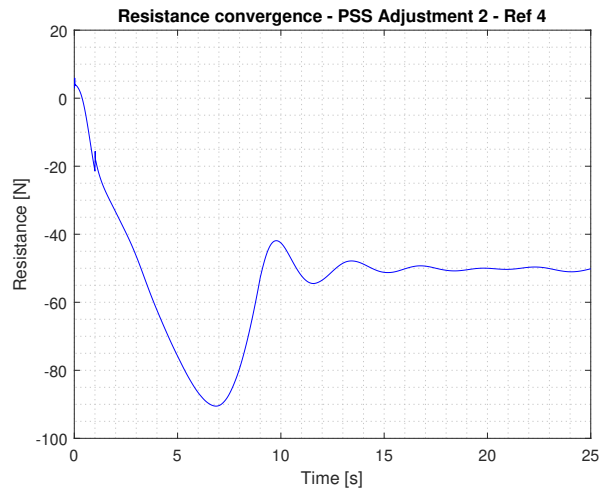


Figure D.8: Resistance convergence - Adjustment 2 of angular position of stator blade. Conducted with gridding corresponding to refinement 4 given in Table 5.15 and adjustments of PSS as given in Table 3.3.

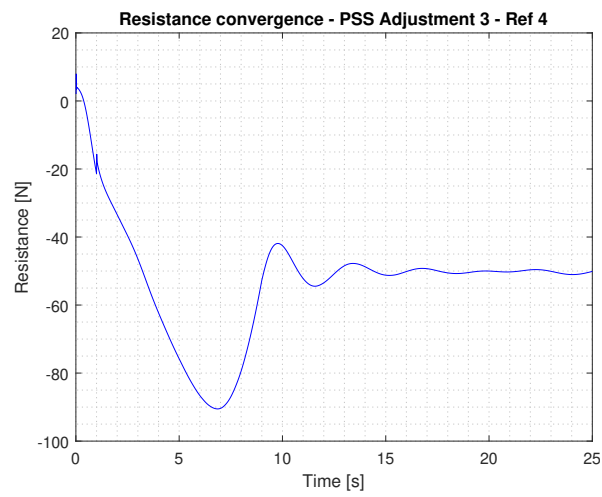


Figure D.9: Resistance convergence - Adjustment 3 of angular position of stator blade. Conducted with gridding corresponding to refinement 4 given in Table 5.15 and adjustments of PSS as given in Table 3.3.

E Propeller Performance

E.1 Original hull w and w/o PSS

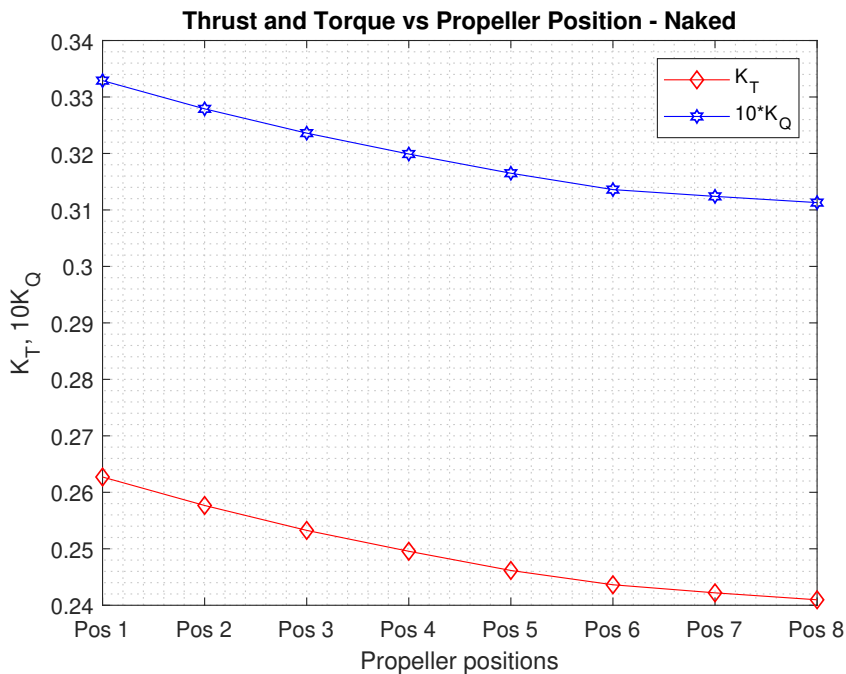


Figure E.1: Thrust and Torque coefficients vs Propeller location - Naked hull

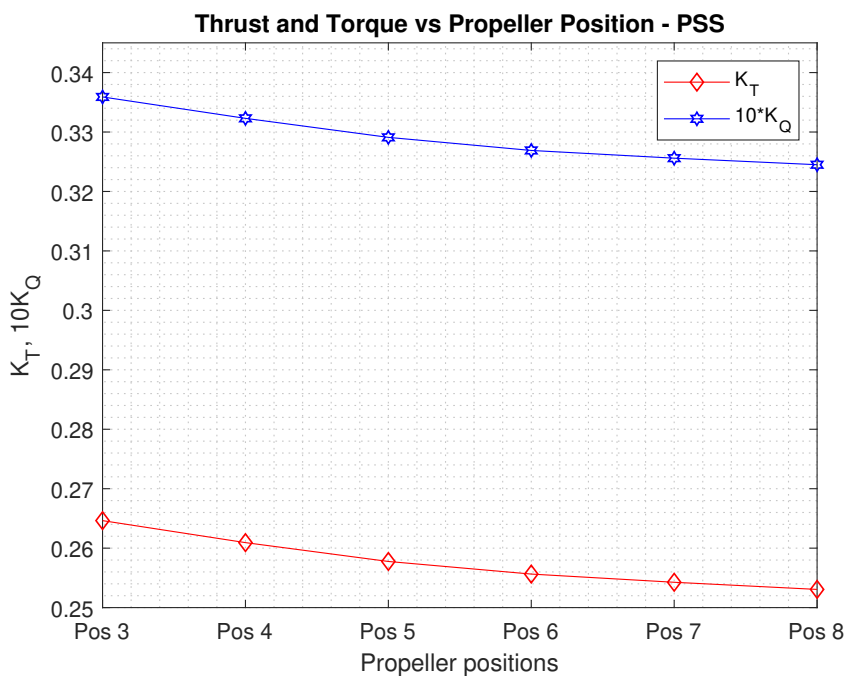


Figure E.2: Thrust and Torque coefficients vs Propeller location - with PSS

E.2 Different advance number

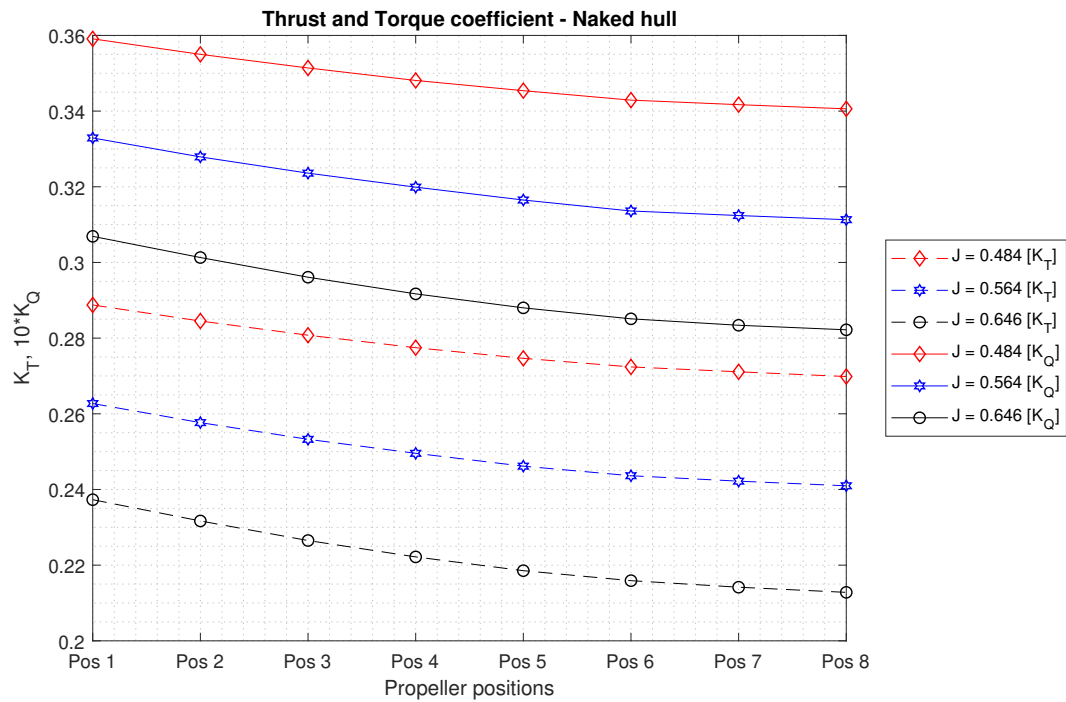


Figure E.3: Thrust and Torque coefficients for all three advance numbers - Naked hull

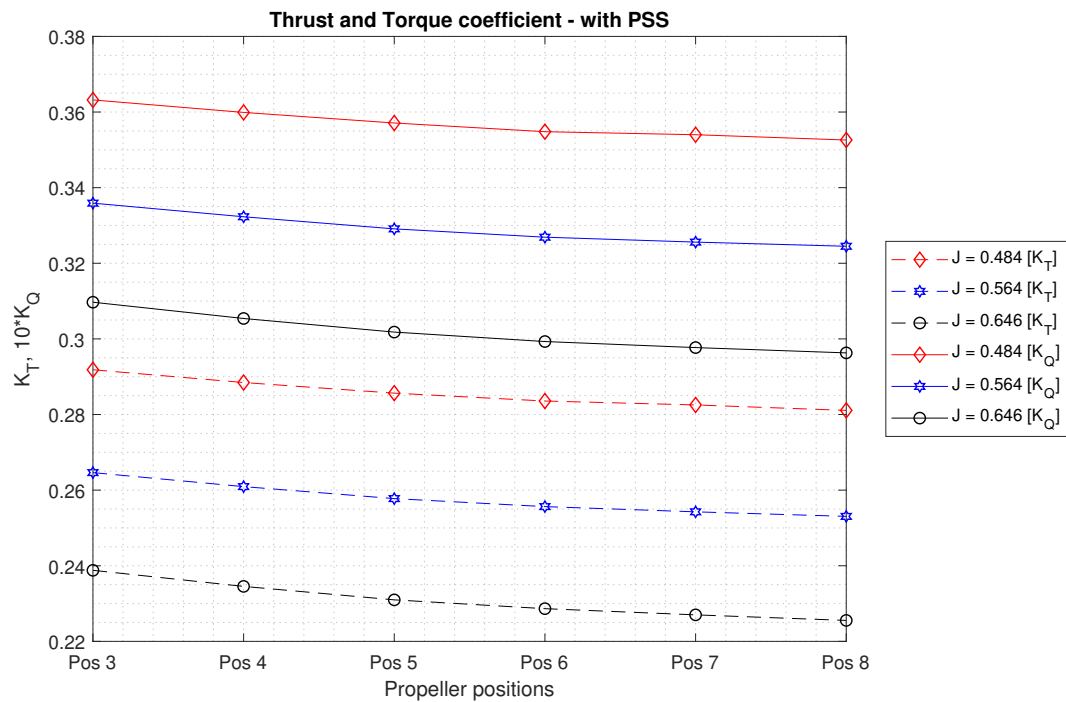


Figure E.4: Thrust and Torque coefficients for all three advance numbers - with PSS

E.3 Adjusted PSS orientation

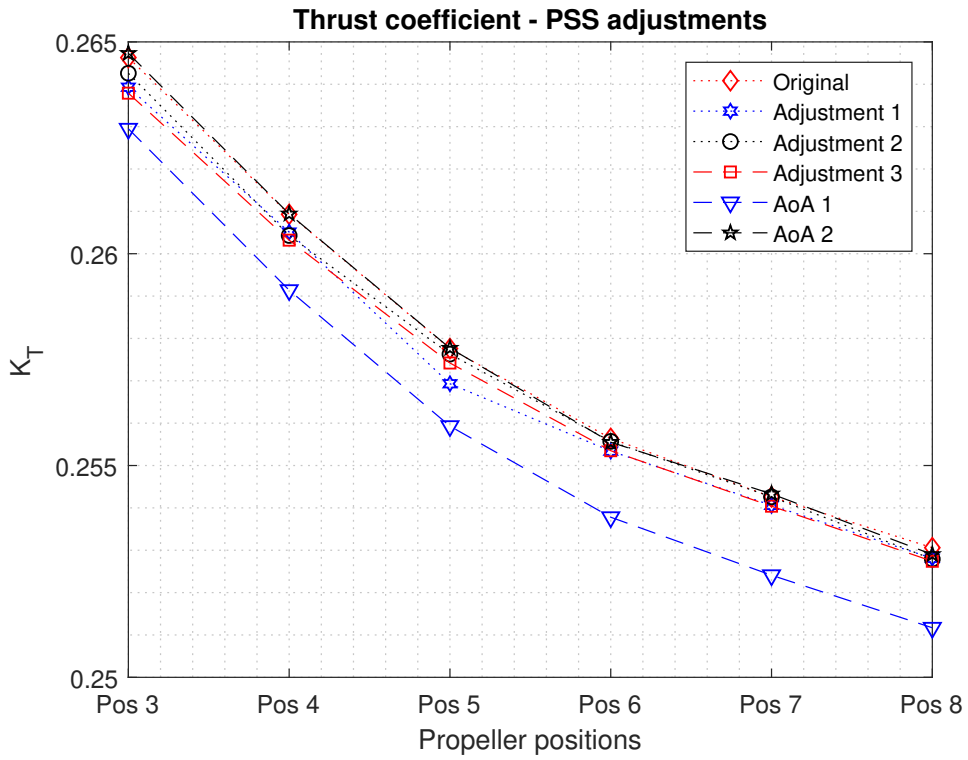


Figure E.5: Thrust comparison for different PSS adjustments.

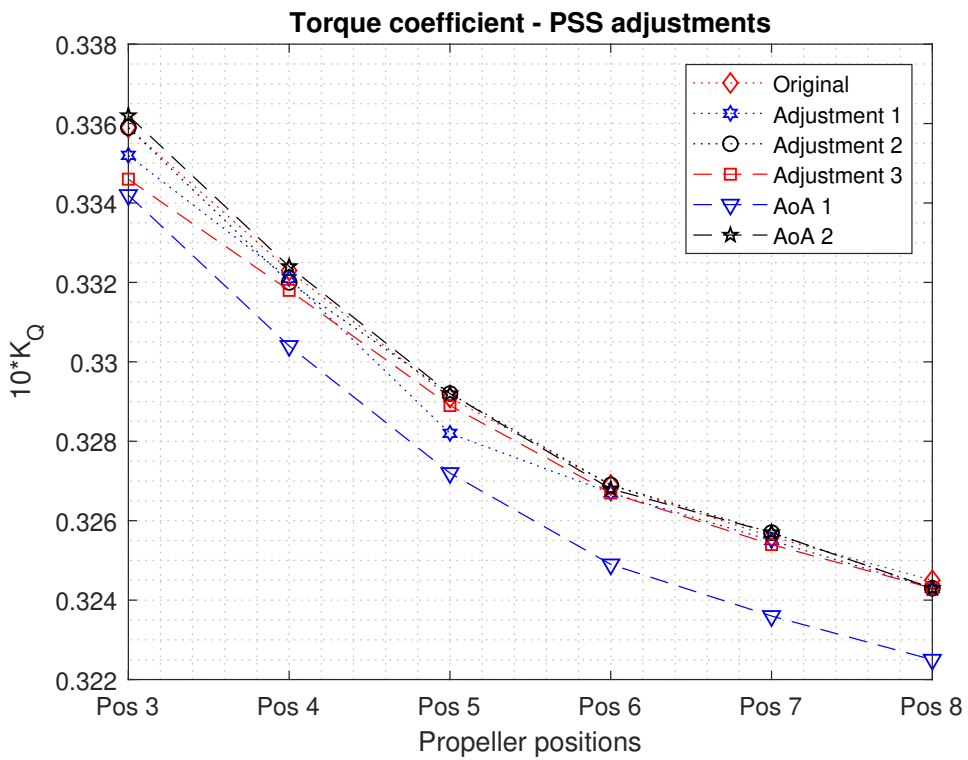


Figure E.6: Torque comparison for different PSS adjustments.

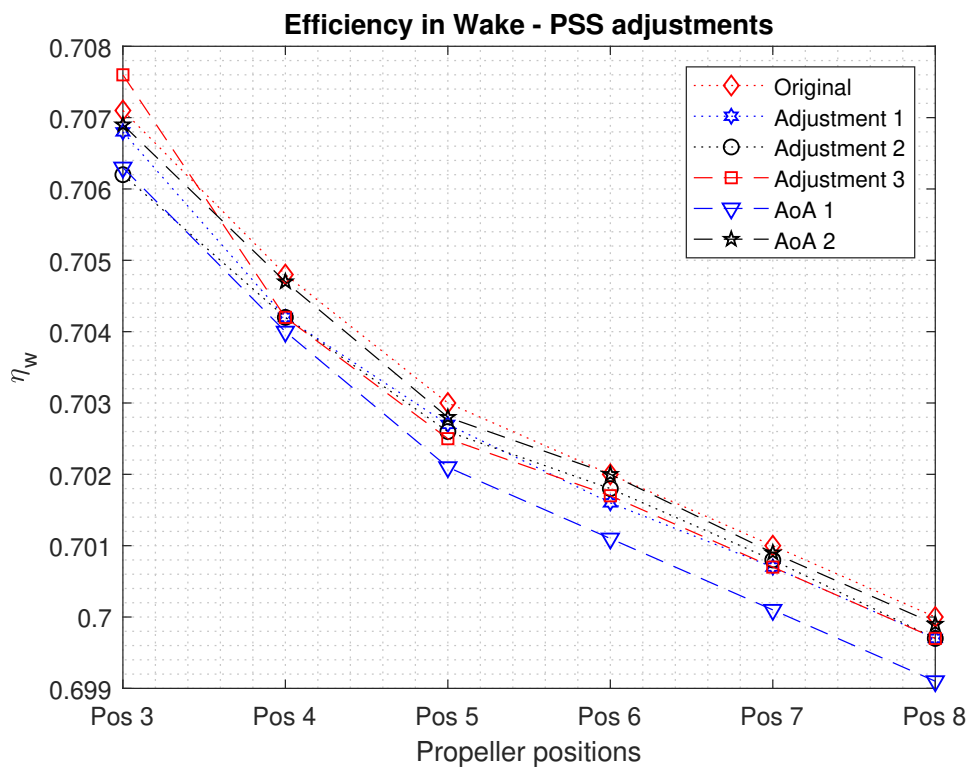


Figure E.7: Efficiency in wake comparison for different PSS adjustments.

E.4 Performance coefficients

Positions	3	4	5	6	7	8
Original	0.26463	0.26093	0.25776	0.25564	0.25426	0.25306
Adjustment 1	0.26393	0.26051	0.25693	0.25534	0.25406	0.25281
Adjustment 2	0.26426	0.26043	0.25763	0.25557	0.25426	0.25279
Adjustment 3	0.26379	0.26032	0.25742	0.25535	0.25404	0.25274
AoA 1	0.26295	0.25914	0.25593	0.25378	0.25241	0.25117
AoA 2	0.26473	0.26094	0.25777	0.25555	0.25433	0.25290

Table 2: Thrust coefficient for all PSS orientations

Positions	3	4	5	6	7	8
Original	0.03359	0.03323	0.03291	0.03269	0.03256	0.03245
Adjustment 1	0.03352	0.03321	0.03282	0.03267	0.03255	0.03243
Adjustment 2	0.03359	0.03320	0.03292	0.03269	0.03257	0.03243
Adjustment 3	0.03346	0.03318	0.03289	0.03267	0.03254	0.03243
AoA 1	0.03342	0.03304	0.03272	0.03249	0.03236	0.03225
AoA 2	0.03362	0.03324	0.03292	0.03268	0.03257	0.03243

Table 3: Torque coefficient for all PSS orientations

F Wake Field

F.1 Naked hull

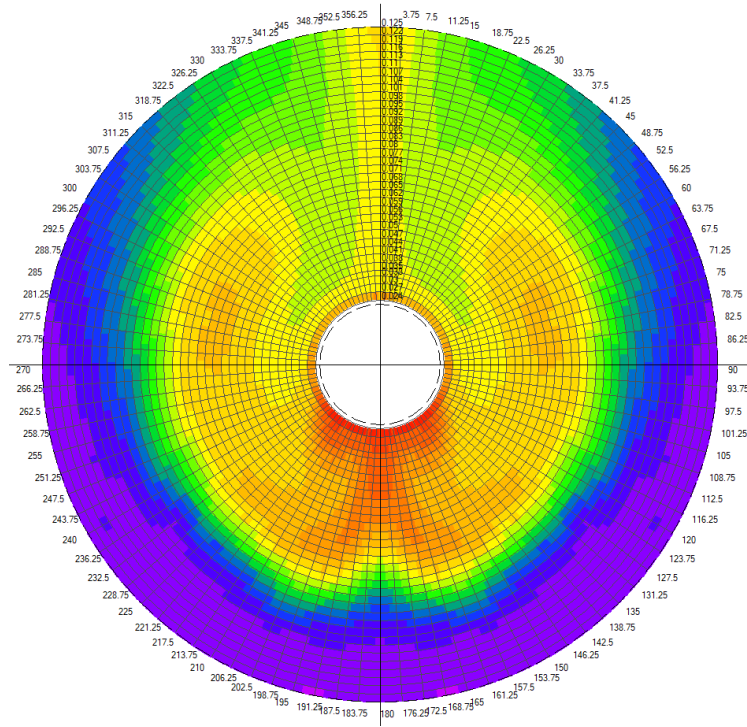


Figure F.1: Nominal Wake Ref 1 Pos 4 - Naked

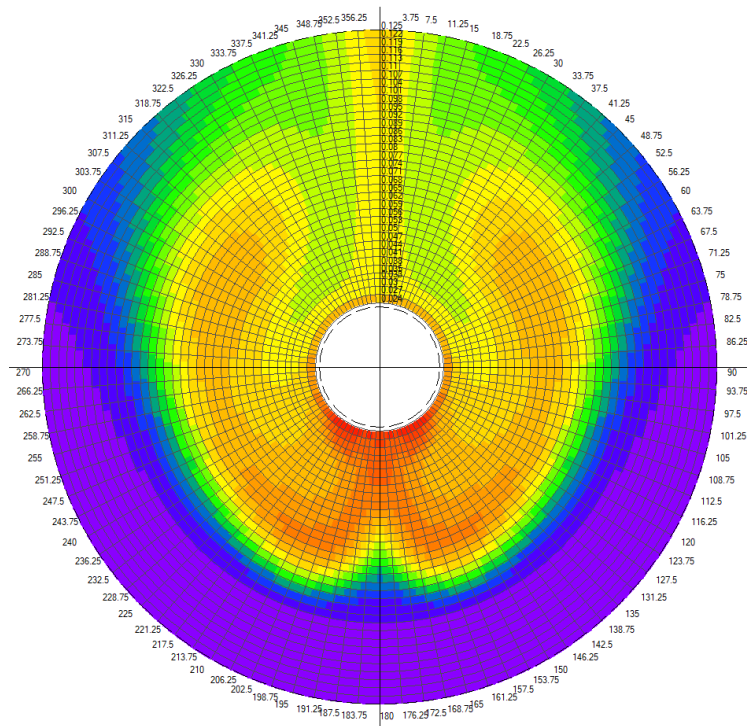


Figure F.2: Nominal Wake Ref 2 Pos 4 - Naked

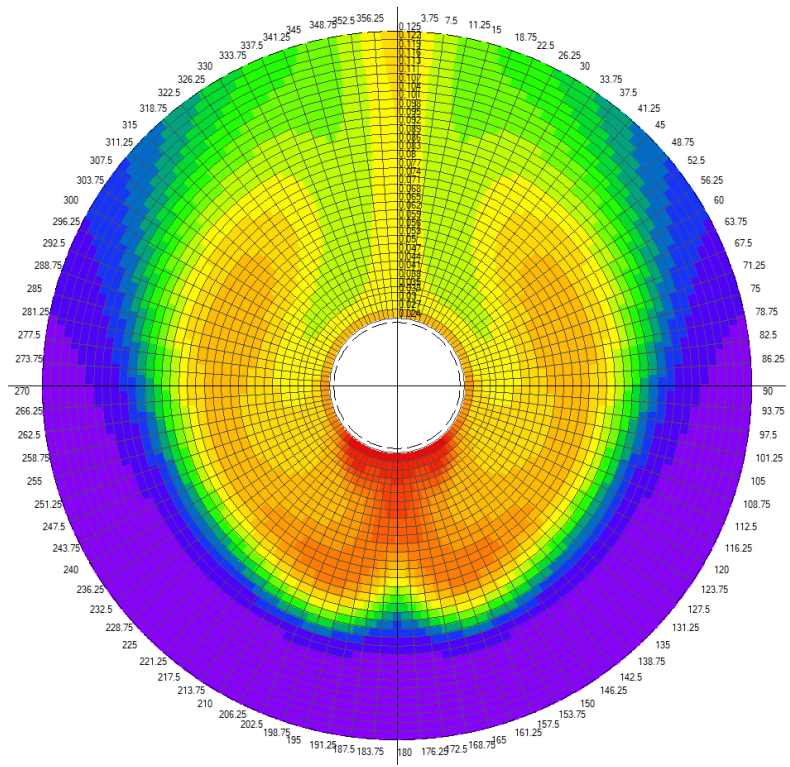


Figure F.3: Nominal Wake Ref 3 Pos 4 - Naked

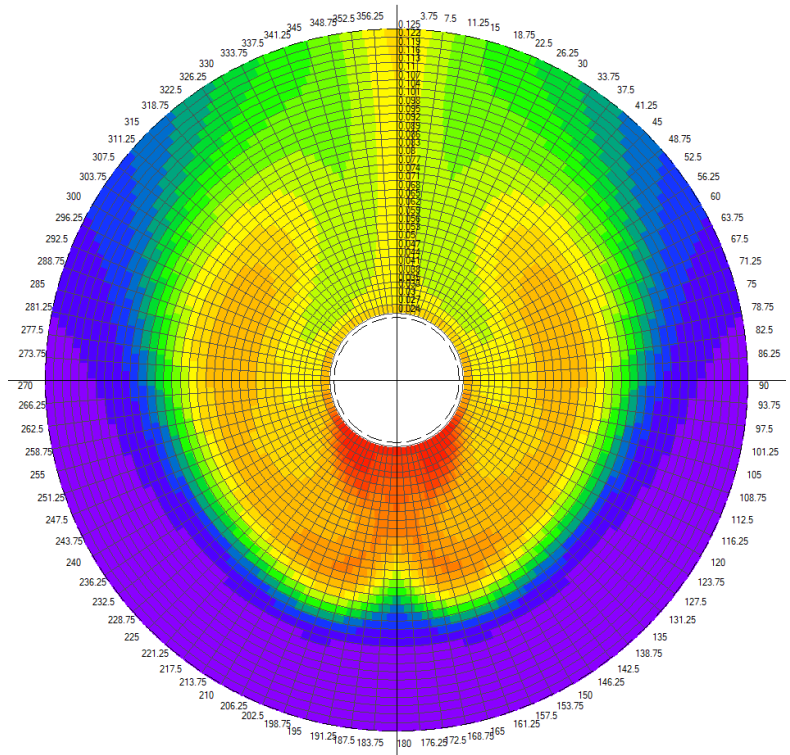


Figure F.4: Nominal Wake Ref 4 Pos 4 - Naked

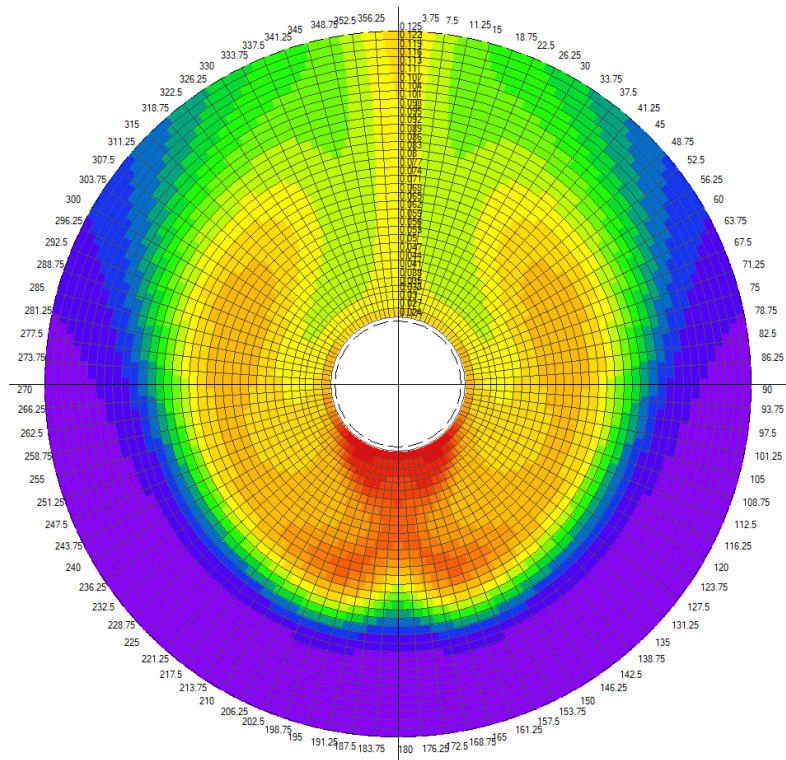


Figure F.5: Nominal Wake Ref 5 Pos 4 - Naked

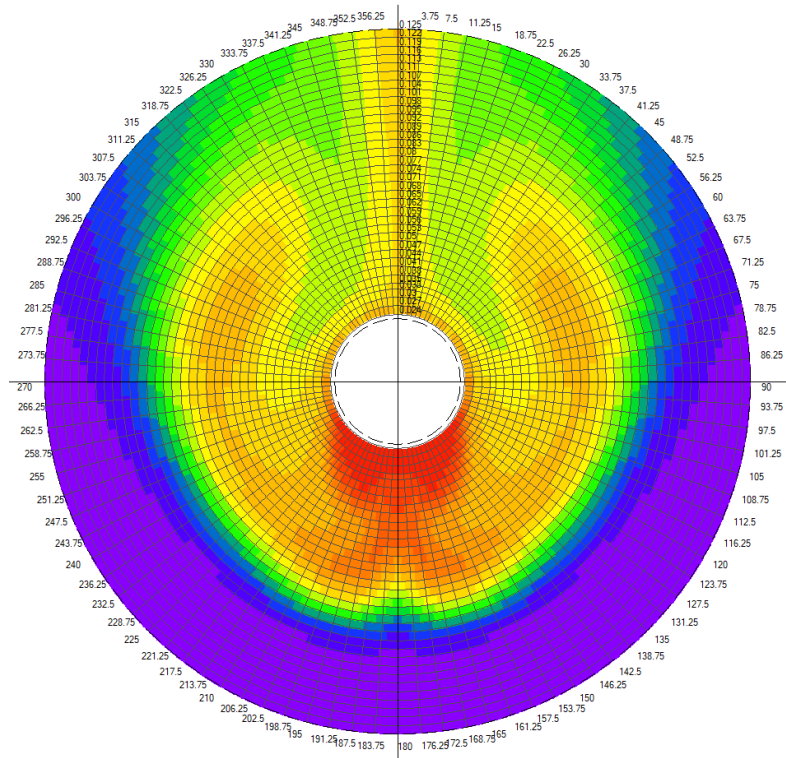


Figure F.6: Nominal Wake Ref 6 Pos 4 - Naked

F.1.1 Effective Wake

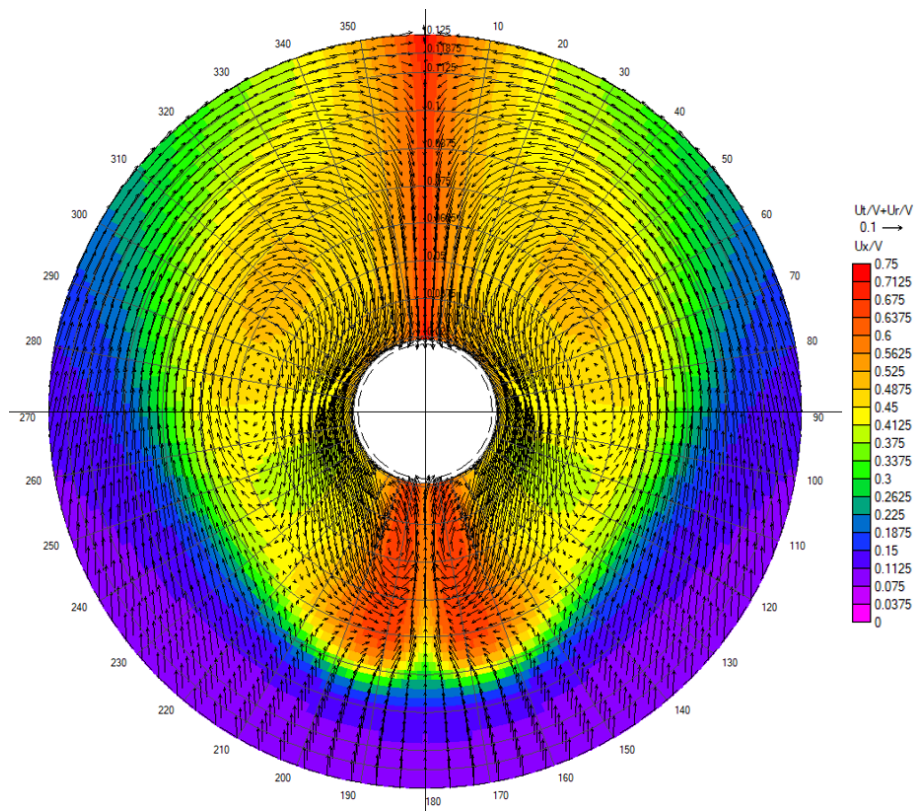


Figure F.7: Effective Wake - Naked Position 1

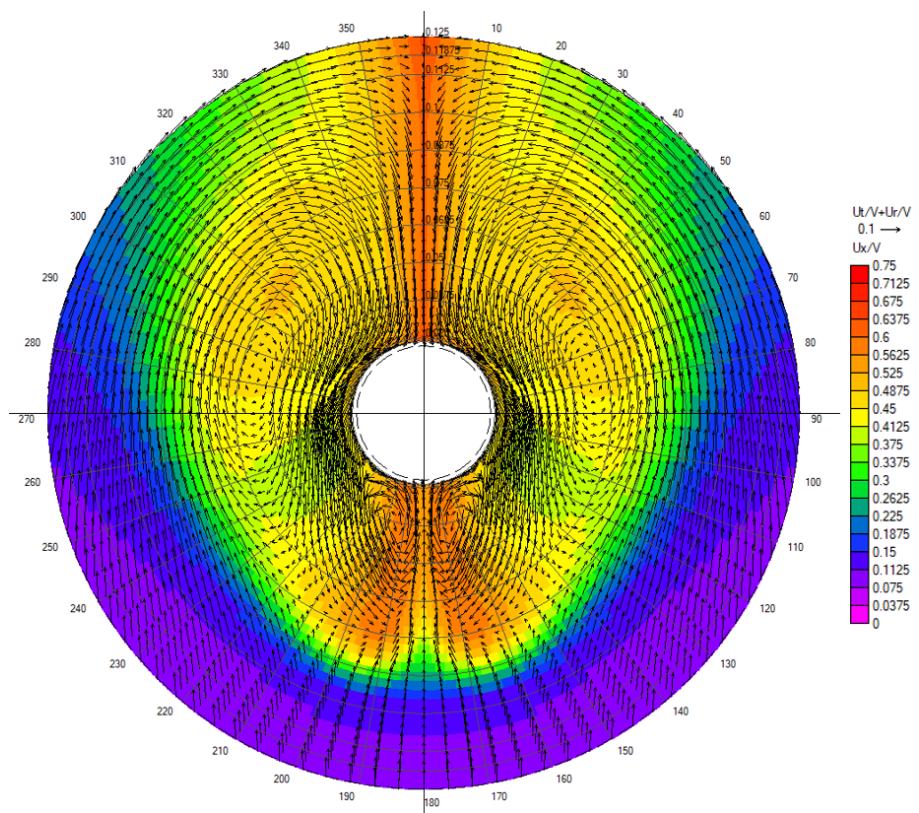


Figure F.8: Effective Wake - Naked Position 2

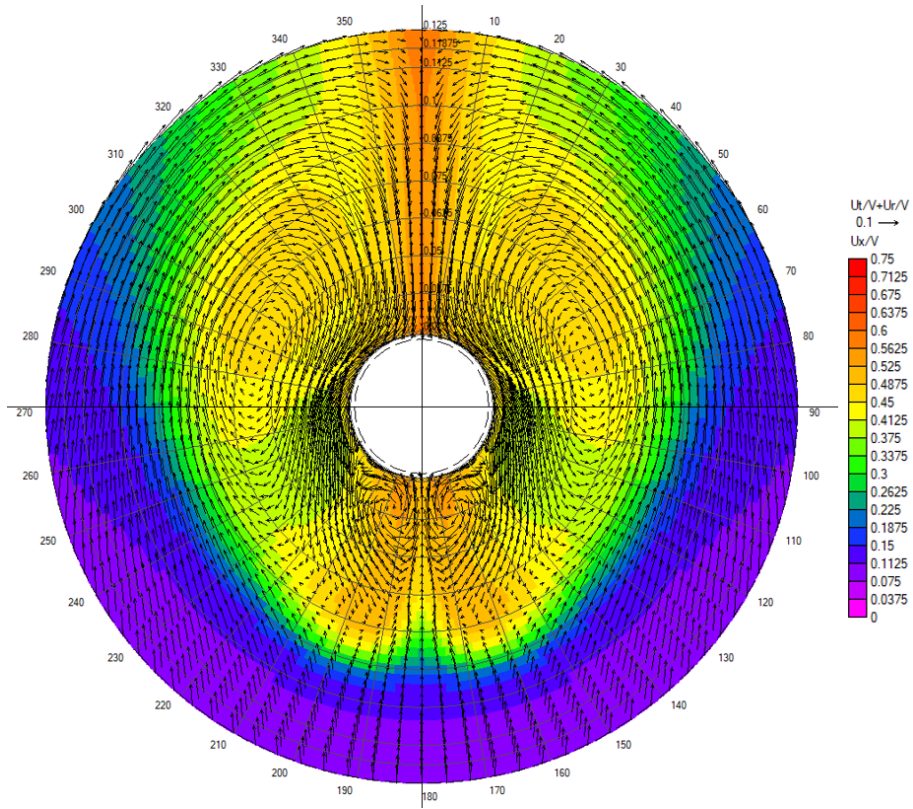


Figure F.9: Effective Wake - Naked Position 3

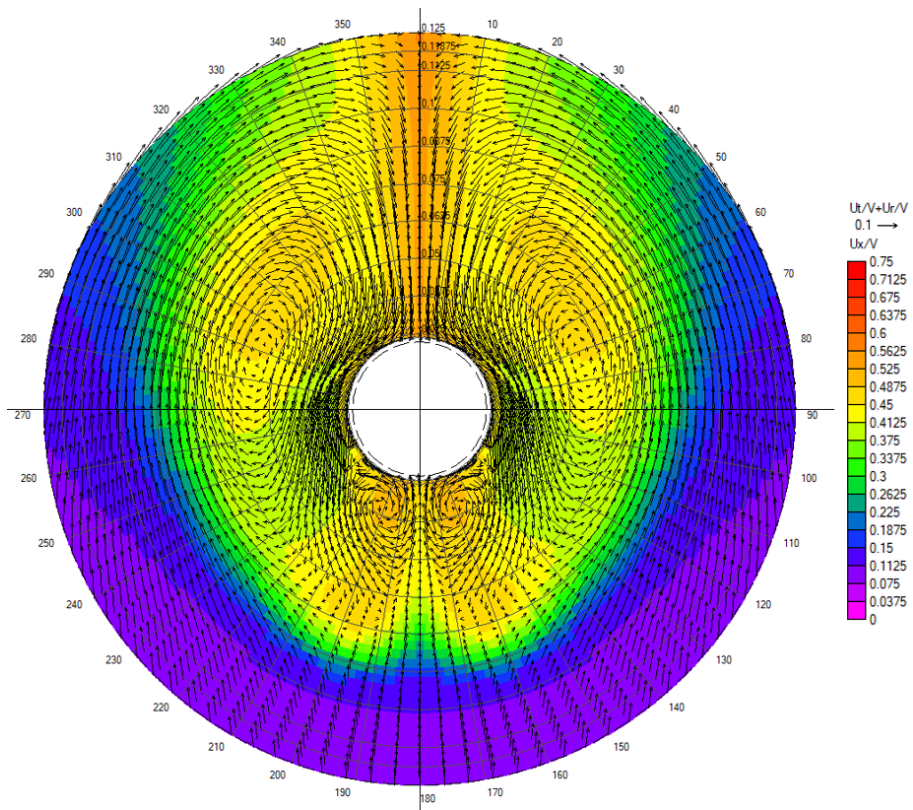


Figure F.10: Effective Wake - Naked Position 4

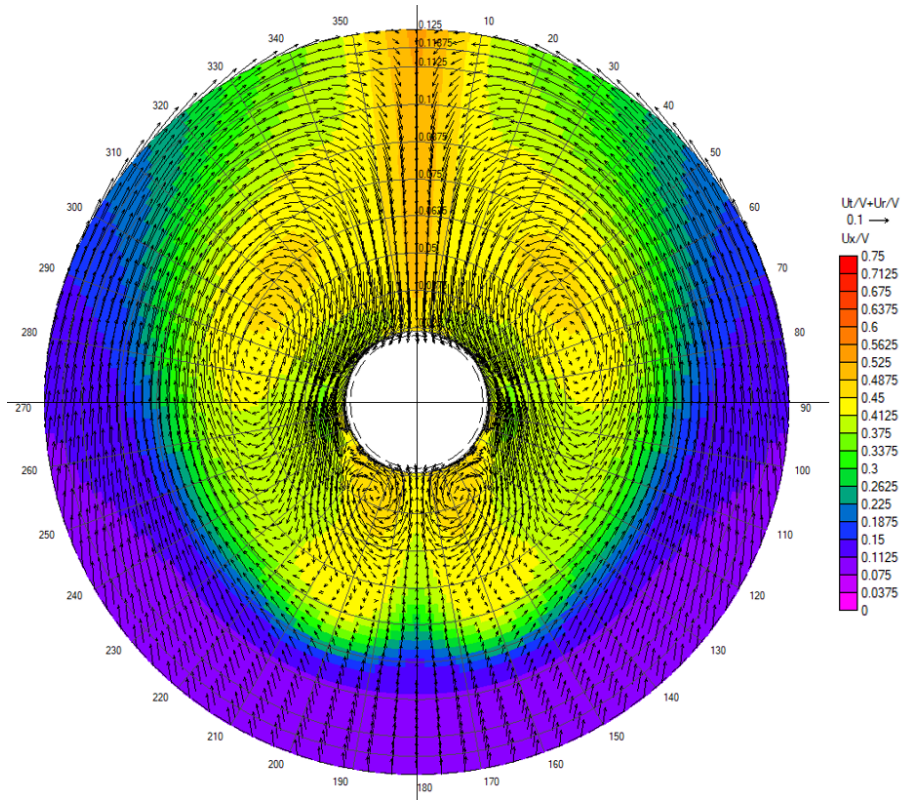


Figure F.11: Effective Wake - Naked Position 5

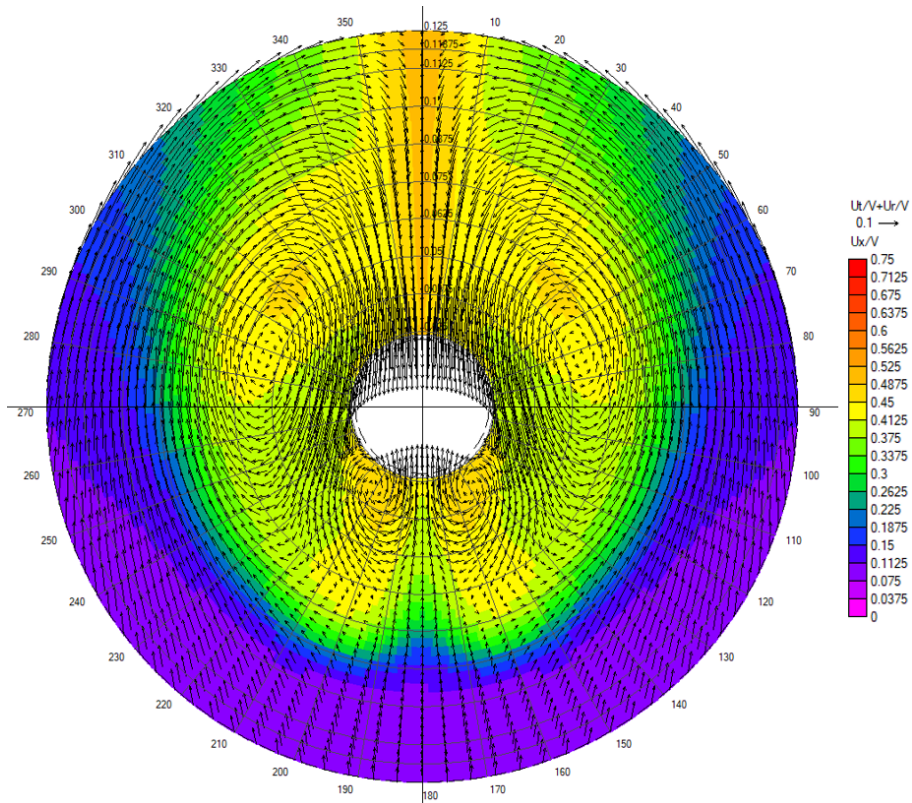


Figure F.12: Effective Wake - Naked Position 6

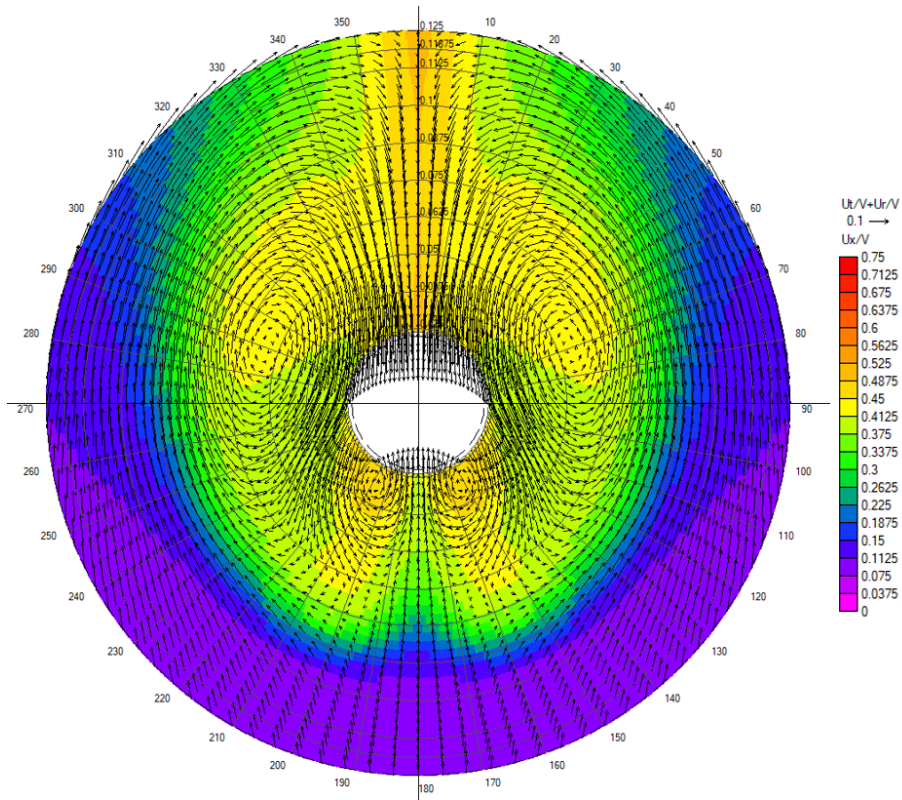


Figure F.13: Effective Wake - Naked Position 7

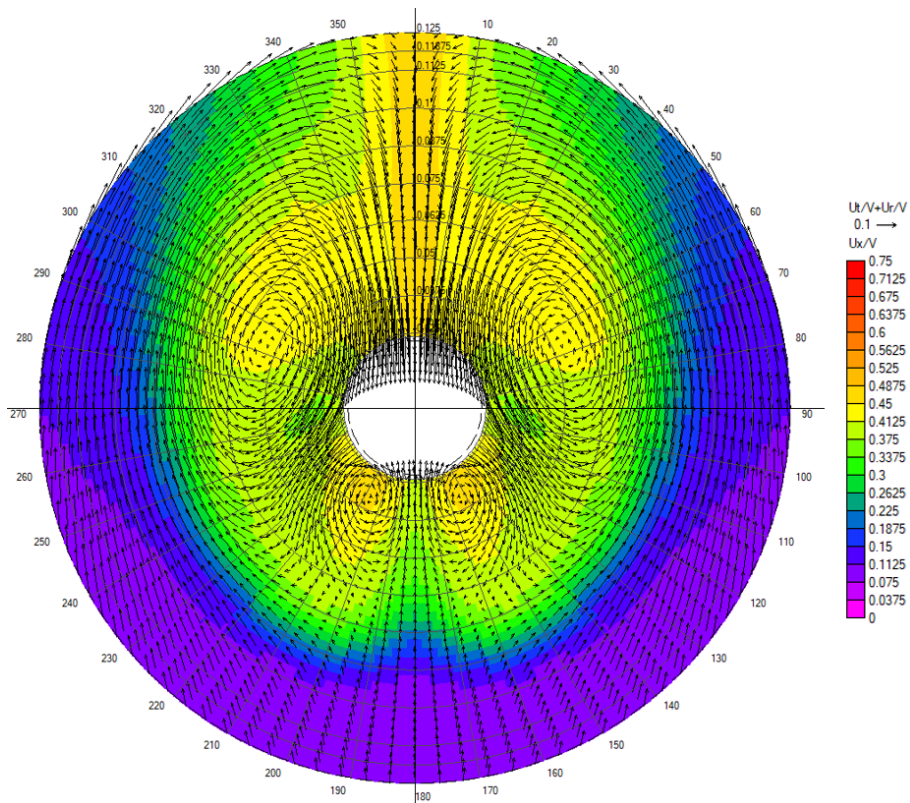


Figure F.14: Effective Wake - Naked Position 8

F.2 Hull with PSS

F.2.1 Nominal Wake

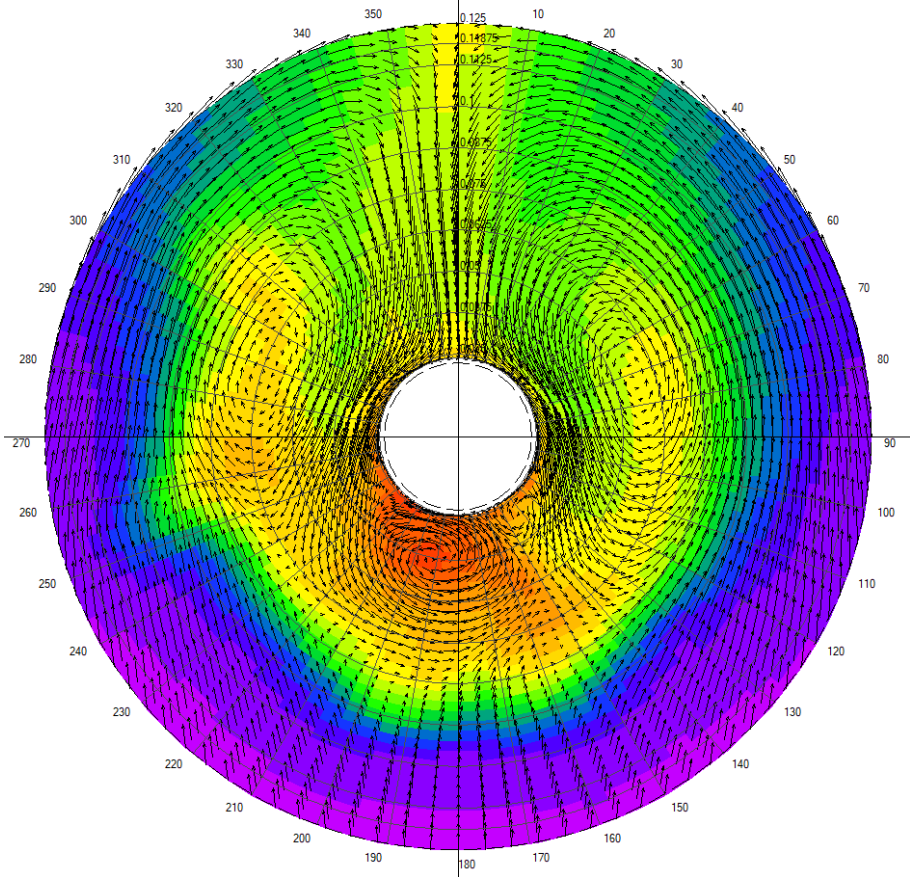


Figure F.15: Nominal Wake Ref 1 Pos 4 - PSS

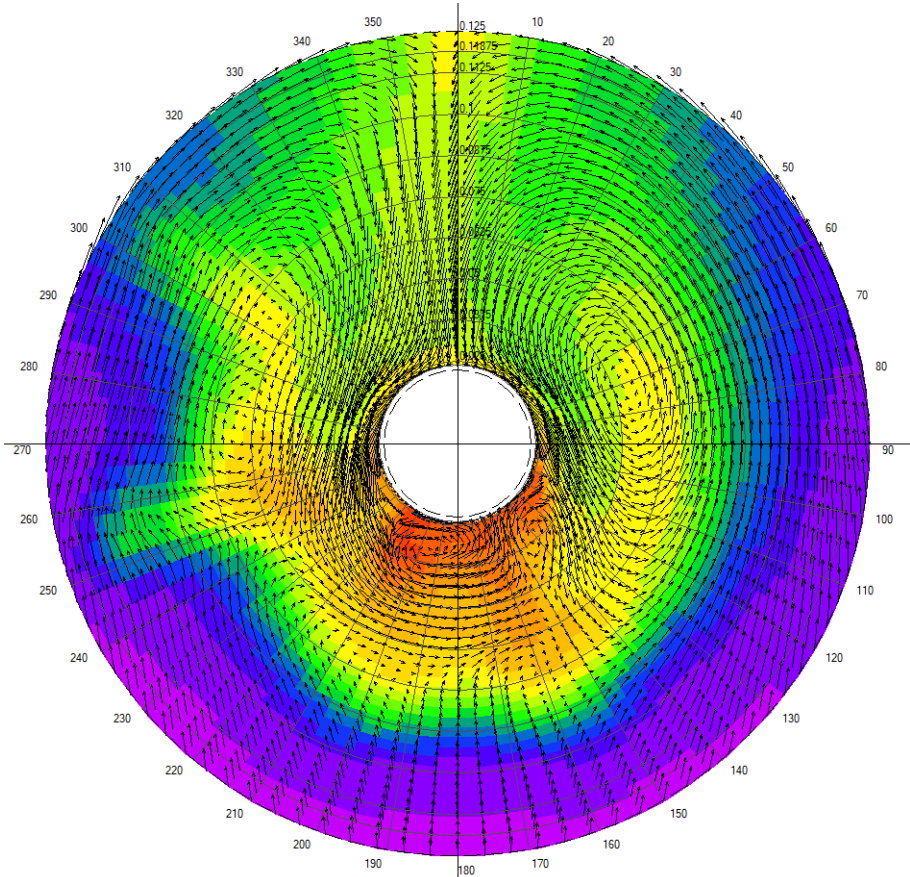


Figure F.16: Nominal Wake Ref 2 Pos 4 - PSS

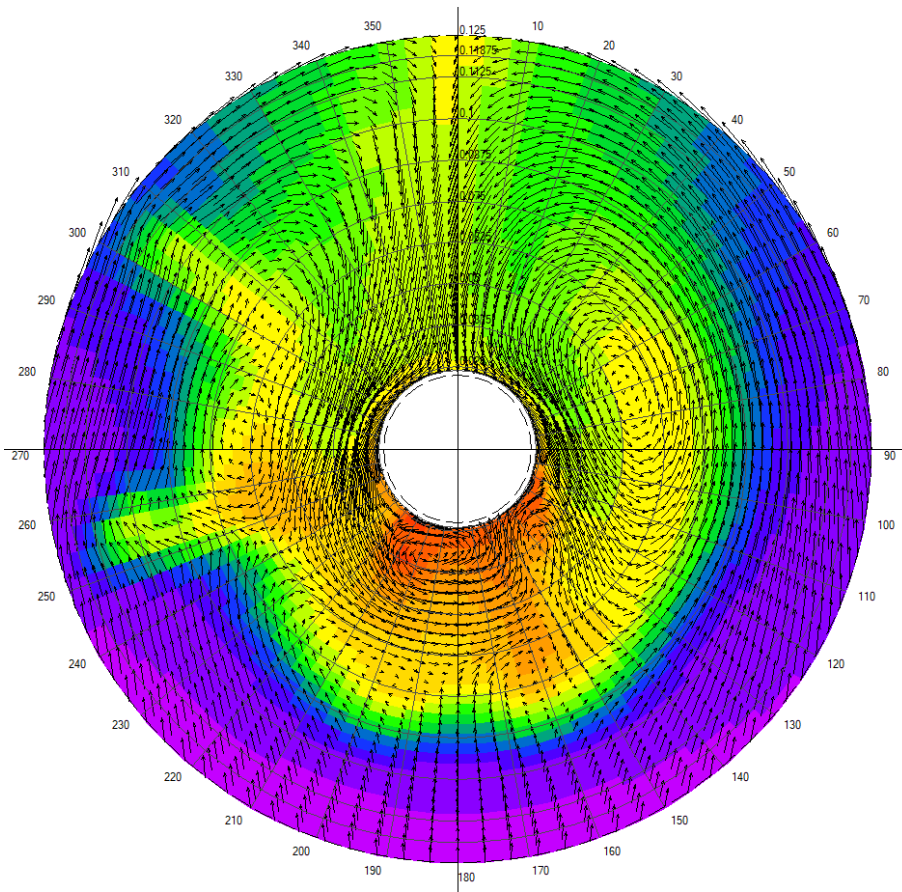


Figure F.17: Nominal Wake Ref 3 Pos 4 - PSS

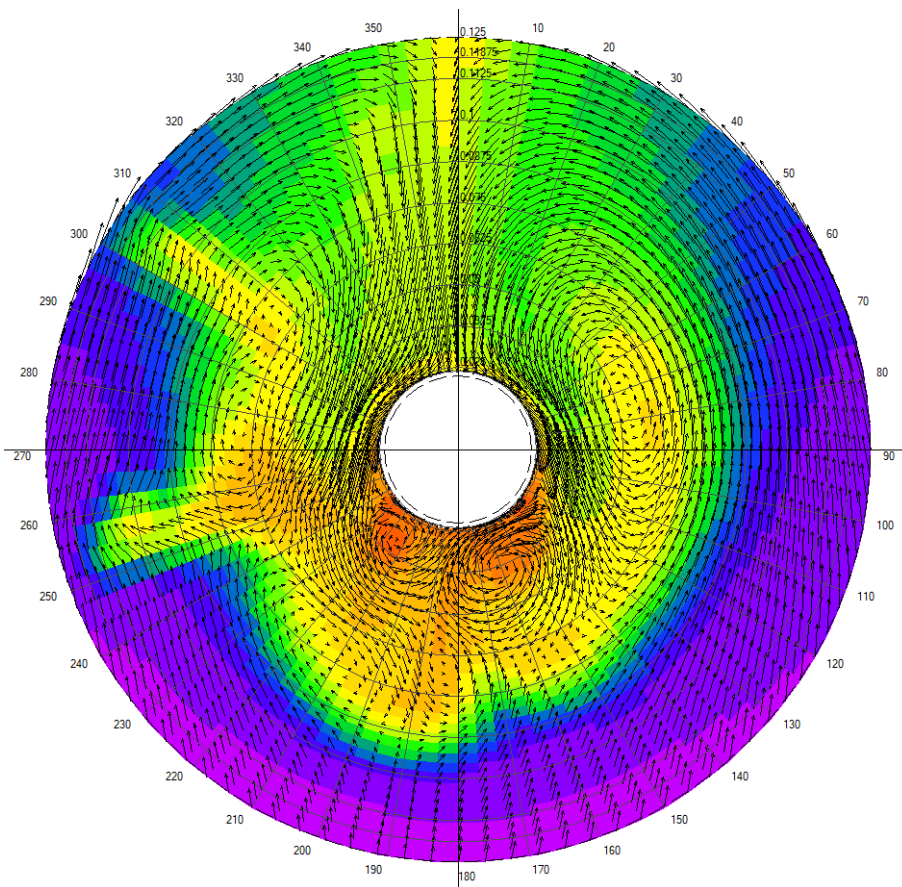


Figure F.18: Nominal Wake Ref 4 Pos 4 - PSS

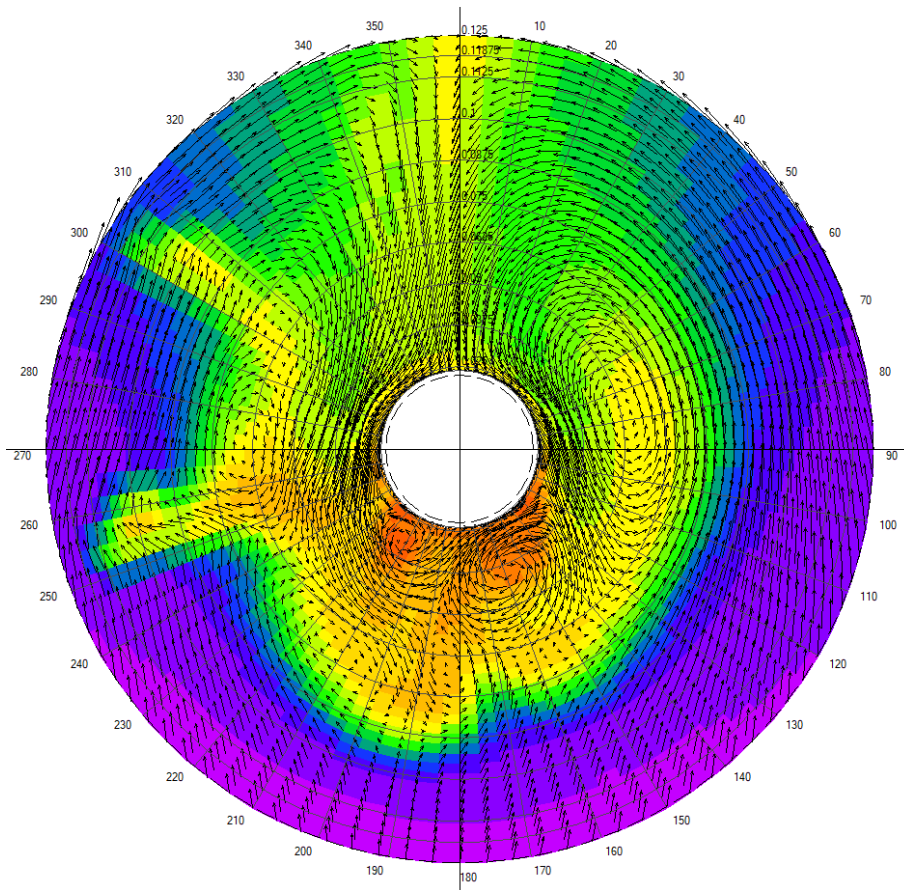


Figure F.19: Nominal Wake Ref 5 Pos 4 - PSS

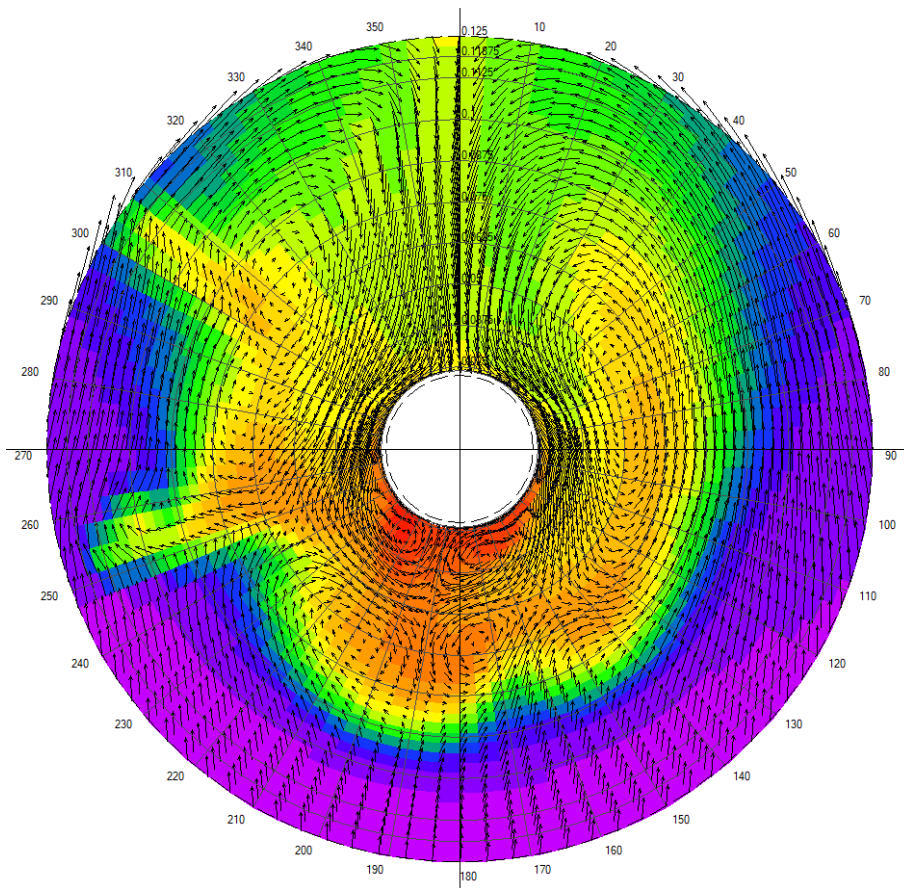


Figure F.20: Nominal Wake Ref 6 Pos 4 - PSS

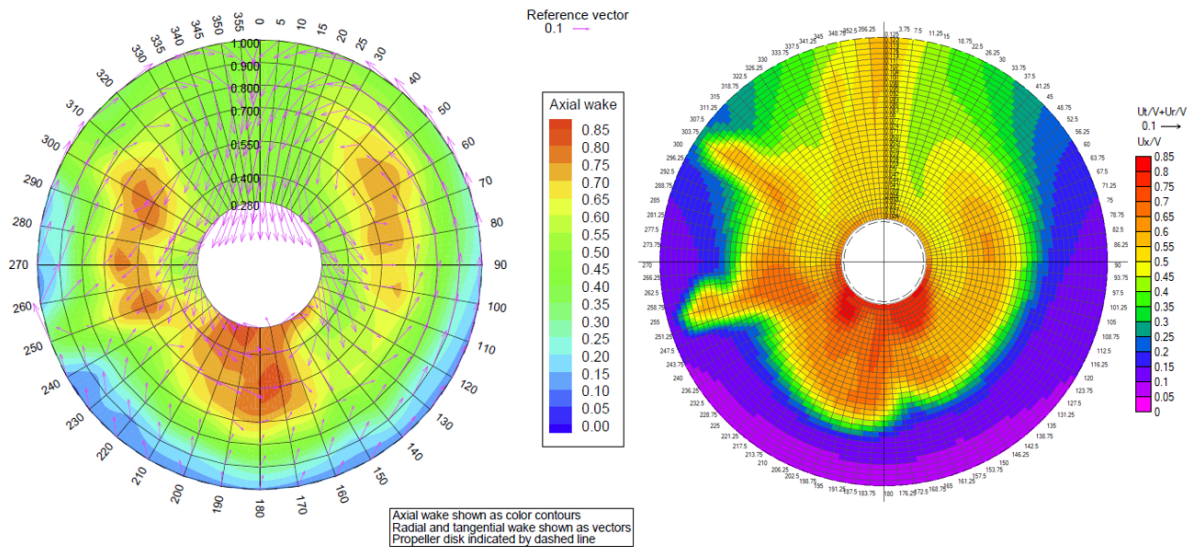


Figure F.21: Comparison of nominal wake at propeller location. Formerly conducted CFD by SINTEF (left) and obtained results from refinement 4 (right)

F.2.2 Effective Wake

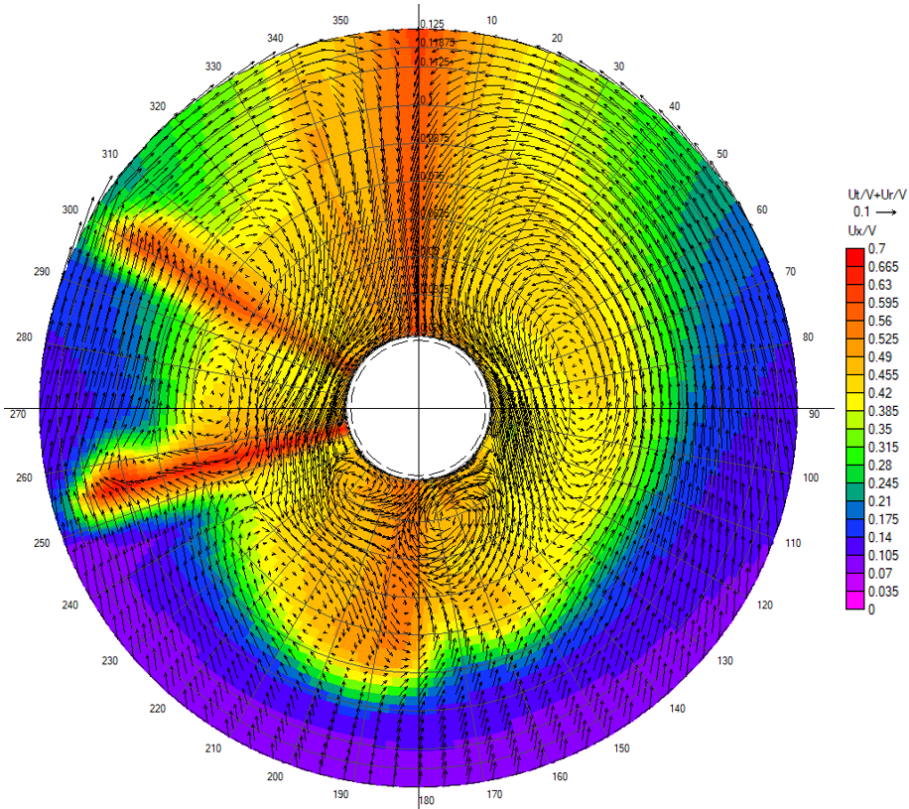


Figure F.22: Effective Wake - PSS Adjustment 1 Position 3

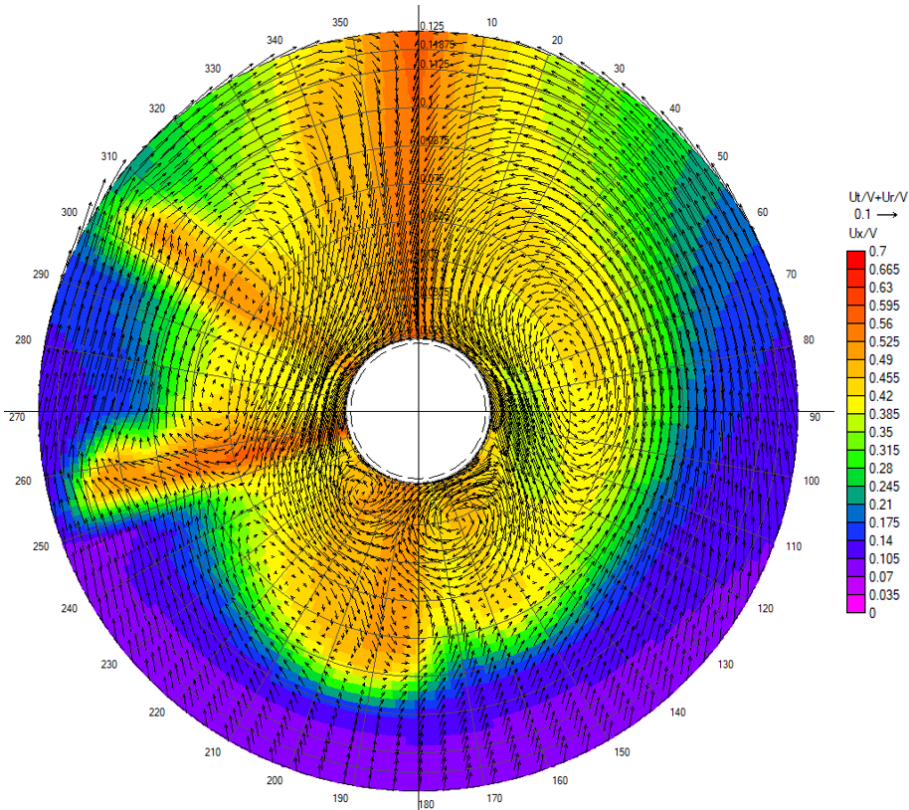


Figure F.23: Effective Wake - PSS Adjustment 1 Position 4

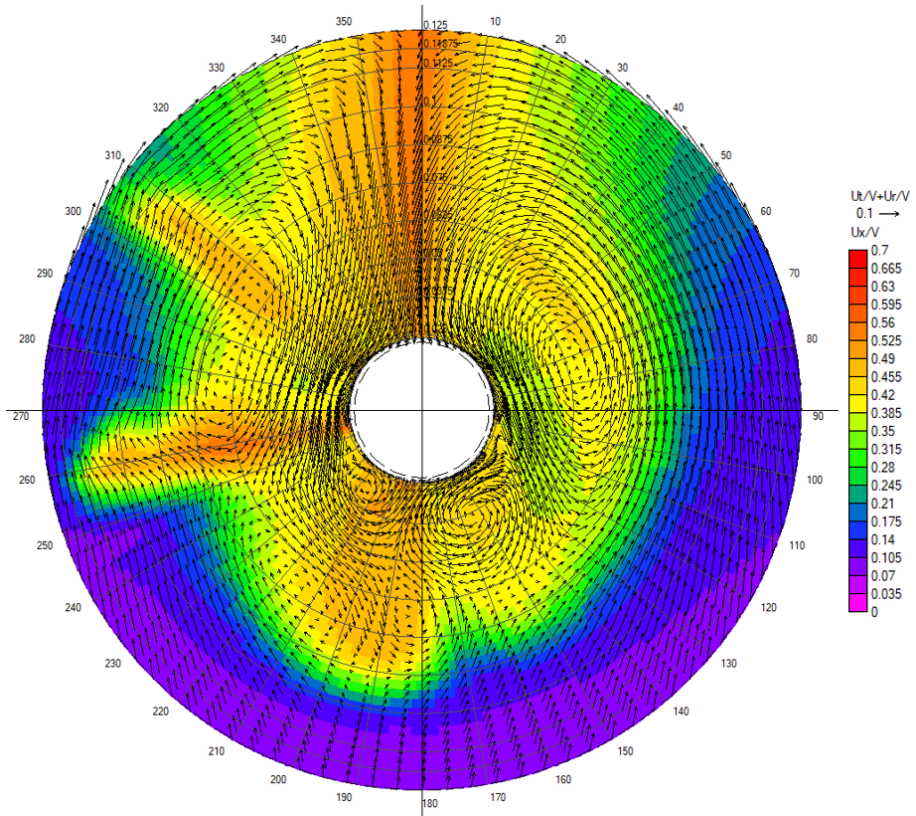


Figure F.24: Effective Wake - PSS Adjustment 1 Position 5

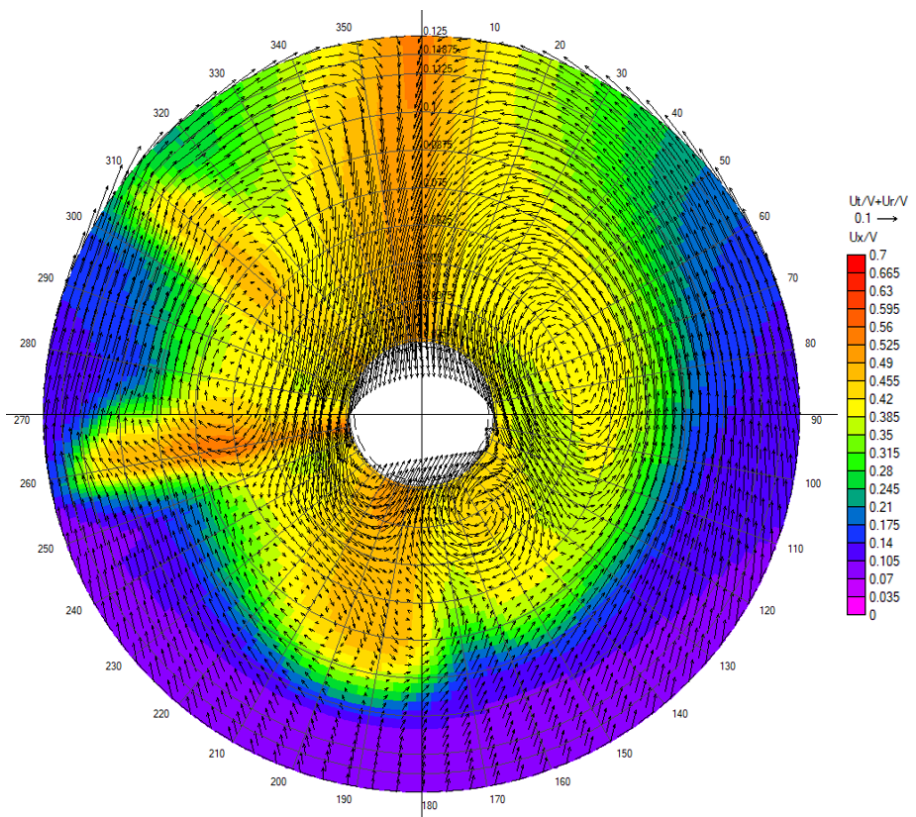


Figure F.25: Effective Wake - PSS Adjustment 1 Position 6

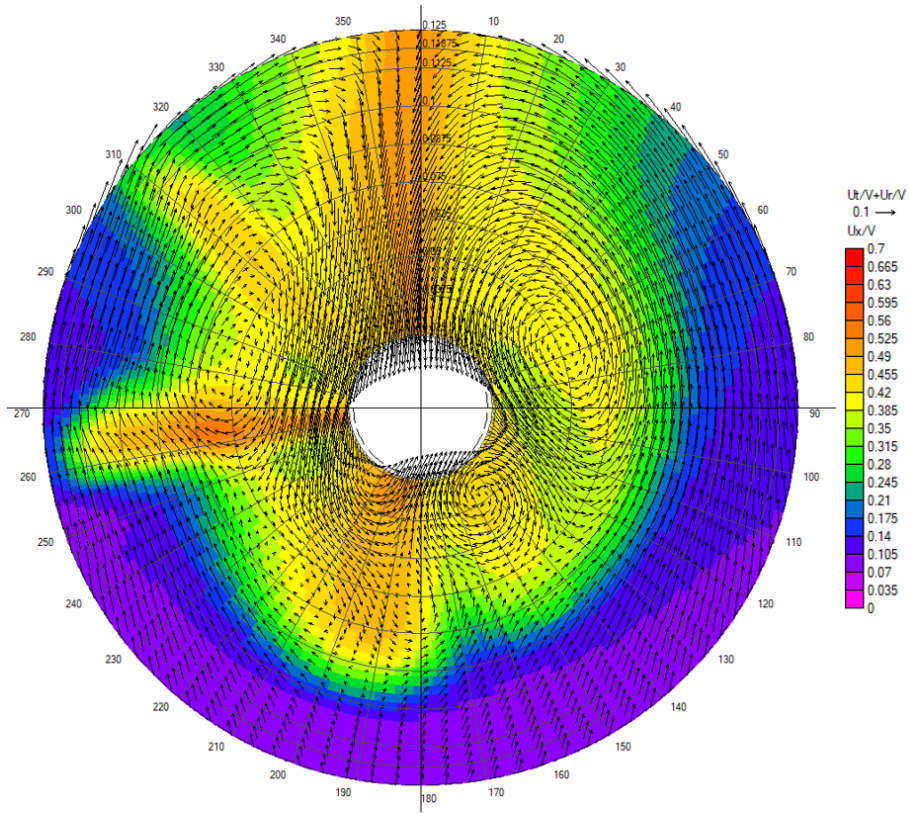


Figure F.26: Effective Wake - PSS Adjustment 1 Position 7

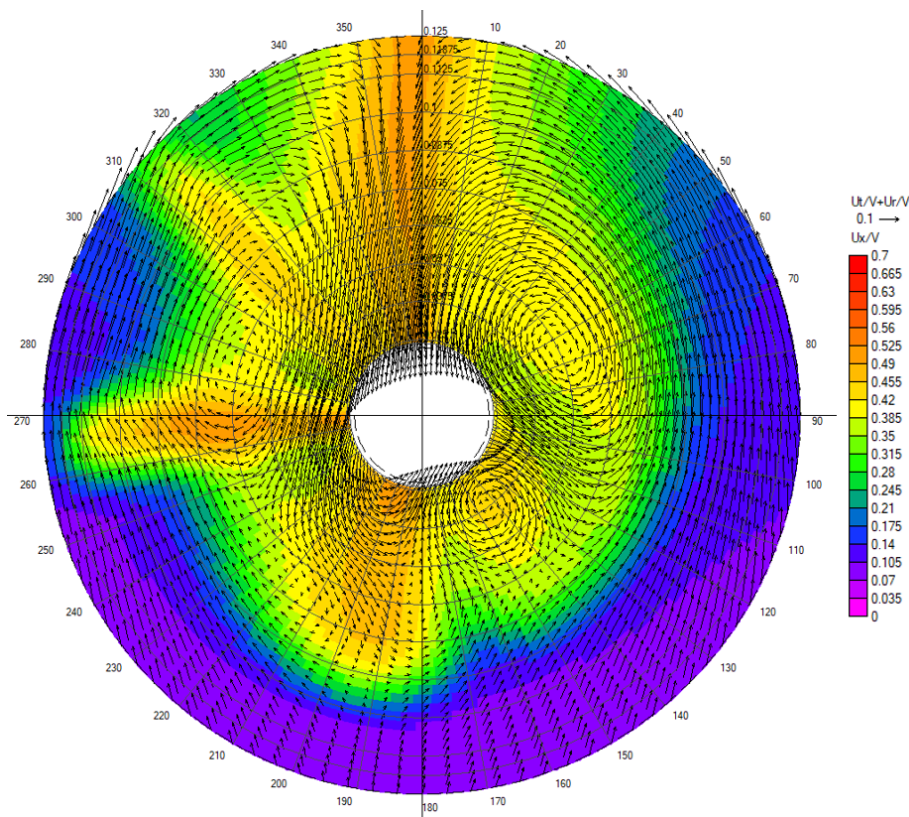


Figure F.27: Effective Wake - PSS Adjustment 1 Position 8

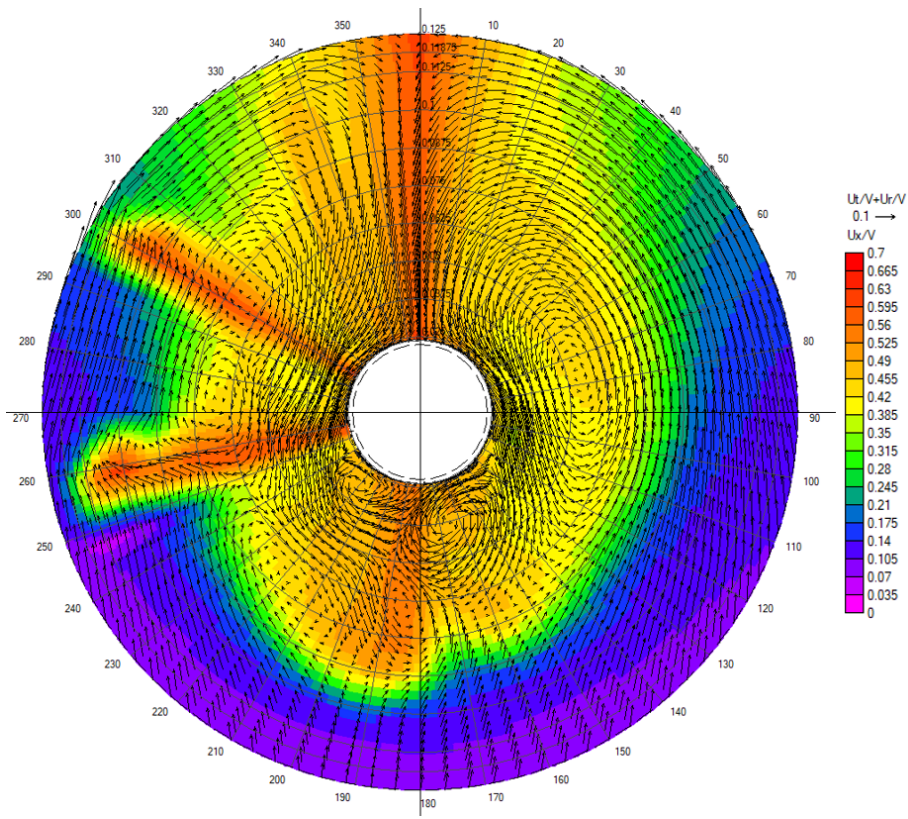


Figure F.28: Effective Wake - PSS Adjustment 2 Position 3

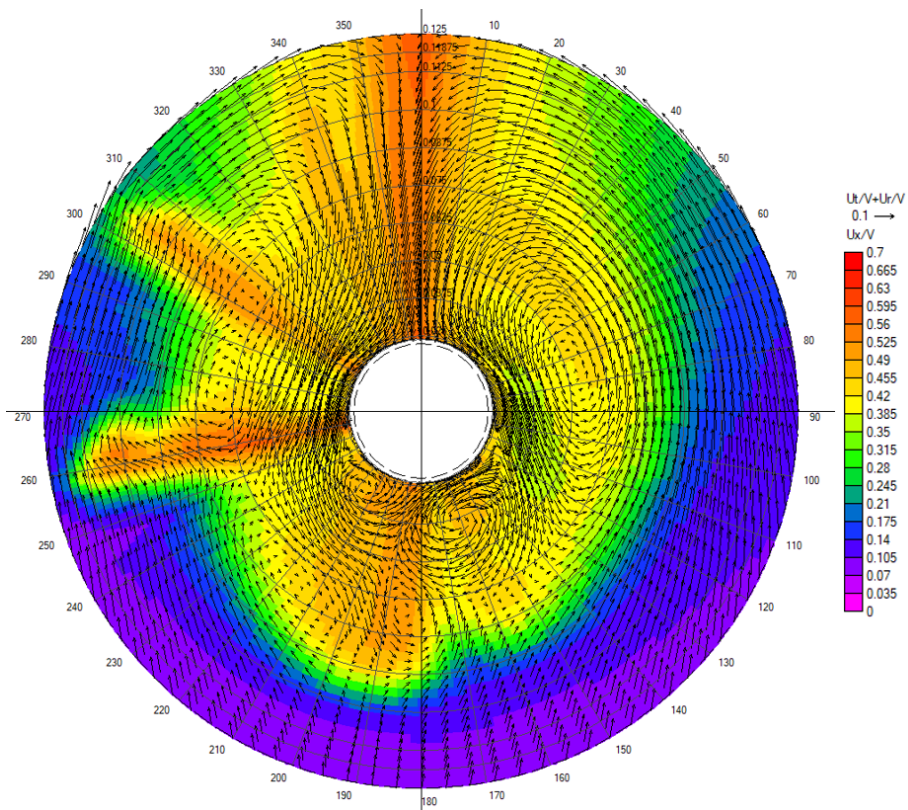


Figure F.29: Effective Wake - PSS Adjustment 2 Position 4

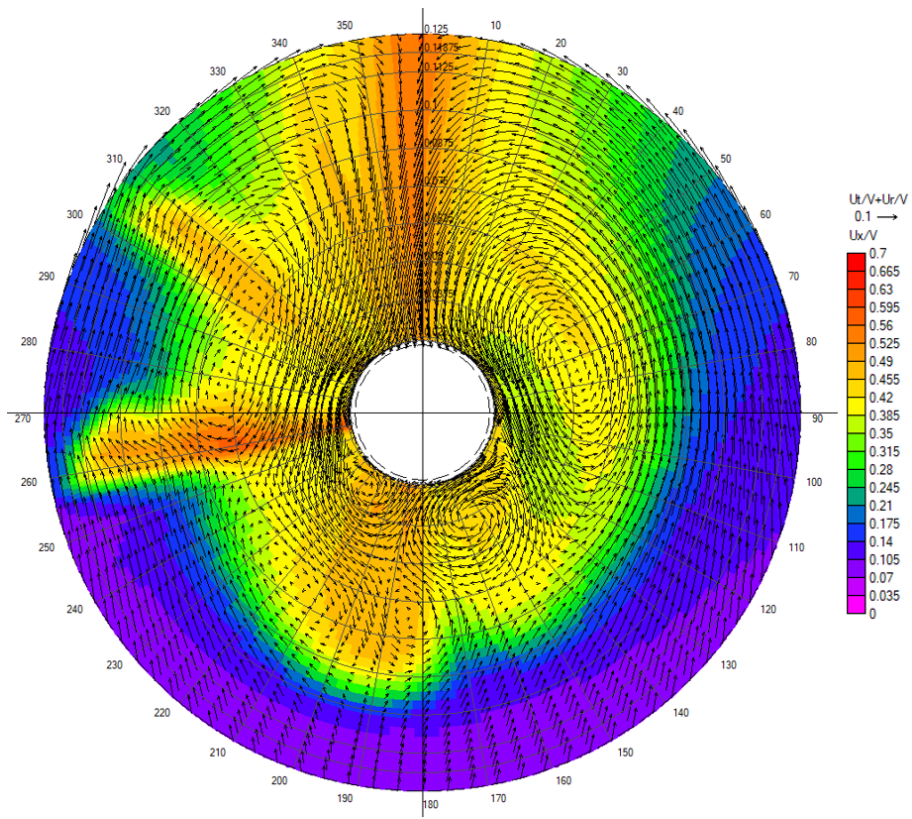


Figure F.30: Effective Wake - PSS Adjustment 2 Position 5

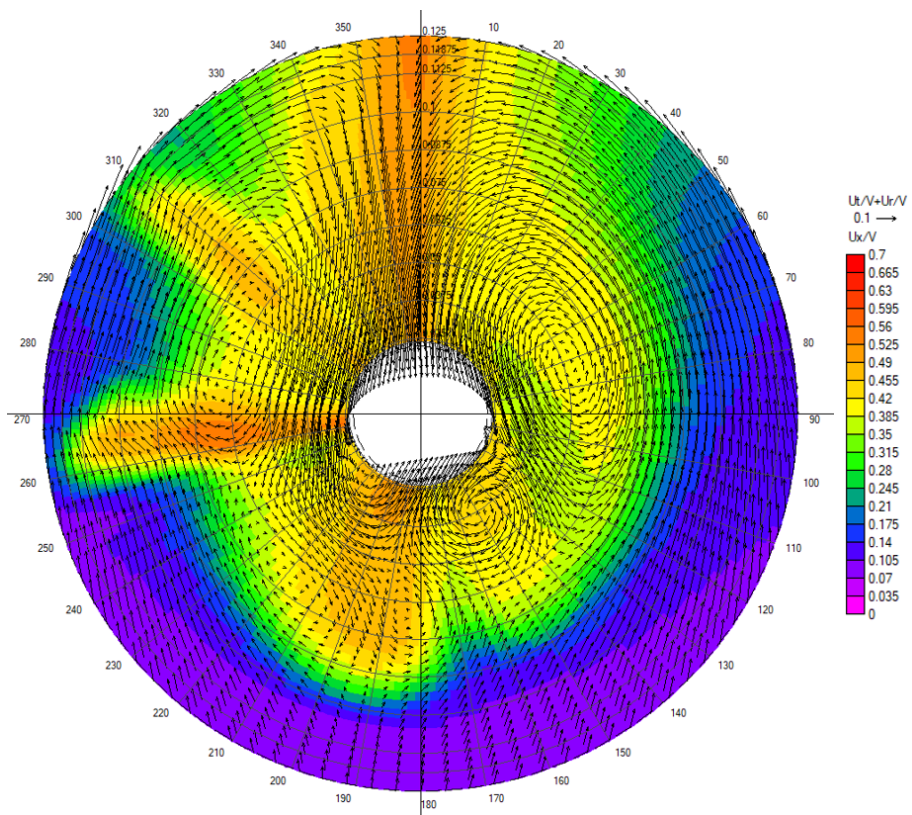


Figure F.31: Effective Wake - PSS Adjustment 2 Position 6

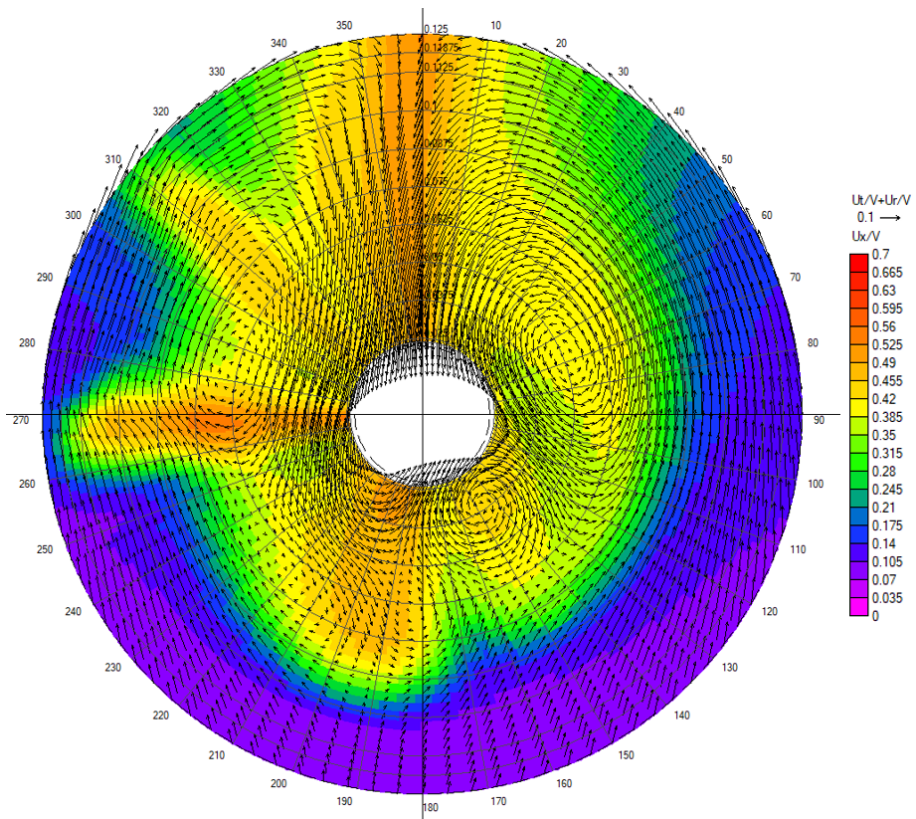


Figure F.32: Effective Wake - PSS Adjustment 2 Position 7

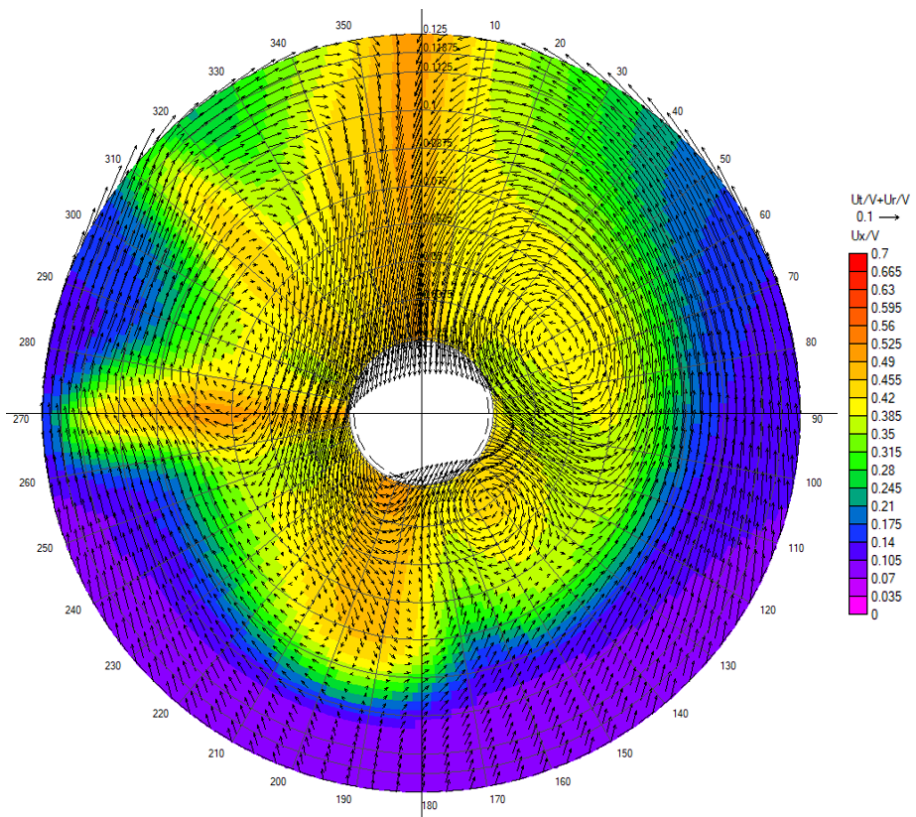


Figure F.33: Effective Wake - PSS Adjustment 2 Position 8

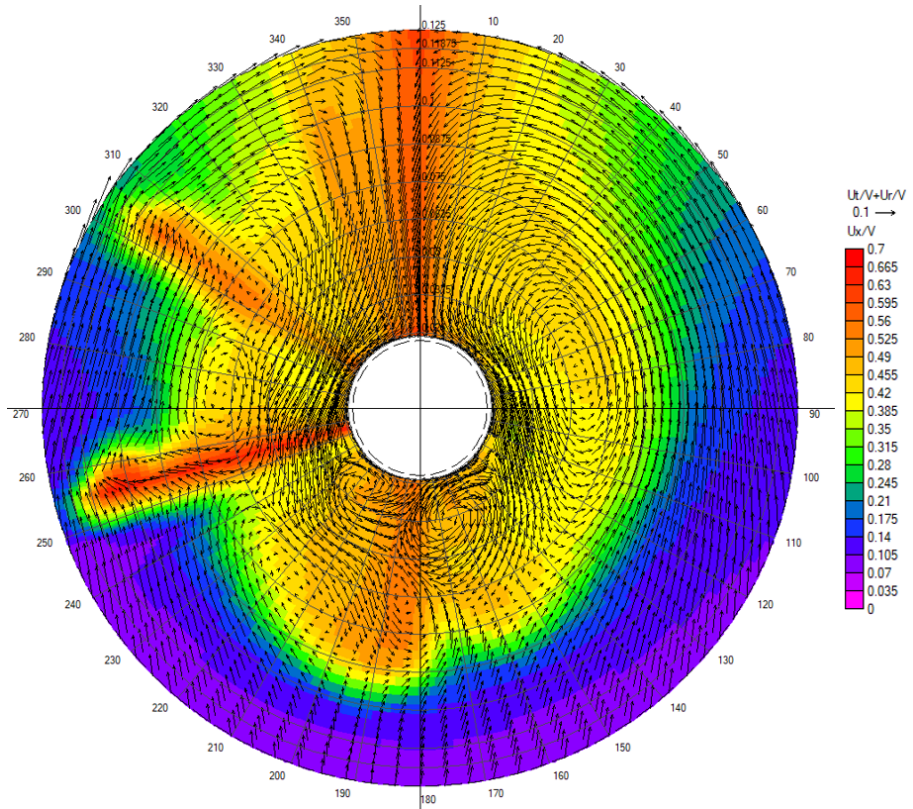


Figure F.34: Effective Wake - PSS Adjustment 3 Position 3

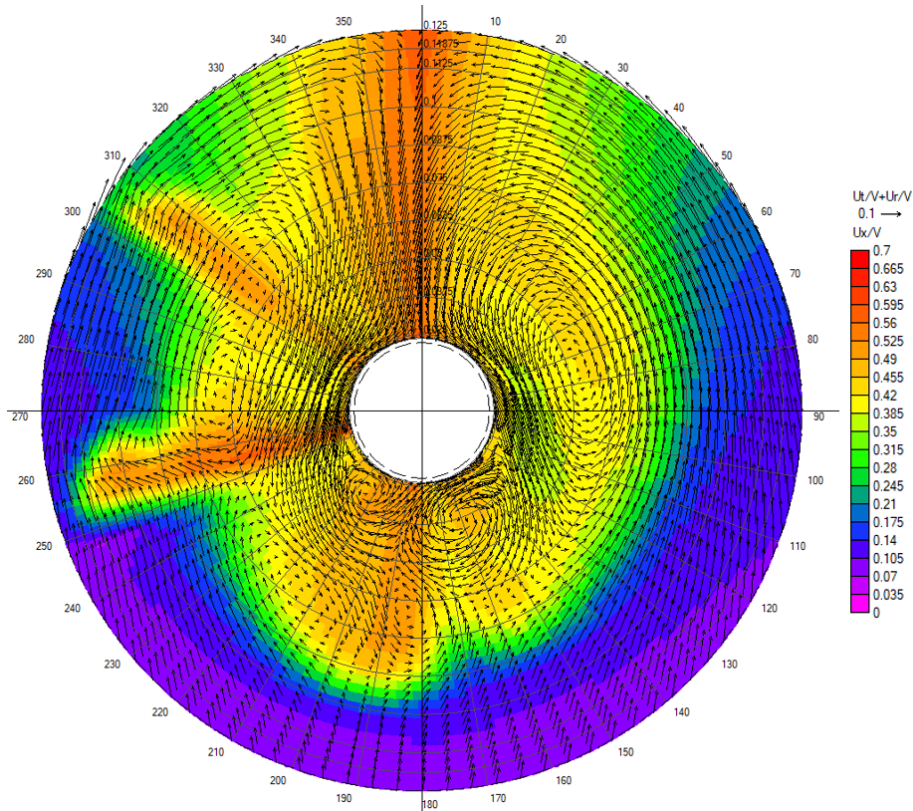


Figure F.35: Effective Wake - PSS Adjustment 3 Position 4

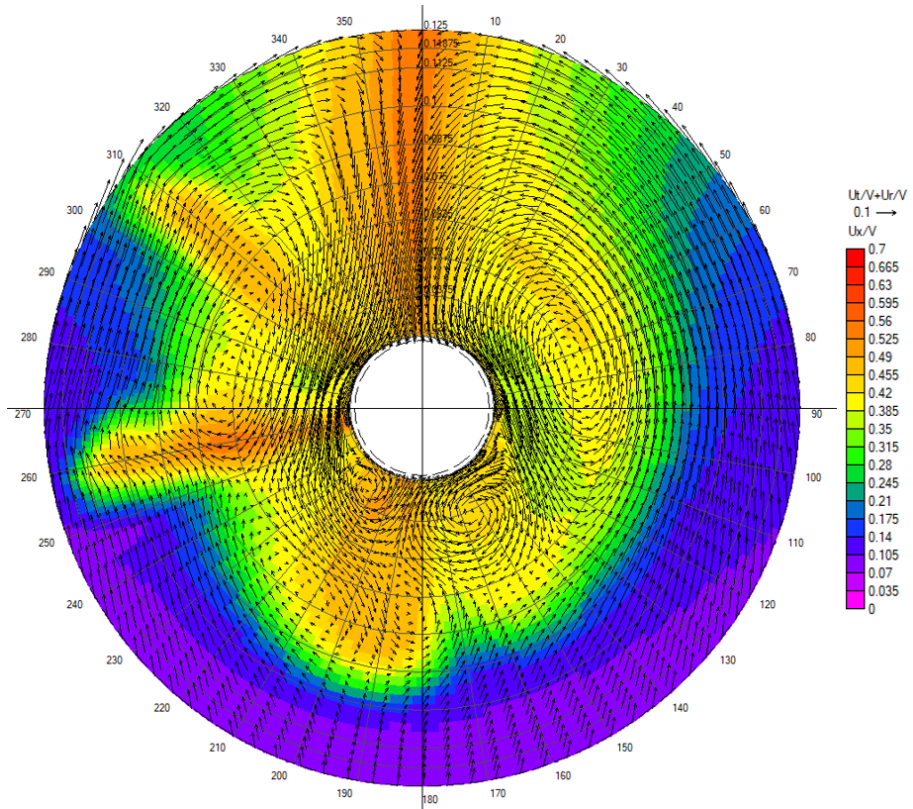


Figure F.36: Effective Wake - PSS Adjustment 3 Position 5

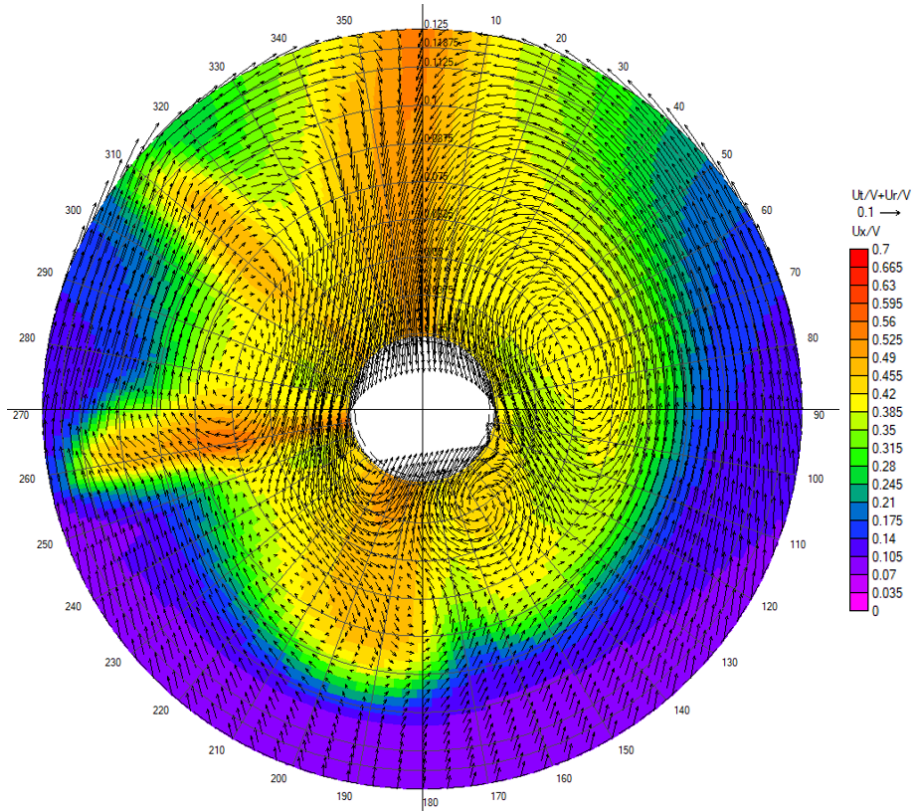


Figure F.37: Effective Wake - PSS Adjustment 3 Position 6

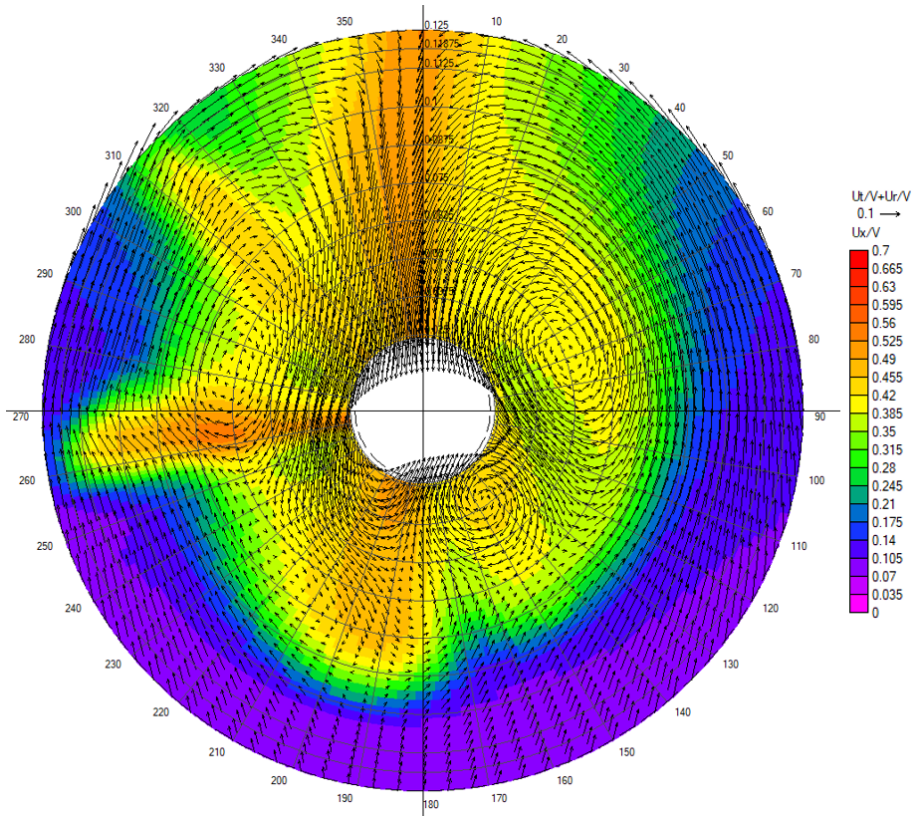


Figure F.38: Effective Wake - PSS Adjustment 3 Position 7

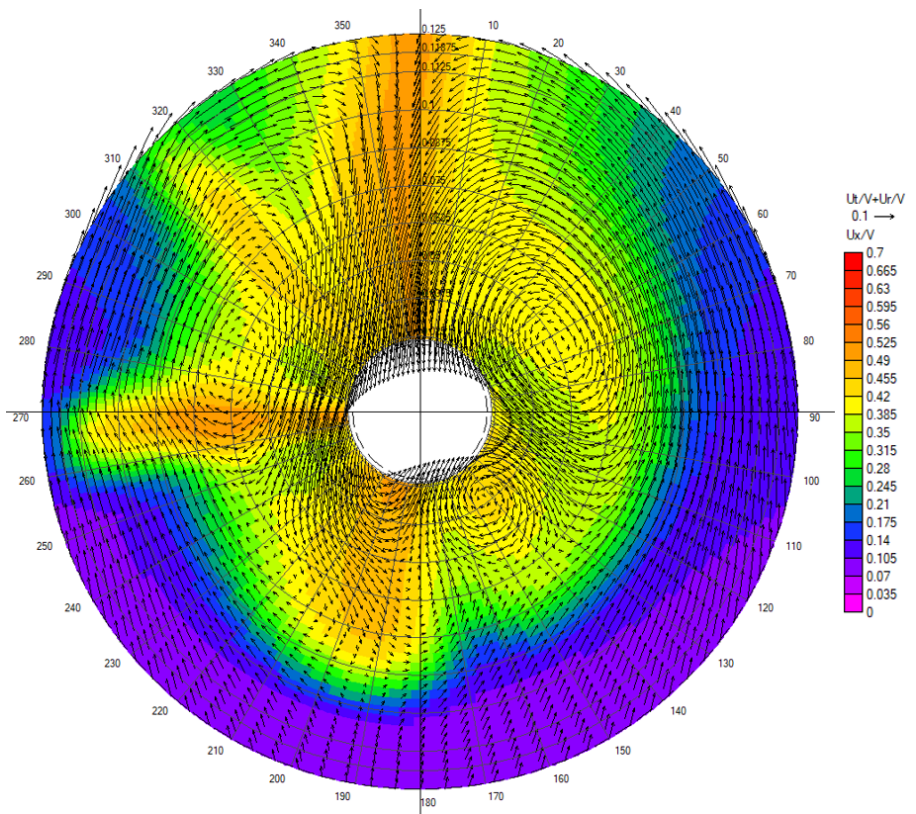


Figure F.39: Effective Wake - PSS Adjustment 3 Position 8

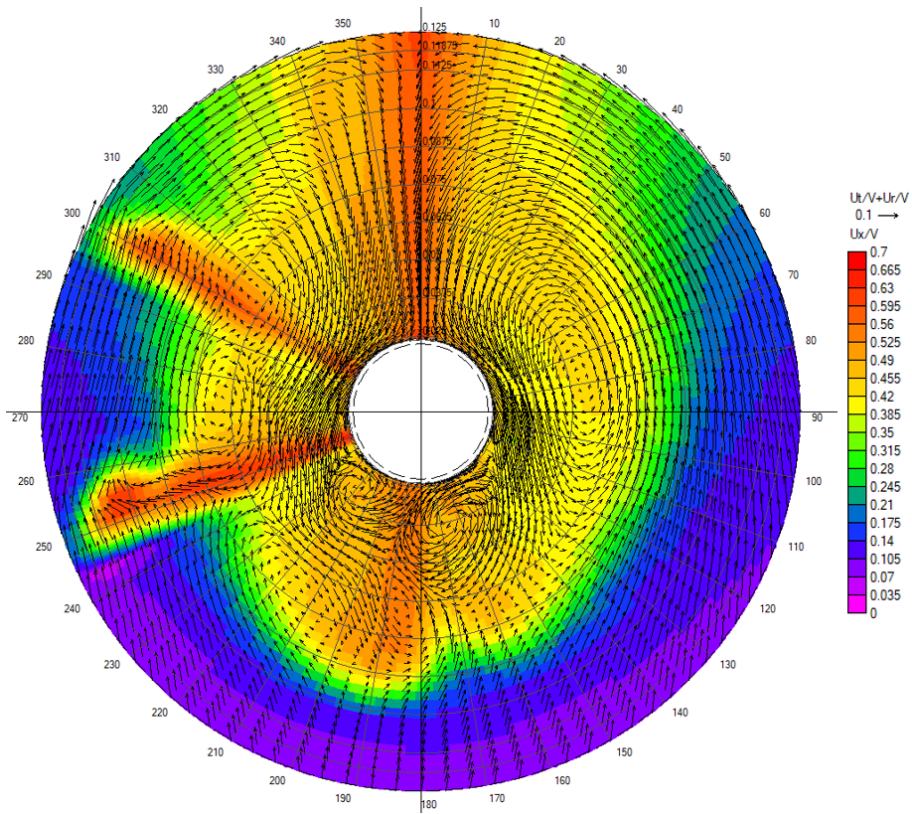


Figure F.40: Effective Wake - PSS AoA 1 Position 3

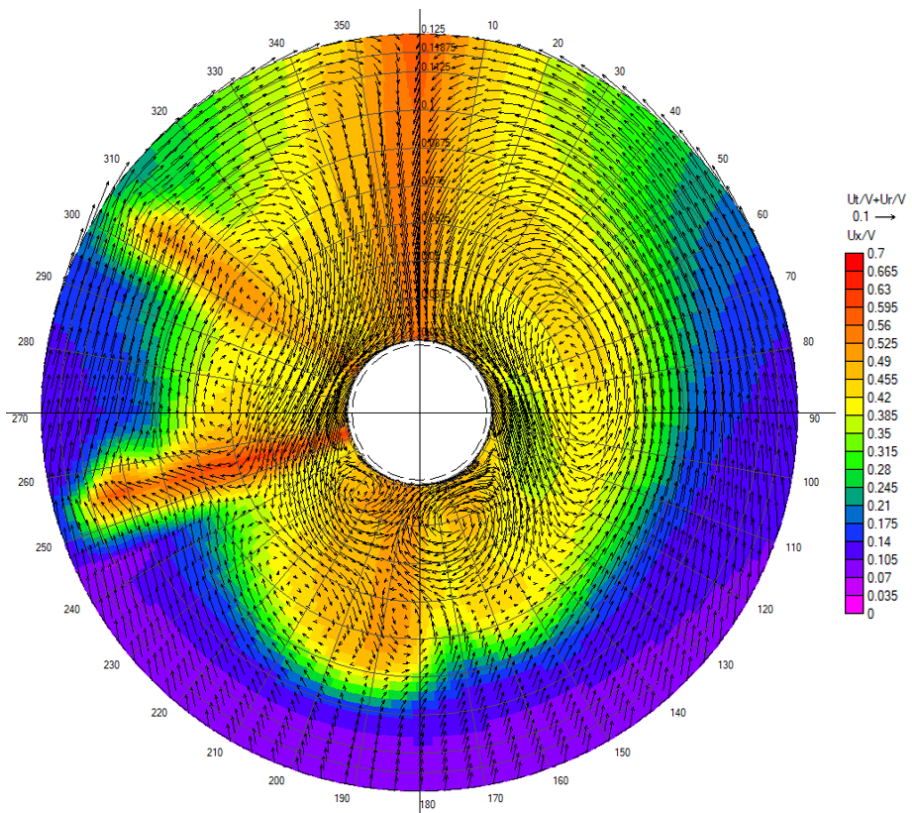


Figure F.41: Effective Wake - PSS AoA 1 Position 4

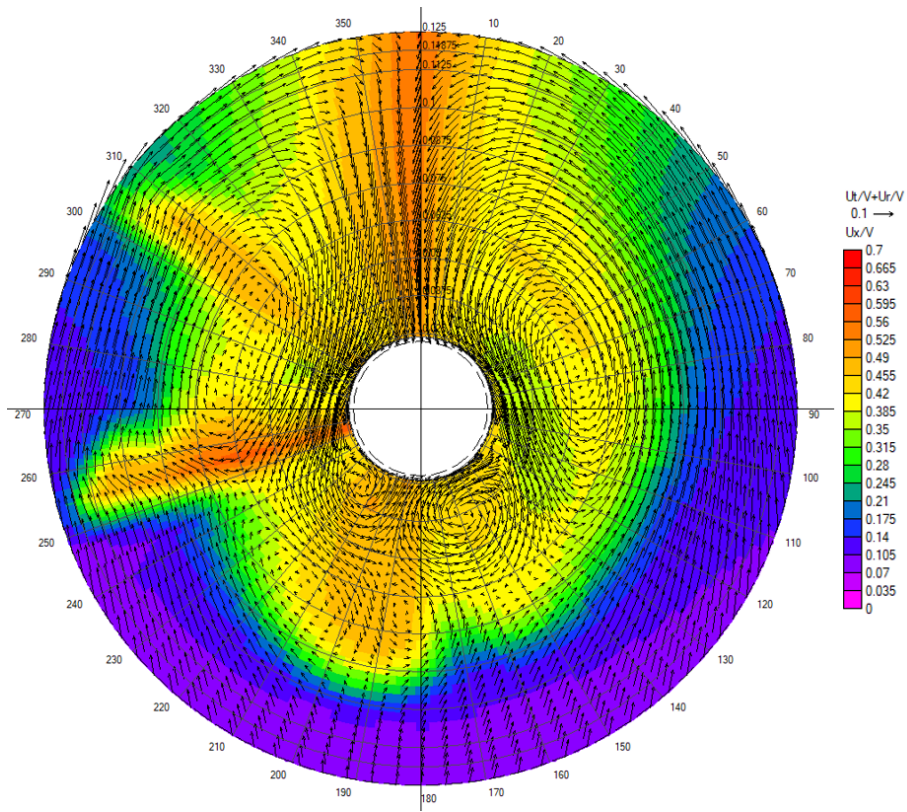


Figure F.42: Effective Wake - PSS AoA 1 Position 5

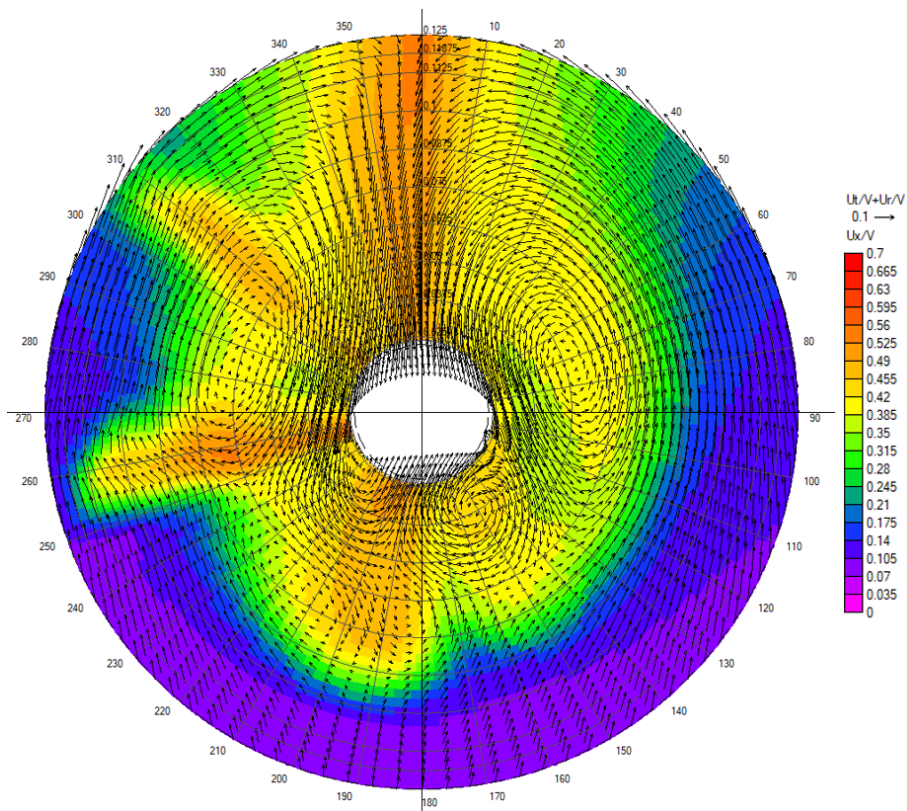


Figure F.43: Effective Wake - PSS AoA 1 Position 6

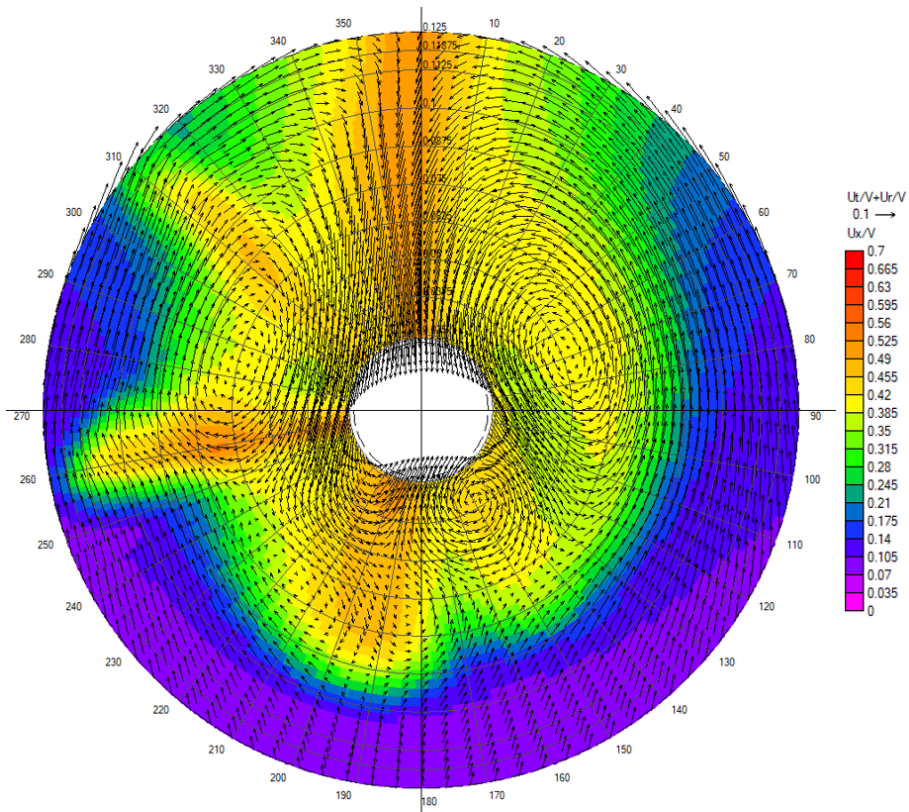


Figure F.44: Effective Wake - PSS AoA 1 Position 7

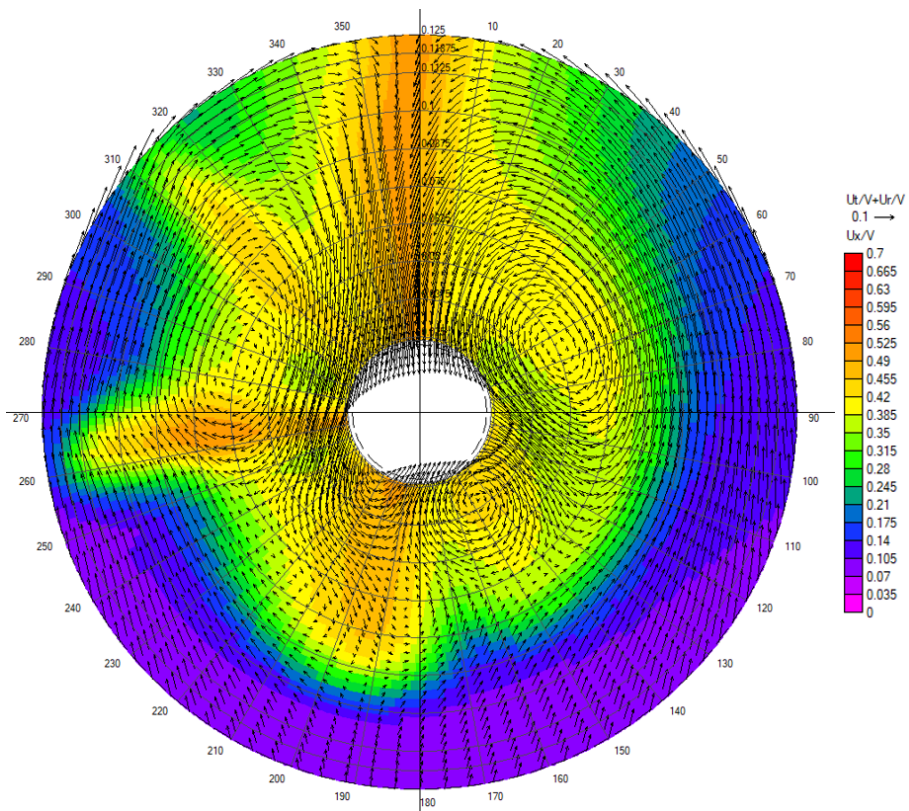


Figure F.45: Effective Wake - PSS AoA 1 Position 8

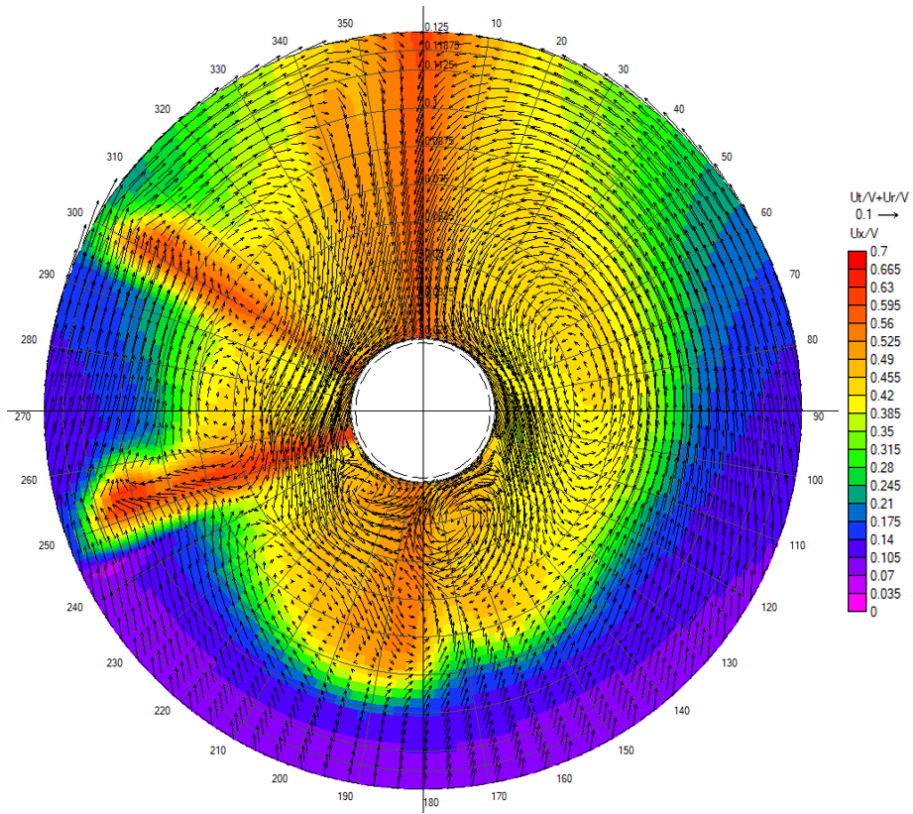


Figure F.46: Effective Wake - PSS AoA 2 Position 3

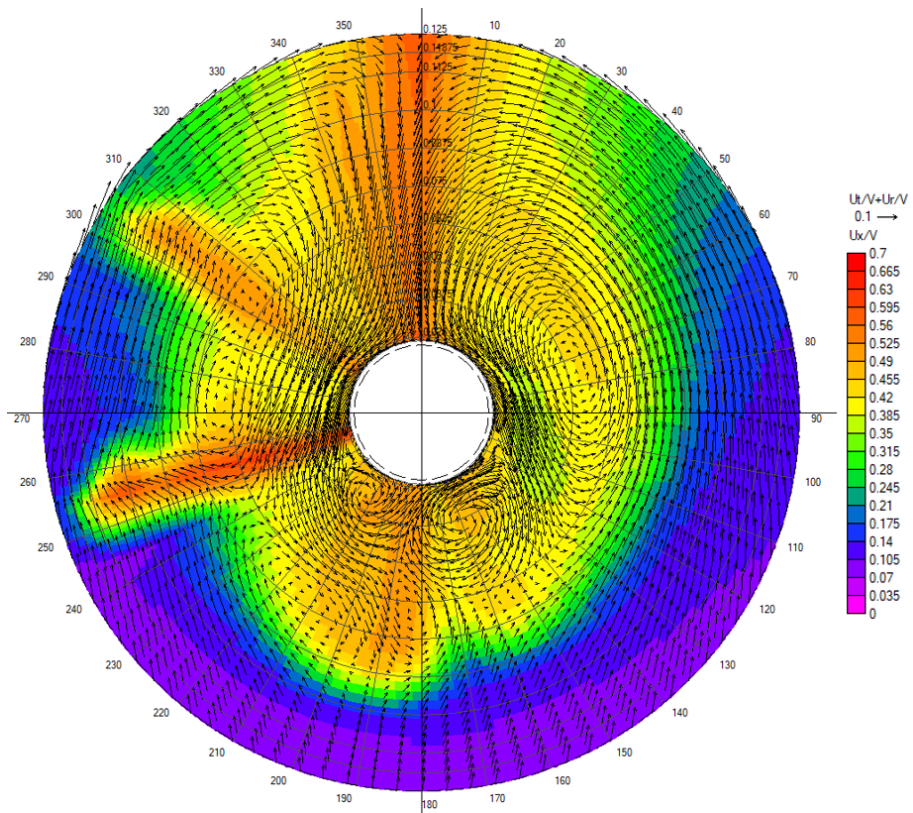


Figure F.47: Effective Wake - PSS AoA 2 Position 4

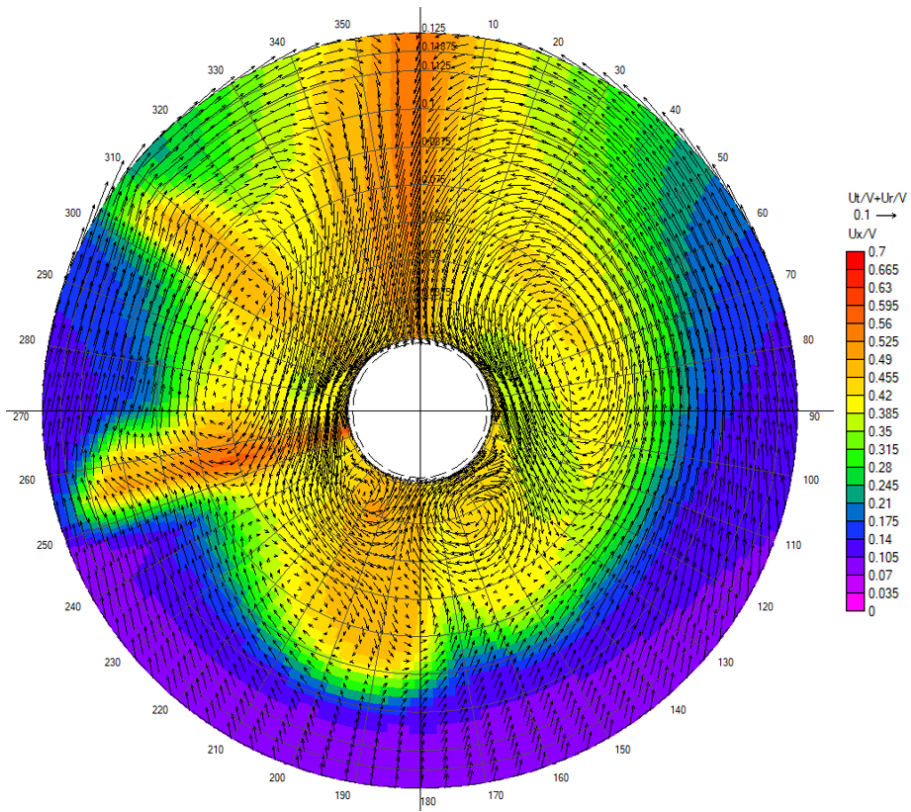


Figure F.48: Effective Wake - PSS AoA 2 Position 5

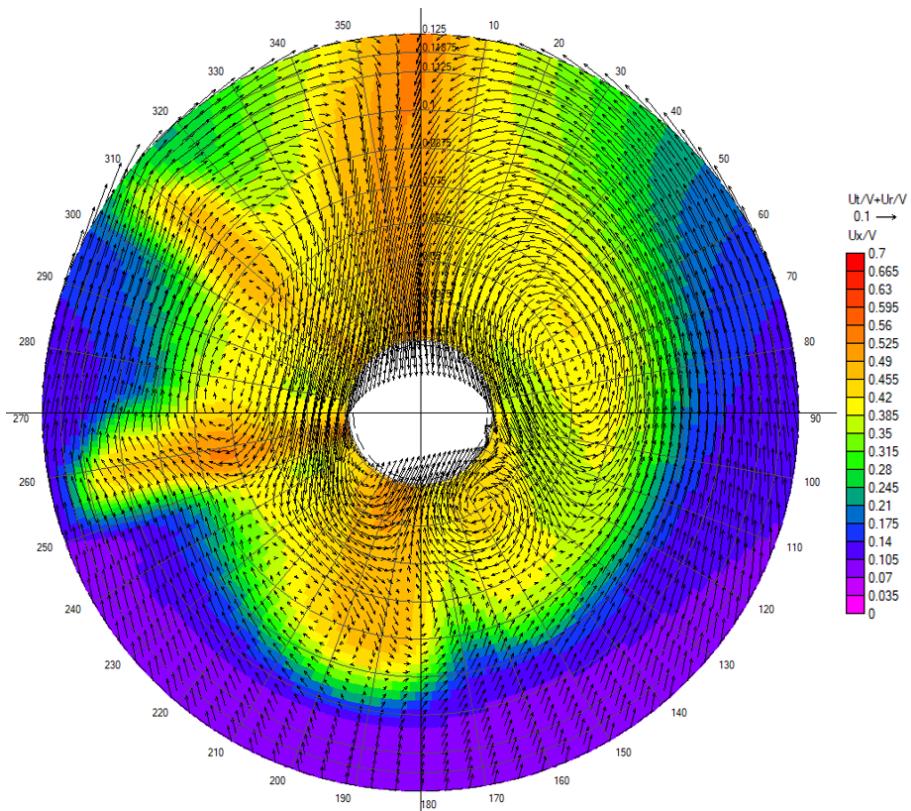


Figure F.49: Effective Wake - PSS AoA 2 Position 6

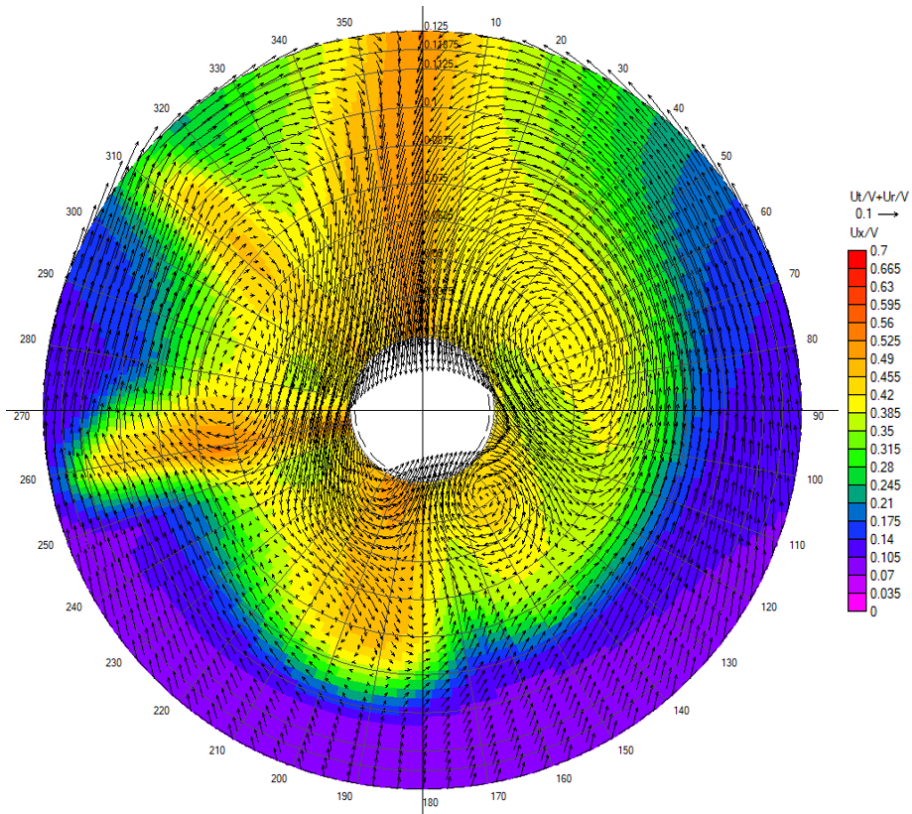


Figure F.50: Effective Wake - PSS AoA 2 Position 7

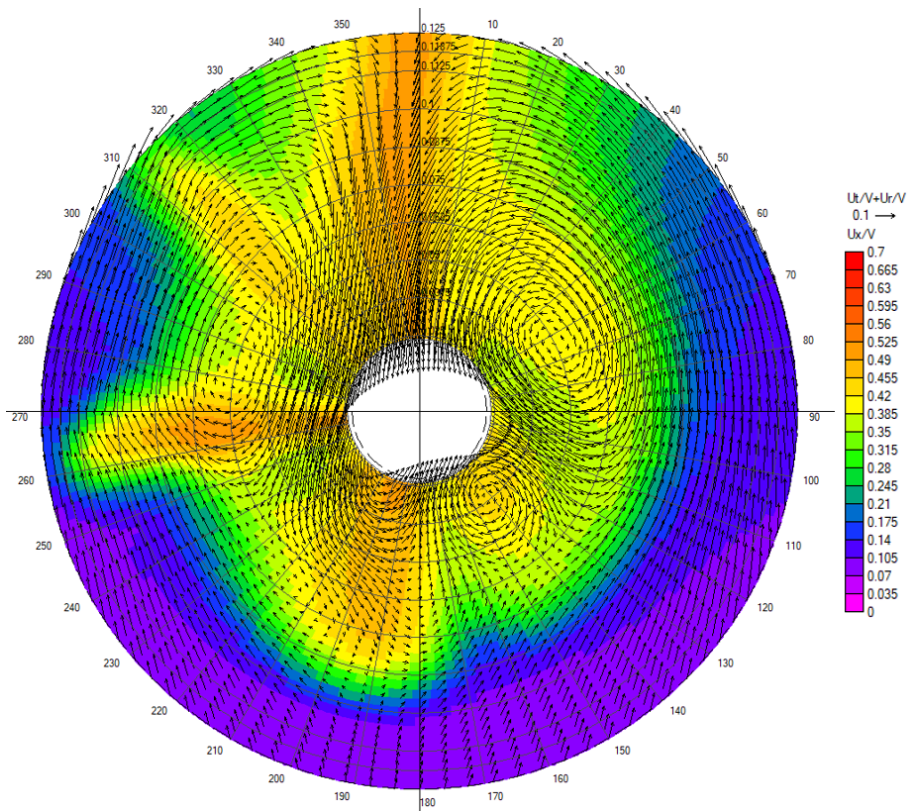


Figure F.51: Effective Wake - PSS AoA 2 Position 8

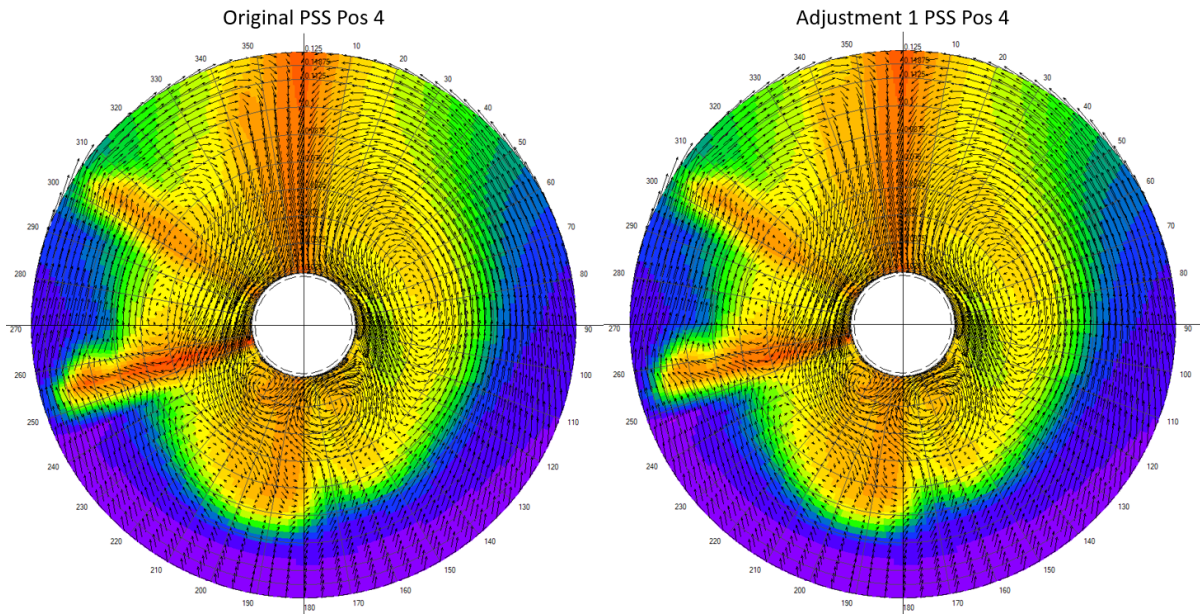


Figure F.52: Effective Wake - PSS Adjustment Comparison - Original vs Adjustment 1

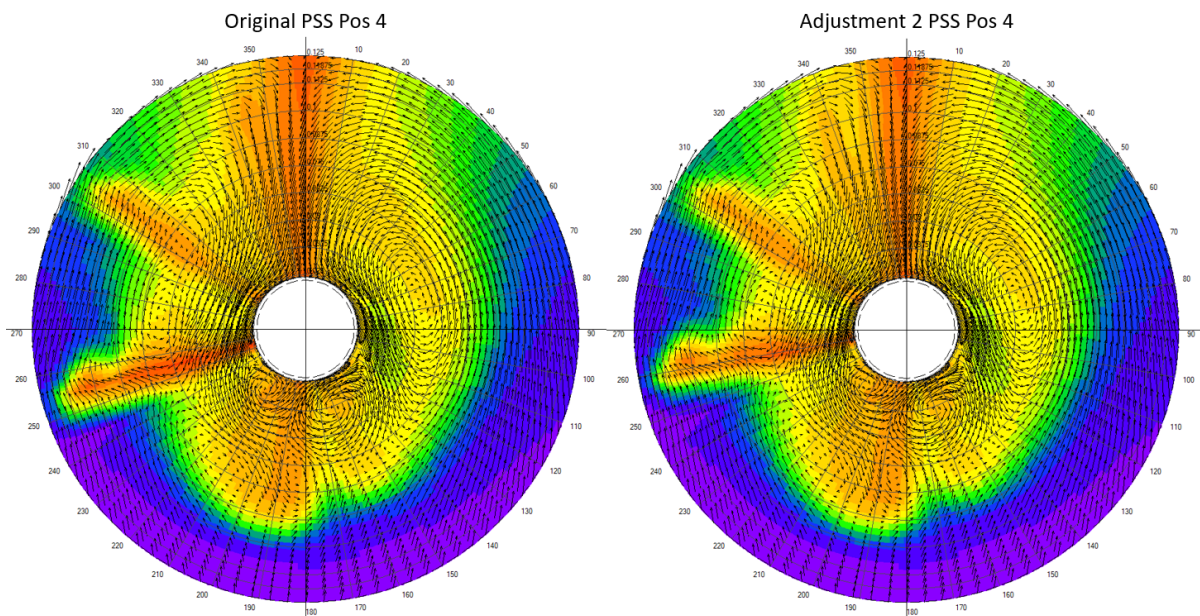


Figure F.53: Effective Wake - PSS Adjustment Comparison - Original vs Adjustment 2

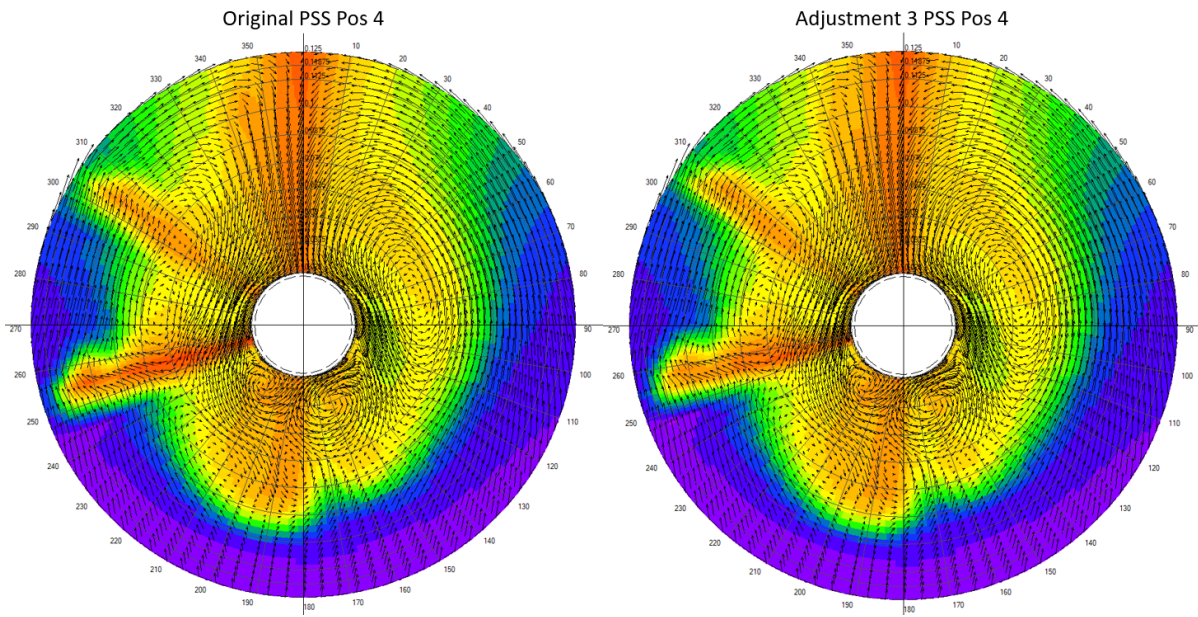


Figure F.54: Effective Wake - PSS Adjustment Comparison - Original vs Adjustment 2

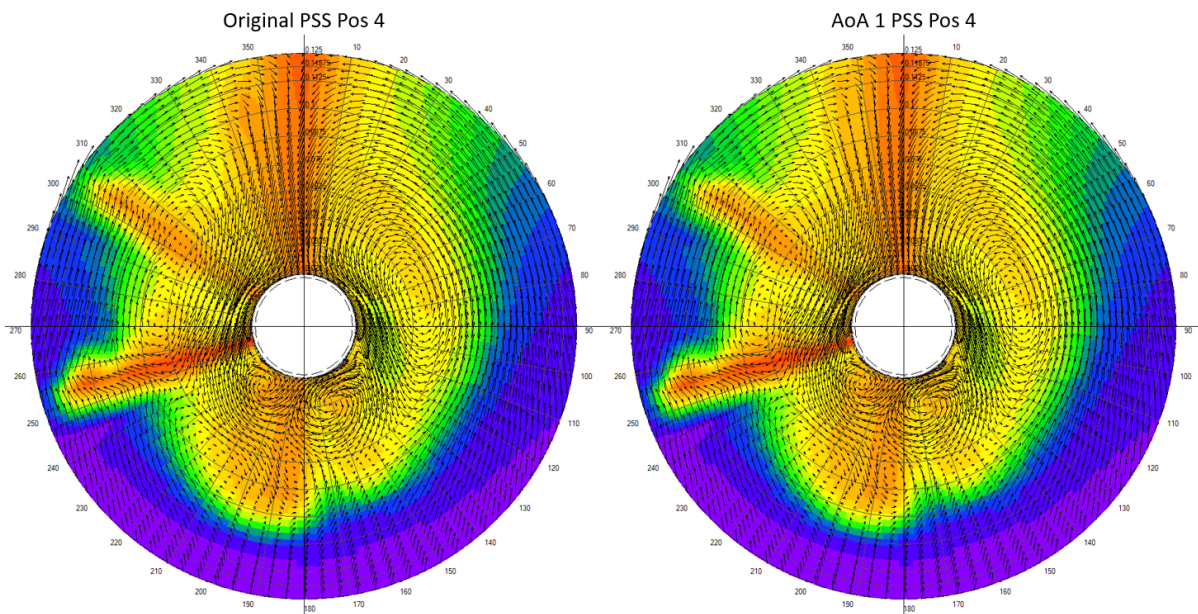


Figure F.55: Effective Wake - PSS Adjustment Comparison - Original vs AoA 1

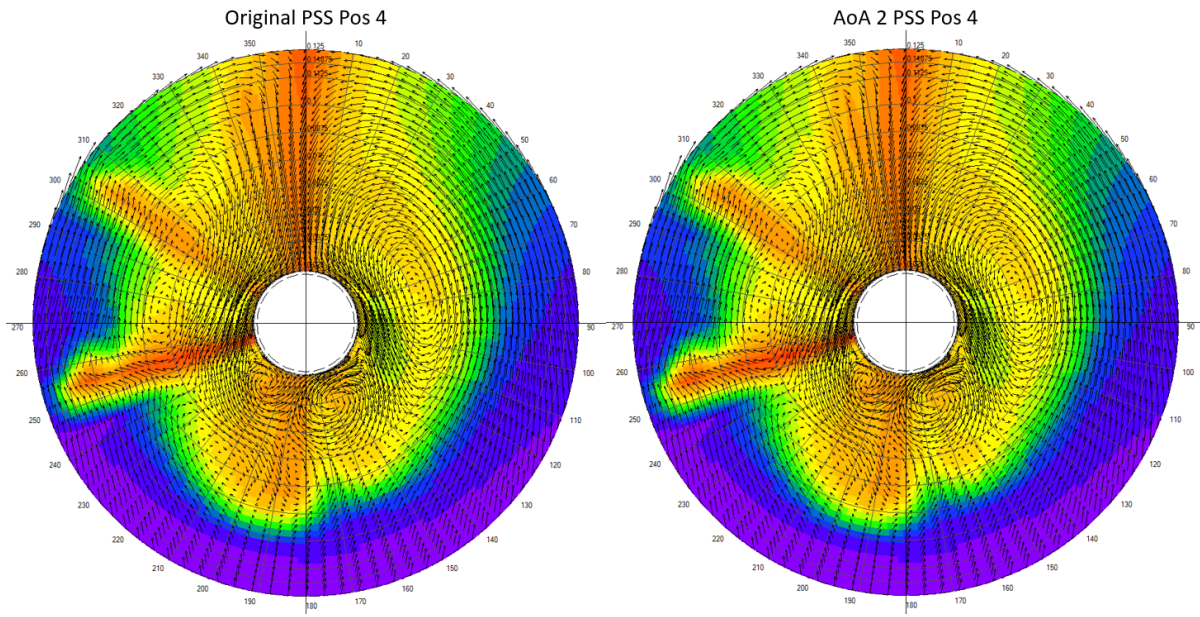


Figure F.56: Effective Wake - PSS Adjustment Comparison - Original vs AoA 2

F.3 Wake Fraction

Positions	1	2	3	4	5	6	7	8
Naked [12kn]	0.3500	0.3346	0.3207	0.3084	0.2976	0.2913	0.2858	0.2808
Naked [14kn]	0.3487	0.3332	0.3193	0.3071	0.2964	0.2904	0.2853	0.2804
Naked [16kn]	0.3524	0.3369	0.3231	0.3111	0.3006	0.2949	0.2899	0.2851
Original [12kn]	—	—	0.3377	0.3247	0.3139	0.3072	0.3016	0.2962
Original [14kn]	—	—	0.3332	0.3204	0.3094	0.3032	0.2978	0.2927
Original [16kn]	—	—	0.3348	0.3222	0.3114	0.3056	0.3002	0.2952
Adjustment 1	—	—	0.3310	0.3176	0.3068	0.3014	0.2964	0.2912
Adjustment 2	—	—	0.3297	0.3174	0.3076	0.3023	0.2971	0.2911
Adjustment 3	—	—	0.3299	0.3171	0.3069	0.3015	0.2962	0.2909
AoA 1	—	—	0.3311	0.3182	0.3072	0.3010	0.2956	0.2904
AoA 2	—	—	0.3317	0.3189	0.3078	0.3017	0.2963	0.2911

Table 4: Effective Wake fraction WT for all computations

G Cavitation Analysis

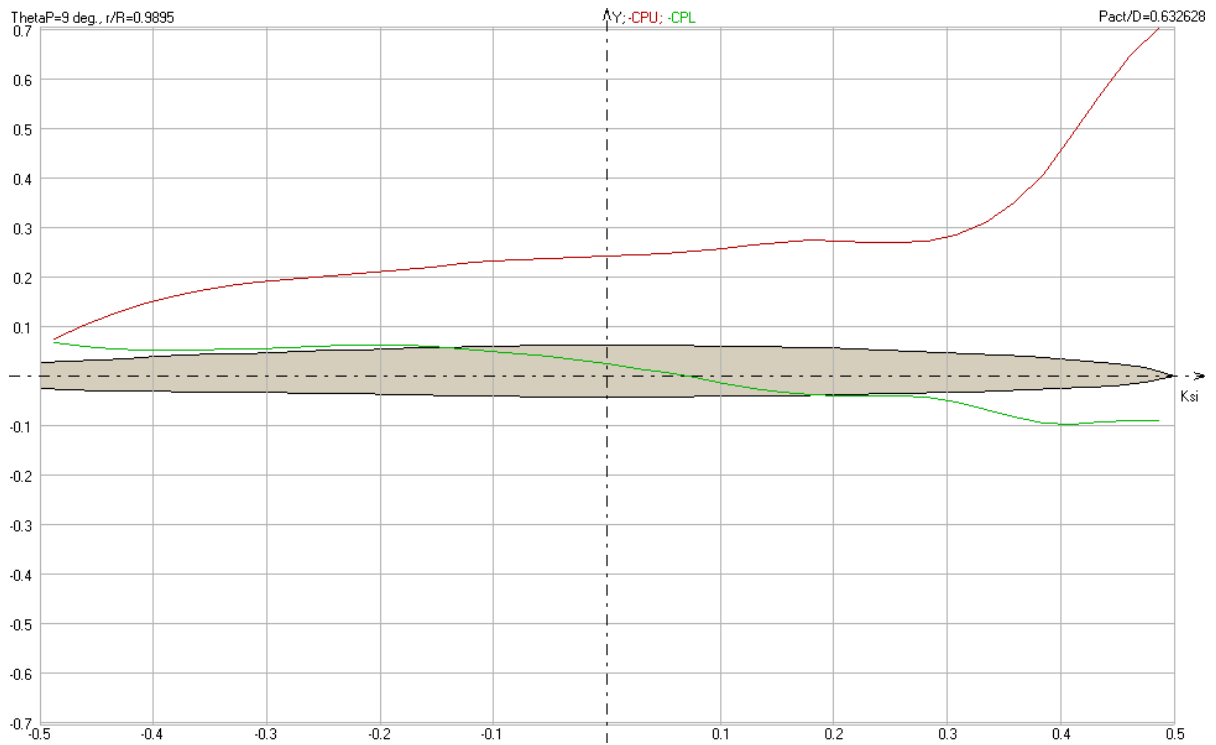


Figure G.1: Original PSS Pos 4 - Pressure distribution upper (CPU) and lower (CPL) blade surface at 9°rotation. Radial position $r/R = 0.9895$

H Pressure distribution PSS

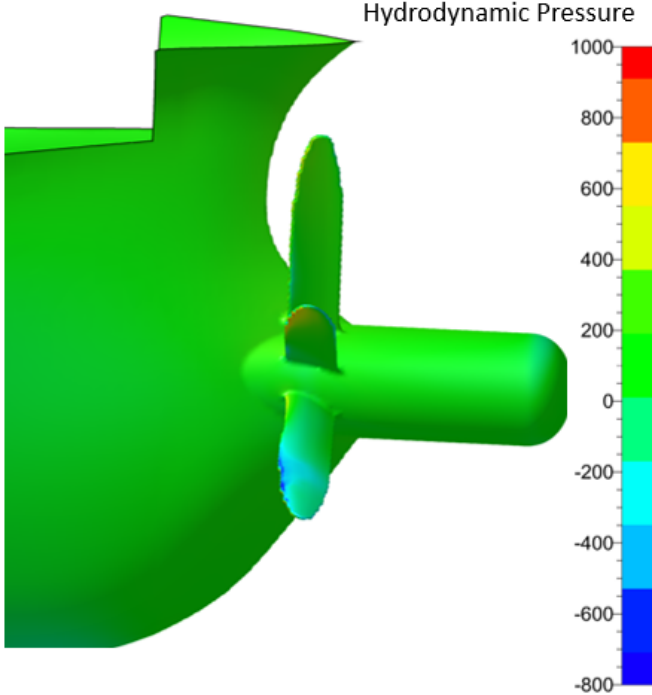


Figure H.1: Pressure distribution PSS Adjustment 1 (1)

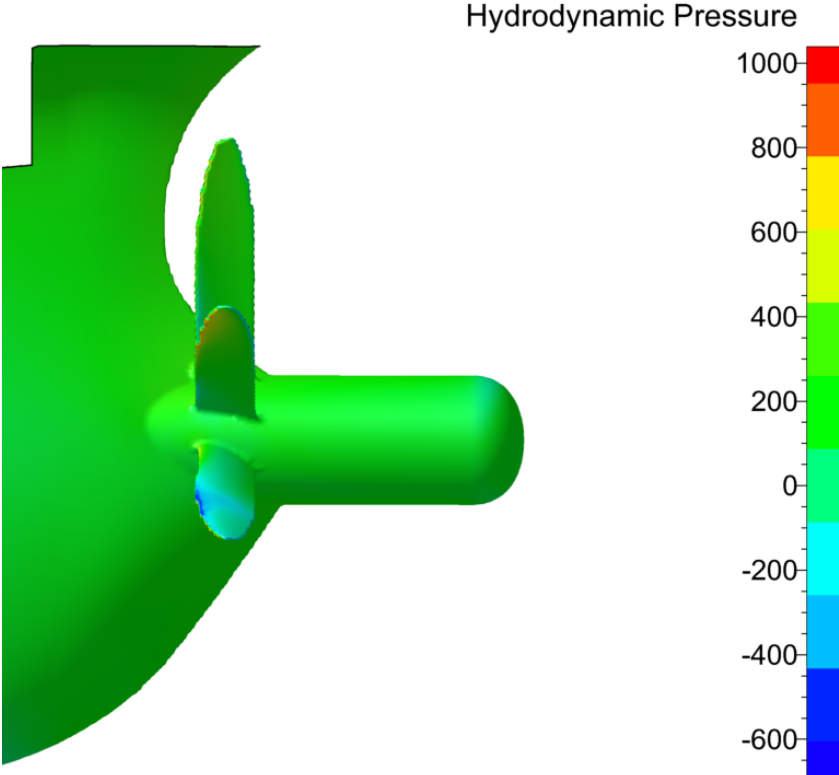


Figure H.2: Pressure distribution PSS Adjustment 2 (1)

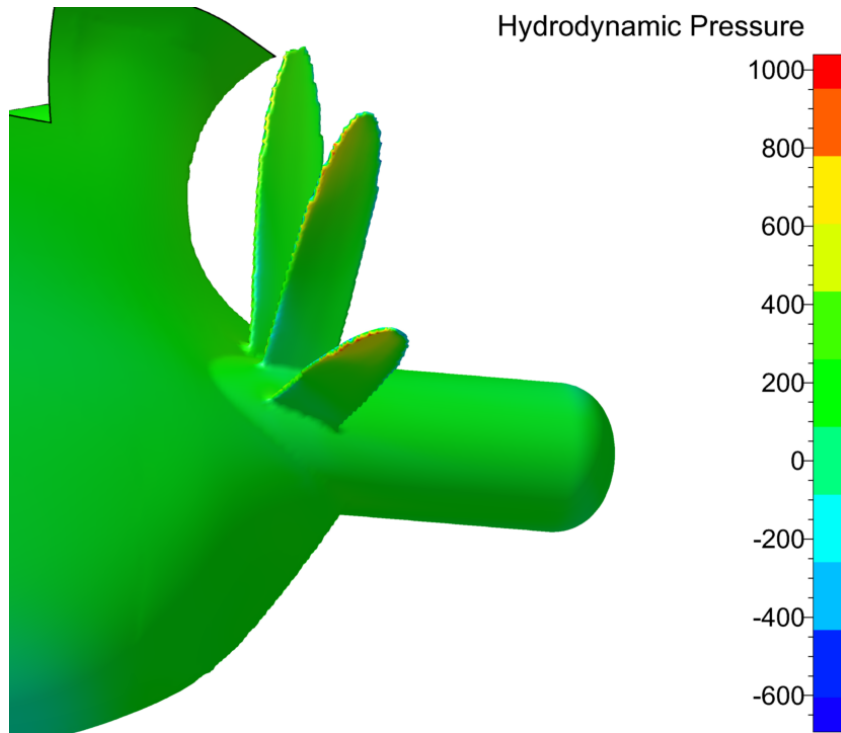


Figure H.3: Pressure distribution PSS Adjustment 2 (2)

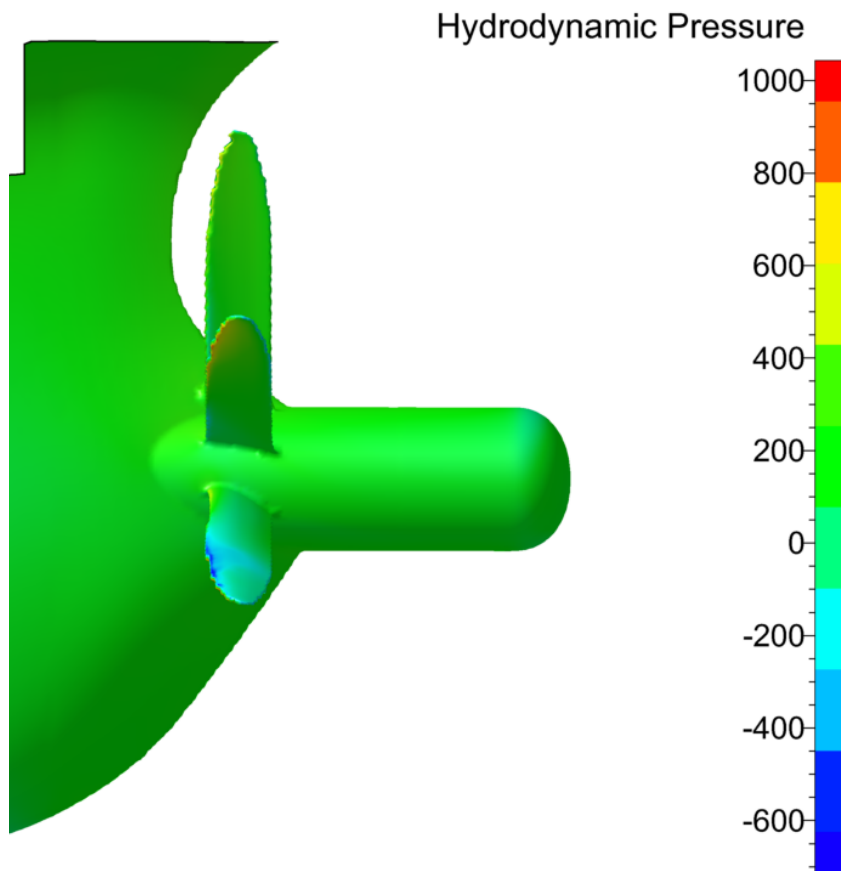


Figure H.4: Pressure distribution PSS Adjustment 3 (1)

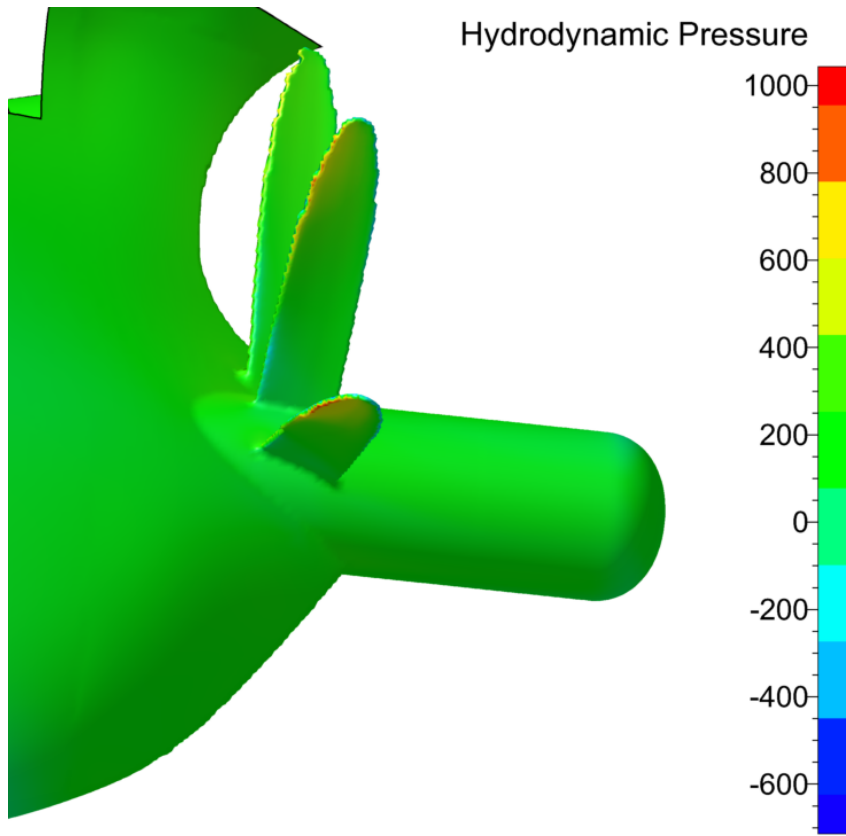


Figure H.5: Pressure distribution PSS Adjustment 3 (2)

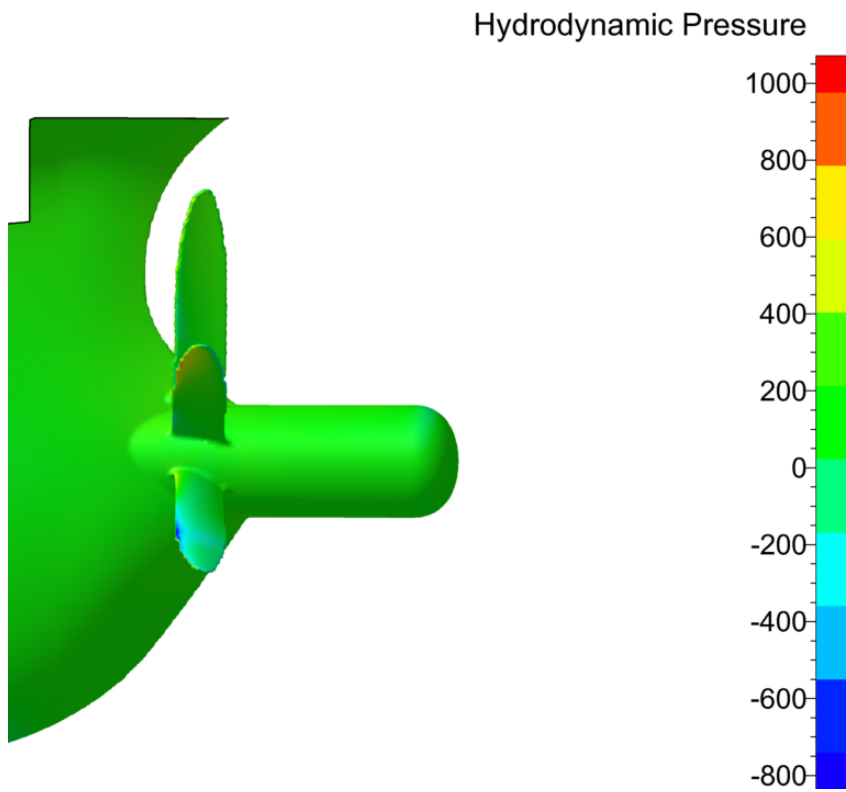


Figure H.6: Pressure distribution PSS AoA 1 (1)

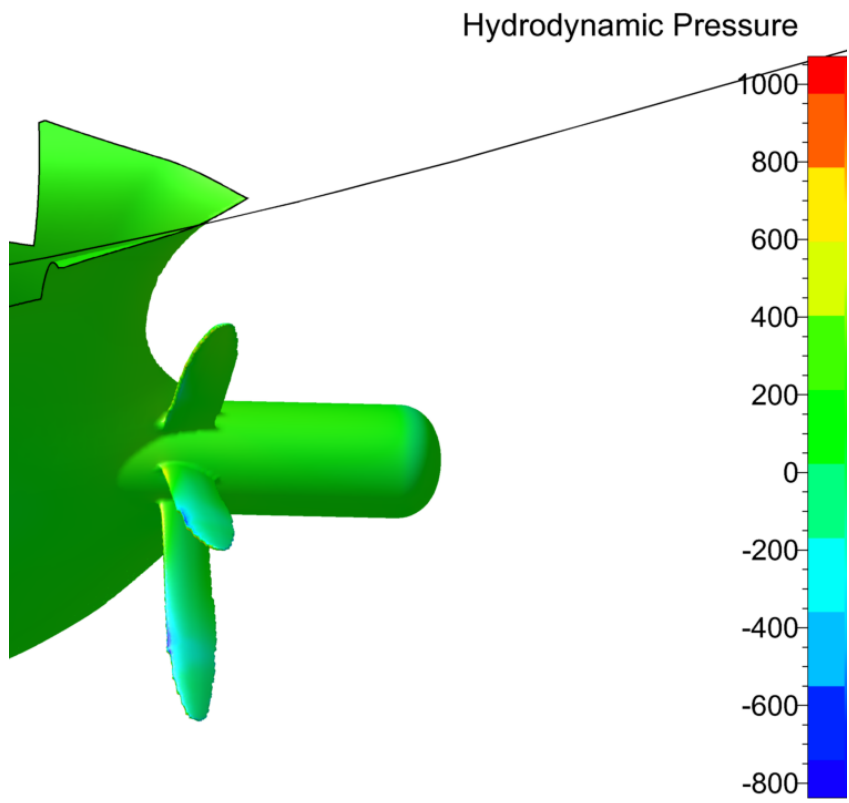


Figure H.7: Pressure distribution PSS AoA 1 (2)

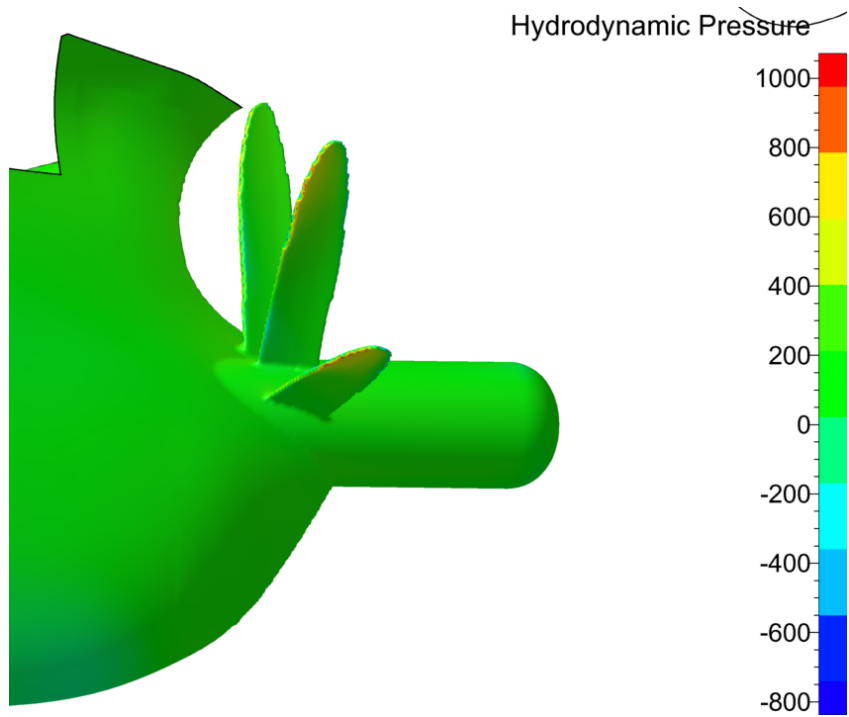


Figure H.8: Pressure distribution PSS AoA 1 (3)

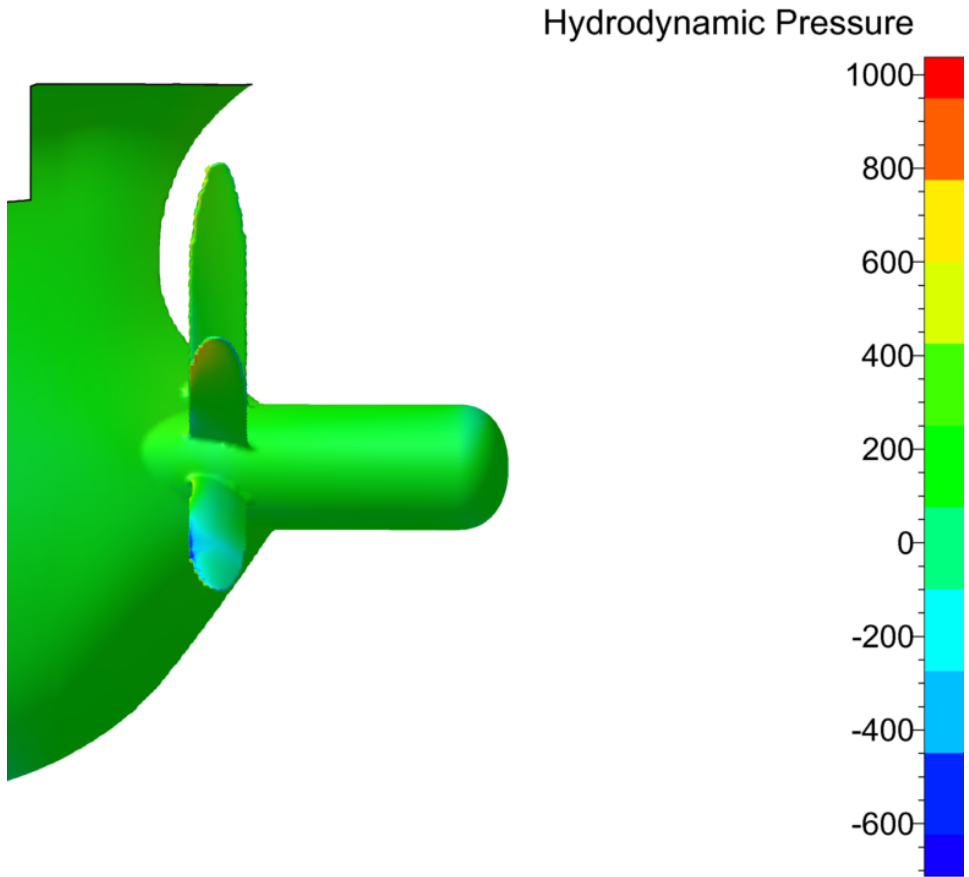


Figure H.9: Pressure distribution PSS AoA 2 (1)

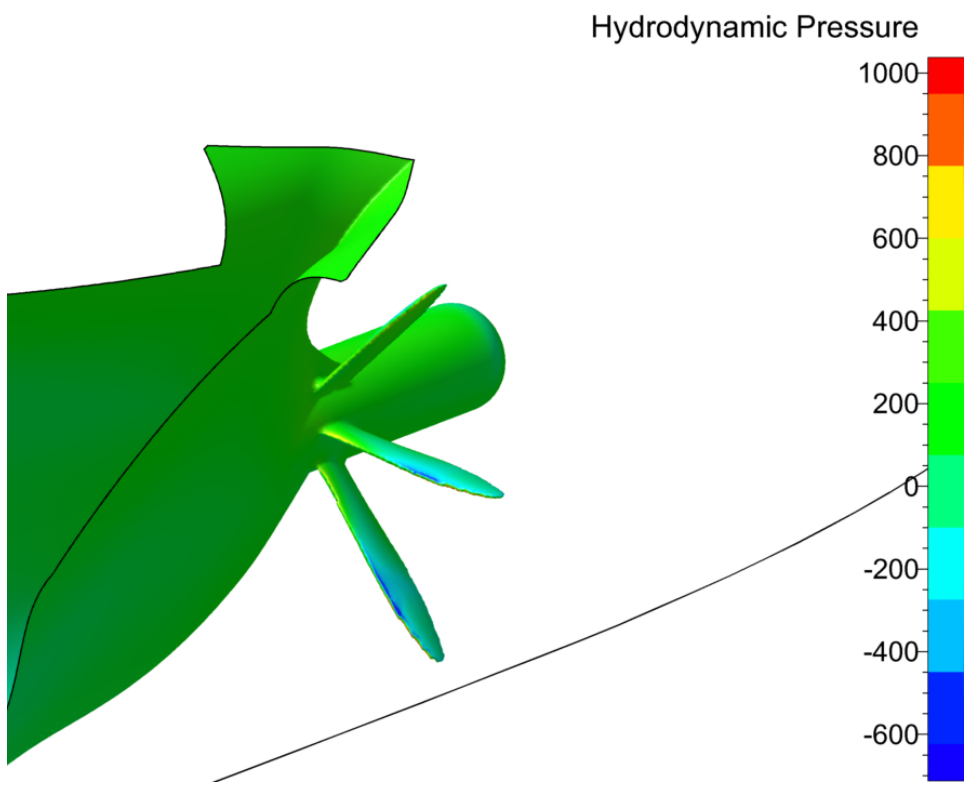


Figure H.10: Pressure distribution PSS AoA 2 (2)

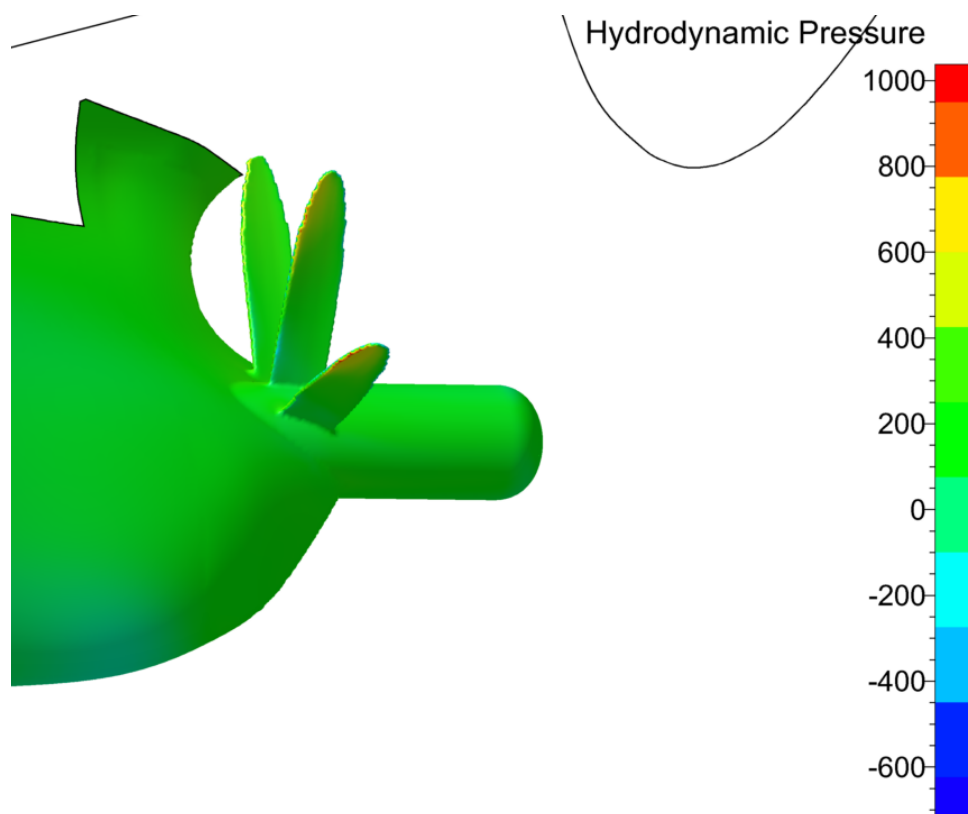


Figure H.11: Pressure distribution PSS AoA 2 (3)

I Programming

I.1 Python

```
1 #!/bin/bash
2 # list of distances to propeller plane
3 positions=(0.0615 0.0410 0.0205 0 -0.0205 -0.0410)
4 # list of directories to explore SIMULATIONS WITH ESD
5 DIRS=( NorSingProp_w_ESD_Ref_1/NorSingProp_w_ESD_Run_1)
6
7 # save current directory as top directory
8 topDir='pwd'
9
10 # loop over list of directories run wakeflow tool
11 for DIR in "${DIRS[@]}"
12 do
13 # loop over list of distances to propeller plane
14 for pos in "${positions[@]}"
15 do
16 # print case
17 echo "${DIR} ${pos}:"
18 # replace keyword "position" in input file with numerical value and
19 # copy input file to sim directory
20 sed "s/position/${pos}/" wake_flow_pp.input > $DIR/wake_flow_pp.
21 input
22 # move to simulation directory
23 cd "${DIR}"
24 # run wake flow tool
25 wake_flow_ppmarine72 -print -relative < wake_flow_pp.input
26 # save wake flow output to separate subdirectory (overwrites
27 previous files)
28 rm -r "Wake_pos_${pos}"
29 mkdir "Wake_pos_${pos}"
30 mv wake* "Wake_pos_${pos}"/
31 # move back to top directory
32 cd "$topDir"
33 done
34 done
```

I.2 MATLAB

I.2.1 Code - Read FM data create AKPA file

```
1 %% Import data using 'readwaketable.m' function
2 clear all
3 close all
4 clc
5
6 Refstep = 6;    % Number of refinements
7 Runstep = 1;   % Number of runs
8 Posstep = 6;   % Number of positions to evaluate
9
10 %% Read wake data and save to .mat files
11 for ii = 1:Refstep
12     for j = 1:Runstep
13         for k = 1:Posstep
14             filename = ['C:\Users\stian\OneDrive\Documents\
15 Skole - NTNU\2019 - Vr\PostPro\matlab\Speed1.41ms\ESD\
16 wake_flow_ESD\Ref_' num2str(ii) '\Wake_pos_' num2str(k) '
17 \wake_flow.txt'];
18             startRow = 15;
19             endRow = 111;
20
21             fid = fopen(filename,'r');    %open file and
22 read
23
24             l1 = fgetl(fid);
25             l2 = fgetl(fid);
26             l3 = fgetl(fid);
27             l4 = fgetl(fid);
28             l5 = fgetl(fid);
29             l6 = fgetl(fid);
30             l7 = fgetl(fid);
31             l8 = fgetl(fid);
32             l9 = fgetl(fid);
33             output = strsplit(l6,' ');
34             nb_angles = str2num(output{5});
35
36             rD = strsplit(l9,' ');    %collects radial
37 data
38             rD = rD(3:end);    %collects only
39 numbers in string
40
41             for i = 1:length(rD)
42                 rr(i) = str2num(rD{i}); %from string to
43 numbers
44             end
45         end
46     end
47 end
```

```

37
38     %Extract data from line 3
39     B = regexp(l3, '[0-9]+.[0-9]+', 'match'); %find
numbers 000.000
40     XP = str2num(cell2mat(B(2)));
41     YP = str2num(cell2mat(B(3)));
42     ZP = str2num(cell2mat(B(4)));
43     Uref = str2num(cell2mat(B(5)));
44
45     fclose(fid); %stop reading file
46
47     %% Collect the three different velocity
components
48     axial = readwaketable(filename,15,15+
nb_angles-1); %(:,from,to)
49     tan = readwaketable(filename,15+nb_angles
+5,15+nb_angles+5+nb_angles-1);
50     radial = readwaketable(filename,15+nb_angles
+5+nb_angles+5,15+nb_angles+5+nb_angles+5+nb_angles-1);
51     theta = axial(1:end,1); %extract the
exact angular position
52     theta(end) = 360;
53
54     axial = axial(1:end,2:end); %extract
only velocity components
55     tan = tan(1:end,2:end); %
56     radial = radial(1:end,2:end); %
57
58     R = rr.*0.25; %exact
radial position
59
60     r1 = strcat('wake_ESD_Ref_', num2str(ii));
61     r2 = strcat('_Run_', num2str(j));
62     r3 = strcat('_Pos', num2str(k));
63     save([strcat(r1,r2,r3, '.mat')], 'axial', 'tan', '
radial', 'R', 'theta', '-v7.3');
64
65     end
66     end
67 end
68
69 %% Create AKPA input files
70 for iii = 1:Refstep
71     for jj = 1:Runstep
72         for kk = 1:Posstep
73

```

```
74         load(['wake_ESD_Ref_' num2str(iii) '_Run_'
num2str(jj) '_Pos' num2str(kk) '.mat']);
75         Refstep = iii;
76         Posstep = kk;
77         AKPA_Input_Files_rev1(axial,tan,radial,theta,R,
Refstep,Posstep); % see function
78
79         cd 'C:\Users\stian\OneDrive\Documents\Skole -
NTNU\2019 - Vr\PostPro\matlab\Speed1.41ms\ESD'
80     end
81 end
82 end
```

I.2.3 Function - Create AKPA Input files

```
1 function [] = AKPA_Input_Files(axial,tan,radial,theta,R,  
    Refstep,Posstep)  
2 %% Create readable files for AKPA from files collected from  
    FINE/Marine  
3 axial = [theta axial];  
4 tan = [theta tan];  
5 radial = [theta radial];  
6  
7 for i = Refstep  
8     for j = Posstep  
9         %Return to AKPA directory  
10        cd 'C:\AKPA\AKPA-CP-DT_60\P1500mod_BAR=0'  
11        % cd 'C:\Users\stian\OneDrive\Documents\Skole - NTNU  
    \2019 - Vr\PostPro\matlab\Speed1.41ms\ESD'  
12  
13        %Check if folder exist, if not create  
14        if ~exist(['ESD_Ref_' num2str(i) '_Pos' num2str(j)],  
    'dir')  
15            newFolder = mkdir(['ESD_Ref_' num2str(i) '_Pos'  
    num2str(j)]);  
16            end  
17  
18            %Directs to current working directory.  
19            cd(['ESD_Ref_' num2str(i) '_Pos' num2str(j)])  
20            filename = 'inputvel.frw'  
21  
22            %Create the document  
23            fid = fopen(filename,'w')  
24            fclose(fid)  
25  
26            A = length(axial(:,1));  
27            B = length(axial(1,:))-1;  
28  
29            % Read and write the needed information into the  
    document  
30            fid = fopen(filename,'r+')  
31            fprintf(fid, ' "AK-QSPA-POD-RUD". TWO-STAGE  
    PROPULSOR/POD/RUDDER QUASI-STEADY ANALYSIS CODE. (version  
    3.0)\n\n')  
32  
33            fprintf(fid, ' I N P U T   D A T A   O N   T H E   I  
    N F L O W   V E L O C I T Y   F I E L D\n')  
34            fprintf(fid, '  
    -----  
n')
```



```

35         fprintf(fid, '                F O R   T H E   F O R W
A R D   S T A G E\n')
36         fprintf(fid, '
-----\n\n')
37
38         fprintf(fid, '   Project name :   \n')
39         fprintf(fid, '   c). Comments : uniform inflow field\
n\n\n')
40
41
42         fprintf(fid, '   COMPONENT OF THE CIRCUMFERENTIAL
NON-UNIFORM INFLOW VELOCITY FIELD \n')
43         fprintf(fid, '   PRESCRIBED AT THE PROPELLER DISK (
BRL-SECTION)\n\n')
44
45         fprintf(fid, [' * Number of the r-sections NRU='
num2str(B) '\n'])
46         fprintf(fid, [' * Number of the Theta-positions NTU
=' num2str(A) '\n\n'])
47
48         fprintf(fid, ' * RU      - r-coordinate of the
section to prescribe the inflow;\n')
49         fprintf(fid, ' * THETU - angular positions of the
points to prescribe the inflow.\n')
50         fprintf(fid, '          ( ! must be the same for all
three components ! )\n\n')
51
52         fprintf(fid, '          Inflow velocity field is defined
in the global fixed cylindrical\n')
53         fprintf(fid, '          coordinate system upstream the
propeller \n\n')
54
55         fprintf(fid, ' * Axial Ux/V (positive to forward):\n
n')
56         fprintf(fid, ' * Key for definition of Ux ( 1 - Ux,
2- (1-Ux) ) Key_Ux=1\n')
57         fprintf(fid, '
-----\n\n')
58         fprintf(fid, '          |   Radial sections, RU [m]\n
n')
59         fprintf(fid, '          THETU
|-----\n\n')
60
61         fprintf(fid, '          ')
62         for rad = 1:length(R)

```

```

63         fprintf(fid, ' % .5f ' ,R(rad))
64     end
65
66     fprintf(fid, '\n
-----+-----
\n')
67
68     for row = 1:size(axial, 1)
69         startline = ftell(fid);           % get current
position
70         fseek(fid, 0, 'cof');
71         for col = 1:size(axial,2)
72             fprintf(fid, '%10.5f', axial(row, col));
73         end
74         fprintf(fid, '\n');
75         fseek(fid, startline, 'bof');    % return to
beginning of line
76         fgetl(fid);
77     end
78
79     fprintf(fid, '
-----+-----
\n\n')
80     fprintf(fid, ' * Tangential Ut/V (positive to
clockwise (right) direction):\n')
81     fprintf(fid, '
-----+-----
\n')
82     fprintf(fid, '          |   Radial sections, RU [m]\n
')
83     fprintf(fid, '          THETU
|-----+-----
\n')
84
85     fprintf(fid, '          ')
86     for rad = 1:length(R)
87         fprintf(fid, ' % .5f ' ,R(rad))
88     end
89
90     fprintf(fid, '\n
-----+-----
\n')
91
92     for row = 1:size(tan, 1)
93         startline = ftell(fid);           %get current
position
94         fseek(fid, 0, 'cof');

```

```

95         for col = 1:size(tan,2)
96             fprintf(fid, '%10.5f', tan(row, col));
97         end
98         fprintf(fid, '\n');
99         fseek(fid, startline, 'bof'); %return to
beginning of line
100         fgetl(fid);
101     end
102
103     fprintf(fid, '
-----
\n\n')
104     fprintf(fid, ' * Radial Ur/V (positive radially
outward, to propeller blade tip):\n')
105     fprintf(fid, '
-----
\n')
106     fprintf(fid, '          | Radial sections, RU [m]\n
')
107     fprintf(fid, '          THETU
|-----
\n')
108
109     fprintf(fid, '          ')
110     for rad = 1:length(R)
111         fprintf(fid, ' % .5f ', R(rad))
112     end
113
114     fprintf(fid, '\n
-----+
\n')
115
116     for row = 1:size(radial, 1)
117         startline = ftell(fid); %get current
position
118         fseek(fid, 0, 'cof');
119         for col = 1:size(radial,2)
120             fprintf(fid, '%10.5f', radial(row, col));
121         end
122         fprintf(fid, '\n');
123         fseek(fid, startline, 'bof'); %return to
beginning of line
124         fgetl(fid);
125     end
126     fprintf(fid, '
-----
\n')

```

```
127  
128     end  
129 end  
130 end
```

